Rekenmodellen voor de dwarskrachtsterkte van geprefabriceerde voorgespannen liggers uit staalvezelbeton

Design Models for the Shear Strength of Prestressed Precast Steel Fibre Reinforced Concrete Girders

Tim Soetens

Promotor: prof. dr. ir. S. Matthys
Proefschrift ingediend tot het behalen van de graad van
Doctor in de Ingenieurswetenschappen: Bouwkunde

Vakgroep Bouwkundige Constructies
Voorzitter: prof. dr. ir. L. Taerwe
Faculteit Ingenieurswetenschappen en Architectuur
Academiejaar 2014 - 2015

UNIVERSITEIT GENT

ISBN 978-90-8578-791-4
NUR 955
Wettelijk depot: D/2015/10.500/35

My will to win will always be greater than the fear to fail

Supervisor

Prof. dr. ir. Stijn Matthys

Research institute

Magnel Laboratory for Concrete Research
Department of Structural Engineering
Faculty of Engineering and Architecture
Ghent University, Belgium

Examination Committee

Prof. dr. ir. Luc Taerwe (chairman)
Ghent University, Department of Structural Engineering, Ghent, Belgium

Prof. dr. ir. Robby Caspeele (secretary)
Ghent University, Department of Structural Engineering, Ghent, Belgium

Prof. dr. ir. Stijn Matthys (supervisor)
Ghent University, Department of Structural Engineering, Ghent, Belgium

Prof. dr. ir. Joaquim Barros
University of Minho, ISISE, Department of Civil Engineering, Guimarães, Portugal

Prof. dr. ir. Lucie Vandewalle
Catholic University of Leuven (KU Leuven), Department of Civil Engineering, Leuven, Belgium

Prof. dr. ir. Wim Moerman
Willy Naessens Group, Belgium
Ghent University (guest professor)

Prof. dr. ir. Wouter De Corte
Ghent University, Department of Industrial Technology and Construction, Ghent, Belgium

Research funding

The author would like to thank the company MEGATON (part of the Willy Naessens Group) and the Agency for Innovation by Science and Technology (IWT) for the financial support through the Baekeland research project with ref. 100686.

Dankwoord

Tijdens dit doctoraatsonderzoek heb ik de kans gekregen om mijn kennis over beton in het algemeen en meer specifiek over staalvezelbeton verder uit te diepen. Daarbij lag voornamelijk de focus of de technische en wetenschappelijk aspecten. Deze zijn dan ook zorgvuldig neergeschreven in het boek dat u nu in de hand hebt. Het zou echter verkeerd zijn om enkel en alleen deze resultaten aan de buitenwereld te tonen.

Naast alle nieuw verworven wetenschappelijke inzichten op het vlak van beton, is het minstens even belangrijk om ook eens stil te staan bij de talrijke ervaringen en de verrijkingen op menselijk vlak die onlosmakelijk verbonden zijn aan een doctoraat. Zoiets is moeilijk in woorden te vatten, maar degenen die het mij al hebben voorgedaan zullen dit wellicht kunnen beamen.

Gedurende vier jaar lang heb ik, met veel passie, inzet en doorzettingsvermogen, getracht om alle uitdagingen, opportuniteiten en problemen het hoofd te bieden. Anderzijds moet ik, met alle respect, ook toegeven dat de honger naar kennis en studie stilletjes aan ook gestild aan het geraken is.

Niettemin ben ik fier om u dit boek ter lezing aan te bieden en is het tevens mijn plicht om vele mensen te bedanken die mij op financieel, technisch, wetenschappelijk, en emotioneel vlak gedurende de afgelopen vier jaar hebben bijgestaan.

Eerst en vooral wil ik mijn industriële promotor, ir. Frederik Cornelis, bedanken om als directeur van de firma Megaton nv te kiezen voor een innovatief beleid en op die manier te kiezen voor een traject van product- en productieoptimalisatie met een grondig wetenschappelijke ondersteuning. Dit boek dient dan ook gezien te worden als het begin voor een verdere implementatie van staalvezels in het dagelijks gebruik van producenten van geprefabriceerde betonelementen voor structurele doeleinden. Tevens bedank ik u om alle faciliteiten van de firma Megaton nv voor dit onderzoeksproject aan mij beschikbaar te stellen.

Daarnaast wil ik ook een groot woord van dank richten aan mijn wetenschappelijke promotor, prof. dr. ir. Stijn Matthys, zonder wie dit onderzoek nooit hetzelfde hoge niveau zou bereikt hebben. Bedankt om vanaf het prille begin tot het bittere einde van deze vier jaar al mijn teksten na te lezen en te verbeteren en om mij op professionele wijze te begeleiden. Door u kon ik mezelf ook altijd motiveren om na ietwat tegenvallende resultaten toch altijd de draad terug op te pakken.

Al het experimenteel werk kon slechts worden uitgevoerd mits de medewerking van het Laboratorium Magnel voor Betononderzoek. Daarvoor wil ik prof. dr. ir. Luc Taerwe bedanken om alle faciliteiten van het labo voor mijn onderzoek beschikbaar te stellen.

I would also like to thank the members of the jury for reviewing this PhD thesis. Thank you prof. Matthys, prof. Taerwe, prof. Caspeele, prof. Barros, prof. Vandewalle, prof. Moerman, prof. De Corte.

Verder wens ik nog een aantal personen in het bijzonder te bedanken voor de logistieke, mentale en technische hulp. Eerst en vooral Ann Van Gysel, omdat haar doctoraatsproefschrift heeft gediend als basis voor mijn verder onderzoek; Pieter Verlé en Chris Van Holsbeek, voor de opvolging van mijn onderzoeksproject en de hulp bij het vervaardigen van de voorgespannen liggers bij Megaton; Stijn Hertelé, voor de ondersteuning bij de DIC-metingen, Ann Lambrechts en Steven Pouillon van de firma Bekaert, voor het ter beschikking stellen van talloze kilo's staalvezels; Jos Costers, voor de optimalisatie van de verwerkbaarheid van verschillende mixen staalvezelbeton.

Ook alle collega's van het Labo Magnel verdienen een vermelding in mijn dankwoord: Tom en Nathan, voor het maken van beton en te helpen bij het vervaardigen van de aanvullende proefstukken bij de voorgespannen liggers; Peter Van Den Bussche, om ervoor te zorgen dat alle metingen correct werden uitgevoerd; Dieter, om eender welke proefopstelling voor mij in elkaar te steken; Stefan, voor het maken van bekistingen en mee te denken en te helpen bij de opbouw van mijn proeven op liggers; Marc, om alle proefstukken te verzagen; Peter Lampaert, voor het plakken van 1080 demec-puntjes en Tommy, om alles zorgvuldig in te plannen en waar nodig bij te springen.

I would also like to thank all of my colleagues who helped me with the large scale tests for the assistance during the manual measurements.

For all of the evenings in Ghent we partied until dawn, I would like to thank the legendary Magnel Party Crew. Those who believe to be part of it, have just been mentioned. During these nights out in Ghent, many things happened which should never be forgotten. They will always have a place in my heart.

Aan de mannen van de Fanny's wil ik ook een woord van dank richten voor de vele avonden op café om bij te praten over onze studietijd en het werk in "de bouw".

Ook op het thuisfront dienen een aantal mensen bedankt te worden. Daarbij wil ik alle vrienden van de Chiro van Sinaai bedanken om in het weekend af te spreken en bij pot en pint bij te praten over vroeger en nu. Hierdoor was het gemakkelijker om het hoofd eens vrij te maken van betononderzoek en met een frisse blik het onderzoek terug aan te kunnen vangen.

Ik wil ook dankjewel zeggen aan mijn mama en papa om mij van kinds af aan te begeleiden tot wie ik nu ben. Zonder jullie steun en liefde zou ik dit immers nooit bereikt hebben.

De mate waarin mijn vrouw Claudia bedankt dient te worden kan niet met woorden worden beschreven. Toch waren het net haar woorden van motivatie en liefde, die de afgelopen vier jaar de grootste bron zijn geweest om de moed niet op te geven en er steeds voor te blijven gaan. Bedankt!

Table of contents

List of abbreviations and symbols

Abbreviations

ACI	American Concrete Institute
ASTM	American Society for Testing and Materials
CEB	Comité Euro-International du Béton
CMOD	Crack Mouth Opening Displacement
CTOD	Crack Tip Opening Displacement
CoV	Coefficient of Variation
DAfStb	Deutscher Ausschuss für Stahlbeton
DICT	Digital Image Correlation Technique
EC2	Eurocode 2
EFNARC	European Federation of National Associations Representing producers and applicators of specialist building products for Concrete
EN	European Norms
FEM	Finite Element Model
fib	Fédération International du Béton – International Federation for Structural Concrete
FRC	Fibre Reinforced Concrete
JCI	Japan Concrete Institute
JSCE	Japan Society of Civil Engineers
LoA	Level of Approximation
LVDT	Linear Variable Displacement Transducer
MC2010	Model Code 2010
MC78	Model Code 1987
MC90	Model Code 1990
MCFT	Modified Compression Field Theory
NBN	Belgian Bureau for Standardisation
PC	Prestressed Concrete
RC	Reinforced Concrete
SFRC	Steel Fibre Reinforced Concrete
SLS	Serviceability Limit State
SVB	Staalvezelbeton
UNI	Ente Nazionale Italiano di Unificazione
ULS	Ultimate Limit State

Symbols

Roman letters

a	Shear span	mm
A	Empirical constant for the crack dilatancy behaviour	-
a_1	Shear span length at section 1	mm
a_2	Shear span length at section 2	mm
A_c	Cross sectional area of concrete	mm²
A_{ct}	Uncracked concrete section	mm²

A_{EXP}	Area beneath the experimental curve	Nm
A_f	Cross sectional area of fibre	mm²
a_g	Aggregate size	mm
A_{IA}	Area beneath the curve determined by means of inverse analysis	Nm
A_p	Cross sectional area of prestress steel	mm²
$A_{p,bot}$	Cross sectional area of prestress steel at the bottom of the section	mm²
$A_{p,top}$	Cross sectional area of prestress steel at the top of the section	mm²
A_s	Cross sectional area of mild reinforcement steel	mm²
B	Empirical constant for the crack dilatancy behaviour	-
b	Correction factor of the strength model	
b_f	Flange width	mm
b_i	Width of layer i	mm
b_i	Width of layer i	mm
B_n	Flexural thoughness up to a deflection equal to the span length ratio n	
b_w	Web width	mm
$C_{1,2}$	Empirical correlation factor	N/mm²
C_p	Empirical correlation factor for the effect of prestress on the shear strength of plain concrete	-
C_R	Correlation factor for shear of reinforced concrete without stirrups	-
d	Effective depth	mm
D	Deviatoric force	N
D_c	Secant stiffness matrix for concrete	
$D_{c,loc}$	Local secant stiffnes matrix for concrete	
d_f	Fibre diameter	mm
$D_{s,loc}$	Local reinforcement stiffness matrix	
D_{tot}	Total local secant stiffnes matrix	
E_c	Young’s modulus of concrete	N/mm²
E_{c1}	Secant stiffness modulus in tension	N/mm²
E_{c2}	Secant stiffness modulus in compression	N/mm²
E_p	Young’s modulus of prestressing steel	N/mm²
E_s	Young’s modulus of mild reinforcement steel	N/mm²
F	Fibre factor	
f_c	Average cylinder compressive strength	N/mm²
f_c^*	Effective concrete compressive strength	N/mm²
$f_{c,cub}$	Average cube compressive strength	N/mm²
$f_{c,max}$	Maximum cylinder compressive strength	N/mm²
$f_{c,min}$	Minimum cylinder compressive strength	N/mm²
f_{ck}	Characteristic cylinder concrete compression strength	N/mm²
f_{cm}	Cylinder compressive strength	N/mm²
f_{ct}	Concrete tensile strength	N/mm²
$f_{ct,fl}$	Flexural tensile strength	N/mm²
f_{ctk}	Characteristic concrete tensile strength	N/mm²
f_{ctm}	Average concrete tensile strength	N/mm²
f_{Ftu}	Ultimate post-cracking tensile strength of SFRC	N/mm²
f_{Ftuk}	Characteristic ultimate post-cracking tensile strength of SFRC	N/mm²
f_{Ftum}	Average ultimate post-cracking tensile strength of SFRC	N/mm²
f_{fy}	Fibre yield strength	N/mm²
f_i	Local normal force at layer i	N

f_{p0}	Initial stress in the prestress strands	N/mm²
F_{PO}	Pull-out force	N
$f_{R,1}$	Residual tensile stress at CMOD=0.5 mm	N/mm²
$f_{R,2}$	Residual tensile stress at CMOD=1.5 mm	N/mm²
$f_{R,3}$	Residual tensile stress at CMOD=2.5 mm	N/mm²
$f_{R,4}$	Residual tensile stress at CMOD=3.5 mm	N/mm²
$F_{R,i}$	Resiudal load at $CMOD_i$ (i=0.5-3.5 mm)	kN
$f_{Rk,i}$	Characteristic value of the residual tensile stress at $CMOD_i$	N/mm²
$f_{Rm,i}$	Average residual tensile stress at $CMOD_i$	N/mm²
f_{spf}	Splitting tensile strength of SFRC	
f_t^*	Effective concrete tensile strength	N/mm²
f_y	Yield strength of reinforcement	N/mm²
f_{yk}	Characteristic yield strength of reinforcement	N/mm²
f_{ym}	Average yield strength of reinforcement	N/mm²
g_k	Characteristic value of the self-weight	kN/m
h_{crit}	Height at shear-critical cross-section	mm
h_f	Flange heigth	mm
h_i	Height of layer i	mm
h_i	Height of layer i	mm
h_{sp}	Prism height above notch	mm
I	Second moment of inertia	mm^4
k	Size effect factor	-
k_{cp}	Influence factor for confining stress on the direct shear capacity	-
k_f	Influence factor for the effect of flanges on the shear capacity	-
k_v	Influence factor for the concrete shear strength	-
l	Span length	m
L_{emb}	Embedded length of fibre	mm
L_f	Fibre length	mm
L_{sp}	Spalling length	mm
M	Bending moment	kNm
M_{cr}	Cracking moment	kNm
M_f	Fibre weight	kg
M_{int}	Internal bending moment	kNm
$M_{Sd,mid}$	Design value of the bending moment at midspan	kNm
M_u	Ultimate bending moment	kNm
n	Span length ratio	-
N_{ext}	External normal force	kN
N_f	Number of fibres	-
N_{int}	Internal normal force	kN
n_{layer}	Number of layers	-
N_p	Number of prestress strands	-
$n_{sect1,i}$	Normal force at layer i for section 1	N
$n_{sect2,i}$	Normal force at layer i for section 2	N
P_0	Initial prestress force	kN
p_k	Characteristic value of the dead load	kN/m
Q	Point load	kN
q_k	Characteristic value of the variable load	kN/m
R	Relative error	-

s	Slip displacement	mm
S	First moment of inertia	mm³
$s_{m\theta}$	Average inclined crack spacing	mm
s_{sect}	Distance between two sections	mm
s_x	Horizontal crack spacing	mm
s_{xe}	Equivalent crack spacing in the longitudinal direction	mm
s_y	Vertical crack spacing	mm
T	Transformation matrix	
t	Time	days
t_0	Reference starting time	days
V	Shear load	kN
$V_{2.5,cal}$	Calculated shear strength at a crack opening equal to 2.5 mm	kN
$V_{2.5,exp}$	Experimentally obtained shear strength at a crack opening equal to 2.5 mm	kN
v_c	Reduction factor for the concrete compressive strength	kN
V_c	Shear strength capacity of concrete	kN
V_{cr}	Cracking shear strength	kN
V_f	Fibre content	kg/m³
$V_{f,exp}$	Experimentally determined fibre content	kg/m³
$V_{f,req}$	Required fibre content	kg/m³
V_{fibres}	Shear strength capacity of fibres	kN
v_i	Local shear force at layer i	N
$V_{max,cal}$	Calculated maximum shear strength	kN
$V_{max,exp}$	Experimental maximum shear strength	kN
V_{MODEL}	Shear strength capacity according to the considered MODEL	kN
V_R	Shear resistance	kN
V_{Rd}	Design value of shear resistance	kN
V_s	Shear strength capacity of reinforcement steel	kN
V_{Sd}	Shear design load	kN
$V_{Sd,crit}$	Design value of the shear load at the shear-critical section	kN
V_u	Ultimate shear strength	kN
w	Crack width	mm
w_0	Initial crack opening of the tri-linear post-cracking tensile law	mm
w_1	first crack opening of the tri-linear post-cracking tensile law	mm
w_2	second crack opening of the tri-linear post-cracking tensile law	mm
w_u	ultimate crack opening of the tri-linear post-cracking tensile law	mm
x	Horizontal projection length of the shear crack	mm
z	Internal lever arm	mm
z_i	Distance between the top of the cross-section and the center of layer i	mm

Greek letters

α_i	Pull-out direction	°
$\bar{\gamma}$	Cross-sectional average shear strain	-
$\bar{\varepsilon}$	Cross-sectional average longitudinal strain	-
α_f	Fibre inclination angle with respect to the longitudinal axis	°
β	Reliability index	°
β_f	Fibre inclination angle with respect to the vertical axis	°

γ_{xy}	Shear strain	-
Δ	Vertical pull-out displacement	mm
δ	Relative error of the strength model	-
Δ_f	Displacement of the fibre end	mm
ε_1	Principal tensile strain	-
ε_2	Principal compressive strain	-
$\varepsilon_{c,lim}$	Limit strain of concrete in compression	°
ε_{cr}	Crack strain	°
ε_{eq}	Equivalent strain in the fibre	-
ε_x	Longitudinal strain	-
ε_x	Longitudinal strain	-
ε_y	Transverse strain	-
ε_y	Transverse strain	-
ζ	Orientation of fibre in the xy-plane	°
η	Ratio of prestress losses	-
η_θ	Orientation number	-
θ	Inclination angle of compressive strut	°
θ_{cr}	Inclination of compressive strut at cracking	°
θ_f	Fibre inclination angle	°
θ_{f0}	Initial fibre inclination	°
θ_{fm}	Average fibre inclination	°
μ	Friction coefficient	-
ξ	Orientation of fibre in the yz-plane	°
ρ_f	Fibre reinforcement ratio	-
ρ_l	Longitudinal reinforcement ratio	-
ρ_w	Transverse reinforcement ratio	-
σ_1	Principal tensile stress	N/mm²
$\sigma_{1,res}$	Residual tensile stress	N/mm²
σ_2	Principal compressive stress	N/mm²
σ_{cp}	Concrete prestress at neutral axis	N/mm²
σ_{cx}	Compressive stress in the longitudinal direction	N/mm²
σ_{eq}	Equivalent stress in the fibre	-
σ_f	Post-cracking tensile strength of SFRC	N/mm²
$\sigma_{f,0}$	Post-cracking tensile strength of SFRC at crack opening w_0	N/mm²
$\sigma_{f,1}$	Post-cracking tensile strength of SFRC at crack opening w_1	N/mm²
$\sigma_{f,2}$	Post-cracking tensile strength of SFRC at crack opening w_2	N/mm²
$\sigma_{f,u}$	Post-cracking tensile strength of SFRC at crack opening $L_f/4$	N/mm²
σ_{px}	Tensile stress in prestress strands	N/mm²
σ_{sx}	Tensile stress in mild reinforcement	N/mm²
σ_x	Longitudinal stress	N/mm²
σ_y	Vertical stress	N/mm²
σ_θ	Standard deviation of fibre inclination	N/mm²
τ_{agg}	Shear stress capacity due to aggregate interlocking	N/mm²
τ_b	Bond shear stress of fibres	N/mm²
τ_{conf}	Shear stress capacity due to a confining stress	N/mm²
τ_f	Shear stress capacity due to fibres	N/mm²
$\tau_{max,cal}$	Maximum calculated shear stress	N/mm²
$\tau_{max,exp}$	Maximum experimental shear stress	N/mm²

τ_{SFRC}	Shear stress capacity of SFRC	N/mm^2
τ_{xy}	Shear stress	N/mm^2
χ	Curvature	-

Summary

In a way to improve the production process and to optimize the economics of precast concrete elements, it has been investigated to what extent fibres can be used as a replacement of traditional steel stirrups. By the use of Steel Fibre Reinforced Concrete (SFRC), the production time of prestressed girders can be decreased due to the elimination of labour-intensive placing of stirrups. However, current design standards do not provide any design equations for the shear capacity of (prestressed) SFRC elements and the majority of design engineers are not familiar with SFRC for shear resistance applications. During the past decade, a number of design guidelines have been published in Europe by RILEM and fib. In these pre-normative documents, different design approaches for the shear resistance of SFRC are provided. In this doctoral study the feasibility and accuracy of available design equations and a newly proposed engineering model, are investigated in view of implementation in the daily practice of a precast concrete company.

The research strategy adopted in this study can be summarized by the following steps:

(1) The post-cracking behaviour of SFRC has been studied (experimentally, numerically and analytically) at the material level in order to understand how fibres bridge a crack for different types of crack opening behaviour (i.e. mode I tensile crack width opening or mixed mode cracking combining crack opening and transverse crack dilatation).

(2) The shear behaviour of full-scale prestressed SFRC girders has been determined by means of 23 shear tests conducted on 9 different I-shaped and 2 IV-shaped girders.

(3) The observations from both the material testing and the full-scale shear tests have been combined to develop an analytical model which predicts the shear behaviour of the prestressed SFRC girders. In addition to this detailed model capable to describe the complete shear stress-crack propagation path, a more simple engineering model is proposed for the prediction of the shear capacity for design purpose.

(4) Shear resistance models have been evaluated by means of an assembled shear test database and inherent model uncertainties have been determined. By taking into account the model uncertainties, the safety levels of existing shear strength models have been reconsidered and suggestions for a practical design engineering model are proposed.

Research at the micro- and mesoscale level

For the design of SFRC structures, the most important parameter to be known is the post-cracking tensile strength. Currently, it is widely accepted to test the post-cracking behaviour of the adopted SFRC mix by means of (standardized) quality control or material characterization tests. Hereby, the mode I post-cracking tensile behaviour can be either derived directly from axial tensile tests, or indirectly from bending tests. Since the uni-axial tensile test is relatively hard to perform, from a practical point of view, the standard three-point bending test according to EN 14651 is more frequently applied. According to this

standard, the residual post-cracking bending tensile strength is evaluated as a function of the Crack Mouth Opening Displacement (CMOD).

Hence, though the best method to derive the post-cracking tensile constitutive law for SFRC is the uni-axial tensile test, due to the complexity of such direct test method, indirect methods are more often used to determine the flexural toughness of SFRC. Hereby, the measured flexural stresses have to be transformed to an equivalent axial stress to obtain the mode I post-cracking constitutive law. Furthermore, in order to derive a characteristic value of the residual flexural strength, a sufficient number of tests must be performed.

In this study, different methods have been verified to model the uni-axial and bending behaviour of hooked-end SFRC. Taking into account the available (semi-) analytical models for the pull-out behaviour of single fibres, an analytical model is developed to derive the mode I post-cracking constitutive law taking into account the fibre orientation and embedded length distribution, the fibre strength and the concrete strength. Further to this analytical model, a new method to implement the fibre pull-out behaviour into a 3D finite element model has been proposed. With this FEM model, the multiple cracking of SFRC prisms subjected to four-point bending can be modelled successfully. In due consideration of the observed mode I behaviour, a tri-linear constitutive law is proposed for the flexural toughness of SFRC, which is also able to represent the pseudo-hardening behaviour observed for SFRC containing low amounts of high-performance type of fibres.

Since the propagation of shear cracks will not be similar to a pure mode I crack opening, the effect of fibres crossing a shear crack plane has been investigated by means of direct shear tests. Hereby, a double notched SFRC prism is symmetrically subjected to two in-plane shear forces. The adopted test method is based on the push-through test setup initially proposed as the JSCE-SF6 test setup. In order to investigate the effect of lateral compression on the direct shear behaviour, the traditional unconfined test setup has been modified to apply a horizontal confinement perpendicular to the shear plane.

It is found that the maximum direct shear strength is linearly related to the fibre dosage and that the shear stress transfer capacity of SFRC increases further as a function of applied confining stress. This latter increase is related to the square root of lateral confining pressure. In this study, as an extension of the available direct shear strength models, a direct shear behaviour model is developed based on the involved shear friction phenomena such as crack propagation behaviour, fibre pull-out influence by the transverse pull-out and aggregate interlocking. This analytical model is able to predict the maximum shear friction capacity of cracked SFRC, as well as the post-cracking branch of the stress-slip curve.

Research at the macro-scale level

In total, 11 precast concrete girders have been manufactured by Megaton, part of the Willy Naessens Group, and 27 shear tests have been conducted in the Magnel Laboratory for Concrete Research. The main research variables are fibre content and shear span to depth ratio. Since the span of the girders is equal to 20 m or more, the shear test is conducted at both ends. Between each testing phase, the supports are moved in order to avoid the damaged zone of the previous tests. For four girders, a third test has been conducted to study the shear response of the girders when loaded further away from the prestressed girder end blocks. All tested girders failed in shear as intended, though some differences in the failure aspect details have been observed.

For all of the tested girders, special attention has been given towards the crack propagation of shear cracks in the thin web. This has been monitored by means of a grid of extensometers at one hand, and by means of a Digital Image Correlation Technique (DICT) at the other hand. Hence, the shear crack displacement behaviour of the shear critical area is continuously monitored as a function of the applied shear load. By comparing the applied shear load at a crack opening equal to 2.5 mm and at the maximum shear capacity of the girders, it has been found that fibres are more effective to limit the crack opening, than to increase largely the maximum shear strength. For the tests with a shear span to depth-ratio (a/d-ratio) equal to 3.0, the observed relationship between the increase of residual flexural stress (increase of nominal fibre dosage) with respect to the increase in shear capacity is more distinct, as for this a/d-ratio the influence of direct transfer of shear load to the support through an arching effect is less pronounced.

Based on the observations from the full-scale shear tests and the gained insights into the behaviour of SFRC on the material level, a sectional model has been developed taking into account the equilibrium and compatibility conditions analogously to the Modified Compression Field Theory (MCFT). The existing formulations have been adapted in order to introduce the SFRC constituent behaviour in agreement with the experimental observations on the macroscale as well as the material meso-scale.

The developed model is able to describe the post-cracking shear behaviour of full-scale prestressed SFRC girders. However, for lower values of residual flexural strength and for beams without any shear reinforcement, the difference between the modelled and experimentally observed maximum shear capacity is relatively large. For girders containing fibre dosages between 40 and 60 kg/m^3 and for the girders with traditional reinforcement, the sectional model output matches the experimental results relatively accurate. Generally speaking, the sectional model was observed to yield conservative results. This can be explained by keeping in mind that this model is a beam-like shear model, so that it is unable to take into account direct load transfer to the support and inherent arching action.

Given that the iterative calculation procedure of the MCFT approach is less desirable for straightforward design calculations in engineering practice, a new resistance model is proposed in this work. This proposed engineering model is based on the iterative MCFT shear capacity model given in the Model Code 2010, yet converting it in a closed-form solution through observed correlations with physical phenomena influencing the shear strength such as dowel action, shear span to depth ratio, size effect and level of prestress.

Shear design

In order to evaluate current design shear resistance models, a shear test database has been assembled based on shear test results available in literature. When selecting these test results, a sufficient amount of information has to be available on the post-cracking tensile stresses (e.g. f_R-values, compressive strength, prestress, etc.) to enter the database. After collecting shear test results available in literature, a selection of suitable results have been made and 99 test results have been retained, covering both reinforced and prestressed concrete members. Since the majority of results reported in literature corresponds with tests on members with relatively limited dimensions and without the presence of a prestressing force, the obtained shear test results from the full-scale prestressed girders are of great value to extend the database.

The considered models that have been verified with respect to the test database are those provided by RILEM, the Model Code 2010 (both the empirical model and the model based on the simplified MCFT) and a model based on the plasticity theory. Furthermore, the newly proposed engineering model has been included as well, in this verification of accuracy of the resistance models. The analysis has been done for the whole database and for subsets of reinforced and prestressed concrete girders only. It has been found that current design provisions will yield an acceptable design in case of reinforced concrete beams, but for most models a very conservative design is obtained for the case of prestressed girders. Improved model accuracy is obtained with the proposed engineering model.

Extending on the quantified accuracy of the resistance models, an assessment has been performed on using these models as design equations targeting for a safe design in terms of reliability index. This assessment resulted in calculated values of the model safety factor of each of the considered design formulations.

Based on these reconsidered safety factors, two design cases for SFRC roof girders have been conducted. Following, these IV-shaped roof girders have been manufactured and tested to verify the design procedure. For both roof girders, with an applied fibre dosage of 20 and 35 kg/m^3 respectively, it was found that the maximum obtained shear capacity was much higher than the design value of the shear resistance. Regarding the crack opening behaviour, a stable crack control has been observed up to shear failure.

For an economical application of steel fibres as shear reinforcement, high quality SFRC mixes should be executed in the precast production environment so that scatter on the post-cracking tensile response of the SFRC is kept within boundaries and hence more beneficial characteristic values of the fracture toughness of the SFRC mix are obtained for a given concrete type, fibre type and fibre dosage.

Samenvatting

Om het gebruik van voorgespannen beton door materiaaltechnologische innovaties economisch interessanter te maken, is in deze studie onderzocht in welke mate staalvezels kunnen gebruikt worden ter vervanging (deels of volledig) van traditionele beugelwapening. Door een bepaald aantal staalvezels tijdens het mix-proces aan het beton toe te voegen, wordt een deel van het productieproces van voorgespannen ligger gereduceerd door het vermijden van de arbeidsintensieve bewerkingen zoals het knippen, plooien en plaatsen van beugels. Echter zijn er tot op heden nog geen ontwerpmethoden voor voorgespannen liggers uit staalvezelbeton (SVB) beschikbaar in de berekeningsnormen en zijn de ontwerpingenieurs vaak niet vertrouwd met de eigenschappen en de werking van het composietmateriaal SVB. Gedurende de afgelopen 10 jaar zijn er door RILEM en fib een aantal ontwerprichtlijnen gepubliceerd die kunnen beschouwd worden als pre-normatief. Naast het experimenteel luik van dit onderzoeksproject, wordt ook gekeken naar de mogelijkheden van bestaande ontwerpmodellen om de dwarskrachtcapaciteit van voorgespannen SVB liggers te voorspellen (inclusief met oog op structurele veiligheid en kosten efficiëntie) en welke modellen geschikt zijn om toe te passen voor dagelijks gebruik in studiebureaus van prefab betonproducenten.

De hiertoe ondernomen onderzoeksstappen kunnen als volgt samengevat worden:

(1) Eerst is op niveau van de composietwerking (cf. micro- en mesoniveau) onderzocht hoe vezels bijdragen tot het scheuroverbruggend vermogen van SVB wanneer het scheurvlak enerzijds onderworpen wordt aan een uitsluitend axiale component en anderzijds waarbij het scheurvlak onderworpen wordt aan een hoofzakelijk transversale component.

(2) Op het macroniveau zijn in totaal 23 dwarskrachtproeven uitgevoerd op 9 liggers met ware grootte (20 m overspanning).

(3) De onderzoeksresultaten die verworven worden op zowel het materiaalniveau als op het structureel niveau zijn samengevoegd ter ontwikkeling van een model waarmee het gedrag van voorgespannen SVB liggers kan geanalyseerd en gesimuleerd worden.

(4) Verschillende beschikbare rekenmodellen voor de dwarskrachtcapaciteit van SVB elementen zijn afgetoetst aan de hand van een database met resultaten van relevante dwarskrachtproeven. Op basis van de berekende modelonzekerheden zijn de huidige veiligheidsmarges herbekeken en worden voorstellen gedaan voor een praktisch dwarskrachtontwerp met SVB.

Onderzoek op micro- en macroniveau

Bij het ontwerp van staalvezelbeton is het van onmisbaar belang de nascheurtreksterkte van het SVB te kennen. Tegenwoordig is het algemeen aanvaard dat de eigenschappen die in rekening gebracht worden bij ontwerp voor elk type van SVB afzonderlijk dienen geverifieerd te worden door proeven. De nascheurtreksterkte kan enerzijds bepaald worden door axiale trekproven (directe methode) en anderzijds via indirect wijze door middel van buigproeven op standaardprisma's. Aangezien de correcte uitvoering van axiale trekproeven vaak moeilijk uit te voeren valt, wordt er vaak gebruik gemaakt van de gestandaardiseerde drie-puntsbuigproef op gekerfde prisma's. Door middel van deze proef wordt het spanning-scheuropening diagram verkregen op basis waarvan door transformatieformules een constitutieve materiaalwet voor SVB wordt afgeleid. Verder dienen er ook een voldoende aantal proeven uitgevoerd te worden opdat de spreiding van de proefresultaten gekend is en een karakteristieke waarde van de ontwerpparameter kan bepaald worden.

In deze studie worden ter bepaling van de constitutieve materiaalwet van SVB na scheurvorming verschillende methoden ter modellering voorgesteld en geëvalueerd. Vertrekkende van bestaande (semi-)analytische modellen die het uittrekgedrag van gehaakte vezels beschrijven, is een analytisch model ontwikkeld om het Mode I nascheurgedrag van SVB te simuleren. Hierbij wordt rekening gehouden met het orientatieprofiel van de staalvezels, de ingebedde lengte, de sterkte van de vezel en de betonkwaliteit. Naast het analytisch model is er ook een manier voorgesteld om het nascheurgedrag van een vezel te implementeren in een eindige-elementenmodel. Aldus wordt een standaard buigproef driedimensionaal gemodelleerd en kan het buigingsgedrag met meervoudige scheurvorming gesimuleerd worden. Ten derde wordt op basis van een inverse analyse van buigproefresultaten een vereenvoudigd trilineair model voorgesteld dat kan gebruikt worden ter bepaling van het nascheurgedrag waarbij ook onderscheid kan gemaakt worden tussen pseudo-hardening gedrag, wat typisch is waargenomen bij SVB met lage gehaltes aan hoog-performante vezels in combinatie met een relatief hoge betonkwaliteit.

Aangezien, de scheurvorming bij dwarskracht niet identiek is aan een puur Mode I scheurpropagatie, wordt ook het effect onderzocht van staalvezels op het nascheurgedrag van SVB wanneer het onderworpen wordt aan directe afschuiving. Daartoe wordt een standaardprisma symmetrisch belast met een geconcentreerde afschuifbelasting. De aangewende proefmethode is gebaseerd op de door het JSCE ontwikkelde doorschuifproefmethode JSCE-SF6. Bovendien is deze proefmethode verder aangepast om het effect in acht te nemen van een zijdelingse drukkracht die horizontaal inwerkt loodrecht op het afschuifvlak.

Er is vastgesteld dat de afschuifsterkte lineair toeneemt in functie van het vezelgehalte. Verder kan de afschuifsterkte verder verhoogd worden door het toepassen van een zijdelings drukspanning, maar deze toename is gecorreleerd met de wortel van de toegepaste zijdelings spanning. In tegenstelling tot de beschikbare modellen voor de maximale afschuifsterkte, die voorgesteld zijn op basis van eerder verkregen proefresultaten, is er in dit onderzoek getracht een model te ontwikkelen dat kan gebruikt worden om het volledige schuifspanning-slip diagram te beschrijven. Daarbij kan in het model rekening gehouden worden met de belangrijkste invloedsparameters zoals de relatie tussen scheurwijdte en slip, de transversale vezelpull-out, en de haakweerstand van het ruwe afschuifvlak (aggregate interlocking). Naast de maximale waarde van de afschuifsterkte kan ook de residuele tak van het afschuifspanning-slipdiagram bepaald worden.

Onderzoek op macroniveau

In totaal zijn er door de firma Megaton, onderdeel van de groep Willy Naessens, 11 voorgespannen I-liggers geproduceerd waarop 27 dwarskrachtproeven uitgevoerd zijn in het Laboratorium Magnel voor Betononderzoek. Hierbij is voornamelijk de invloed van de vezeldosering en de a/d-verhouding nagegaan op de dwarskrachtsterkte nagegaan. De reproduceerbaarheid van de dwarskracht proefresultaten is nagegaan door dezelfde liggers meervoudig op dwarskracht te testen. Gezien de lengte van de balken gelijk is aan 20 m, worden voor alle liggers beide uiteinde beproefd, en zijn een aantal liggers een derde keer beproefd. Tussen elke dwarskrachtproef per balk, zijn de steunpunten verplaatst om geen ongewenste effecten te verkrijgen ten gevolge van de eerder gevormde dwarskrachtscheur.

Bij alle uitgevoerde dwarskrachtproeven is voornamelijk gekeken naar de scheurontwikkeling in de lijfplaat van de ligger. Dit is voor alle uitgevoerde proeven opgemeten door middel van een vast grid van extensometers en voor een groot deel van de proeven door middel van een DIC (Digital Image Correlation) techniek. Hierdoor was het mogelijk om de ontwikkeling van de dwarskrachtscheuren in functie van de opgelegde dwarskracht te monitoren voor de volledig dwarskrachtzone. Voor alle balken is een dwarskrachtbreuk waargenomen. Wanneer gekeken wordt naar de dwarskrachtsterkte voor een scheuropening gelijk aan 2.5 mm, kan geconcludeerd worden dat de toevoeging van vezels aan het beton voornamelijk effect heeft op het belemmeren van de scheurpropagatie, eerder dan op het sterk verhogen van de bezwijklast van de liggers. Voor de dwarskrachtproeven uitgevoerd met een verhouding a/d = 3 is, in vergelijking met a/d = 2.5, een meer uitgesproken stijgend verband waargenomen tussen de residuele buigtreksterkte en de bezwijklast.

Op basis van de waargenomen proefresultaten op liggers met ware grootte en de verworven inzichten met betrekking tot de scheuroverbruggende werking van vezels voor zowel een axiale als een transversale scheuropening, is een sectionaalmodel ontwikkeld dat steunt op de principes van de Modified Compression Field Theory (MCFT). Hiertoe zijn de bestaande materiaalwetten herbekeken om rekening te houden met de aanwezigheid van staalvezels in het beton en de waargenomen scheurpropagatie bij de dwarskrachtproeven op liggers.

Het ontwikkelde model kan gebruikt worden om het volledig niet-lineaire gedrag van de staalvezelbetonbalken te beschrijven. Voor liggers met vezelgehaltes lager dan 20 kg/m³ en voor balken zonder dwarskrachtwapening is het verschil tussen de gemodelleerde en experimenteel bepaalde dwarskrachtsterkte relatief groot. Bij hogere vezelgehaltes en bij liggers met traditionele wapening geeft het model betere benaderingen. Algemeen gezien, geeft het sectionaalmodel conservatieve resultaten. Inderdaad, rekening houdend met het feit dat het sectionaalmodel een balkmodel benadering is voor de dwarskrachtwerking, kan er geen rekening gehouden worden met de effecten van boogwerking.

Ontwerpmodellen

Om de bruikbaarheid van bestaande ontwerpmodellen na te gaan is een database van dwarskrachtresultaten samengesteld op basis van de beschikbare resultaten in de literatuur. Bij de selectie van deze resultaten dient er rekening mee gehouden te worden dat er voldoende informatie wordt gegeven met betrekking tot de eigenschappen van het staalvezelbeton (residuele buigtreksterkte, betondruksterkte, voorspanning, etc.). Na het verzamelen van alle resultaten van dwarskrachtproeven, en het toepassen van de selectiecriteria zijn er in totaal 76 testresultaten weerhouden om op te nemen in de database. Aangezien het merendeel van deze resultaten afkomstig zijn van proeven op relatief kleine balken zonder voorspanning, zijn de proefresultaten uit deze studie van zeer groot belang om de verscheidenheid van parameters in de database verder uit te breiden. Uiteindelijk is er een dataset bekomen waarbij 30 resultaten afkomstig zijn van proeven op voorgespannen liggers en 69 op gewapende balken.

De beschouwde modellen die afgetoetst zijn aan de samengestelde database zijn deze van RILEM, Model Code 2010 (twee verschillende methoden), de plasticiteitstheorie en een nieuw voorgesteld ingenieursmodel. De dwarskrachtcapaciteit van deze vijf modellen zijn vergeleken met de volledige dataset en verder voor de subsets van enkel voorgespannen of gewapende balken. Daarbij is tevens gekeken naar de invloed van de treksterkte van het beton (gerelateerd aan de betondruksterkte) en de nascheurtreksterkte in geval van SVB. Op basis van deze vergelijking is gevonden dat de traditionele modellen over het algemeen voor gewapende balken een goede inschatting maken van de dwarskrachtsterkte maar waarbij toch een relatief hoge modelonzekerheid dient in acht genomen te worden. Bij voorgespannen elementen wordt de dwarskrachtsterkte vaak sterk onderschat. Meer accurate voorspellingen worden bekomen met het voorgestelde ingenieursmodel.

Na de bepaling van de modelonzekerheden is voor elk rekenmodel de veiligheidsmarge herbekeken, op basis waarvan twee rekenvoorbeelden voor het dwarskrachtontwerp zijn uitgevoerd voor dakliggers met veranderlijke hoogte. Beide liggers, ontworpen met een vezelgehalte van respectievelijk 20 en 35 kg/m², zijn vervolgens onderworpen aan een dwarskrachtproef. Hierbij is gevonden dat de maximale dwarskrachtcapaciteit veel hoger is dan de ontwerpwaarde en dat na scheurvorming de vezels voor een stabiele scheurpropagatie zorgen. Als aandachtspunt dient hierbij opgemerkt te worden dat het noodzakelijk is om een goede kwaliteitswaarborging toe te passen in het productieproces, om op die manier het benodigd aantal vezels voor een vooropgestelde karakteristieke residuele buigtreksterkte economisch optimaal te houden.

1 INTRODUCTION

1.1 General

During the last 50 years, the use of precast concrete for construction has experienced a strong growth [1]. Not only the quality of the concrete elements is enhanced by means of the controlled production environment, but also the construction time can be reduced strongly. Precast concrete girders are, due to their typically larger spans, designed to resist high bending moments and in a way to improve the effectiveness and economical use of concrete for the precast industry, cross-sections are generally reduced which results in the development of T, double-T and I-shaped cross-sections. For roof girders, a variable height is applied in order to reduce the self-weight and to provide automatically a slope. Hence, an optimal economic design of precast girders is a challenge for further innovation.

However, due to the limited web thickness, slender beams become more sensitive for other failure mechanisms such as buckling, torsion and shear. As a result, special attention is needed for the resistance of precast members against these actions.

1.2 Problem statement

In the current design codes a distinction is made between the shear resistance of zones with or without bending cracks present in the Serviceability Limit State (SLS) [2]. In the case of prestressing however, bending cracks are not likely to occur in the SLS and the effect of prestress has to be taken into account to evaluate the design shear crack load. When the design shear load is lower than the design shear crack load, the shear forces are taken by the concrete and the prestress action. However, a minimum amount of transverse reinforcement has to be placed in order to provide sufficient ductility when reaching the Ultimate Limit State (ULS). If the design shear crack load is lower than the design shear load, the concrete contribution shall be neglected and the shear capacity of the girder shall be provided by transverse rebars only. As a result, the application of current design procedures for shear [2, 3] will automatically lead to the placement of either minimum or calculated amounts of transverse reinforcement.

In order to find a way to further improve the economics of precast concrete elements, solutions are sought to reduce both material and labour costs within the manufacturing process. Since the placing of traditional stirrups are labour-intensive, several alternatives to omit (partially or completely) traditional stirrups as shear reinforcement have been investigated in the past.

One of the most promising techniques widely investigated, is the use of steel fibres in reinforced concrete. Fibres can be easily added to the concrete during the mixing process and provide significant increase of toughness and ductility after cracking. If fibres can provide sufficient post-cracking strength to the concrete, the use of traditional stirrups can be reduced or replaced and the precast production process speed will be increased and labour costs can be reduced significantly. Hereby, the decrease of labour costs should balance at least the increase in material costs due to the use of high quality materials such as fibres and high strength concrete.

Although the use of fibres as shear reinforcement has been proven to be feasible under laboratory conditions by the scientific community [4-9], real life structural applications are rather limited. Only one example of the application of steel fibres as shear reinforcement in practice is known to the author: for a warehouse built in 2005 in Dortmund, 22 m span ceiling girders were manufactured of Steel Fibre Reinforced Concrete (SFRC) to resist shear forces [10]. The lack of practical case studies can be attributed to an insufficient material knowledge by design engineers and the absence of internationally accepted design guidelines. In order to increase the overall acceptance of this new technique within the daily practice of design engineers, the transfer of knowledge acquired through research should be facilitated. In this respect, the experimental investigation of the shear capacity of full-scale prestressed girders is fairly unique, when compared to shear test data available in literature.

A first step in the development of a unified approach to the shear design of SFRC was proposed by the RILEM committee TC-TDF 162 in 2002 [11] . More recently, the Model Code 2010 [12] provides two design procedures that can be used for the shear design of SFRC elements. Nevertheless, it has not yet been proven or investigated whether these procedures yield economical solutions or safe designs in the case of prefabricated prestressed concrete girders.

In short, the following problem statement is addressed in this study: although shear design of SFRC members is recently implemented in design guidelines, no evidence is yet available on the feasibility of these models towards the design of full-scale precast concrete girders when replacing traditional stirrups by SFRC.

1.3 Aim of the thesis and research objectives

It is the aim of this study to verify experimentally to what extent steel fibres can be used to either reduce or replace traditional stirrups as shear reinforcement in full-scale precast concrete girders and to evaluate existing or to propose new shear design procedures which can be adopted in the daily practice of design engineers. In order to reach this, research will be done on different sub-domains or scale levels, and the following research objectives are defined:

At micro- and mesoscale level:

Since the enhanced post-cracking toughness of SFRC is mainly attributed to the pull-out behaviour of both straight and deformed fibres, a first research objective is defined on the micro- and mesoscale level. To better understand the post-cracking behaviour of SFRC in bending and direct shear, it is the objective to establish an analytical relationship between the single fibre pull-out behaviour and the composite behaviour at mesoscale level (e.g. tests on standard prisms), both for the case of predicting the tensile response and the direct shear response.

At macroscale level:

On the macro scale level, the shear behaviour of full-scale prestressed SFRC will be experimentally investigated. In this part of the research, it is the objective to evaluate the effectiveness of steel fibres used as shear reinforcement and to enlarge the existing set of experimental data available in literature. Special focus will be given to the shear crack opening behaviour as a function of applied shear load.

At engineering level:

At engineering level, it is the objective to develop an analytical model for the prediction of the shear behaviour and shear resistance of full-scale SFRC girders. This is done by making use of the experimental test results and findings at micro-, meso- and macrolevel. A second objective at engineering level is the evaluation of resistance models in terms of a safe design (i.e. corresponding with a target reliability index), and their further application in a design example of SFRC roof girders, which are finally tested up to failure to confirm the design methodology

1.4 Outline of the thesis

Following this first chapter, in which the scope and objectives of the doctoral study are given, in Chapter 2, a state of the art overview with respect to the mechanical properties of SFRC subjected to axial and shear loading is provided at the mesoscale or material level.

An overview of relevant literature concerning shear behaviour and the use of fibres as shear reinforcement, is given in Chapter 3. In this overview, special attention is given to shear design equations for reinforced or prestressed concrete beams without stirrups and with steel fibres as the only shear reinforcement.

Chapter 4 provides all research results obtained on the material level of SFRC in which further distinction is made between pull-out behaviour and composite behaviour. Based on the experimental observations at meso-scale and available semi-analytical models for the pull-out behaviour of hooked-end fibres, different modelling techniques (numerical and analytical) are developed and evaluated to analyse the post cracking behaviour in both mode I (opening) and mixed mode (shear friction) loading conditions.

Concerning the experimental work done at the macroscale level, research results are described in Chapter 5 for the 23 full-scale shear tests performed on prestressed I-shaped girders. In total, 9 girders were manufactured in a precast concrete plant and tested in laboratory conditions. Additional to the strain and deflection measurements of the girders as a function of the applied shear load, the shear behaviour of the prestressed girders is also investigated in terms of the crack propagation behaviour of the critical shear cracks in the thin web. This is done by means of a Digital Image Correlation Technique.

In Chapter 6, a method to model the shear behaviour of the full-scale prestressed SFRC girders is proposed. This model is implemented in a sectional analysis software tool, based on the theoretical principals of the Modified Compression Field Theory (MCFT), which is updated with the constitutive material models of SFRC. A verification of this analytical model is performed on the basis of the experimental data from Chapter 5.

A shear test database is assembled in Chapter 7 and used to evaluate the accuracy of different shear resistance models. As an extent to the existing state of the art, a simplified design model is proposed based on the experimental observations of Chapter 5 and behaviour models from Chapter 6. Furthermore in Chapter 7, an evaluation is performed of the design safety factors when applying these shear resistance models for design purpose and aiming for a target reliability index.

As a case study given in Chapter 8, the design procedure is applied on two different girders with variable height. These girders are also produced and tested up to failure. Hereby, general observations are made towards the implementation of fibres in both the production and design stage of prestressed SFRC girders.

Finally, general conclusions are drawn and suggestions are made for further research in Chapter 9.

1.5 References

[1] fib. (2004). "Bulletin No. 29 - Precast Concrete Bridges". Lausanne, Switzerland.

[2] CEN. (2004). "EN1992-1-1:2004 - Eurocode 2: Design of concrete structures - Part 1-1: General rules and rules for buildings". Brussels, Belgium.

[3] Collins, M. P., Kuchma, D. (1999). "How safe are our large, lightly reinforced concrete beams, slabs and footings". *ACI Structural Journal*, Vol. 96(4), pp. 482-490.

[4] De Pauw, P., Taerwe, L., Van den Buverie, N., Moerman, W. (2008). "Steel fibre concrete as an alternative for traditional shear reinforcement in pretensioned concrete beams". *7th international RILEM symposium on fibre reinforced concrete: design and applications (BEFIB 2008)*, pp. 887-898.

[5] Minelli, F. (2005). "*Plain and Fibre Reinforced Concrete Beams under Shear Loading: Structural Behaviour and Design Aspects*" (PhD-thesis). Brescia, University of Brescia.

[6] Narayanan, R., Darwish, I. Y. S. (1987). "Shear in prestressed concrete beams containing steel fibres". *The International Journal of Cement Composites and Lightweight Concrete*, Vol. 9(2), pp. 81-90.

[7] Voo, Y. L., Foster, S. J. (2008). "Shear strength of steel fiber reinforced ultra-high performance concrete beams without stirrups". *5th international Specialty Conference on Fibre Reinforced Materials*, pp. 177-184.

[8] Cuenca, E., Serna, P. (2013). "Shear behavior of prestressed precast beams made of self-compacting fiber reinforced concrete". *Construction and Building Materials*, Vol. 45(August 2013), pp. 145–156.

[9] Gustafsson, J., Noghabai, K. (1999). "Steel fibers as shear reinforcement in high strength concrete beams". *International Journal of Nordic Concrete Research*, Vol. 22, pp. 1-18.

[10] Krampe Harex. (2015). http://www.krampeharex.com, 09/02/2015.

[11] RILEM. (2003). "Final Recommendation of RILEM TC 162-TDF: Test and design methods for steel fibre reinforced concrete sigma-epsilon-design method". *Materials and Structures*, Vol. 36(262), pp. 560-567.

[12] fib. (2010). "Model Code for Concrete Structures 2010". Lausanne, Switzerland, fédération internationale du béton.

2 LITERATURE REVIEW ON SFRC

2.1 Steel Fibre Reinforced Concrete

2.1.1 Historical background

More than 4500 years ago, in the ancient cultures of Mesopotamia and Egypt, natural fibres were used to strengthen sun-dried mud or clay bricks. These fibres, e.g. straw or flax fibres, were used to prevent the sun-dried bricks from crumbling during transportation or manipulation [1]. Other examples of the early use of composites in human history can be found in Roman culture around 500-400 BC. The Romans used lime-mortars and concrete made of 'puzzalano trass' strengthened with horse- and goat hair.

Although the use of concrete was widespread around that time, together with the fall of the Roman Empire, the use of natural cements for concrete construction disappeared completely. It was waiting until the discovery and development of the modern Portland cement in the early 19th century by Joseph and William Aspdin, for concrete to become more popular again and being applied as a construction material [2]. However, engineers recognized the major deficiency of the concrete to have low tensile strength capacity and its brittle nature.

Around that time, the French engineer Joseph-Louis Lambot experimented with wire reinforcement which led to the use of ferrocement. Later in 1868, Joseph Monier was granted a patent for the invention of a new system of reinforcement which led to the development of reinforced concrete as known today. The use of continuous steel bars to bridge cracks in a concrete section led evidently to the popularity of reinforced concrete as an economical construction material.

However, instead of placing steel wires or bars into concrete in order to sustain tensile stresses after cracking, the idea of using fibres as a homogenous type of reinforcement to increase the tensile strength of concrete was challenging many researchers at that time. The first inventions which led to the development of modern fibre reinforced concrete were made in the late 19th century. The first was made by Ludwig Hatschek, who produced thin sheets made of 90 % cement-paste and 10% asbestos fibres. Since then, the use of asbestos fibres began to spread worldwide and was used for the production of both internal- and external cladding and roofing materials [3]. Another invention was made by A. Berard, who filed his patent in 1874 for the production of concrete with dispersed steel grains of waste materials [4]. Around 1910, the use of nails, wire segments and metal chips were mentioned in experimental test reports and patents [3]. Around 1940, glass fibres were first used in construction in Russia.

Although several attempts were made to improve the tensile capacity of concrete during the early 20th century, serious scientific work in the field of fibre reinforced concrete started in the 1960’s. Initially, it was believed that fibres could enhance the tensile strength of the concrete. First serious attempts to investigate the composite behaviour were done by Romualdi & Batson [5] and Romualdi & Mandel [6]. Based on linear fracture mechanics, they found that the toughness of Fibre Reinforced Concrete (FRC) is related to the square root of fibre spacing. However, no significant benefits could be addressed to the use of fibre reinforcement at that time.

During the 1970’s, due to improved testing equipment and analysis procedures, the concepts of energy absorption and fracture toughness were further introduced. The benefits of fibres towards the improved post-cracking stress-strain relationship of FRC were first reported by Shah and Rangan [7]. They observed that the most significant effect of fibres was derived after cracking of the matrix, enhancing the fracture toughness instead of the concrete tensile strength (see Fig. 2.1, left). From their experimental work, it was concluded that the post-cracking toughness of FRC was mostly influenced by the fibre length, orientation and stress-strain relationship. In 1972, Naaman [8, 9] studied the behaviour of FRC containing straight smooth steel fibres used in relatively high dosages. This can be seen as a key point in history towards the development and analysis of modern types of FRC.

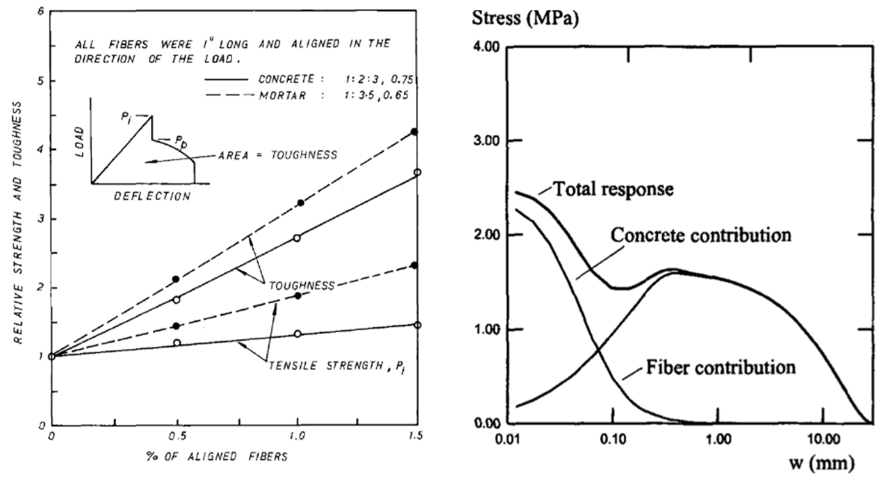

Fig. 2.1 – Influence of fibres on the increase of tensile strength and post-cracking toughness (from Shah and Rangan [7]) and concept of fibre bridging (from RILEM [10])

The experimental results of Shah and Rangan (Fig. 2.1, left) evidence the enhancement of post-cracking toughness rather than the increase of tensile strength of the concrete matrix. In the right graph of Fig. 2.1, the total post-cracking response of SFRC is schematically visualised as the summation of a concrete and fibre contribution. This graph shows that the fibres are mainly contributing to the tensile behaviour of the composite for higher values of the crack opening. A typical view of fibres bridging a crack is shown in Fig. 2.2.

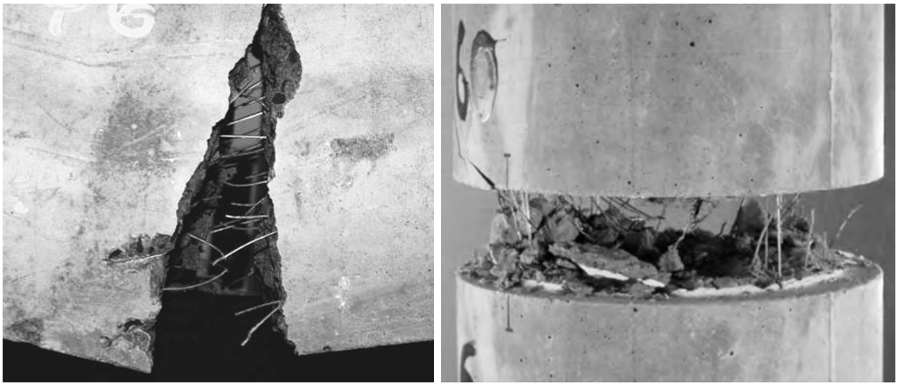

Fig. 2.2 – Bending (left) and axial (right) tensile failure planes of SFRC

2.1.2 Steel fibre types

The first types of steel fibre reinforced concrete were made by using high dosages of short straight fibres [1, 3]. However, it was found that for relatively high dosages, the increase of post-cracking tensile strength was rather limited. As a consequence, different types of fibres have been developed with a wide range of shape, length, diameter and wire strength. An overview of various possible shapes of modern types of fibres is given in Fig. 2.3. In Table 2.1, the range of variation of different material properties are summarized.

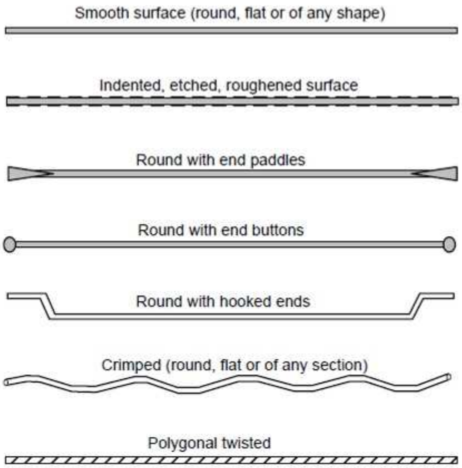

Fig. 2.3 – Different types of fibres and their particular shape (from Naaman [11])

Table 2.1 – Typical range of steel fibre properties

Property	Range
Tensile strength [N/mm²]	1000-3000
Ultimate strain [-]	1-5 %
Fibre length L_f [mm]	10-60
Fibre diameter d_f [mm]	0.2-1
Aspect ratio (L_f/d_f)	20-100

One of the most popular types of deformed fibres is the hooked-end fibre which provides high post-cracking ductility due to plastic deformation of the hook during pull-out. For fibre types with increased anchorage capacity, a loss of ductility is observed by either failure of the concrete matrix or by fibre rupture. The first failing mechanism is more likely to occur for a combination of a low-strength matrix and high strength fibre, while the second brittle failure mechanism is caused by the combination of high strength concrete with a relatively low fibre tensile strength. The anchorage capacity of a single fibre has been studied in the past by means of pull-out testing for both aligned and inclined configurations. A more detailed description of the pull-out process of hooked-end fibres is given in Section 2.2.

2.1.3 SFRC in the fresh state

Both the workability and the final performance of concrete with steel fibres can be adversely affected, if the effect of addition of fibres to the concrete is not properly taken into account. During the mixing of SFRC, fibres are either added and mixed first together with the dry components or added to the fresh concrete afterwards. A too fast addition rate of fibres can cause fibres sticking together and forming a fibre ball. Most common is a dry fibre ball which is formed by tangling of loose fibres and covering of this tangled fibres with a layer of concrete. Inside the ball, only fibres and dry sand is present. In general, balling and clustering of fibres, due to a bad dispersion, will cause undesirable cavities and an overall loss of performance. To overcome the fibre balling, a suitable fibre integration method should be adopted. This can be done by decreasing the fibre addition rate of loose fibres or by using glued fibres which will induce the release of fibres in the concrete when the glue is dissolved by the mixing water. Wet balling can occur when the mixing time is too long, when the grading of the concrete is not optimized and if the aggregate size is too large for the used type of fibre. The risk of balling generally increases for higher fibre lengths and inherent aspect ratio.

When fibres are added to concrete, special attention should be addressed to the concrete mix composition. In general, for increasing fibre content, the workability of the SFRC decreases [12] and in order to overcome workability issues, the concrete grading has to be optimized with respect to the adopted type of fibre and dosage. This can be done by increasing the mortar fraction and the use of water reducing agents. In order to avoid workability issues for SFRC mixes containing very high volumes of fibres (> 1.5%), self-compacting concrete types are often used. Since the orientation of fibres can be influenced by the concrete flow during filling of the formwork, attention should be paid towards the possibility of undesirable orientation of fibres with respect to the main cracking pattern expected. The influence of fibre dosage on the slump (flow) and consistency were experimentally investigated by Markovich [12]. In Fig. 2.4, the effect of the fibre factor (i.e. fibre volume fraction multiplied with the ratio between fibre length and diameter) on the slump flow of self-compacting concrete has been shown for a SFRC containing only short (13 mm) and both short and long (60 mm) fibres.

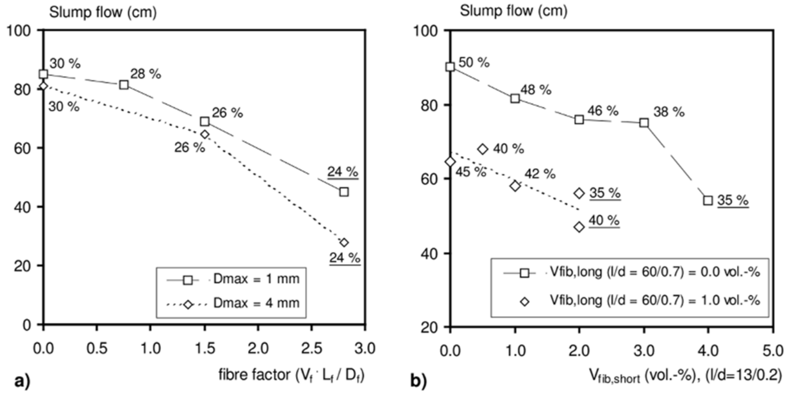

Fig. 2.4 – Influence of fibre dosage on the workability of SFRC [12]

Further it should be noted that adding fibres can increase the air-content and have a negative effect on the porosity of the concrete. Due to the presence of fibres, the packing density of the concrete matrix is affected and, if the concrete matrix design is not optimized, it can eventually lead to a decrease of overall performance. Moreover, for increasing air-content, the bond strength of fibres will decrease due to the presence of air-bubbles at the fibre/matrix interface. For normal concrete, the air-content will be around 1.5-2.0 of Vol-%. However, when fibres are included, the air-content may increase to around 5%. The effect of fibres on the packing density is schematically shown in Fig. 2.5.

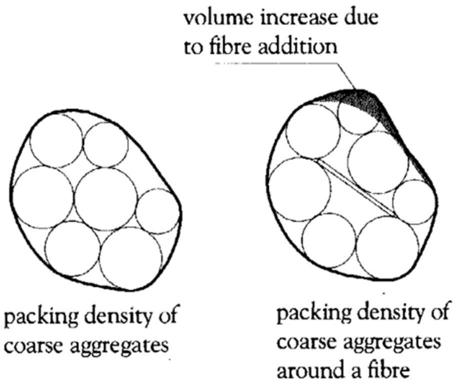

Fig. 2.5 – Schematic visualisation of the effect of fibre addition on the packing density of concrete (from Bartos and Hoy [13])

2.2 Pull-out behaviour of hooked-end fibres

2.2.1 General principles

Since the post-cracking tensile strength capacity of SFRC is inherent to the anchorage of fibres in the matrix, understanding the mechanisms of fibre pull-out of both straight and deformed fibres have been thoroughly investigated in the past. For the case of hooked-end fibres, the entire pull-out mechanism can be divided in two main parts: a debonding phase and a mechanical deformation phase (i.e. the actual pull-out). A schematic of the pull-out response of a hooked-end fibre is shown in Fig. 2.6.

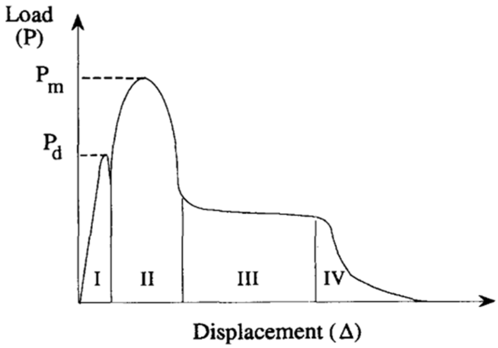

Fig. 2.6 – Schematic of the pull-out response of hooked-end fibres [14]

During the debonding phase, shear stresses along the fibre-matrix interface provide pull-out resistance. For the case of aligned straight fibres, the debonding load P_d (Fig. 2.6, Zone I) will lead to a completely debonded fibre/matrix interface and will lead to the pull-out failure. For the particular case of single or double hooked-end fibres, the existence of additional curved segments at the fibre ends provides a mechanical anchorage contribution equal to P_m-P_d (Fig. 2.6, Zone II) which is much larger than the resistance provided by the bond shear stresses only. When the fibre debonds, an increase of the pull-out resistance is caused by the coulomb friction effects along the curved length of the fibre as well as the plastic deformation due to bending of the deformed hooks [15, 16].

When the fibre is completely debonded along its embedded length, the maximum pull-out force has been reached. From this point, any further slipping of the fibre through the pull-out channel will cause a gradual decrease of pull-out resistance. In a first stage of the pull-out phase, the hooked-ends are straightened representing the drop in the pull-out curve, after reaching the maximum pull-out load P_m. After passing the last inflection point, the hook is roughly straightened, providing an almost constant residual pull-out strength (Fig. 2.6, Zone III), until the embedded length becomes too short and no pull-out forces can be transferred anymore and a complete decay of pull-out force is observed (Fig. 2.6, Zone IV).

For the case of crimped fibres, fibres with conical or paddled ends (cf. Fig. 2.3) and fibres with more than two bended segments at the fibre ends, the pull-out forces will become very high due to an almost perfect anchorage of the hook. This implies that there is no significant slipping phase when the fibre has no ductility. Hence, the crack bridging ability of fibres for higher crack-width has to be provided by a plastic elongation of the debonded fibre length. As a result, pull-out failure will occur either by loss of anchorage due to failure of the concrete matrix or by excessive plastic deformation of the fibre.

2.2.2 Influencing parameters

2.2.2.1 Fibre dimension and relative strength

The main parameters influencing the pull-out behaviour of hooked-end fibres are the embedded length, tensile strength and diameter of the fibre and the concrete compressive strength. Van Gysel [16] studied the effect of these parameters on the pull-out response of hooked-end fibres with a length of 60 mm and different fibre diameters of 0.50 and 0.80 mm for both low and high carbon content steel fibres mixed in a low and high strength concrete matrix. Typical average pull-out curves are compared in Fig. 2.7.

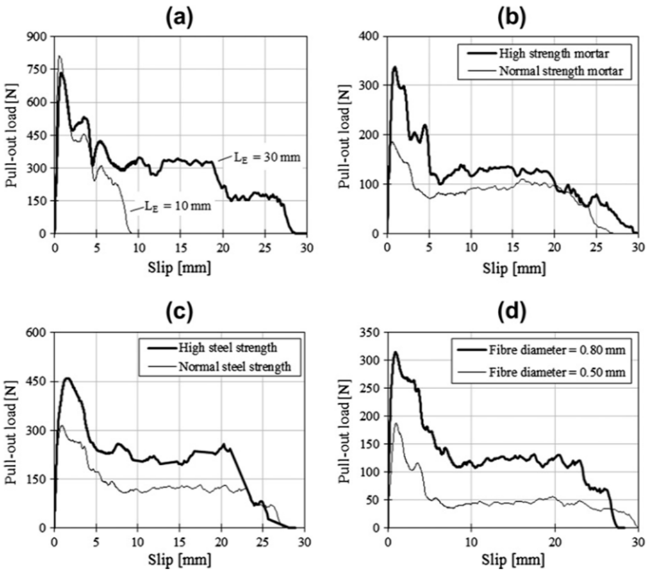

Fig. 2.7 – Influence of embedded length (a), concrete compressive strength (b), fibre tensile strength (c) and diameter (d) on the pull-out response of a hooked-end fibre (from Soetens et al. [17])

From Fig. 2.7, it can be seen that the influence of embedded length has a negligible effect on the debonding phase of the pull-out process. However, since the fibre can only be pulled out over its embedded length, the residual stresses can only be transferred until a maximum slip equal to the embedded length. Considering crack widths up to 2 to 3 mm as the ultimate limit state of crack opening, the embedded length is a parameter of minor importance in case of single fibre pull-out.

For both an increase of fibre tensile strength and concrete compressive strength, a constant increase of pull-forces over the entire slipping range has been observed. For higher concrete strengths, the bonding mechanism between the fibre and the matrix is stronger and for a higher steel strength, the deformation of the hooked-end requires more energy.

A logical increase of pull-out force has been observed for higher fibre diameter since the stresses in the fibre will be more or less constant. Further, it was found by Van Gysel that the residual pull-out strength is influenced by the fibre diameter, concrete compressive strength and fibre yield strength. An empirical formulation for the residual capacity of the hook after being rectified by pulling it through the mortar channel, has been proposed as follows:

$$F_{h,res} = \frac{1}{325} f_c f_y d_f^2 \qquad \text{Eq. 2.1}$$

Whereby, f_c is the compressive strength, f_y is the yield strength of the fibre and d_f is the fibre diameter.

2.2.2.2 Fibre inclination

Since fibres are randomly dispersed in the concrete matrix, all fibres crossing the crack plane will be pulled out for a given inclination angle. The influence of fibre inclination on the pull-out response has been investigated by several researchers [16-19]. Robins et al. [18] performed pull-out tests on hooked-end fibres embedded at different inclination angles. The average pull-out curves for each inclination are shown in Fig. 2.8.

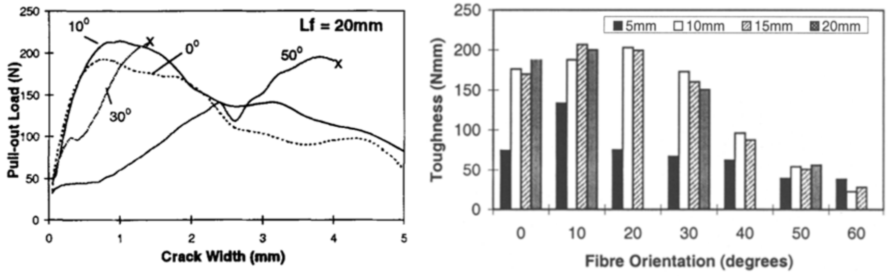

Fig. 2.8 – Influence of fibre inclination on the pull-out response [18]

As can be seen form Fig. 2.8 (left), the inclination of fibres will lead to an increase of fibre pull-out resistance. This increase is caused by the additional frictional effects and mechanical anchorage due to bending of the fibre at the crack surface. Due to local stress concentrations at the fibre exit point, the concrete at the fibre exit point will be damaged causing the fibre to be able to undergo an extra rotating displacement. This phenomenon will lead to higher crack openings when reaching the maximum pull-out load. For higher values of the inclination angle, the coulomb friction at the fibre exit point will become large enough to change between ductile pull-out failure to a more brittle fibre rupture failure and a decrease of toughness (Fig. 2.8, right).

2.2.2.3 Mutual fibre interaction

When the embedded length of fibres is relatively small, the occurrence of matrix rupture or splitting is possible. Further, when fibres are spaced closely (i.e. for high fibre dosages), the chance of fibres damaging the anchorage zone and influencing the embedded conditions of nearby positioned fibre is possible. In Fig. 2.9, an idealized situation of three fibres in one plane is shown and for which the second fibre is influencing the nearby positioned fibre (i.e. fibre 3).

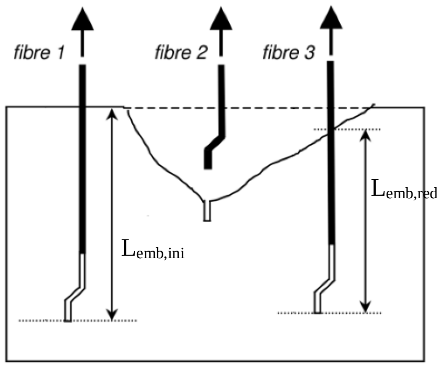

Fig. 2.9 – Fibre interaction due to a splitting failure of the surround matrix (from Markovich [12])

From Fig. 2.9, it can be seen that due to the anchorage failure of fibre 2, a concrete cone is being removed. Since the volume of this irregular cone also contains a part of fibre 3, the embedded length of fibre 3 shall be decreased suddenly and consequently, a lower fibre pull-out capacity for fibre 3 will be observed. When the post-cracking tensile capacity is analysed as the summation of the pull-out forces of all fibres, the mutual fibre interaction will decrease the post-cracking capacity of the SFRC composite. Since the damaging of the anchorage zone will be more pronounced for higher fibre dosages, a non-proportional increase of the post-cracking tensile strength of SFRC with respect to the total amount of fibres crossing the crack plane can be observed. A comparison between the effective amount of fibres actually being pull-out and the total amount of fibres crossing the crack is shown in Fig. 2.10.

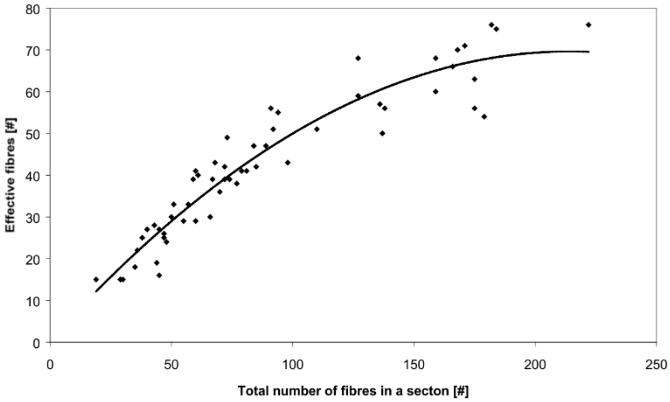

Fig. 2.10 – Comparison between effective fibres versus total fibres crossing the crack plane (from Dupont [20])

2.2.3 Pull-out models

The basis for pull-out models of deformed fibres is the analytical description of the debonding of the straight part. Based on pull-out tests on straight fibres, different models are proposed by Stang [21, 22], Grey [23-25], Naaman & Namur [26] and Wang et al. [27], to predict the pull-out frictional stress decay as a function of pull-out distance. The pull-out model of a straight fibre, as proposed by Wang [27] is given in Fig. 2.11. The load on the fibre increases linearly, until reaching a maximum bond capacity. After this, the load drops to the frictional shear strength of the fibre which further decays with increasing pull-out distance. This decreasing pull-out force is modelled as linear, and relates to the increasing damage of the fibre-matrix interface.

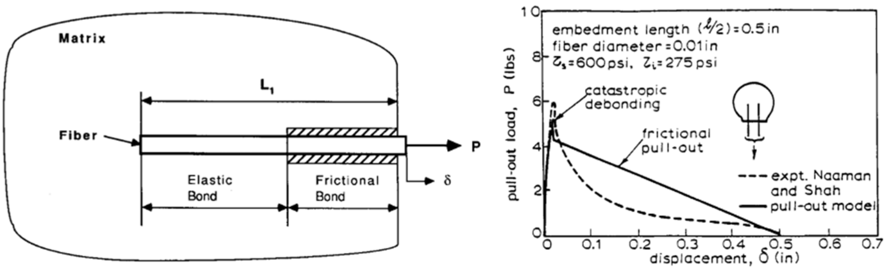

Fig. 2.11 – Modelling concept of fibre debonding according to Wang [27].

With respect to deformed fibres, the most important contribution to the pull-out modelling has been done by Chanvillard [15], by proposing a method based on the principals of virtual work to calculate the pull-out response. This model was later optimized, based on the experimental results from about 120 pull-out tests by Van Gysel [16].

In the semi-analytical pull-out model developed by Van Gysel [17], the debonding of the straight part is taken into account by the implementation of the shear lag model for which the mathematical description has been proposed by Stang [21]. Furthermore, the model takes into account several parameters such as fibre inclination, fibre shape, tensile strength, embedded length and concrete compressive strength. A comparison between modelled and experimental pull-out curves is shown in Fig. 2.12. Detailed information about the model with a calculation example can be found in [17].

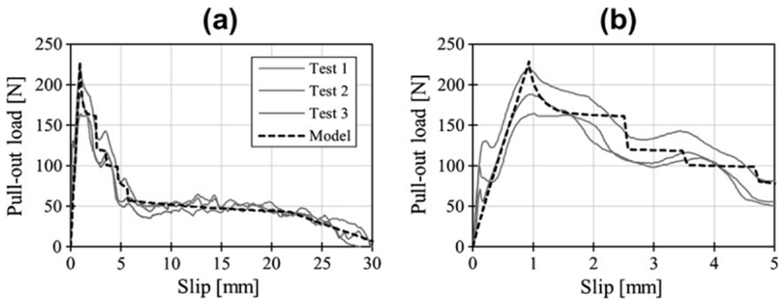

Fig. 2.12 – Comparison between experimental and modelled pull-out curves by Van Gysel et al. [16] for a normal strength concrete: a) complete curve and b) detail for a slip between 0-5 mm

A simplified empirical approach has been developed by Alwan et al. [28]. The pull-out load slip curve is defined by four key-points corresponding to the pull-out load P_{1-4} and inherent slip Δ_{1-4}. Similarly, another model has been proposed by Laranjeira [19]. The schematic representations of the pull-out curve of both models are shown in Fig. 2.13.

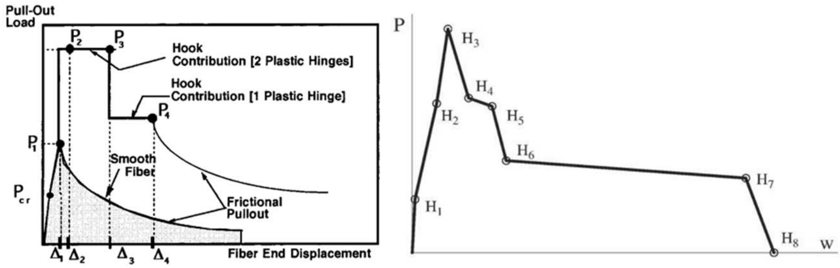

Fig. 2.13 – Schematic representation of the pull-out process according to Alwan [28] (left) and Laranjeira [19] (right)

Regarding the shape of the modelled pull-out curve shown in Fig. 2.13 (right), the pull-out behaviour is mainly defined by eight distinct points. According to Laranjeira, these points (H_{1-8}) are related to the specific pull-out situations as shown in Fig. 2.14.

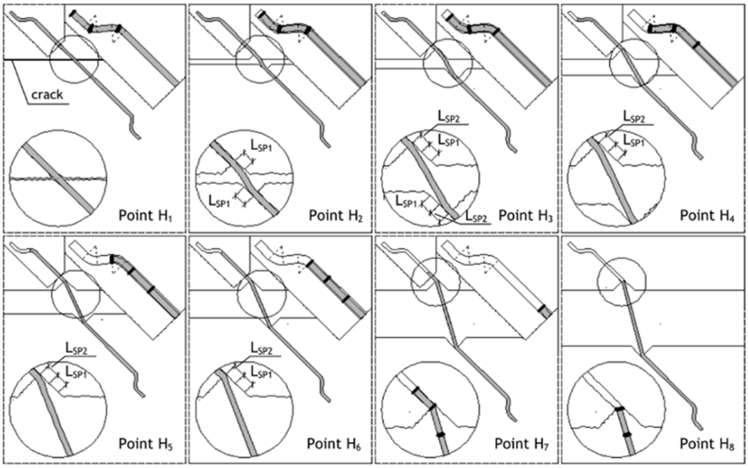

Fig. 2.14 – Different stages defining the pull-out curve

The spalling lengths L_{SP1} and L_{SP2} are determined iteratively as a function of fibre inclination, pull-out force and coulomb friction coefficient between fibre and matrix. The first spalling length is denoted as L_{SP1}, while L_{SP2} is the additional length of spalling due to progressive fibre pull-out and related deformation at the fibre exit point. In contrast to the spalling criterion adopted by Van Gysel, whereby a compressive failure is assumed (contact pressure induced concrete wedge failure), the model as proposed by Laranjeira, takes into account the fibre inclination by means of a spalling criterion based on the tensile capacity of a concrete wedge being pushed off.

2.3 Post-cracking behaviour

2.3.1 Crack propagation

When a plain concrete element is subjected to internal or external loadings, it will either fail in tension or in compression from the moment the principal stresses reach the tensile or compressive strength, or a combination of both (i.e. biaxial stress state). For both the initiation and propagation of a tensile failure, there are in general three different crack propagation modes (see Fig. 2.15), defined as opening (Mode I), sliding (Mode II) and tearing (Mode III).

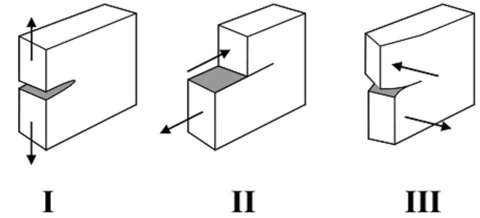

Fig. 2.15 – Different failure modes

Mode I is one of the most common crack propagation modes, since it occurs in uniaxial, splitting and bending tensile failure. For Mode II it should be noted that in plane shear stresses will generally not only cause crack sliding but also crack opening. The latter is due to the irregularity of the crack plane. This results in crack dilatation and is further referred to as a mixed mode crack opening (i.e. Mode I and II). Out of plane shear or tearing (Mode III) is rare in reinforced concrete analysis, for which often a plane stress state can be assumed.

A schematic of pure Mode I and a mixed mode opening displacement for a crack in SFRC is shown in Fig. 2.16.

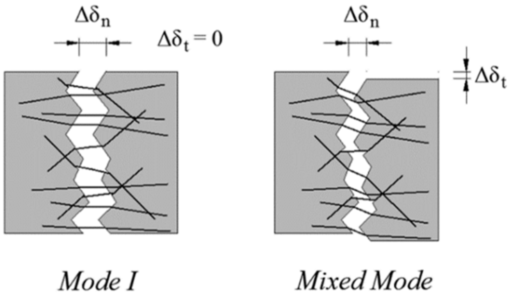

Fig. 2.16 – Schematic representation of a pure Mode I crack opening (left) and a mixed mode crack opening displacement (right)

Given the two different types of crack propagation, the crack bridging mechanism will be substantially different. For a pure mode I crack opening behaviour the only resistance of further crack opening is provided by the anchorage of fibres in between the two crack faces. Hence, by superposition of the individual pull-out response of all fibres crossing the crack, the post-cracking stress capacity of SFRC in Mode I can be described.

For the mixed mode crack propagation, the contribution of fibre pull-out has to be decomposed in an axial and transverse component (i.e. dowel action at micro scale level). Furthermore, the additional friction between the two rough crack interfaces will lead to an increase of shear stresses needed to further enlarge the normal ($\Delta\delta_n$) and tangential ($\Delta\delta_t$) crack displacements.

2.3.2 Tensile behaviour

2.3.2.1 General

In the early stages of the developments and research in the field of fibre reinforce concrete, it was the aim to increase the tensile strength of plain concrete and similar to other composites, the rule of mixtures was adopted to describe the material properties of the new cementitious composite. Today, it is generally acknowledged that the use of steel fibres only affects the post-cracking behaviour of concrete instead of the tensile strength of the concrete itself. This post-cracking response, determining the performance of steel fibre reinforced concrete, has to be measured by means of material testing, whereby uni-axial or bending tests are adopted in order to derive post-cracking parameters needed for design.

Most commonly, the Mode I (i.e. pure opening, Fig. 2.16 left) post-cracking constitutive law of SFRC is obtained from experimental bending tests. In order to compare test results and to derive design strengths parameters, these bending tests are included in (inter)national standards. In Sections 2.3.2.2 and 2.3.2.3, the most frequently used tests are described and the relationship between the results obtained from different test methods are discussed.

2.3.2.2 Uni-axial tension test

Although it can be stated that the best way of determining the post-cracking response of SFRC is directly done by means of uni-axial testing, no standard method is available yet. In general, uni-axial tests are difficult to perform and specialised test equipment and experienced personnel is needed. Dog-bone shaped test specimens and notched specimens with round or square cross-sections are the most used types of test specimen. Examples of the most frequently used test setups are shown in Fig. 2.17.

The main difficulty of the uni-axial test is the positioning of the specimen in order to apply a uniform tensile stress on the crack plane. In reality, the tensile load will be applied with a certain eccentricity and undesired bending moments will cause stress concentrations at the crack surface.

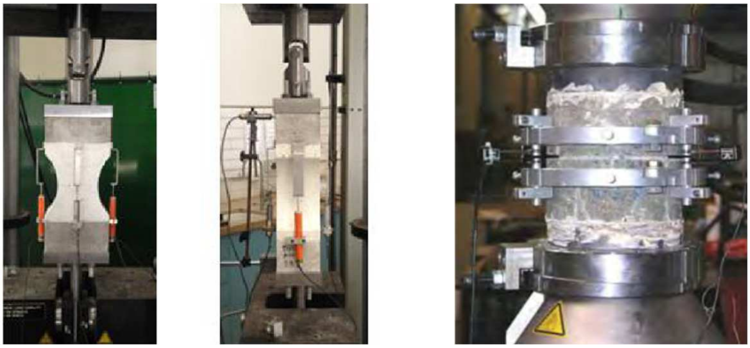

Fig. 2.17 – Different uni-axial tensile test setups: dog-bone [29] (left and middle) and notched cylindrical specimens (right) [4]

From the uni-axial tensile test, the Mode I relationship between tensile stress and crack opening is measured directly. A typical example of derived stress-crack opening curves is shown in Fig. 2.19. These results are obtained by Laranjeira [30] for a normal strength SFRC containing fibres with a length of 60 mm, a diameter of 0.75 mm and fibre dosages between 20-60 kg/m³.

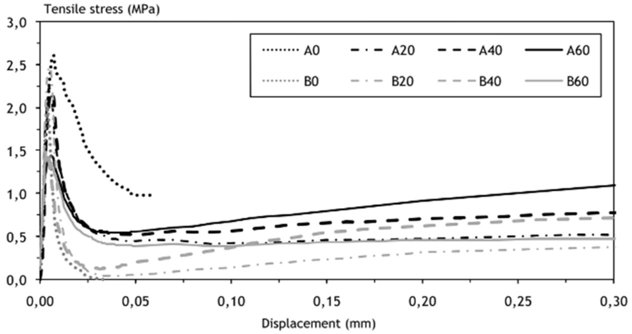

Fig. 2.18 – Post-cracking tensile response obtained from uni-axial testing (initial response at cracking, range till 0.3 mm)

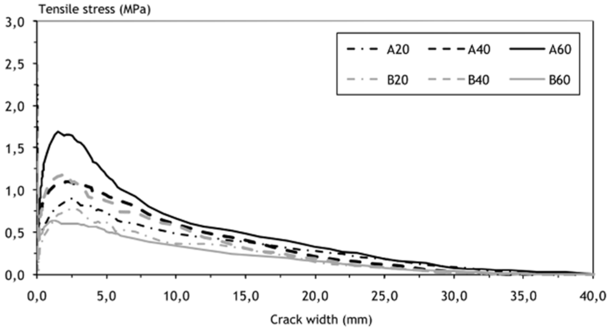

Fig. 2.19 – Post-cracking tensile response obtained from uni-axial testing until complete fibre pull-out

2.3.2.3 Bending tests

In order to avoid the difficulties inherent to the direct tensile test methods, the post-cracking behaviour of SFRC is generally determined by more feasible bending tests. In literature, different types of test setups and specimens can be found and a variety of bending test standards have been published over the last 30 years. An overview of the most frequently used bending tests and their corresponding parameters used to indicate the SFRC post-cracking toughness is given in the following.

<u>*ASTM C 1018 (1984)*</u>

In 1984, the American standard ASTM C 1018 was first adopted for the determination of toughness relative to the toughness up to first cracking. This toughness is defined as the area up to a specified deflection δ expressed as a multiple of the deflection measured at first cracking. By dividing this toughness by the toughness at first cracking, a toughness index I_a is determined. After a revision of this standard in 1989, additional residual strength factors were defined as the average strength retained at a certain deflection as a percentage of the first cracking strength (see Fig. 2.20).

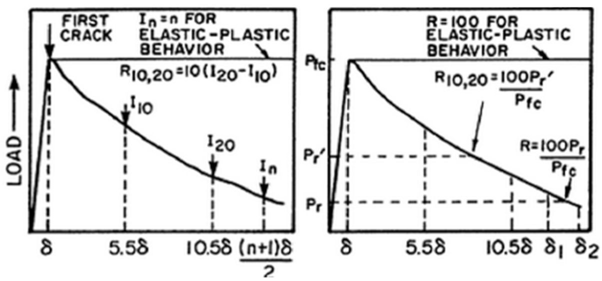

Fig. 2.20 – Toughness indices and residual strength parameters determined by means of ASTM C 1018

The load-deflection curves as shown in Fig. 2.20 are obtained by means of four-point bending test (often referred to as a third-point bending test because at each third of the span length, a point-load is applied) conducted on prisms with a standard size of 153 mm x153 mm x 533 mm (i.e. 6 in x 6 in x 21 in). After withdrawal of this test method in 2006, current SFRC post-cracking properties are derived by a four point bending test according to ASTM C 1609. Hereby, from the obtained load-deflection curve, the residual flexural strength at a deflection equal to L/600 and L/150 are determined (Fig. 2.21) by means of Eq. 2.2

$$f_n = \frac{T_n}{HB^2}\frac{L}{n} \qquad \text{Eq. 2.2}$$

In which n is equal to 150 or 600 and T_n is the area under the load-deflection curve until a deflection of L/n. H and B are the height and width of the cross-section.

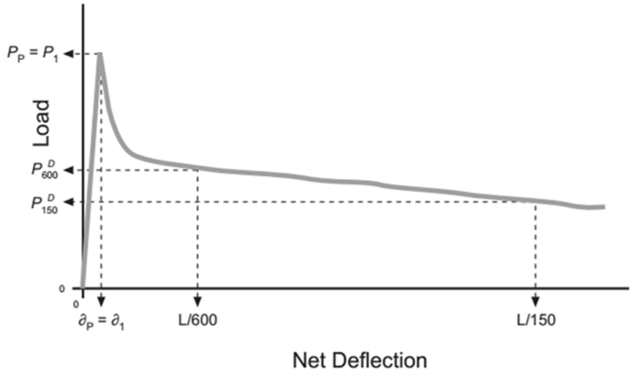

Fig. 2.21 – Toughness indices and residual strength parameters determined by means of ASTM C 1609

<u>*JCI-SF4 (1984)*</u>

Also in 1984, the Japan Concrete Institute proposed to determine toughness of SFRC by means of a four point bending test. Similar to the test method described in the ASTM C 1018 (and ASTM C 1609) the toughness T_b is evaluated as the area under the load deflection point up to a deflection of the span length divided by 150. Further, an equivalent flexural strength σ_b is determined by converting the toughness by using elastic bending formula.

$$\sigma_b = \frac{T_b}{HB^2}\frac{L}{\delta} \qquad \text{Eq. 2.3}$$

with H and B, the height and width of the cross-section. The ratio of L and δ is equal to 150.

<u>*NBN B15-238 (1992)*</u>

In the Belgian standard NBN B15-238, the load versus midspan deflection is measured by means of a four-point bending test using 150 mm x 150 mm x 600 mm standard prisms with a span length of 450 mm. The flexural toughness B_n is evaluated at a deflection of 1.5 mm and 3 mm, corresponding to the span length ratios L/300 and L/150 respectively (n = 300 or 150). The equivalent flexural strength is defined as the flexural toughness averaged over the prescribed deflection distance.

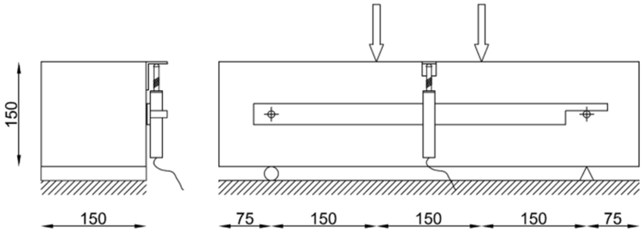

Fig. 2.22 - Four-point bending test setup

$$f_{f,n} = \frac{B_n n}{BH^2} \qquad \text{Eq. 2.4}$$

For n equal to 150, the equivalent flexural strength is the same as determined by using the JSCE-SF4 method.

<u>*DBV (2003)*</u>

According to the German guidelines for steel fibre reinforced concrete, the flexural parameters are obtained by means of four point bending tests conducted on 150 mm x 150 mm x 700 mm. Based on the load deflection curve, the residual flexural stresses at a deflection of 0.5 and 3.5 mm are determined to evaluate the post-cracking performance of SFRC and to define the performance classes as defined by the magnitude of both $f_{cfl,L1}$ and $f_{cfl,L2}$ [31].

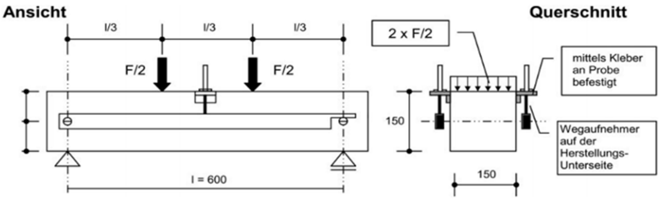

Fig. 2.23 - Four-point bending test setup according to DAfStb Richtlinie Stahlfaserbeton [31]

At a deflection of 0.5 and 3.5 mm, the following residual flexural stresses are determined:

$$f_{cfl,Li} = \frac{F_i L}{BH^2} \qquad \text{Eq. 2.5}$$

In which F_i is the load at a deflection of 0.5 and 3.5 mm. The first value ($f_{cfl,L1}$) represents the post-cracking flexural strength at the Serviceability Limit State (SLS) while for a deflection of 3.5 mm ($f_{cfl,L2}$) the Ultimate Limit State (ULS) is considered.

<u>*UNI 11039-2 (2003)*</u>

On the basis of the Italian standards UNI 11039-2, the toughness evaluation of SFRC is determined by means of four point bending tests performed on 150 mm x 150 mm x 600 mm specimens. The specimens have a central notch with a height a_0 of 45 mm (Fig. 2.24). During testing, the applied load is monitored as a function of Crack Tip Opening Displacement (CTOD).

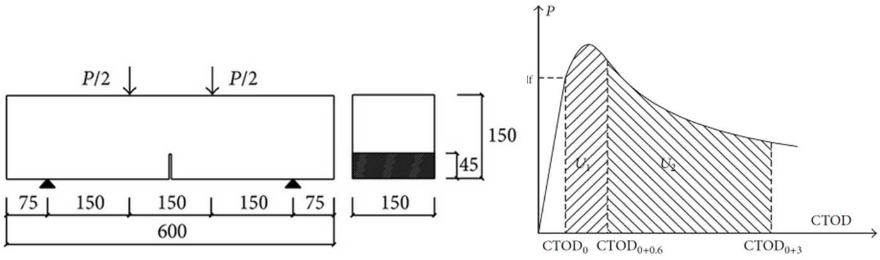

Fig. 2.24 – Schematic test setup and load-CTOD curve according to UNI 11039-2

The post-cracking performance of SFRC is expressed in terms of an equivalent flexural stress calculated by using the following equations.

$$f_{eq(0-0.6mm)} = \frac{U_1 L}{0.6B(H-a_0)^2} \qquad \text{Eq. 2.6}$$

$$f_{eq(0.6-3mm)} = \frac{U_2 L}{2.4B(H-a_0)^2} \qquad \text{Eq. 2.7}$$

In which U_1 and U_2 denote the absorbed energies (grey hatched areas under the load-CTOD curve as shown in Fig. 2.24) within the ranges of 0-0.6 mm and 0.6-3 mm.

<u>*RILEM TC 162-TDF (2003) & EN 14651 (2005)*</u>

The standard test method as given in the European standard EN 14651 is similar to the method described in the final recommendations of the RILEM technical committee TC 162-TDF which was first published in 2003. According to this recommendation, the residual flexural strength of SFRC is obtained by means of a three-point bending test on a notched prism (a_0 = 25 mm) with standard size of 150 mm x 150 mm x 600 mm and with a span length L equal to 500 mm. The applied load is monitored as a function of Crack Mouth Opening Displacement (CMOD). A schematic of both the test setup and a typical load-CMOD curve are shown in Fig. 2.25 and Fig. 2.26.

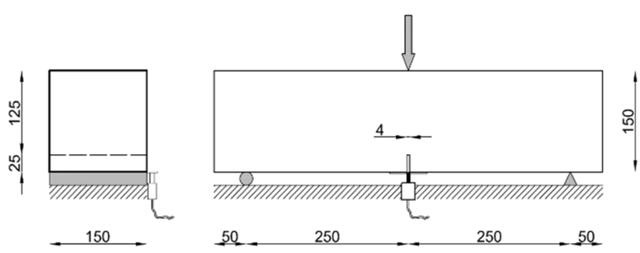

Fig. 2.25 - Three-point bending test setup with notch

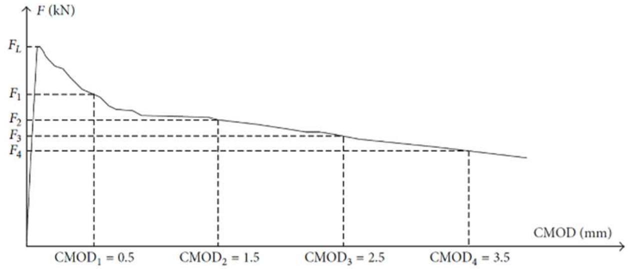

Fig. 2.26 – Load-CMOD curve according to EN 14651

Based on the load-CMOD curve, residual stresses are calculated by using Eq. 2.8 at CMOD values equal to 0.5 (i=1), 1.5 (i=2), 2.5 (i=3) and 3.5 mm (i=4), respectively.

$$f_{R,i} = \frac{3}{2}\frac{F_i L}{B(H-a_0)^2} \qquad \text{Eq. 2.8}$$

Additional to the residual strength, an equivalent flexural stress is defined by RILEM TC 162-TDF. Hereby, the area under the load-deflection curve is considered as shown in Fig. 2.27.

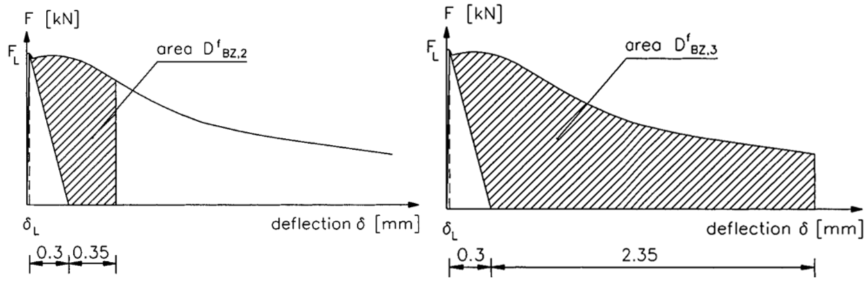

Fig. 2.27 – Load-deflection curves with the definition of energy absorption capacity (grey-hatched zones) for a deflection range of 0.35 mm (left) and 2.35 mm (right)

The equivalent stresses are given by

$$f_{eq,2} = \frac{3}{2}\left(\frac{D^f_{BZ,2}}{0.50}\right)\frac{L}{B(H-a_0)^2} \qquad \text{Eq. 2.9}$$

$$f_{eq,3} = \frac{3}{2}\left(\frac{D^f_{BZ,3}}{2.50}\right)\frac{L}{B(H-a_0)^2} \qquad \text{Eq. 2.10}$$

Round panel test (ASTM C 1550)

From the experimental work of Bernard [32], it was found that the reproducibility of test results was better for round panel tests than for bending tests on standard prisms. The methodology has been adopted in ASTM C1550, using standard panels with a thickness of

75 mm and a diameter of 800 mm and centrally loaded while vertically supported on three points positioned at 120° degrees from each other. The deflection is measured at the centre of the panel. A schematic of the test setup is shown in Fig. 2.28.

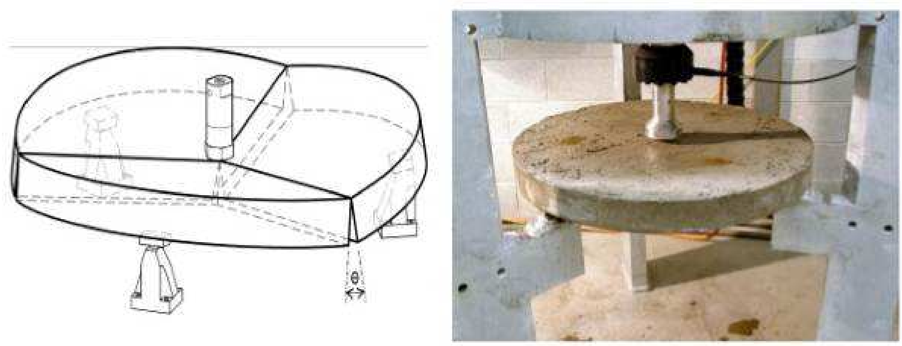

Fig. 2.28 – Schematic of the round panel test method according to ASTM C 1550

<u>*Square panel test (EN 14488-5)*</u>

Alternative to the ASTM round panel test, a square panel test method was developed by the European Federation of National Associations Representing producers and applicators of specialist building products for Concrete (EFNARC) [33] for determining the flexural toughness of sprayed SFRC applied for tunnel linings. This test method was later transformed into EN 14488-5. The square panel has a side length of 600 mm and a thickness of 100 mm. The load is applied centrally on a square of 100 mm x 100 mm and the panel is linearly supported on a square with dimensions equal to 500 mm x 500 mm. A schematic of the test setup is shown in Fig. 2.29.

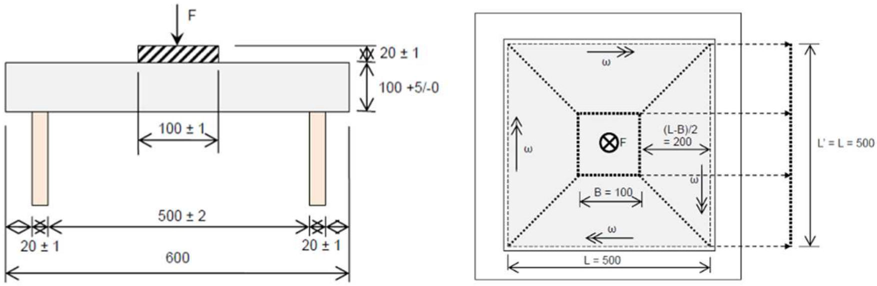

Fig. 2.29 – Schematic of the square panel test method according to EN 14488-5

2.3.2.4 Correlation between test methods

As discussed in Section 2.3.2.3, for the evaluation of the flexural toughness of SFRC a wide range of possible test methods is available. The choice of which test is used will depend on the purpose of using the obtained parameters. For example: the EN 14651 will be used when the Model Code 2010 design formulations are used to determine the bending or shear design capacities. Further, the ease of handling and testing of specimens can be important: casting of specimens and performing panel tests is more elaborate compared to the four-point bending test setup. For a standard test on a notched beam, the position and dimension of the notch have to be treated with great care.

Given the number of different test methods, a comparison of performance between SFRC mixes is difficult. For SFRC prisms tested according to the Belgian standard NBN B15-238 [34], the equivalent flexural strength can be converted into the residual strength defined in EN 14651 [35]. In Fig. 2.30, the correlation between residual stresses $f_{R,1}$ and $f_{R,4}$ and equivalent flexural stresses $f_{eq,2}$ and $f_{eq,3}$ are shown for SFRC mixes containing hooked-end fibres with a length of 60 mm and a diameter of 0.75

Minelli et al. [36] determined empirical correlations between the flexural parameters as derived by means of EN 1465, UNI 11039 and the ASTM round panel test method. The adopted SFRC mixes contained 20 and 30 kg/m³ of hooked-end normal strength (1100 N/mm²) cold drawn wire fibres with a length of 50 mm and a diameter of 1 mm.

Other correlations have been established between three-point bending, four-point bending and different panel tests with varying specimen size, e.g. by Minelli & Plizzari [36]. It was concluded that the correlation between different values of toughness and ductility performance parameters determined by either large or small round panel tests and the standard bending test on small prisms are strongly correlated (see Fig. 2.31)

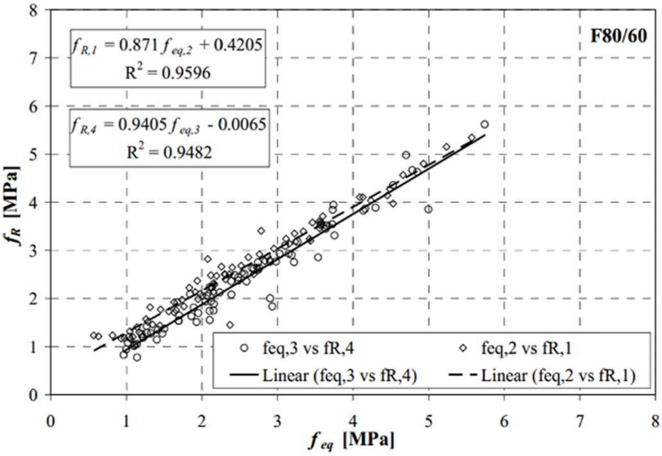

Fig. 2.30 – Correlation between equivalent and residual flexural stresses obtained from RILEM standard prism tests (from Barros et al. [35])

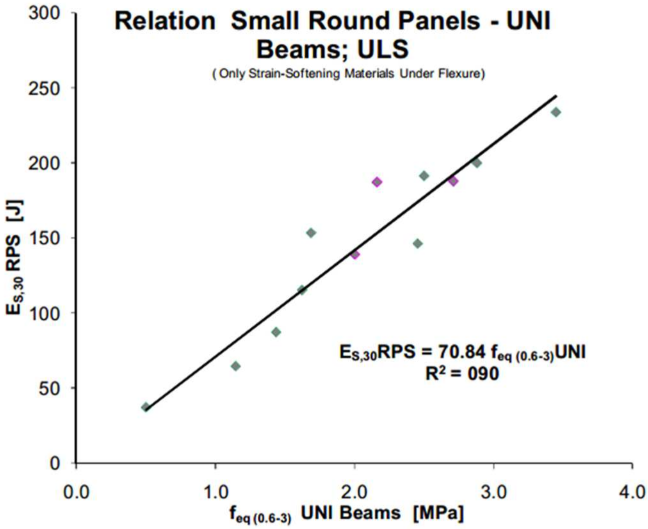

Fig. 2.31 – Correlation between round panel tests and Italian standard bending test (from Minelli et al. [36])

2.3.3 Scatter of post-cracking tensile behaviour

One of the most important issues related to the determination of post-cracking strength parameters of SFRC is the obtained scatter of test results [37-39]. This scatter is mainly attributed to

- Variation in mix homogeneity
- Orientation and embedded length distribution of fibres in a crack plane
- Magnitude of the crack plane area
- Concrete strength and fibre dosage variations

The homogeneity of a SFRC mix is influenced by the mixing procedure and rheological properties of the concrete. In order to obtain a good distribution of the fibres within the concrete matrix, the stability of the concrete mix in terms of segregation sensitivity is of concern. Furthermore, an appropriate mixing time should be respected in order to distribute the fibres into the concrete. A bad dispersion of fibres into the concrete mix will directly lead to an unequal distribution of the amount of the fibres in specimens cast form the same batch. For a discussion on mix design aspects, reference is made to section 2.1.3.

Even when a SFRC concrete mix is sufficiently homogeneous, the observed scatter of test results can be addressed to the localisation of fibres in the crack plane, the fibre distribution and embedded length. For the case of self-compacting concrete, the flow of the concrete will influence the alignment of the fibres with respect to the casting direction and can influence the magnitude of the post-cracking residual parameters measured on prisms and due to the influence on fibre orientation, in some cases a reduction of the scatter of test results has been observed [40, 41].

However, the flow of concrete can also have a detrimental effect on the post-cracking strength of SFRC. In the research conducted by Abrishambaf [42], the influence of the general fibre orientation with respect to the crack plane has been investigated by performing uni-axial tensile tests on specimens drilled from a slab. Fig. 2.32 shows the difference between the test results for specimens with a notch perpendicular and parallel to the flow direction.

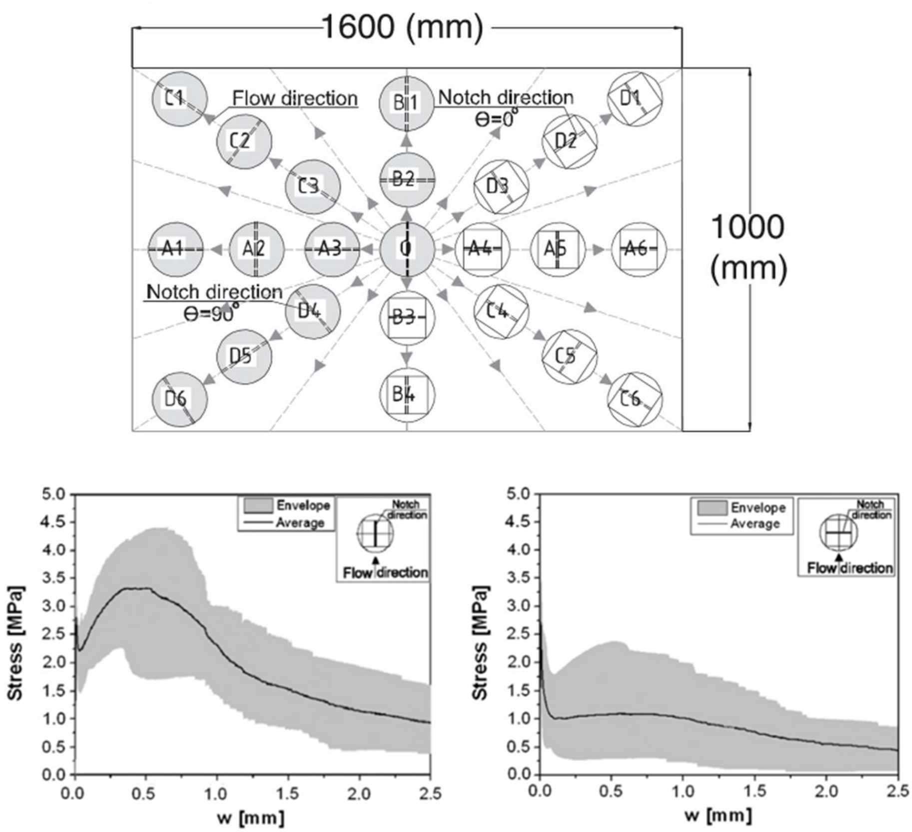

Fig. 2.32 – Stress crack opening curves obtained from cores, drilled out of a slab for different flow directions of fibres (from Abrishambaf [42])

From Fig. 2.32, it can be seen that the relative orientation of fibres due to the flow of the concrete during pouring is significantly influencing the post-cracking tensile strength of SFRC. For the case of flow direction parallel to the notch (Fig. 2.32, left), the average post-cracking stresses are about three times as high as for the case of flow direction perpendicular to the notch (Fig. 2.32, right).

Another parameter influencing the observed scatter of test results, is the adopted experimental test used to derive post-cracking bending tensile behaviour. Studies have proven the observed scatter of post-cracking strength is reduced significantly by using test procedures with higher effective cracking areas. Parmentier et al. [37] proved that for the round and square panel tests on SFRC the coefficient of variation (CoV) of the post-cracking tensile stresses is around 5-10 % instead of typical values of 15-25% for the experimental results obtained by means of standard prisms with cross-sectional dimensions of 150 mm by 150 mm (Fig. 2.33, left).

Based on 96 performed standard prism bending tests, Kooiman [39] found that the scatter of test results decreases for higher beam widths (Fig. 2.33, right), while for beams with constant width and variable height, the magnitude of observed scatter was nearly constant.

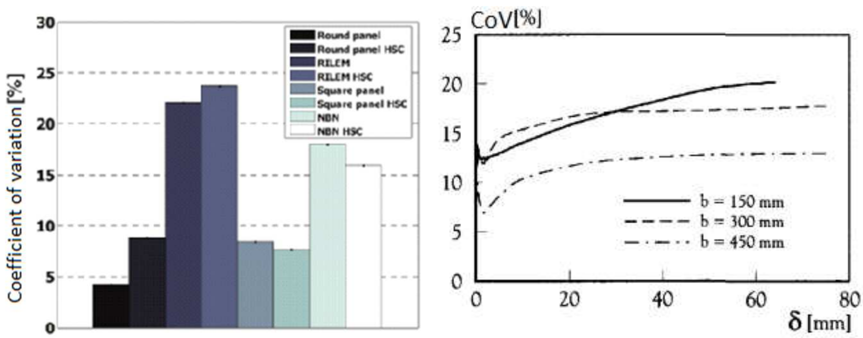

Fig. 2.33 – Influence of test method (left [37]) and beam width (right [39]) on the dispersion of post-cracking strength of SFRC

Furthermore, in the study performed by Kooiman, it was pointed out that for higher fibre dosages and higher concrete compressive strength lower values of CoV for the residual tensile strength can be expected.

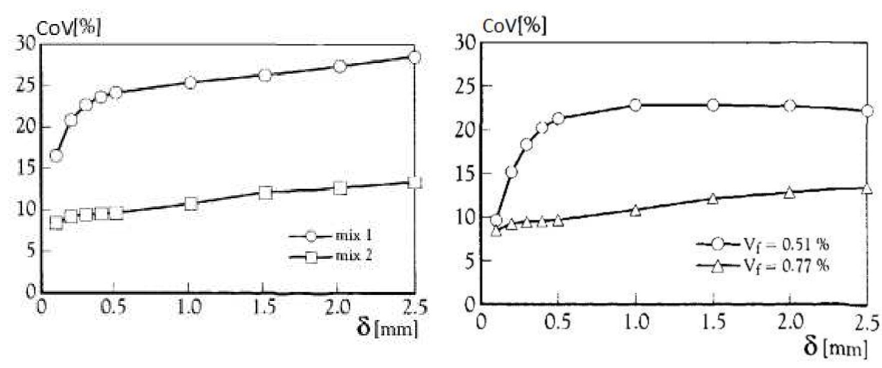

Fig. 2.34 – Influence of concrete strength and fibre dosage on the scatter of post-cracking stress [39]

In the left graph of Fig. 2.34, the CoV of the residual flexural stress as a function of deflection is shown for a normal (mix 1) and high strength concrete (mix 2). For the higher strength concrete, the CoV is about half of the value observed for the normal strength concrete. The scatter of test results tends to increase at higher deflections for both concrete mixes. For an increase of fibre dosage from 0.51 % (40 kg/m³) to 0.77 % (60 kg/m³), the CoV was reduced with about 50%. Between a deflection of 0 and 0.5 mm, the CoV increases from 10% to almost 25% for a fibre dosage of 0.51%.

Since relatively high scattering of test results is inherent to the composite behaviour of SFRC, the obtained test results will be used to derive a characteristic value for design purpose. Based on the number of tests conducted to obtain the residual flexural parameters (cf. EN 14651), the characteristic value of f_{Ri} is derived by:

$$f_{Rk,i} = f_{Rm,i} - ks_{Ri} \qquad \text{Eq. 2.11}$$

In which $f_{Rk,i}$ is the characteristic value of the residual flexural strength obtained from a given number of tests on standard prisms from the same SFRC batch , $f_{Rm,i}$ is the average value of obtained residual strength and s_{Ri} is the batch standard deviation.

The appropriate values of k as a function of the number of samples are summarized in Table 2.2 (see also [43]).

Table 2.2 – Values of k as a function of number of tests

n	3	4	5	6	10	20	30	∞
k	1.89	1.83	1.80	1.77	1.72	1.68	1.67	1.64

As a concluding remark, it should be mentioned that the amount of scatter of the post-cracking tensile strength is directly influenced by the scatter of mechanical properties of the concrete matrix itself. In order to reduce the scatter, it is essential to pay attention to mixing quality and curing of the concrete.

2.3.4 Constitutive models for tension

2.3.4.1 General

In general, different approaches can be adopted to model the constitutive tensile stress-crack width relationship of SFRC. Thereby, a distinction can be made between three main methods:

1) Direct approach based on fibre pull-out,

2) Indirect approach based on predefined correlations

3) Indirect approach based on inverse analysis.

The direct modelling approach considers the single fibre pull-out mechanism as the basis for a Mode I post-cracking law, while the indirect approaches start from bending test results from which the post-cracking stress-crack opening law is obtained by either predefined formulations to convert the residual flexural stress to a post-cracking tensile stress or by a more complex, but more accurate, inverse analysis.

The tensile constitutive law can be formulated as a stress-crack opening (σ-w) or a stress-strain (σ-ε) constitutive law. The advantage of using a σ-w relation offers straightforward compatibility with respect to uni-axial tensile test results. On the other hand, for conventional reinforced concrete calculations, it is more convenient to use a stress-strain relationship similar to the adopted stress-strain relationships for concrete in compression and conventional steel reinforcement in tension. When a σ-w constitutive law is transformed into a σ-ε, the concept of characteristic length needs to be considered, relating a crack width to the corresponding strain by means of a length l_{cs} (Eq. 2.12):

$$\varepsilon = \frac{w}{l_{cs}} \qquad \text{Eq. 2.12}$$

For the analysis of RC-structures, the characteristic length is often taken as the average distance between cracks. Hence, the stress-strain post-cracking constitutive law is size dependent and should be treated carefully [44]. In finite element modelling, the magnitude of l_{cs} is related to the finite element size (i.e. the area in one element covered by an integration point). Hence, by taking into account a fixed stress-crack opening law, the stress-strain constitutive law for SFRC is a function of element size and average crack spacing.

2.3.4.2 Direct approach based on fibre pull-out

By means of the direct approach, the Mode I constitutive law of SFRC is determined by taking into account the stress transfer mechanisms between crack surfaces. Considering the experimental results or semi-analytical models which describe the pull-out response of single fibres, the σ-w relationship is obtained by superposition of the individual contribution of all fibres as a function of embedded length and fibre inclination. For a detailed description of the models available in literature reference is made to [30, 45-51]. A summary is given in the next paragraphs.

One of the simplest forms of the post-cracking σ-w law has been proposed in 1987 by Lim [45], by assuming a constant post-cracking stress up to an ultimate strain. This is called a rigid-plastic model (see Fig. 2.35). The rigid plastic models are characterised by a sudden drop of stresses just after reaching the tensile strength of the concrete matrix, after which a stress plateau is maintained up to the ultimate strain. In the model suggested by Lim, the magnitude of post-cracking tensile stress is related to the amount of fibres crossing the crack plane combined with the average bond stress for each fibre. Lim [45] used a bi-linear bond stress-slip law for the pull-out response of both straight and hooked-end single fibres and proposed a resulting post-cracking σ-w response based on the average maximum tensile stress in the fibres. A similar model taking into account the average fibre stress based on the bond stress slip relationship for straight fibres has been developed by Li [49] and the post-cracking stress-crack opening relationship of high strength concrete with fibre dosages ranging from 0.5 to 2 % were modelled successfully. The considered pull-out stress-slip behaviour of the straight fibres was modelled by taking into account the analytical formulations developed by Stang et al. [22].

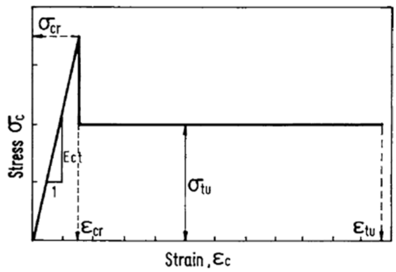

Fig. 2.35 – Load-CMOD curve according to Lim et al [45].

With respect to the modelling techniques developed by Lim [45] and Li [49], an improved direct approach has been suggested by Armelin [46]. By means of the pull-out response of inclined pull-out tests on hooked-end fibres with a length of 30 mm and a diameter of 0.5 mm, the pull-out behaviour was modelled by adopting a regression analysis. A lumping of fibre contributions up to a crack opening of 3 mm provided satisfactory simulation accuracy.

Further improvement for the direct approach modelling of SFRC has been done by Voo & Foster by the development of the Variable Engagement Model (VEM [47]). By the analysis of the pull-out response of inclined fibres it was observed that the engagement of fibres to provide tensile stress to the SFRC is influenced by the fibre inclination angle. The model is able to deal with varying fibre inclination, embedded length, concrete compressive strength, straight and hooked-end fibres with different length and diameter. Similar techniques have been adopted by Prudencio, Laranjeira and Luccioni [48].

Next to the available analytical or semi-analytical models available in literature, a direct approach by means of finite element analysis has been developed by Cunha et al. [51]. By introducing a two phase method, the matrix volume is modelled as a plain concrete and the fibres are modelled as straight embedded reinforcement elements, randomly distributed in the matrix volume (Fig. 2.36).

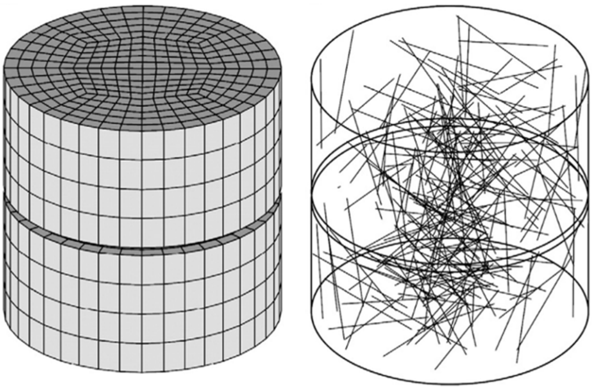

Fig. 2.36 – Two phase model components: concrete matrix 3D-mesh (left) and discrete fibre elements (right) (from Cunha et al. [51])

As a concluding remark it should be noted that although the direct modelling approaches are quite accurate for the prediction and simulation of the σ-w constitutive law, the methods require the input of a large number of both mechanical and geometrical properties and are very difficult to be implemented in a day by day engineering practice. However, from a scientific point of view, these modelling techniques are the most rational and deal with the majority of physical crack-bridging mechanisms involved. Furthermore, these models can only be used to estimate the post-cracking tensile response. In order to derive the real composite behaviour, experimental test results have to be considered.

2.3.4.3 Indirect approach based on predefined correlations

Since the uni-axial tensile test is difficult to perform and given the complexity of a direct modelling approach by the assumption of different parameters such as fibre spacing and inclination and inherent pull-out behaviour, more simple methods to derive a sufficiently accurate constitutive law have been proposed in literature. Many of these methods take into account the experimental results of different bending tests available in standards or (inter)national guidelines (see also section 2.3.2.2).

The most relevant design guidelines providing constitutive laws for the tensile stress-crack opening or stress-strain behaviour are proposed by the RILEM TC 162-TDF [43] and by the fib in the latest Mode Code 2010 [52]. In the RILEM recommendations, a stress-strain relationship for SFRC is considered by assuming a constant stress along the cracked section. The height of this cracked part is taken equal to 2/3 of the section height for the case of CMOD = 0.5 mm and 0.9 times the section height for the case CMOD = 3.5 mm (Fig. 2.37). When the bending moment calculated by means of the assumption of a rigid plastic post-cracking tensile law is equated to bending moment based on the residual flexural stresses at corresponding CMOD, the relationship between residual stresses f_{R1} an f_{R4} and σ_2 and σ_3 can be obtained (Eq. 2.13 and Eq. 2.14).

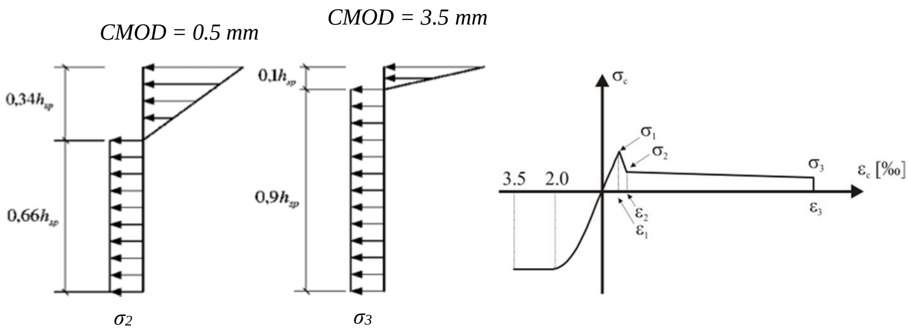

Fig. 2.37 – Stress-strain laws for SFRC in tension and compression according to RILEM TC 162-TDF

$$\frac{bh_{sp}^{2}}{6} f_{R,1} = b \cdot 0.66h_{sp} \cdot 0.56h_{sp} \cdot \sigma_2 \qquad \text{Eq. 2.13}$$

$$\frac{bh_{sp}^{2}}{6} f_{R,4} = b \cdot 0.90h_{sp} \cdot 0.50h_{sp} \cdot \sigma_3 \qquad \text{Eq. 2.14}$$

For the stress-strain relationhsip as shown in Fig. 2.37, the following values defining the post-cracking bilinear constitutive law are obtained:

$$\sigma_1 = 0.7(1600 - d) f_{ctm,fl} \qquad \text{Eq. 2.15}$$

$$\sigma_2 = 0.45 f_{R,1} \kappa_h \qquad \text{Eq. 2.16}$$

$$\sigma_3 = 0.37 f_{R,4} \kappa_h \qquad \text{Eq. 2.17}$$

$$E_c = 9500 f_{cm}^{1/3} \qquad \text{Eq. 2.18}$$

$$\varepsilon_1 = \frac{\sigma_1}{E_1} \qquad \text{Eq. 2.19}$$

$$\varepsilon_2 = \varepsilon_1 + 0.01\% \qquad \text{Eq. 2.20}$$

$$\varepsilon_3 = 2.5\% \qquad \text{Eq. 2.21}$$

$$\kappa_h = 1 - 0.6\left(\frac{h - 125}{475}\right), \; 125 \le h \le 600 \qquad \text{Eq. 2.22}$$

In which d is the effective depth and h the height of the standard prism, both in mm.

In MC2010, the constitutive stress crack-opening law of SFRC is based on the values of f_{R1} and f_{R3}. Two different models can be adopted for design purposes: a) rigid plastic or b) softening/hardening (Fig. 2.38).

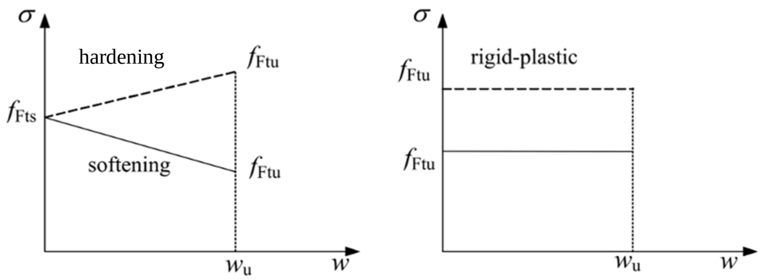

Fig. 2.38 – Load-CMOD curve according to MC2010

According to the rigid plastic model, the mode I crack-bridging stress is taken equal to $f_{R3}/3$ up to a critical crack opening w_u. The second model allows to calculate a linear softening or hardening branch after cracking. The tensile stress as a function of crack opening w is given by Eq. 2.23 and Eq. 2.24.

$$\sigma_F(w) = f_{Fts} - \frac{w}{2.5}\left(f_{Fts} - 0.5 f_{R3} + 0.2 f_{R1}\right),\ \geq 0 \qquad \text{Eq. 2.23}$$

$$f_{Fts} = 0.45 f_{R1} \qquad \text{Eq. 2.24}$$

Alternatively, Model Code 2010 provides also a stress-strain curve for SFRC. Thereby, a distinction is made between strain-softening (Case I, Fig. 2.39) and strain-hardening behaviour (Case II and III, Fig. 2.40). The stress levels f_{Fts} an f_{Ftu} are calculated by means of Eq. 2.23 and Eq. 2.24. The corresponding SLS and ULS strains are determined by Eq. 2.25 and Eq. 2.26.

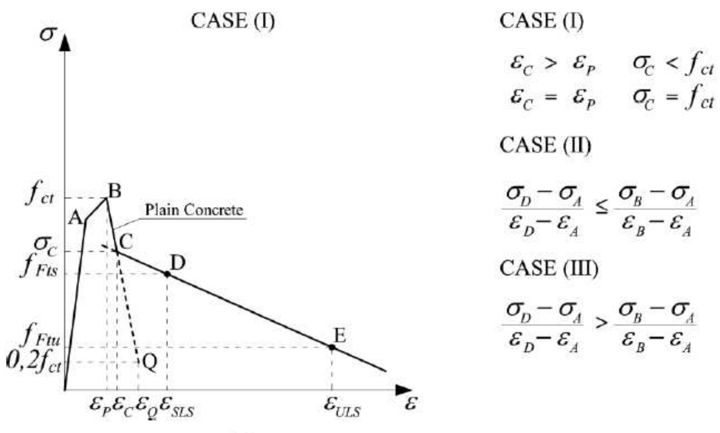

Fig. 2.39 – Stress strain curve laws according to MC2010 (case I)

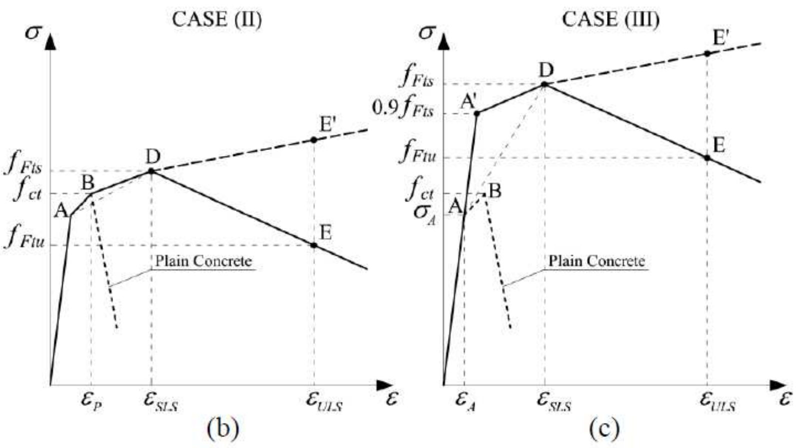

Fig. 2.40 – Stress strain curve laws according to MC2010 (Cases II and III)

$$\varepsilon_{SLS} = \frac{CMOD_1}{l_{cs}} \quad \text{Eq. 2.25}$$

$$\varepsilon_{ULS} = \min\left(\varepsilon_{Fu}, \frac{2.5}{l_{cs}}\right) \quad \text{Eq. 2.26}$$

in which ε_{SLS} is the strain considered in the SLS, ε_{ULS} is the strain considered in the ULS, l_{cs} is the crack spacing length and ε_{Fu} is the ultimate strain taken as 2% for bending and 1% for uni-axial tension.

As a modification to the rigid-plastic model, a two steps rigid plastic model has been proposed by Dupont [20] (Fig. 2.41) for which the stress levels are related to the residual flexural stresses as derived by a standardised three-point bending tests according to EN 14651.

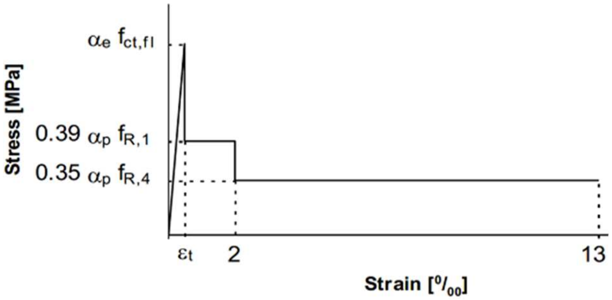

Fig. 2.41 – Load-CMOD curve according to Dupont [20]

In addition to rigid plastic models, bilinear softening models have been propsed by Di Prisco [53]. Their schematic representations are shown and Fig. 2.42.

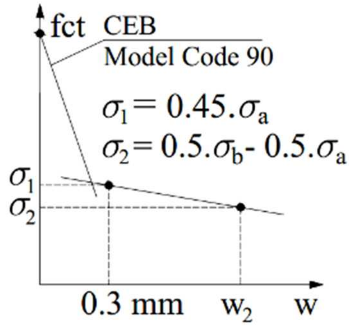

Fig. 2.42 – Load-CMOD curve according to Di Prisco [53]

Di Prisco et al. related the values of σ_1 and σ_2 to the post-cracking equivelant stresses $f_{eq,0\text{-}0.6}$ (i.e. σ_a) and $f_{eq,0.6\text{-}3}$ (i.e. σ_b) (see Section 2.3.2.3). The crack opening at which the second branch starts is kept constant at 0.3 mm.

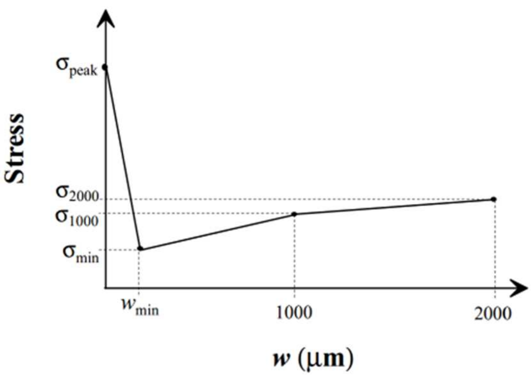

Fig. 2.43 – Load-CMOD curve according to Barragan [54]

The tri-linear model suggested by Barragan [54] is merely an adaptation of the rigid plastic model to deal with the drop op residual stresses at small crack openings and an increase of fibre engagement (see also VEM [47]) for larger crack openings.

2.3.4.4 Indirect approach based on inverse analysis

By means of an inverse analysis, experimentally obtained bending test results can be simulated by taking into account an assumed post-cracking stress-crack opening or stress-strain Mode I constitutive law. In general, the inverse analysis starts with the estimation of a first post-cracking law and simulating the bending test. Then, the difference between the simulated and experimentally obtained bending response is evaluated and the parameters of the assumed law are adopted. Iteratively, a solution is found when the error between the modelled and experimental bending response is sufficiently low.

Based on the obtained load-CMOD curves by means of the standard three point bending tests, an effective way to estimate the Mode I uni-axial tensile crack opening law is done by applying inverse analysis (IA) procedures as described in the Model Code 2010 (section 5.6) [52]. The solution procedure consists of the following five steps:

1. Divide the beam in a sufficient amount of n layers with a defined height Δh
2. Assume, for a specific value of CMOD, a certain deformation in terms of strain (compression), or crack opening (tension) according to the assumed post-cracking constitutive law for SFRC in tension.
3. Apply stresses for SFRC in tension and compression in accordance with the chosen constitutive law (see Fig. 2.44).
4. Solve iteratively by changing deformations assumed in step 2, by solving the horizontal equilibrium using Eq. 2.27
5. Calculate the corresponding moment-CMOD relationship with Eq. 2.28

By performing these five steps at different CMOD values, a complete moment-CMOD curve can be obtained.

$$N = \sum_{i=1}^{n} \sigma_i \cdot \Delta h \cdot b = 0 \qquad \text{Eq. 2.27}$$

$$M = \sum_{i=1}^{n} \sigma_i \cdot \Delta h \cdot y_i \cdot b \qquad \text{Eq. 2.28}$$

with y_i the distance of the centroid of the layer to the neutral axis of the cross-section, Δh the height of the layers, b the width of the layers and σ_i the tensile or compressive stresses as a function of the considered displacement (see Fig. 2.44).

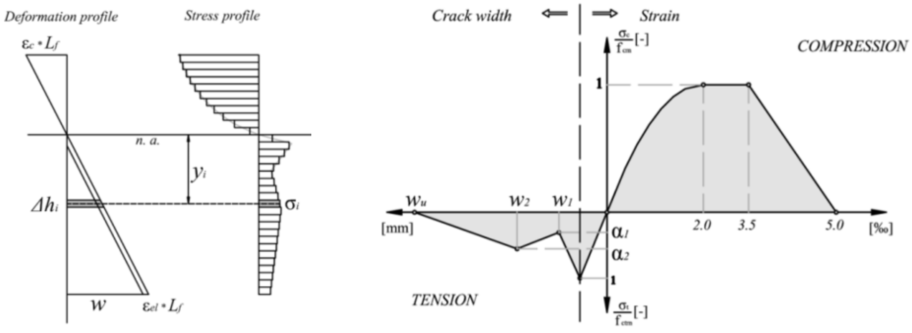

Fig. 2.44 - Schematic of used constitutive laws for tension and compression of SFRC

In order to obtain a complete moment-CMOD curve, the incremental deformation of the standard prism can be done in terms of curvature (strain distribution) or directly in terms of crack width. The difference between both approaches will lead to the use of a characteristic length as defined by Eq. 2.12 or by means of a fictitious length, which concept was introduced by Kooiman [39].

The bilinear softenig model proposed by Kooiman is based on the curve fitting of obtained post-cracking bending behaviour by means of inverse analysis. For the experimental data obtained from SFRC mixes containing 60 kg/m³ of hooked-end steel fibres Kooiman defined the bi-linear softening curve as follows:

- The ratio of $f_{ctm,eq,bil}$ to $f_{ctm,ax}$ is equal to 0.2 – 0.3 for 30 mm and 60 mm long fibres respectively.
- The ratio of w_c/w_0 is in the range of 0.20
- The ratio of w_0/L_f is in the range of 0.33-0.425.

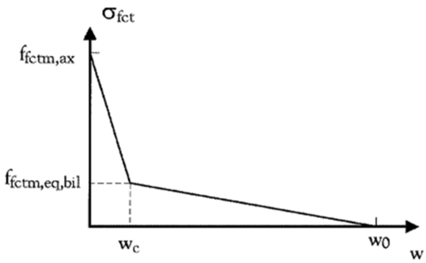

Fig. 2.45 – Load-CMOD curve according to Kooiman [39]

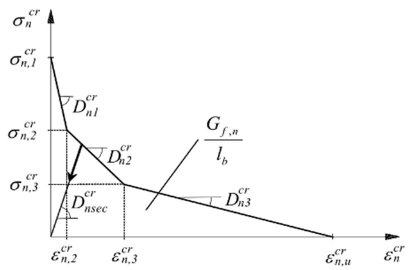

Fig. 2.46 – Load-CMOD curve according to Barros et al.[35]

In order to improve the simulation or prediction accuracy of the constitutive laws, the bi-linear approaches have been extended to multi-linear approaches (Fig. 2.46 and Fig. 2.43). However, increasing the number of ascending and descending branches of the post-cracking law, the degrees of freedom increases as well and will lead to an increased possibility of a non-unique solution when an inverse analysis method is applied.

In order to implement the post-cracking behaviour of SFRC into finite element calculations, Barros et al. proposed a tri-linear σ-w law for tension based on the total fracture energy $G_{f,n}$. A solution is found by means of inverse analysis of the test results obtained from standard bending tests, the values of σ and ε can be obtained [55]. The tri-linear model as shown in Fig. 2.46 consists of three softening branches. However, in order to derive a good fit of flexural test data, the second branch may be ascending as well.

2.3.5 Direct shear behaviour

2.3.5.1 General

When plain concrete is subjected to tensile stresses, a brittle failure is likely to occur. Therefore a suitable type of tensile reinforcement has to be provided, in order to guarantee sufficient post-cracking strength for concrete members subjected to tensile stresses. It has been proven [56-58] that for members subjected to shear, traditional reinforcement can be partially or completely replaced by the use of steel fibre reinforced concrete (SFRC). However, under these loading conditions, the crack propagation behaviour will differ largely from that of a pure mode I crack opening (i.e. tensile stress normal to the plane of the crack). As a result, the material properties of SFRC derived by standard bending tests [59] will not necessarily be representative to be used as design parameters for shear.

2.3.5.2 Direct shear tests

In order to gain more insight into the crack bridging ability of steel fibres when subjected to a combination of both mode I (opening) and mode II (sliding) crack propagation, i.e. mixed mode behaviour of SFRC, different types of direct shear tests have been adopted [60] to investigate the direct shear or shear friction capacity of steel fibre reinforced concrete. Commonly, the following types of specimens are used to investigate the direct shear response of plain and reinforced concrete (Fig. 2.47):

a) Z-type push-off specimen

b) Double notched push-through specimen

c) Single notched FIP-type specimen

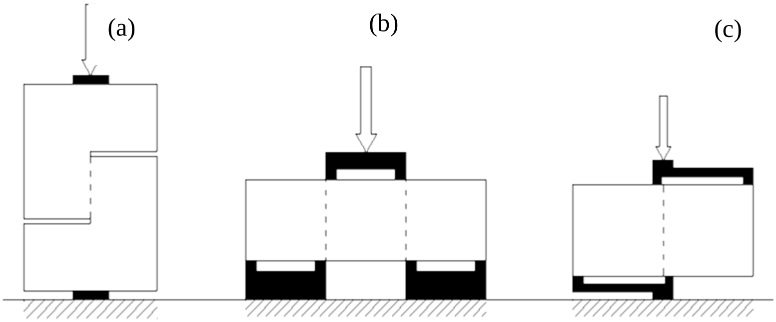

Fig. 2.47 - Different test setups used to investigate the direct shear behaviour op plain and reinforced concrete: (a) Z-type, (b) JSCE-type and (c) FIP-type.

All of the three test setups shown in Fig. 2.47 are designed in order to reduce the effect of bending and hence to achieve a pure state of shear. However, in practice, bending can occur due to irregularities of the test setup. Z-type specimens (Fig. 2.47a) were used by Walraven [61] and Mattock [62] to investigate the fundamentals of aggregate interlock and the shear friction response of pre-cracked concrete with reinforcement passing through the cracking plane under certain inclination angles. Lee [63] used this type of tests to investigate the effects of fibres on the direct shear behaviour of SFRC. Due to the additional reinforcement required in the two L-shaped concrete blocks, the production of this test specimen is elaborate. As a solution, a simple double notched prism (Fig. 2.47b) is used. This test setup is based on the push through configuration of the Japanese standard JSCE-SF6 and was adapted by Mirsayah [64] with a double notch to induce a more controlled crack plane. A third specimen type [65] is a single notched prism used for a direct shear test according to [66] (Fig. 2.47c).

Experimental research has proven that steel fibres can increase the direct shear toughness significantly [65, 67-71]. Valle et al. [69] and Khaloo et al. [70] studied the effect of fibres on the direct shear strength of SFRC by means of the Z-type specimen. The main investigated parameters were concrete compressive strength, fibre aspect ratio and fibre dosage. Valle concluded that the beneficial effect of fibres towards the direct shear capacity is higher for high strength concrete than for normal strength concrete.

Khaloo found similar results based on the experimental results of an extensive test program varying concrete compressive strength (25-75 N/mm²), fibre dosage (0.5-1.5 Vol-%). In this study, hooked-end fibres with two different lengths of 16 and 32 mm, a triangular cross-section and slightly twisted around the longitudinal axis, were adopted. The main influence of all parameters in the toughness is shown in Fig. 2.48. The abbreviations LC, NC, MC and HC denotes low, normal, medium and high strength concrete.

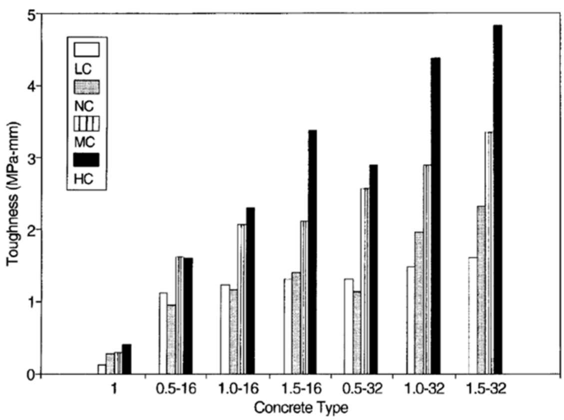

Fig. 2.48 – Influence of concrete compressive strength, fibre dosage and fibre length on the direct shear toughness increase of SFRC.

From Fig. 2.48, it can be seen that for low strength concrete, the addition of fibres has quasi no effect on the direct shear toughness of SFRC. In contrast, for high strength concrete, the toughness increases linearly for higher fibre dosages. Observations of the crack plane after testing have revealed that for the lower strength concrete, fibres were pulled out while for the tests with higher strength concrete, the fibres ruptured due to a better bond between fibres and matrix.

Mirsayah and Banthia [64] adopted the JSCE-SF6 test setup with and without a notch and concluded that for unnotched specimens, the failure plane deviated from the narrow shear plane. Therefore, additional trials were performed adding notches with varying depth. It was found that for a 15 mm deep all-around sawed notch, the direct shear tests (see Fig. 2.47b) were providing reliable and reproducible test results. With respect to the toughness enhancement similar conclusions as Valle and Khaloo were obtained. Additional experimental evidence was later provided by similar direct shear tests performed by Appa Rao [68] and Boulekbache [67].

Khanlou [65] adopted an alternative test setup (see Fig. 2.47c) to evaluate the influence of fibre dosage and concrete strength on the direct shear test. The used fibres were type DRAMIX RC-80/60-BN In contrast to the experimental results obtained by means of the modified JSCE-SF6 test setup, the increase of direct shear strength as a function of fibre content is rather limited.

2.3.5.3 Direct shear strength models

Based on experimental observations, several empirical formulations have been proposed to predict the maximum shear stress transmitted across cracked SFRC [64, 65, 67, 70]. The first reports on the direct shear strength modelling of SFRC focused mainly on the shear strength of plain concrete and the shear strength that can be obtained when adding a certain amount of fibres of different type (crimped, straight, hooked …).

Based on experimental results, empirical equations for τ_{max} are proposed as a function of concrete compressive strength f_c, fibre dosage V_f and the ratio of fibre length L_f to diameter d_f. Thereby, the direct shear strength capacity of SFRC (τ_{SFRC}) is calculated as the superposition of the contribution of plain concrete τ_c and fibres τ_f:

$$\tau_{SFRC} = \tau_c + \tau_f \qquad \text{Eq. 2.29}$$

In which the expressions for τ_c and τ_f are summarized in Table 2.3.

Table 2.3 - Overview of direct shear capacity formulas for SFRC

Shear capacity model	Test type	Fibre type	τ_c [N/mm²]	τ_f [N/mm²]
Boulekbache [67]	JSCE-SF6	Hooked ends	$0.72 f_c^{0.80}$	$0.08 V_f \dfrac{L_f}{d_f}$
Mirsayah & Banthia [64]	JSCE-SF6	Flat ends	7.5	$4.23 V_f$
Khanlou [65]	FIP	Hooked ends	$0.75 f_c^{0.50}$	$4 V_f^{0.90}$
Khaloo & Kim [70]	Z-type	Twisted / hooked ends	$0.65 f_c^{0.50}$	$C_1 V_f + C_2 V_f^2 + C_3 V_f^3$
Mansur [72]	Z-type	No fibres	$0.56 f_c^{0.62}$	-

For all the equations of τ_f given in Table 2.3, the dimension of fibre content V_f is Vol.-%. The constants C_{1-3} used in the equations from Khaloo & Kim are a function of fibre aspect ratio and concrete compressive strength [70].

2.3.6 Compressive behaviour

For lower strength concrete, the compressive stress-strain curve has a quasi-parabolic shape up to the ultimate strain and a softening branch can clearly be observed. However, for higher concrete strengths, after reaching the concrete compressive strength, a more brittle compressive failure occurs and a steep drop of the stress-strain curve occurs. Similar to the enhanced post-cracking ductility for SFRC when subjected to tensile forces, the residual compressive stresses can be increased as a function of higher fibre dosage. For regular types of fibres and for SFRC with relatively low fibre dosages (i.e. < 1%), the compressive strength of concrete itself cannot be improved.

The influence of fibre dosage on the toughness of both low and high strength concrete has been studied by Glavind [73] and Taerwe [74]. Adding fibres to normal strength concrete, causes the softening branch to become more pronounced, while for brittle high strength concrete the addition of fibres is even more effective by providing a significant increase of the post-crushing ductility. The main beneficial effect of fibres on an increase of compression-ductility, has been attributed to the enhanced resistance of the SFRC to the growth of longitudinal splitting cracks after reaching the compressive strength. A schematic description of the effect of fibres to the stress-strain curves for low and high-strength plain and SFRC mixes has been given by Lofgren [4] (Fig. 2.49).

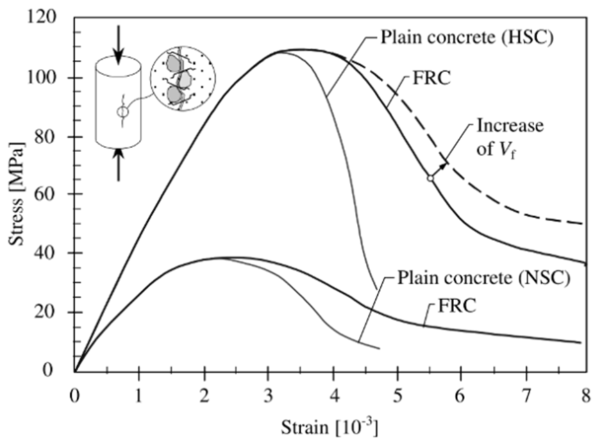

Fig. 2.49 – Schematic compressive stress-strain curves for plain and FRC (from Lofgren [4])

2.4 Conclusions

Regarding the historical evolution towards the experimental and analytical investigations done in the field of SFRC, it can be concluded that a consensus has been found on how the post-cracking behaviour should be quantified. It is now generally acknowledged that the mechanical performance of SFRC has to be determined based on standard flexural tests and to use the results to deduct the post-cracking constitutive laws. However, the main drawback inherent to this concept is that different standard tests have been developed and moreover, several approaches are suggested in order to derive parameters which describe the post-cracking tensile law. More recently, further harmonization towards the mechanical performance characterisation of SFRC has been suggested in the Model Code 2010.

On the other hand, the suggested simplified methods, such as the rigid-plastic or the fixed softening/hardening behaviour, do not provide sufficient information when a more detailed structural analysis has to be made (e. g. numerical analysis). And the models are too simplistic to reflect the fibre bridging mechanisms. Hence, from a more scientifically point of view, it is desirable to know the complete stress-crack opening relationship in relation to the physical and mechanical phenomena involved.

In contrast to the available scientific literature concerning the Mode I crack propagation behaviour of SFRC, less information is available about the post-cracking behaviour of SFRC when subjected to a mixed mode crack propagation (i.e. a simultaneous crack opening and sliding) which is the case for SFRC subjected to shear. Moreover, for the limited amount of available scientific knowledge, research has been focussing on quantifying the increase of ultimate shear strength rather than to understand how fibres bridge a mixed mode crack propagation and how fibres add a significant post-peak shear stress-slip capacity.

Existing empirical formulations for the maximum shear stress capacity at the cracked interface only take into account the fibre dosage and concrete compressive strength. Hence, the general applicability of the suggested models for other types of SFRC is doubtful. A more useful strength model should be made available which takes into account both the shear crack propagation behaviour and residual tensile strength parameters as derived by standard bending tests.

2.5 References

[1] Brandt, A. M. (2008). "Fibre reinforced cement-based (FRC) composites after over 40 years of development in building and civil engineering". *Composite Structures*, Vol. 86(1-3), pp. 3-9.

[2] Collins, P. (2003) "*Concrete, The Vision of a New Architecture*". 2nd ed. McGill-Queen's University Press, p. 472.

[3] ACI. (2001). "544.1R-96: State-of-the-Art Report on Fiber Reinforced Concrete".

[4] Löfgren, I. (2005). "*Fibre-reinforced Concrete for Industrial Construction*" (PhD thesis), p. 276.

[5] Romualdi, J. P., Batson, G. B. (1963). "Mechanics of crack arrest in Concrete". *Journal of the Engineering Mechanics Division*, Vol. 89(3), pp. 147-168.

[6] Romualdi, J. P., Mandel, J. A. (1964). "Tensile strength of concrete affected by uniformly dispersed and closely spaced short lengths of wire reinforcement". *Journal of the American Concrete Institute* Vol. 61(6), pp. 657-672.

[7] Shah, S. P., Rangan, V. (1971). "Fiber Reinforced Concrete Properties". *ACI Journal*, Vol. 68(2), pp. 126-135.

[8] Naaman, A. E. (2007). "*Tensile strain-hardening FRC composites: Historical evolution since the 1960*". In: Advances in Construction Materials 2007 Springer.

[9] Naaman, A. E. (1972). "*A Statistical Theory of Strength for Fiber Reinforced Concrete*", Massachusettes Institute of Technology, p. 196.

[10] RILEM. (2002). "Recommendations of RILEM TC 162-TDF: Test and design methods for steel fibre reinforced concrete; Design of steel fibre reinforced concrete using the sigma-epsilon method: principals and applications". *Materials and Structures,* Vol. 35, pp. 262-278.

[11] Naaman, A. E. (2003). "Engineered Steel Fibers with Optimal Properties for Reinforcement of Cement Composites". *Journal of Advanced Concrete Technology,* Vol. 1(3), pp. 241-252.

[12] Markovich, I. (2006). "*High-Performance Hybrid-Fibre Concrete: Development and Uitilisation*" (PhD-thesis), Delft University of Technology, p. 211.

[13] Bartos, P. J. M., Hoy, C. W. (1996). "Interaction of particles in Fibre Reinforced Concrete". *International RILEM Conference 'Production Methods & Workability of Concrete, Paisley, Scotland*, pp. 451-459.

[14] Pompo, A., Stupak, P. R., Nicolais, L., Marchese, B. (1996). "Analysis of Steel Fibre Pull-out from a Cement Matrix Using Video Photography". *Cement and Concrete Composites*, Vol. 18, pp. 3-8.

[15] Chanvillard, G. (1999). "Modeling the pullout of wire-drawn steel fibers". *Cement and Concrete Research*, Vol. 29, pp. 1027-1037.

[16] Van Gysel, A. (2000). "*Studie van het uittrekgedrag van staalvezels ingebed in een cementgebonden matrix met toepassing op staalvezelbeton onderworpen aan buiging (in dutch)*" (PhD-thesis). Ghent, Ghent University.

[17] Soetens, T., Van Gysel, A., Matthys, S., Taerwe, L. (2013). "A semi-analytical model to predict the pull-out behaviour of inclined hooked-end steel fibres". *Construction and Building Materials,* Vol. 43, pp. 253-265.

[18] Robins, P., Austin, S., Jones, P. (2002). "Pull-out behaviour of hooked steel fibres". *Materials and Structures*, Vol. 35(August 2002), pp. 434-442.

[19] Laranjeira, F., Molins, C., Aguado, A. (2010). "Predicting the pullout response of inclined hooked steel fibers". *Cement and Concrete Research,* Vol. 40(10), pp. 1471-1487.

[20] Dupont, D. (2003). "*Modelling and experimental validation of the constitutive law (sigma-epsilon) and cracking behaviour of steel fibre reinforced concrete*". Leuven, Katholieke Universiteit Leuven.

[21] Stang, H., Li, Z., Shah, S. P. (1990). "Pullout Problem: Stress Versus Fracture Mechanical Approach". *Journal of Engineering Mechanics*, Vol. 116, pp. 2136-2150.

[22] Stang, H., Shah, S. P. (1986). "Failure of fibre-reinforced composites by pull-out fracture". *Journal of Materials Science*, Vol. 21, pp. 953-957.

[23] Gray, R. J., Johnston, C. D. (1987). "The influence of fibre-matrix interfacial bond strength on the mechanical properties of steel fibre reinforced concrete". *The International Journal of Cement Composites and Lightweight Concrete*, Vol. 9(1), pp. 43-55.

[24] Gray, R. J., Johnston, C. D. (1984). "The effect of matrix composition on fibre/matrix interfacial bond shear strength in fibre-reinforced mortar". *Cement and Concrete Research*, Vol. 14, pp. 285-296.

[25] Gray, R. J. (1983). "Experimental techniques for measuring fibre/matrix interfacial bond shear strength". *International Journal of Adhesion and Adhesives*, Vol. 3(4), pp. 197-202.

[26] Naaman, A. E., Namur, G. G., Alwan, J. M., Najm, H. S. (1992). "Fiber Pullout and Bond Slip. I: Analytical Study". *Journal of Structural Engineering*, Vol. 117, pp. 2769-2790.

[27] Wang, Y., Li, V. C., Backer, S. (1988). "Modelling of fibre pull-out from a cement matrix". *The International Journal of Cement Composites and Lightweight Concrete,* Vol. 10(3), pp. 143-149.

[28] Alwan, J. M., Naaman, A. E., Guerrero, P. (1999). "Effect of mechanical clamping on the pull-out response of hooked steel fibers embedded in cementitious matrices". *Concrete Science and Engineering*, Vol. 1(March), pp. 15-25.

[29] Amin, A., Foster, S. J., Muttoni, A. (2013). "Evaluation of the Tensile strength of SFRC as derived from Inverser Analysis of notched bending tests". *8th International Conference on Fracture Mechanics of Concrete and Concrete Structures (FramCos-8), Toledo, Spain*.

[30] Laranjeira, F., Aguado, A., Molins, C. (2008). "Evaluating uniaxial tensile behavior of steel fiber reinforced concrete usign a meso-scale model". *7th RILEM International Symposium on Fibre Reinforced Concrete - BEFIB 20078, Chennai, India*, pp. 1079-1088.

[31] DAfStb. (2012). "Stahlfaserbeton - Ergänzungen und Änderungen zu DIN EN 1992-1-1 in Verbindung mit DIN EN 1992-1-1/NA, DIN EN 206-1 in Verbindung mit DIN 1045-2 und DIN EN 13670 in Verbindung mit DIN 1045-3 - Teil 1: Bemessung und Konstruktion - Teil 2: Festlegung, Eigenschaften, Herstellung und Konformität - Teil 3: Hinweise für die Ausführung".

[32] Bernard, E. S. (2002). "Correlations in the behaviour of fibre reinforced shotcrete beam and panel specimens". *Materials and Structures*, Vol. 35(April 2002), pp. 156-164.

[33] EFNARC. (1996) "*European Specification for Sprayed Concrete*".

[34] NBN. (1992). "B15-238 - Proeven op vezelversterkt beton - Buigproef op prismatische proefstukken". Brussels, Belgium, Belgian Institute for Normalisation.

[35] Barros, J. A. O., Cunha, V. M. C. F., Ribeiro, A. F., Antuns, J. A. B. (2005). "Post-cracking behaviour of steel fibre reinforced concrete". *Materials and Structures*, Vol. 38(275), pp. 47-56.

[36] Minelli, F., Plizzari, G. (2010). "Fiber reinforced concrete characterization through round panel test - part I: experimental study ". *FraMCoS-7: High Performance, Fiber Reinforced Concrete, Special Loadings and Structural Applications,* , pp. 1451-1460.

[37] Parmentier, B., De Grove, E., Vandewalle, L., Van Rickstal, F. (2008). "*Dispersion of the mechanical properties of FRC investigated by different bending tests*". In: Tailor Made Concrete Structures pp. 507-512.

[38] Parmentier, B., Vandewalle, L., Van Rickstal, F. (2008). "Evaluation of the scatter of the postpeak behaviour of fibre reinforced concrete in bending: a step towards reliability". *7th international RILEM symposium on Fibre Reinforced Concrete, Chennai, India*, pp. 133-143.

[39] Kooiman, A. G., van der Veen, C., Walraven, J. C. (2000). "Modelling the post-cracking behaviour of steel fibre reinforced concrete for structural design purposes". *HERON*, Vol. 45(4), pp. 275-307.

[40] Zerbino, R., Tobes, J. M., Bossio, M. E., Giacchio, G. (2012). "On the orientation of fibres in structural members fabricated with self compacting fibre reinforced concrete". *Cement and Concrete Composites*, Vol. 34, pp. 191-200.

[41] Kang, S.-T., Kim, J.-K. (2011). "Investigation on the flexural behavior of UHPCC considering the effect of fiber orientation distribution". *Construction and Building Materials*, Vol. 28(1), pp. 57-65.

[42] Abrishambaf, A., Barros, J. A. O., Cunha, V. M. C. F. (2013). "Relation between fibre distribution and post-cracking behaviour in steel fibre reinforced self-compacting concrete panels". *Cement and Concrete Research*, Vol. 51, pp. 57-66.

[43] RILEM. (2003). "Final Recommendation of RILEM TC 162-TDF: Test and design methods for steel fibre reinforced concrete sigma-epsilon-design method". *Materials and Structures*, Vol. 36(262), pp. 560-567.

[44] fib. (2008). "Bulletin No. 45: Practitioners' guide to finite element modelling". Lausanne, Switzerland.

[45] Lim, T. Y., Paramasivam, P., Lee, S. L. (1987). "Analytical Model for Tensile Behaviour of Steel-Fiber Concrete". *ACI Materials Journal*, Vol. 84(4), pp. 286-298.

[46] Armelin, H. S., Banthia, N. (1997). "Predicting the Flexural Postcracking Performance of Steel Fiber Reinforced Concrete from the pullout of Single Fibres". *ACI Materials Journal*, Vol. 94(1), pp. 18-31.

[47] Voo, J. Y., Foster, S. J. (2004). "Tensile-fracture of Fibre-Reinforced Concrete: Variable Engagement Model". *6th RILEM Symposium on Fibre-Reinforced Concretes (FRC) - BEFIB 2004, Varenna, Italy*, pp. 875-884.

[48] Prudencio Jr., L., Austin, S. A., Jones, P. A., Armelin, H., Robins, P. J. (2006). "Prediction of steel fibre reinforced concrete under flexure from an inferred fibre pull-out response". *Materials and Structures*, Vol. 39(6), pp. 601-610.

[49] Li, V. C., Stang, H., Krenchel, H. (1993). "Micromechanics of crack bridging in fibre-reinforced concrete". *Materials and Structures*, Vol. 26(8), pp. 486-494.

[50] Luccioni, B., Ruano, G., Isla, F., Zerbino, R., Graciela, G. (2012). "A simple approach to model SFRC". *Construction and Building Materials*, Vol. 37(December 2012), pp. 111-124.

[51] Cunha, V. M. C. F., Barros, J., Sena-Cruz, J. (2011). "An integrated approach for modelling the tensile behaviour of steel fibre reinforced self-compacting concrete". *Cement and Concrete Research*, Vol. 41(1), pp. 64-76.

[52] fib. (2010). "Model Code for Concrete Structures 2010". Lausanne, Switzerland, fédération internationale du béton.

[53] di Prisco, M., Ferrara, L., Colombo, M., Mauri, M. (2004). "On the identification of FRC constitutive law in uniaxial tension.". *Sixth RILEM symposium on fibre-reinforced concretes (BEFIB 2004), Varenna, Italy*, pp. 827-836.

[54] Barragán, B., Gettu, R., Agulló, L., Zerbino, R. (2006). "Shear failure of Steel Fiber-Reinforced Concrete Based on Push-Off Tests". *ACI Materials Journals*, Vol. 103(4), pp. 251-257.

[55] Cunha, V. M. C. F., Barros, J. A. O., Sena-Cruz, J. (2012). "Numerical simulations of three-point bending tests: two distinct approaches". *BEFIB 2012, Guimaraes, Portugal*, pp. 1046-1058.

[56] Minelli, F., Plizzari, G. (2013). "On the Effectiveness of Steel Fibres as Shear Reinforcement". *ACI Structural Journal*, Vol. 110(3), pp. 379-389.

[57] De Pauw, P., Taerwe, L., Van den Buverie, N., Moerman, W. (2008). "Steel fibre concrete as an alternative for traditional shear reinforcement in pretensioned concrete beams". *7th international RILEM symposium on fibre reinforced concrete: design and applications (BEFIB 2008)*, pp. 887-898.

[58] Cucchiara, C., La Mendola, L., Papia, M. (2004). "Effectiveness of stirrups and steel fibres as shear reinforcement". *Cement and Concrete Composites*, Vol. 26(7), pp. 777-786.

[59] CEN. (2005). "EN 14651 - Test method for metallic fibered concrete - measuring the flexural tensile strength". Brussels, Belgium, CEN.

[60] Barr, B. (1987). "*The Fracture Characteristics of FRC Materials in Shear*". In: SP105-2. Detroit: American Concrete Institute, pp. 27-53.

[61] Walraven, J. (1980). "*Aggregate Interlock - A theoretical and experimental analysis*" (PhD-thesis), Delft University of Technology.

[62] Mattock, A. H. (1974). "Shear transfer in Concrete Having Reinforcement at an Angle to the Shear Plane, ACI Special Publication 42". pp. 17-42.

[63] Lee, G. G. (2007). "*Direct shear behaviour of steel fibres in a cementitious matrix*" (PhD-thesis). Sydney, Australia, The University of New South Wales.

[64] Mirsayah, A. A., Banthia, N. (2002). "Shear Strength of Steel Fiber-Reinforced Concrete". *ACI Materials Journal*, Vol. 99(5), pp. 473-479.

[65] Khanlou, A., MacRae, G. A., Scott, A. N., Hicks, S. J., Clifton, G. C. (2013). "Shear Performance of Steel Fibre-Reinforced Concrete". *Steel Innovation Conference 2013, Christchurch, New Zealand*.

[66] Fédération Internationale de la Précontrainte (FIP). (1978). "Shear at the interface of precast and in-situ concrete". Lausanne, Switzerland.

[67] Boulekbache, B., Hamrat, M., Chemrouk, M., Amziane, S. (2012). "Influence of yield stress and compressive strength on direct shear behaviour of steel fibre-reinforced cocnrete". *Construction and Building Materials*, Vol. 27(1), pp. 6-14.

[68] Appa Rao, G., Sreenivasa, R. (2009). "Toughness indices of steel fiber reinforced concrete under mode II loading". *Materials and Structures*, Vol. 42(9), pp. 1173-1184.

[69] Valle, M., Büyüköztürk, O. (1993). "Behavior of Fiber Reinforce High-Strength Concrete under Direct Shear". *ACI Materials Journal*, Vol. 90(2), pp. 122-133.

[70] Khaloo, A. R., Kim, N. (1997). "Influence of Concrete and Fiber Characteristics on Behavior of Steel Fiber Reinforced Concrete under Direct Shear". *ACI Materials Journal*, Vol. 94(6), pp. 592-601.

[71] Ahmed, L., Ansell, A. (2010). "Direct shear strength of high-strength fibre concrete". *Magazine of Concrete Research*, Vol. 62(5), pp. 379-390.

[72] Mansur, M. A., Vinayagam, T., Tan, K.-H. (2008). "Shear Transfer across a Crack in Reinforced High-Strength Concrete". *Journal of Materials in Civil Engineering*, Vol. 20(4), pp. 294-302.

[73] Glavind, M. (1992). "*Evaluation of the Compressive Behaviour of Fibre Reinforced High Strength Concrete*" (PhD-thesis), Technical University of Denmark.

[74] Taerwe, L. (1992). "Influence of Steel Fibers on Strain-Softening of High-Strength Concrete". *ACI Structural Journal*, Vol. 88(6), pp. 54-60.

3 LITERATURE REVIEW ON SHEAR

3.1 Shear in reinforced concrete members

More than over 100 years, shear in reinforced concrete beams has been the subject of interest by many researchers. Based on the derived research results in the past, several shear strength formulations have been proposed, further evaluated and updated in order to improve their accuracy. In the following, an overview is given of the development of current approaches to evaluate the shear strength of concrete beams.

3.1.1 Historical background

Given a shear force acting on a cross-section, shear stresses are induced along the depth of the cross-section. In case of pure shear, shear cracks are formed at an inclination angle of 45° when the shear stress equals the tensile strength at the neutral axis. By using Jourawski’s beam shear formula, the cracking shear stress of a concrete section can be derived as follows:

$$f_{ct} = \tau_{cr} = \frac{V_{cr} S(y)}{I b_w (y)} \qquad \text{Eq. 3.1}$$

With S(y), the static moment at a height y in the cross-section, I is the moment of inertia and b_w, the width of the cross-section at the considered height.

However, modelling the shear strength of reinforced concrete is much more complex and cannot be treated as a simple linear elastic problem. The first attempts to model shear critical beams were done by Ritter [1] and Morsch [2], by independently suggesting the concept of truss analogy for a reinforced concrete beam (Fig. 3.1). After the occurrence of shear cracking, the transverse reinforcement acts as tension ties, while the concrete in between these cracks are the compressive struts. At the bottom of the beam, a tensile tie is formed by the longitudinal reinforcement and in the upper region, the compressive zone of the beam is acting as a compressive chord. One of the first methods used as shear reinforcement is known as the Hennebique system as shown in Fig. 3.2, which consisted of flat steel strip bent around the longitudinal reinforcement and anchored in the compression region.

In this conceptual approach of shear, the influence of the concrete in tension is neglected and the shear strength of a reinforced beam is reached when the stirrups yield. Hence the ultimate shear stress at failure is calculated as follows:

$$\tau_u = \frac{A_{s,t} f_y}{b_w s} = \rho_{s,t} f_y \qquad \text{Eq. 3.2}$$

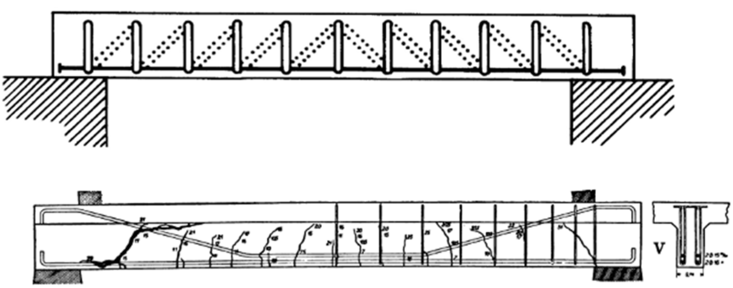

Fig. 3.1 –Truss analogy for reinforced concrete beams subjected to shear [3].

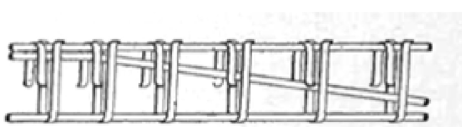

Fig. 3.2 –Hennebique system for shear reinforcement of RC beams [4]

After introducing Ritters truss model in American literature, research by Whitey and Talbot revealed that Eq. 3.2 yields conservative shear strength predictions. In addition, Talbot evidenced the influence of both a/d ratio and the longitudinal reinforcement ratio on the ultimate shear strength of 106 concrete beams without web reinforcement. Despite this early knowledge, the influence of these parameters was not introduced in national design codes at that time. A safe shear design was obtained by limiting the shear stresses to a sufficiently low level [5].

The problem of shear became especially of interest with the collapse of the Wilkins Air Force Depot in Shelby, Ohio which was caused by shear failure of the main girders (Fig. 3.3).

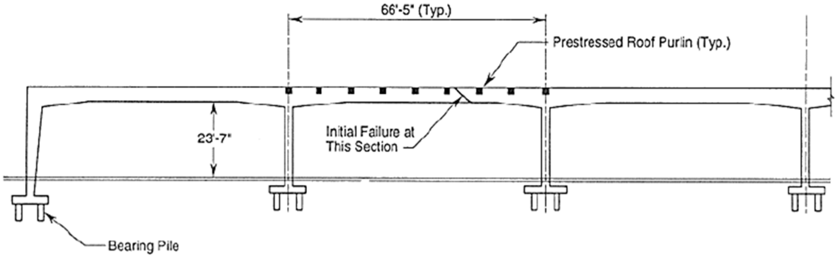

Fig. 3.3 – Localisation of shear failure girder in the Wilkin Air Force Depot (from Shepherd and Frost [6])

Fig. 3.4 – Failed roof girders of the Wilkins Air Force Depot (from Lubell [7])

The shear stresses in the beam at failure were equal to 0.5 MPa, which was only half of the allowable design shear stress [8]. At the time of collapse, the girders were only loaded with the self-weight of the roof. The sudden collapse was caused by the combined effect of loading and shrinkage, which caused the girder to fail in shear even for a lower magnitude of shear stresses. Moreover, the steeper crack inclination caused the shear crack not crossing any of the stirrups [9].

This incident triggred the importance of shear and the effect of parameters such as reinforcement ratio and shear span to depth ratio became a point of interest for many investigations. As such, the Wilkins Air Force Depot shear failure landmarked the development of current shear design rules.

3.1.2 Types of shear failure

When subjecting concrete beams to a shear force, often, the flexural moment will first cause vertical bending cracks to occur in the maximum bending moment region. When increasing the shear load, the bending cracks located near the support, tend to rotate with an inclination angle around 45°. However, when the cross-section has a relatively thin web, diagonal tension cracks can be formed before reaching the flexural cracking moment and shear-tension failure will occur.

This shear-tension failure will occur when the stirrups reach the yield stress (Fig. 3.5a). Antoher type of shear failure is caused by bond failure of the longitudinal reinforcement near the support due to splitting of the concrete, which is often refered to as an anchorage shear failure (Fig. 3.5b).

For the case of bending-shear failure, it is also possible that the height of the compression region becomes too small and reaching the compressive strength of the concrete at the top fibre will lead to bending–shear failure (Fig. 3.5c).

In case of girders with relatively small web thickness and with high values of transverse reinforcement, the concrete compressive stresses in the inclined struts can reach the maximum compressive strength before yielding of the stirrups and the so called web-compression failure will occur (Fig. 3.5d).

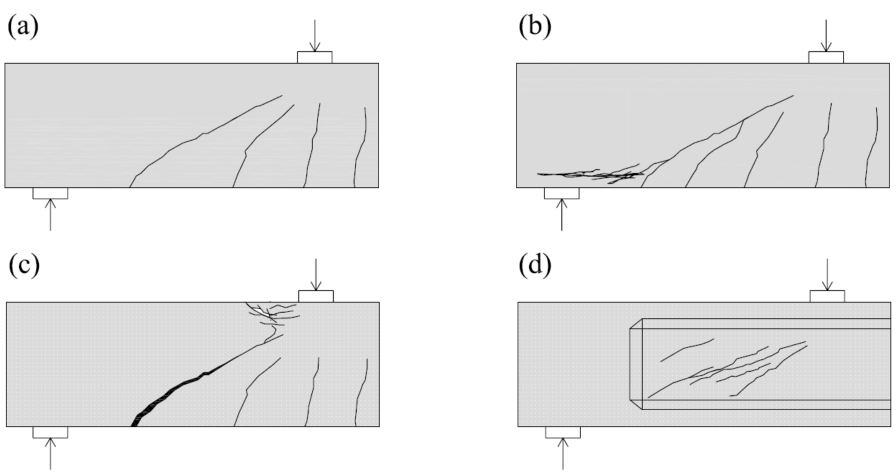

Fig. 3.5 – Different shear failure mechanisms

3.1.3 Shear transfer mechanisms

In a traditionally reinforced beam, the main shear strength contributing mechanisms are:

1) Shear strength of compression zone
2) Friction in the crack interface (i.e. aggregate interlock)
3) Dowel action of longitudinal reinforcement
4) Tensile force in stirrups

Taylor [10] determined experimentally the shear strength components of reinforced beams without shear reinforcement. It was found that the aggregate interlock mechanism is relatively important, contributing for about 33-50% to the total shear strength capacity. The contribution of dowel action is found to be much lower (15-25%) and for the contribution of the compressive zone, values of 20-40% are reported [10-12]. The experimentally determined shear strength components are shown in Fig. 3.6.

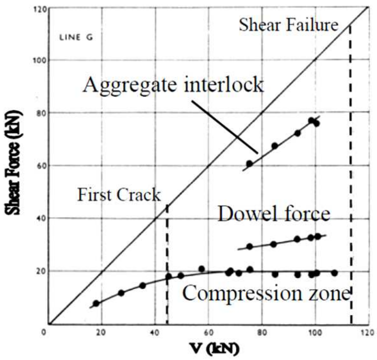

Fig. 3.6 – Shear strength components for beams without shear reinforcement (from Taylor [11, 12]).

Based on shear tests on beams with a compressive strength between 40 and 110 N/mm², Sarkar [13] found values different from Taylor. Sarkar concluded that the most important shear strength mechanism is the dowel action with about 40-50% of the total shear capacity. Aggregate interlock provides an additional 30-40% and the compressive zone represents 10-20% of the ultimate shear strength.

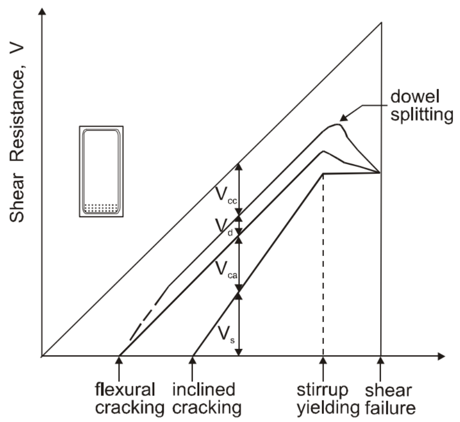

Fig. 3.7 – Distribution of internal shear resistance (from ASCE [14])

3.1.3.1 Shear strength of compressive zone

In a cracked section of a reinforced concrete beam, the compressive zone is subjected to both shear and axial compressive stresses. Considering a plane stress approach for linear elements, the compressive zone will fail when reaching a combination of both compression and shear stresses according to a so called shear failure envelope (see Fig. 3.8).

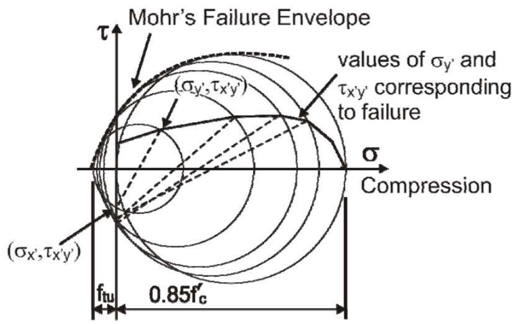

Fig. 3.8 – Geometrical construction of a shear-compression failure.

Based on the principal stress combinations as derived by biaxial failure tests done by Kupfer [15], a Mohr's failure envelope can be constructed. Assuming that the stress $\sigma_{x'}$ can be taken equal to 0 at failure, the shear-compression failure envelope can be constructed geometrically by the points diametrically positioned form the points with coordinates $(0, \tau_{x'y'})$.

Hence, considering a plane stress approach, for which a critical combination of shear stresses and local compressive stress is reached, a compressive shear failure will occur.

3.1.3.2 Aggregate interlock & shear friction

The effect of aggregate interlock is related to the shear friction mechanisms. During the 1980's, different physical and empirical models have been developed. An overview of the most important models and their simplifications are described hereafter.

Two-phase model (Walraven, 1980 [16])

The two-phase model developed by Walraven is a rational approach to the problem of aggregate interlock. In this model, the crack structure is statistically analysed and the stresses acting on the crack faces are described as a function of crack opening and dilatation. The concrete crack and inherent roughness due to the existence of uncracked aggregates is shown schematically in Fig. 3.9. In his theory, the cracks are straight lines and aggregates have an idealized spherical shape.

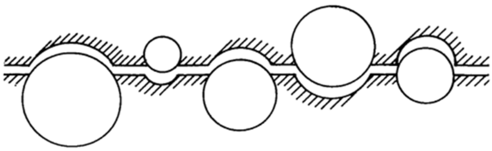

Fig. 3.9 – Shear crack interface model

The contact stresses σ_{pu} and τ_{pu} acting between the matrix and spherical particles is shown more in detail in Fig. 3.10. the tangential stress τ_{pu} is related to the normal stress σ_{pu} by means of a friction parameter:

$$\tau_{pu} = \mu\sigma_{pu} \qquad \text{Eq. 3.3}$$

Horizontal and vertical equilibrium at the crack face with unity width and length, leads to the following general expressions for the shear (τ) and normal stresses (σ):

$$\tau = \sigma_{pu}\left(\Sigma a_n + \mu\Sigma a_t\right) \qquad \text{Eq. 3.4}$$

$$\sigma = -\sigma_{pu}\left(\Sigma a_t - \mu\Sigma a_n\right) \qquad \text{Eq. 3.5}$$

For a given distribution of spherical particles crossing the crack plane, Walraven [16]provided analytical expressions taking into account the total projected areas A_x and A_y in order to be able to calculate the concrete normal and shear stress at the interface.

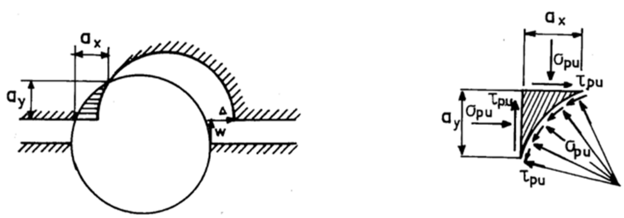

Fig. 3.10 –Normal and tangential component of frictional forces at the crack interface (from Walraven [16]).

In order to derive a more simplified approach, linear relationships were proposed by Walraven & Reinhardt [17] based on regression analysis of test results. Given the crack width w and the shear slip Δ (Fig. 3.10), the best fit of test results is given by:

$$\tau = \frac{-f_{c,cyl}}{30} + (1.8w^{-0.80} + (0.234w^{-0.707} - 0.20)f_{c,cyl})\Delta \qquad \text{Eq. 3.6}$$

$$\sigma = \frac{f_{c,cyl}}{20} - (1.35w^{-0.63} + (0.191w^{-0.552} - 0.15)f_{c,cyl})\Delta \qquad \text{Eq. 3.7}$$

With, $f_{c,cyl}$ the compressive cylinder strength of concrete in N/mm².

<u>Rough-crack model (Gambarova & Karakoç, 1983 [18])</u>

The rough crack model has been introduced by Bazant & Gambarova in 1980 considering regular arrays of trapezoidal teeth representing the roughness of the crack surface (Fig. 3.11).

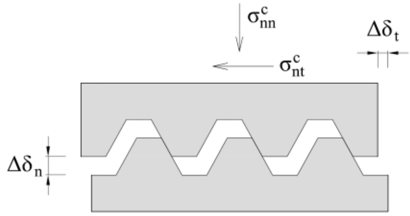

Fig. 3.11 – Rough crack interface model by Bazant and Gambarova

The model is developed taking into account the relative displacement ratio r of the crack surface $\Delta\delta_t/\Delta\delta_n$. For high values of r, it is assumed that the shear stress will be limited asymptotic by the crushing failure of asperities and for very low values of r, the interface shear stress will decrease due to loss of contact when $\Delta\delta_t$ is equal to the half of the average particle size.

Based on the experimental shear friction test results obtained by Paulay & Loeber, a first model was proposed in 1980 by Bazant and Gambarova which was later improved by Gambarova & Karakoç by taking into account the influence of particle size. The transverse and normal components of the shear friction model are given by:

$$\sigma^c_{nt} = \tau_0\left(1 - \sqrt{\frac{2\Delta\delta_n}{D_{max}}}\right) r \frac{a_3 + a_4|r|^3}{1 + a_4 r^4} \qquad \text{Eq. 3.8}$$

$$\sigma^c_{nn} = -a_1 a_2 \sqrt{\Delta\delta_n}\, \frac{r}{(1 + r^2)^{0.25}}\sigma^c_{nt} \qquad \text{Eq. 3.9}$$

with

$$r = \frac{\Delta\delta_t}{\Delta\delta_n}$$ Eq. 3.10

$$a_1 a_2 = 0.62$$ Eq. 3.11

$$a_3 = \frac{2.45}{\tau_0}$$ Eq. 3.12

$$a_4 = 2.44\left(1 - \frac{4}{\tau_0}\right)$$ Eq. 3.13

$$\tau_0 = 0.2 f_{c,cyl}$$ Eq. 3.14

And in which $f_{c,cyl}$ is the compressive cylinder strength of concrete in N/mm² and D_{max} is the maximum particle size in mm.

Contact density model (Maekawa et al., 1989 [19])

Similar to the two-phase model as proposed by Walraven, the contact density model developed by Maekawa, Okamura & Li consists of two main components: the crack surface geometry (Fig. 3.12a) and the interface contact stress as a function of contact displacement and the orientation of the crack surface normal to the crack plane θ (Fig. 3.12c). The crack surface geometry is represented by a probabilistic contact density function Ω(θ) describing the orientation normal to the contact plane (Fig. 3.12b). The density function is independent from strength, size and grading of aggregate particles.

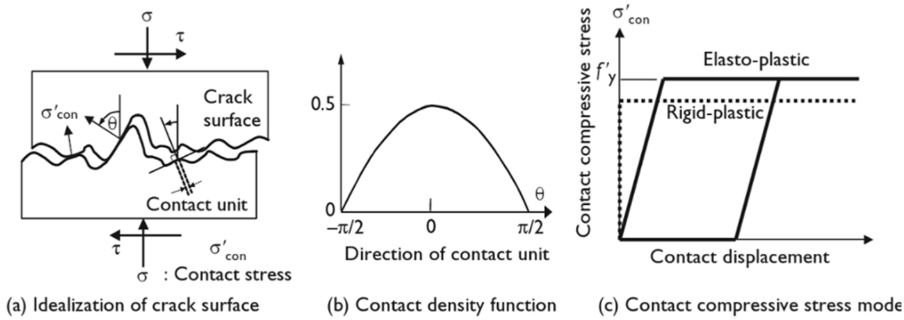

Fig. 3.12 – Contact density model (from Maekawa et al. [20])

The total stress that can be transmitted through the contact areas is calculated by integration of the contact density function over the complete contact area:

$$\tau = \int_{\frac{-\pi}{2}}^{\frac{\pi}{2}} \sigma_{con}(\theta) K(\omega) A_t \Omega(\theta) \sin\theta d\theta$$ Eq. 3.15

$$\sigma = \int_{\frac{-\pi}{2}}^{\frac{\pi}{2}} \sigma_{con}(\theta) K(\omega) A_t \Omega(\theta) \cos\theta d\theta \qquad \text{Eq. 3.16}$$

In which K(ω) is the effective ratio of contact area expressing the loss of contact for increasing crack dilatation and A_t is the surface area of the crack equal to 1.27 times the sectional area of the considered crack plane [19, 20].

Simplified expressions providing the relationship between both shear and normal stresses as a function of crack dilatation were proposed by Li et al. [19] with similarity to the rough crack model by introducing the ratio of transverse to normal displacement of the crack surface.

$$\sigma = 3.83 f_{c,cyl}^{0.333} \left[\frac{\pi}{2} - \cot^{-1} r - \frac{r}{1+r^2} \right] \qquad \text{Eq. 3.17}$$

$$\tau = 3.83 f_{c,cyl}^{0.333} \left[\frac{r}{1+r^2} \right] \qquad \text{Eq. 3.18}$$

Aggregate fracture

Although these aggregate interlock models are very popular and commonly used in e.g. finite element analysis procedures, it should be noted that the main drawback of these models is the assumption that aggregates are stronger than the surrounding matrix. In case of high strengh concrete, cracks are propagating through the aggregates rather than around them which will lead to a decrease of interface roughness. Taking this into consideration, the use of these models in such cases can be doubted. In order to overcome this problem, it is suggested [21] to reduce the particle size artificially as a function of concrete compressive strength.

3.1.3.3 Dowel action

The importance of dowel action to the shear strength contribution is highly influenced by the presence of transverse reinforcement. For members without transverse reinforcement, dowel action shall not be very significant because the development of dowel forces is restricted by failure of the concrete cover due to splitting. The maximum dowel forces are a function of concrete tensile strength and thickness of the concrete cover [22]. Fenwick and Paulay [23] and Taylor [10] found that the contribution of dowel action for beams without shear reinforcement, is not higher than 25 % of the ultimate shear capacity.

For beams with stirrups, the longitudinal reinforcement will be restrained and higher dowel forces can be developed [24]. At the other hand, for beams with transverse reinforcement, the relative increase of shear strength due to dowel action will be rather small, compared to the direct contribution of stirrups. Fig. 3.13 shows schematically the development of dowel forces as a function of dowel displacement for a situation with and without shear reinforcement.

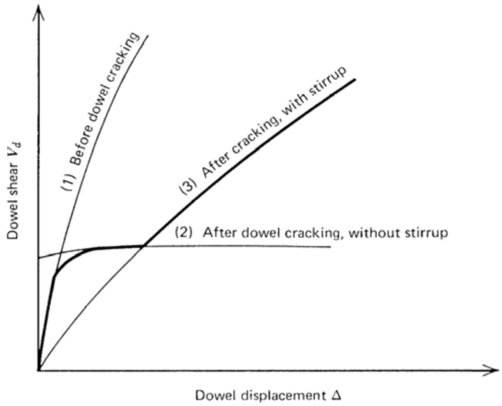

Fig. 3.13 – Dowel shear mechanism as a function of dowel displacement and the presence of stirrups (from Park & Paulay [24])

3.1.4 Important parameters influencing shear strength

For members without transverse reinforcement, the shear strength is mainly influenced by four parameters: 1) the shear span to depth ratio, 2) the depth of the member and 3) the presence of an axial force and 4) the longitudinal reinforcement ratio. In this section, an overview is given of these influencing parameters and additionally, the development of different empirical and rational models for the strength of members without transverse reinforcement is further discussed.

3.1.4.1 Shear span to depth ratio

The influence of shear span to depth ratio (a/d) was first documented by Kani [25] which later on has also be referred to as the “riddle of Kani”. In his “comb with concrete teeth” theory (see also Section 3.1.5.1), a distinction is made between the shear strength corresponding to the strength of the concrete teeth in between flexural cracks and the strength of the remaining arch of the uncracked concrete section, directly transferring shear load to the support. As can be seen on Fig. 3.14, for a/d values between 1 and 5.6 a shear failure is likely to occur. When a/d is lower than 2.5, the shear strength is governed by arch action, rather than beam action.

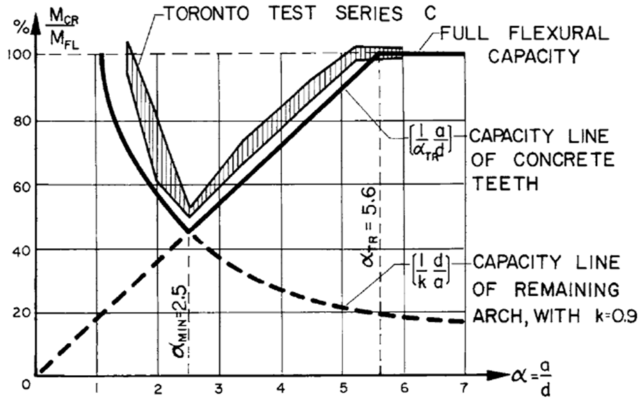

Fig. 3.14 – Arch contribution and concrete tooth strength as a function of shear span to depth ratio, with M_{CR} the bending moment at shear failure and M_{FL} the moment at flexural failure (from Kani [25])

Further explanation of the difference between arch and beam action can be done starting from the main principals of shear resistance. Given the internal bending moment capacity of a given reinforced concrete section with internal lever arm z and tensile strength resultant in the reinforcment N_s , the relationship between the flexural moment M and the corresponding shear force V can be written in the following form:

$$V = \frac{dM}{dx} = \frac{d(N_s z)}{dx} = z\frac{d(N_s)}{dx} + N_s\frac{d(z)}{dx} \qquad \text{Eq. 3.19}$$

In which the first term represents the beam action and the second term the arch action contribution. The variation rate of longitudinal tensile force N_s along the beam length is the bond force applied to the flexural reinforcement per unit length of the beam. Anchorage failure of longitudinal reinforcement or failure of the concrete teeth acting as a cantilever (cf. Kani [25]) can cause inability of the cross section to provide this force component. When this force cannot be provided (either partially or completely), the magnitude of the first term will decrease and N_s has to be replaced by an internal compression force (i.e. compressive force in the inclined struts).

Since the second term of Eq. 3.19 implies that the shear is sustained by the inclined compression, a horizontal tension force, mainly provided by the longitudinal reinforcement, is needed to obtain horizontal equilibrium of forces. Fig. 3.15 shows an idealized situation of a beam with fully anchored tensile reinforcement.

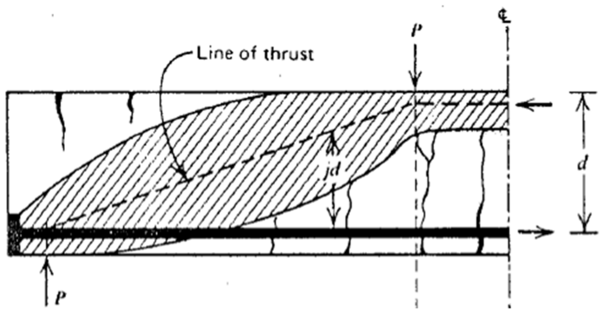

Fig. 3.15 – Variation of internal lever arm and corresponding line of thrust along the shear span (Park and Paulay [24])

From Fig. 3.15 it is clear that when considering a fixed beam height, the distance between the load and the supports will determine the ratio of beam to arch action contribution. For reducing length between load and support the inclination, i.e. the line of thrust becomes steeper and higher parts of the load can be directly transmitted to the support.

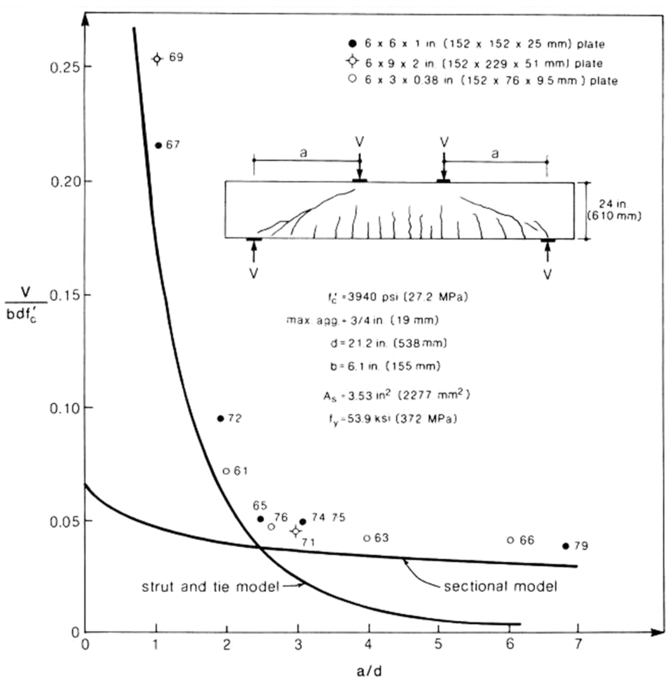

Fig. 3.16 –Arch and beam action as a function of a/d ratio (from Collins & Mitchell [3])

For relatively low values of a/d (< 2), deep beam shear failure will occur due to diagonal compression crushing or splitting. According to Collins & Mitchell [3], the modelling of shear resistance for very low a/d ratios is typically done by using strut and tie models to represent the arch action. Shear failure due to beam action can be analysed by means of sectional models (Fig. 3.16).

3.1.4.2 Depth of the member

Based on experiments on beams width identical reinforcement ratio, width, concrete strength and loading conditions, Kani found that increasing the beam height from 0.15 to 1.20 m (for a constant ratio of a/d) caused a relative decrease of shear strength for about 40% and pointed out that a size reduction factor should be incorporated in order to obtain safe shear designs [8]. Further experimental evidence for this phenomenon was found by Shioya et al. [26], Collins & Kuchma [8], Frosch [27], Lubell et al. [7].

Shioya tested beams with depths ranging from 102 mm to 3.0 m and found that the shear stress at failure for the largest beam was reduced by one third with respect to the smallest beams. Collins and Kuchma drew similar conclusions from their experimental work. It was found that lightly reinforced high strength concrete beams are more sensitive to shear strength reduction due to the size effect. The same conclusions are drawn based on the experiments on large wide beams by Lubell et al.

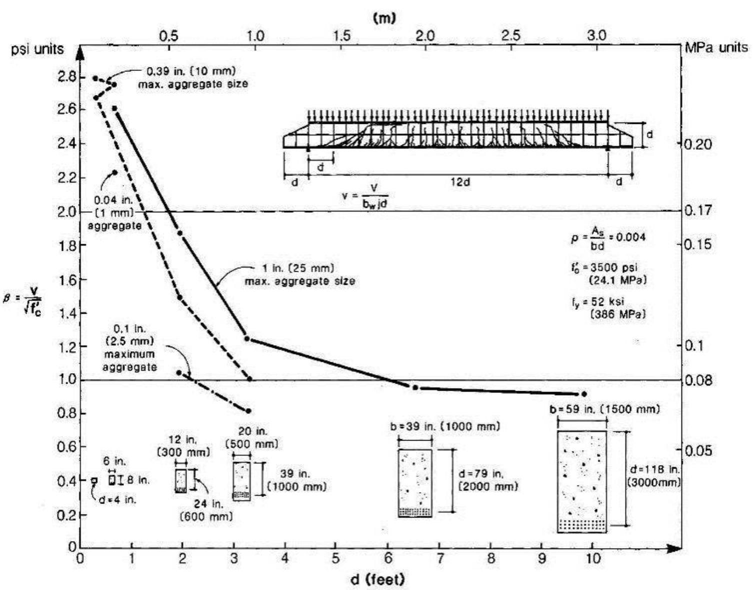

Fig. 3.17 –Shioya's test result for the size effect on the shear strength of concrete beams without transverse reinforcement (from Collins & Mitchell [3])

In general, it is assumed that the size effect is caused by larger crack widths and inherent loss of aggregate interlock mechanisms. Assuming that the main crack width of diagonal cracks is the product of average strain in the longitudinal reinforcement and the crack spacing, Collins [8] found that the size effect is significantly lower for beams with longitudinal reinforcement well distributed along the depth of the beam cross section.

Moreover, since the roughness of a crack interface is inherent to the aggregate size of concrete, the relative roughness of the shear crack decreases for constant particle size and increasing member depth. Considering this, the size effect for shear will even be more important in case of high strength concrete, were the roughness decreases due to fracture of the aggregates.

Using fracture mechanics, Bazant [64] has explained the size effect on the basis of energy release on cracking. The amount of energy released, increases with an increase in size, particularly in depth. Although a portion of the size effect can be attributed to an energy release, Bazant found that the crack-width explanation of size effects fits the test data trends more closely. From another point of view, Bazant and Kim [28] proposed a rational theory for the size effect based on non-linear fracture mechanics where it is assumed that the energy release rate by the formation of a shear crack increases for larger members. It is suggested that there is a transition between a ductile failure related to the strength criterion and the linear elastic fracture mechanics (see Fig. 3.18). The structural size effect factor k, artificially reducing the material strength, as proposed by Bazant is given by (Eq. 3.20).

$$k = \frac{1}{\sqrt{1 + \frac{d_a}{d\lambda_0}}} \qquad \text{Eq. 3.20}$$

with d_a the aggregate size, d the depth of member and λ_0 an empirical constant.

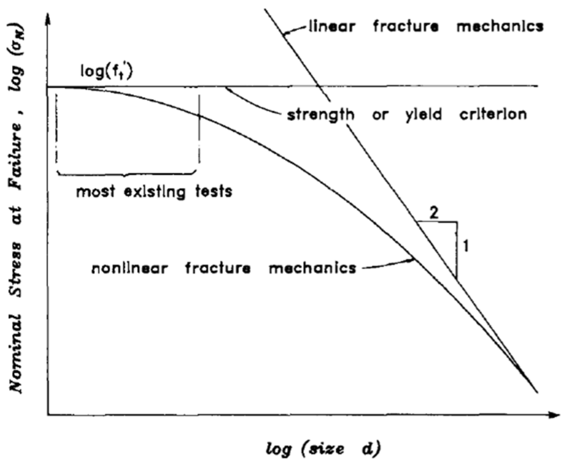

Fig. 3.18 – Size effect as a transition between the strength criterion and linear elastic fracture mechanics (Bazant & Kim [28]).

Other well-known empirical based size effect factors were implemented in the shear strength equations as proposed in RILEM [29] (Eq. 3.21) and EC2 [30] (Eq. 3.22).

$$k = \frac{1600 - h}{1000} \quad (\geq 1) \qquad \text{Eq. 3.21}$$

$$k = 1 + \sqrt{\frac{200}{d}} \quad (\leq 2) \qquad \text{Eq. 3.22}$$

3.1.4.3 Axial force

From a theoretical point of view, the presence of an axial force will cause an increase of first shear crack load and influences the strut inclination. Shear forces acting in a cross section cause principal stresses to occur in the web. When the principal stresses reach the concrete tensile strength, a shear crack will be formed. Due to the presence of a prestress force, the shear stress magnitude needed to cause diagonal cracking is increased. Considering a Mohr's circle, the influence of a prestress force on the cracking shear stress of a beam can be calculated as follows:

$$\tau_{cr} = \sqrt{f_{ct}^2 + f_{ct}\sigma_{cp}} = f_{ct}\sqrt{1 + \frac{\sigma_{cp}}{f_{ct}}} \qquad \text{Eq. 3.23}$$

In which τ_{cr} is the cracking shear stress, f_{ct} is the tensile strength of concrete and σ_{cp} is the compressive stress due to prestress forces.

Secondly the shear crack inclination angle is influenced by the presence of an axial force. Even for non-prestressed members when considering flexural shear cracking, the shear crack inclination tends to be flatter in the concrete compressive zone than for the bottom shear cracks. In case of a prestress force, the shear crack inclination angle will be lower than 45° and for elements subjected to an axial tensile force, the shear crack inclination will be higher than 45°.

3.1.4.4 Longitudinal reinforcement ratio

The effect of increasing longitudinal reinforcement ratio on the shear strength of members without transverse reinforcement is attributed to the reduction of crack widths and inherent increase of aggregate interlock (see Section 3.1.3). Further, the contribution of dowel action is directly related to the amount of longitudinal reinforcement.

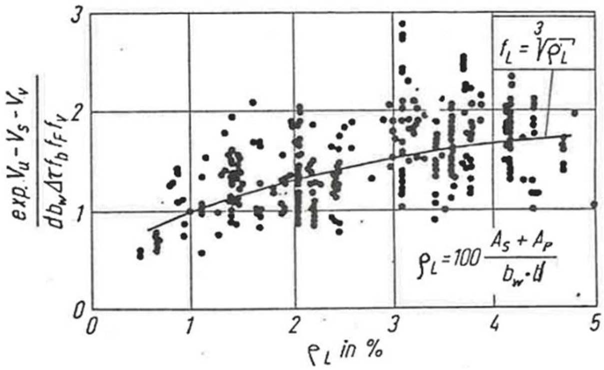

Fig. 3.19 – Influence of longitudinal reinforcement according to Kordina et al[31].

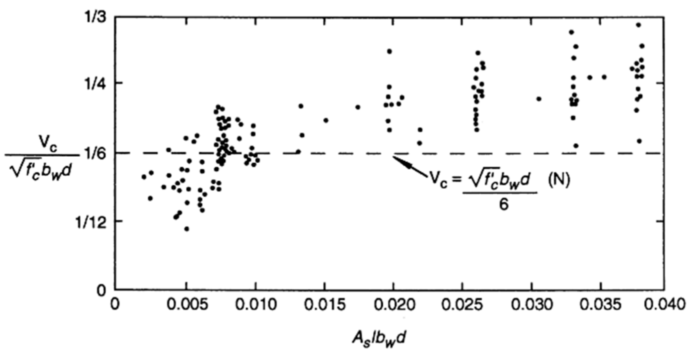

Fig. 3.20 – Influence of longitudinal reinforcement on the shear capacity of RC beams without stirrups (from MacGregor [32])

As can be seen on Fig. 3.19 and Fig. 3.20, the shear capacity is increasing for higher longitudinal reinforcement ratios. However, the observed increase is less than proportional and often related to the cube root of ρ_l . Further, it can be noticed that the simplified shear strength equation according to ACI 318 (see also section 3.1.5) is only valid for longitudinal shear reinforcement ratio values higher than 1%. On the other hand, current shear strength equations as adopted in EC2 limit the increase of concrete shear strength contribution for values of ρ_l higher than 2%.

3.1.5 Shear strength models

Based on literature survey, the available shear strength models can be divided in two main groups: models based on rational approaches and pure empirically determined shear strength models. The first group of rational approaches can be further divided in three main sub-groups of shear strength models based on:

1) Kani’s model

2) Plasticity theory

3) (Modified) Compression Field Theory (CFT/MCFT)

3.1.5.1 Kani's model

Kani [25] considered a beam cracked in bending as a concrete comb, with the compressive zone as a backbone and the concrete in between flexural cracks as concrete teeth (Fig. 3.21). In his theory, two possible types of failure are considered. The beam-like behaviour occurs when the bending capacity of a concrete tooth is exceeded. When the concrete teeth resistance vanishes, the remaining arch is providing shear resistance, which can be significantly higher.

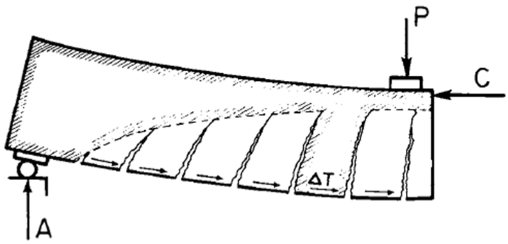

Fig. 3.21 – Comb-like representation of a RC beam subjected to shear and bending (Kani, [25])

In Fig. 3.14 in Section 3.1.4, Kani distinguished two shear governing regions. In the first region (0 < a/d < 2.5), the arch contribution is higher than the strength of concrete teeth. Hence, the shear failure is governed by the arch-action and shear failure is obtained when the compressive strength of the arch has been reached. For a/d-values in between 2.5 and 5.6, the shear failure is governed by the strength of the concrete teeth and beam-failure will occur.

3.1.5.2 Plasticity theory

The most important work in the field of the plasticity theory for the analysis of shear in reinforced beams has been done by Nielsen [33]. For a detailed description background description of the theory reference is made to [33]. In the following, a short description of the main principals behind the theory are discussed.

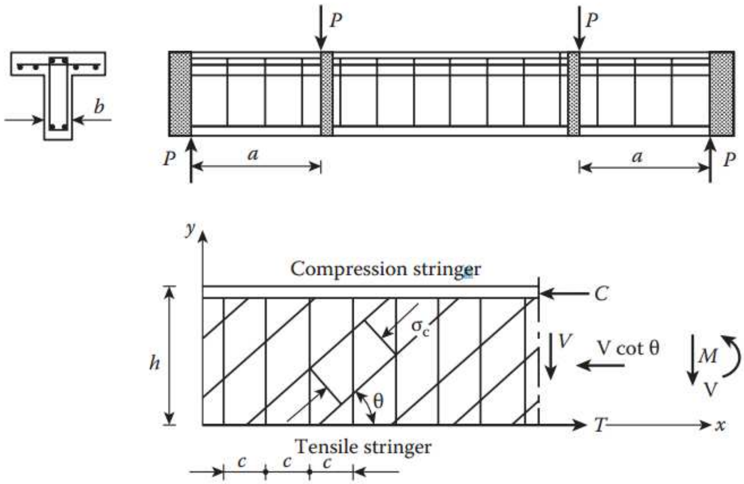

Fig. 3.22 – Geometrical definitions for the plasticity theory (from Nielsen [33])

Considering the vertical shear reinforcement being placed at a constant distance c and b the width of the beam, the transverse reinforcement ratio is defined as

$$\rho_w = \frac{A_s}{cb} \qquad \text{Eq. 3.24}$$

From the shear stress, which is assumed to be constant along the cross-sectional height, the compressive stress in the inclined struts can be obtained from:

$$\sigma_c = \tau\left(\tan\theta + \cot\theta\right) \qquad \text{Eq. 3.25}$$

Further, it is assumed that the vertical stress is equal to zero and the stress in the shear reinforcement can be obtained by

$$\sigma_s = \frac{\tau \tan\theta}{\rho_w} \qquad \text{Eq. 3.26}$$

The basic assumptions of the plasticity theory is that a safe stress field for an RC beam is obtained when the concrete compressive stress is lower than the compressive strength and that the tensile stress in the reinforcement is lower than the yield strength. Hence, the best lower bound solution is found for the following value of the shear stress:

$$\tau = f_c\sqrt{\psi\left(1-\psi\right)} \qquad \text{Eq. 3.27}$$

In which

$$\psi = \frac{\rho_w f_{yw}}{f_c} \qquad \text{Eq. 3.28}$$

From the work equations considered for finding the upper bound solution [33], an identical formulation as for the lower bound solution can be found (cf. Eq. 3.27). Considering the geometrical boundary conditions for the development of the shear crack, the ratio between projected crack length and beam height is taken into account, yielding the following relationship:

$$\tau = \frac{1}{2}\left[\sqrt{1+\left(\frac{a}{h}\right)^2} - \frac{a}{h}\right] + \psi\frac{a}{h} \qquad \text{Eq. 3.29}$$

Both the curves defined by Eq. 3.27 and Eq. 3.29 are shown in Fig. 3.23.

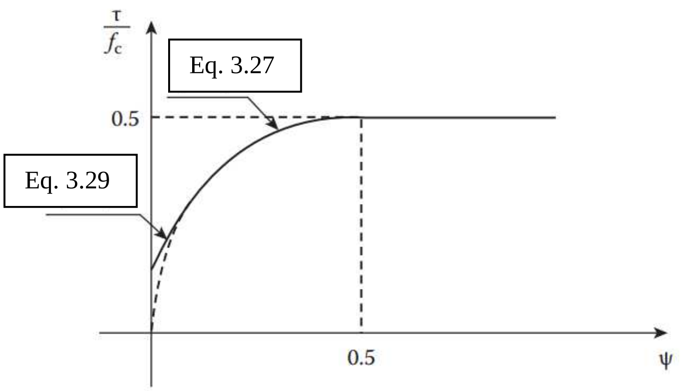

Fig. 3.23 – Geometrical definitions for the plasticity theory (from Nielsen [33])

As can be seen from Fig. 3.23, the shear strength cannot be further increased for values of ψ higher than 0.5.

Although the theory presented herein has an analytical basis, empirical factors have been introduced in order to take into account the effects of element size, longitudinal reinforcement ratio and prestress in order to reduce or to enhance the effectiveness of the compressive strength f_c. For a more detailed description of these reduction parameters, reference is made to Chapter 7, Section 7.2.4, in which the application of the plasticity model for the evaluation of the shear strength of SFRC is discussed.

3.1.5.3 Modified Compression Field Theory

The compression field theories applied for the analysis of the shear resistance of both prestressed and reinforced concrete beams, originates from the tension field theory as proposed by Wagner in 1929 in order to evaluate the residual shear resistance of thin webbed metal girders [34]. In his theory, Wagner assumed that the angle of inclination of the diagonal tensile stresses coincide with the angle of inclination of the principal tensile strains. Applying the theory for reinforced concrete, the shear resistance of the concrete web will be provided by the diagonal compression of the struts.

By using the appropriate equilibrium and compatibility equations from the compression field theory, the complete load-deformation of a member subjected to shear can be obtained. However, the compression field theory neglects the residual tensile stresses in the compression struts and as a result, deformations are overestimated and conservative shear strength capacities are obtained.

To incorporate the effect of residual tensile stresses, caused by tension stiffening of the concrete in between the inclined shear cracks, the modified compression field theory (MCFT) was developed by Collins and Mitchell in 1986 [35]. Fig. 3.24 shows the complete set of equilibrium and compatibility equations that has to be solved for a given state of deformation, expressed in terms of principal strains.

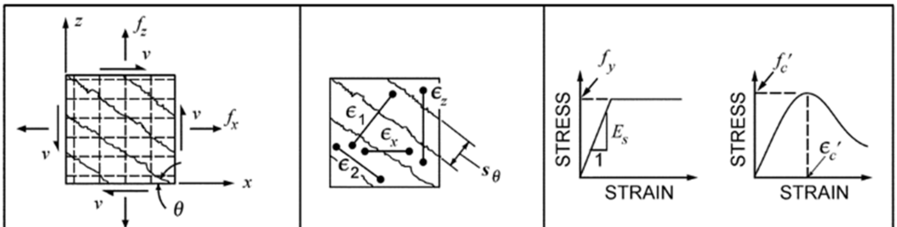

Equilibrium:

Average Stresses:

$$f_x = \rho_x f_{sx} + f_1 - v\cot\theta \quad (1)$$

$$f_z = \rho_z f_{sz} + f_1 - v\tan\theta \quad (2)$$

$$v = (f_1 + f_2)/(\tan\theta + \cot\theta) \quad (3)$$

Stresses at Cracks:

$$f_{sxcr} = (f_x + v\cot\theta + v_{ci}\cot\theta)/\rho_x \quad (4)$$

$$f_{szcr} = (f_z + v\tan\theta - v_{ci}\tan\theta)/\rho_z \quad (5)$$

Geometric Conditions:

Average Strains:

$$\tan^2\theta = \frac{\epsilon_x + \epsilon_2}{\epsilon_z + \epsilon_2} \quad (6)$$

$$\epsilon_1 = \epsilon_x + \epsilon_z + \epsilon_2 \quad (7)$$

$$\gamma_{xz} = 2(\epsilon_x + \epsilon_2)\cot\theta \quad (8)$$

Crack Widths:

$$w = s_\theta \epsilon_1 \quad (9)$$

$$s_\theta = 1 \Big/ \left(\frac{\sin\theta}{s_x} + \frac{\cos\theta}{s_z} \right) \quad (10)$$

Stress-Strain Relationships:

Reinforcement:

$$f_{sx} = E_s \epsilon_x \le f_{yx} \quad (11)$$

$$f_{sz} = E_s \epsilon_z \le f_{yz} \quad (12)$$

Concrete:

$$f_2 = \frac{f_c'}{0.8 + 170\epsilon_1}\left[2\frac{\epsilon_2}{\epsilon_c'} - \left(\frac{\epsilon_2}{\epsilon_c'}\right)^2 \right] \quad (13)$$

$$f_1 = 0.33\sqrt{f_c'} \Big/ \left(1 + \sqrt{500\,\epsilon_1}\right) \text{ MPa} \quad (14)$$

Shear Stress on Crack:

$$v_{ci} \le \frac{0.18\sqrt{f_c'}}{0.31 + \dfrac{24\,w}{a_g + 16}} \text{ MPa, mm} \quad (15)$$

Fig. 3.24 – Set of 15 equations of the MCFT (Bentz [21])

Assuming that in a cracked concrete section of a beam subjected to both shear, axial forces and bending moments, there are no vertical stresses and the stress in the web reinforcement equals the yield stress at maximum shear strength, Eq. 5 from Fig. 3.24 can be rewritten as:

$$v = v_{ci} + \rho f_y \cot\theta \qquad \text{Eq. 3.30}$$

Similarly, Eq. 2 from Fig. 3.24 can be rearranged as

$$v = f_1 \cot\theta + \rho f_y \cot\theta \qquad \text{Eq. 3.31}$$

In Eq. 3.30 and Eq. 3.31, v is the average shear stress, v_{ci} is the local shear stress due to friction at the crack surface and f_1 is the principal tensile stress.

Based on the MCFT, both the value of v_{ci} and f_1 are related to the concrete compression strength and hence, Eq. 3.30 and Eq. 3.31 can be rewritten in a general form of a concrete contribution v_c and a contribution of stirrups v_s:

$$v = v_c + v_s = \beta\sqrt{f_{cm}} + \rho f_y \cot\theta \qquad \text{Eq. 3.32}$$

with

$$\beta = \min\begin{cases} \sim f_{1,res}(\varepsilon_1) \\ \sim v_{ci} \end{cases} \qquad \text{Eq. 3.33}$$

The first term in Eq. 3.33 represents the residual tensile stress of the concrete between cracks due to the existence of tension softening. The second term is accounting for the maximum frictional stresses that can be transmitted as a function of crack width. It should be noted that in the modified compression field theory, the aggregate interlock and tensile strength of the concrete is related to the square root of the concrete compressive strength. According to the MCFT, the tension softening curve of concrete after cracking is expressed as follows:

$$f_{1,res}(\varepsilon_1) = \left(\frac{C_1}{1+\sqrt{C_2\varepsilon_1}}\right)\sqrt{f_{cm}} \qquad \text{Eq. 3.34}$$

In which C_1 is equal to 0.33 and C_2, determined by curve fitting of test results equals 200, 500 and 1500 according to experimental work of Vecchio, Collins and Mitchell, and Tamai respectively [36].

The second term in Eq. 3.33 represents the shear stress capacity between cracks due to the existence of aggregate interlocking. Based on the experimental work conducted by Walraven [16], Vecchio [35] proposed the following simplified relationship:

$$v_{ci} = v_{ci,max}\left[0.18 + 1.64\frac{f_{ci}}{v_{ci,max}} - 0.82\left(\frac{f_{ci}}{v_{ci,max}}\right)^2\right] \qquad \text{Eq. 3.35}$$

with

$$v_{ci,max} = \frac{\sqrt{f_{cm}}}{0.31 + \dfrac{24w}{a_g + 16}} \qquad \text{Eq. 3.36}$$

According to Adebar & Collins [37], the shear strength of members without shear reinforcement, is found for a deformation situation representing intersection values for β taking into account Eq. 3.33 - Eq. 3.36. A number of different possibilities are summarized in Fig. 3.25.

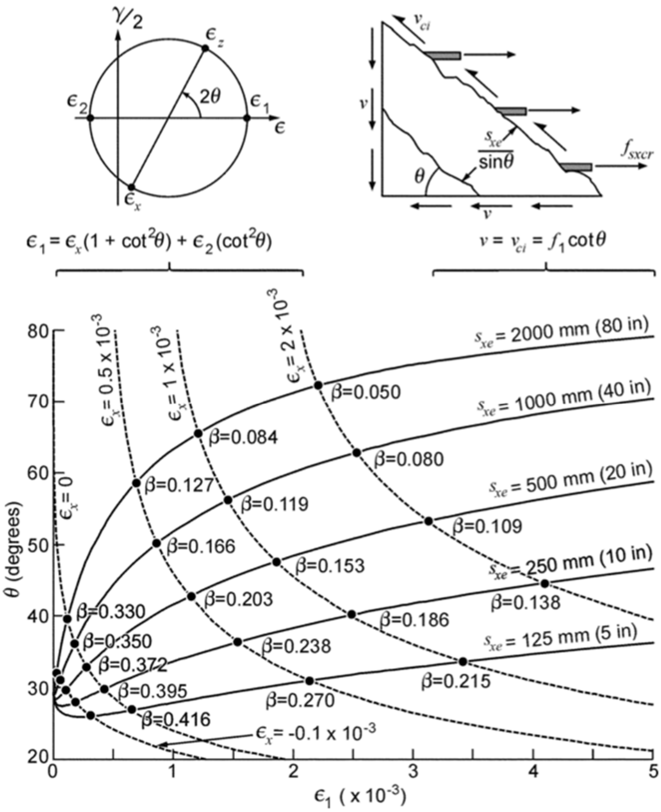

Fig. 3.25 – Concrete contribution factors β for different combinations size and strain deformation of a member (Bentz [21])

The longitudinal strain of a cross section is determined by taking into account both the bending moment and axial forces acting on a cross section, which are transformed in a principal tensile strain (ε_1). The crack width at which v_{ci} has to be evaluated is calculated as the product of the principal tensile strain and the average crack spacing $s_{xe}/\sin\theta$.

Although the MCFT is a well-established rational approach to solve the problem of shear, some remarks can be made:

- The influence of aggregate interlock has been introduced in the MCFT by the term v_{ci}, which is a function of crack opening and aggregate size. It should be noted that the shear slip displacement is not taking into account. However, based on the available aggregate interlock models, it is the relative increase of opening and sliding which will determine the magnitude of shear friction stresses.

- The concrete contribution term related to the residual tensile stresses has been evaluated from shear panel tests containing reinforcement. Hence, it is doubtful whether the suggested relationships are still valid for members without shear reinforcement.
- The MCFT, is a sectional analysis method which neglects the arch action contribution and for lower values of shear span to depth ratios, the shear strength will be underestimated.
- The deformation at mid-depth of the section is taken as half of the strain at the bottom of the cross-section. However, for prestressed sections with I- or T-shape this relationship can be different.

3.1.5.4 Empirical models

In order to provide an explanation for the shear strength capacity of reinforced concrete beams without transverse reinforcement, it is suggested by Morsch to take into account the tensile strength of the concrete in the truss model. The additional shear strength term attributed to the plain concrete is implemented in the most common shear strength formulas by the root of the concrete compressive strength. The simplest formulation is suggested by ACI as a lower bound for the shear capacity (Table 3.1, Eq. 3.37). However, this equation is only valid for longitudinal reinforcement ratios higher than 1%.

Additional research on the shear strength of reinforced concrete beams without stirrups has led to the development of improved empirical formulations taking into account the effect of three main parameters: longitudinal reinforcement ratio, size effect and shear span to depth ratio. In 1962, the ACI proposed a new equation based on 194 tests on beams subjected to both single and double point-loads and distributed loads. Later in 1977, it was decided by the ACI-ASCE committee 426 to no longer use the equation and to use the lower limit equation again.

In 1971, an empirical equation has been proposed by Zsutty [38] which takes into account all of the main influencing parameters except the size effect ratio. Hence, the use of Zsutty's equation will lead to an overestimation of the ultimate shear strength for beams with large depths. Other improvements were suggested in both the Model Codes 1978 and 1990 and later in the European Standard EN 1992 (EC2). The empirical formulation proposed in the MC78 resulted from a statistical analysis by Hedman and Losberg [39]. Later, the equations have been revised by Remmel [40] to the formulations now implemented in EC2.

An overview of the empirical equations as suggested by ACI, Zsutty, MC78 and EC2 is given in Table 3.1.

Table 3.1 - Overview of the most relevant empirical shear strength formula for RC beams without stirrups

ACI (lower bound solution)	$v = \frac{\sqrt{f_{cm}}}{6}$	Eq. 3.37
ACI [1962]	$v = \frac{1}{7}\left(\sqrt{f_{cm}} + 120\rho\frac{d}{a}\right)$	Eq. 3.38
Zsutty [1971]	$v = 2.138\left(f_{cm}\frac{d}{a}\rho_l\right)^{1/3}$	Eq. 3.39
MC78 [1978]	$v = 0.092k\left(1+50\rho_l\right)\sqrt{f_{cm}}$, with $k = 1.6 - d\ (\leq 1)$	Eq. 3.40
EN 1992 (EC2) [1994]	$v = C_R k\left(100\rho_l f_{cm}\right)^{1/3}$, with $k = 1 + \sqrt{\frac{200}{d}}$ and with C_R an empirical constant equal to 0.18	Eq. 3.41

When concrete members are subjected to a prestressing force (it is further assumed that prestress cables are straight and consequently, no vertical shear strength component has to be taken into account), both the approaches suggested by the ACI and EC2 differentiate between zones with and without the occurrence of flexural cracks. Due to the presence of a prestress force, it is possible that web shear cracks occur when the lower flange is still under compression. A schematic of a crack pattern with these different zones is shown in Fig. 3.26.

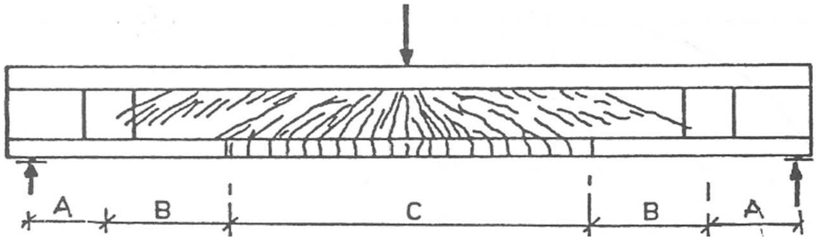

Fig. 3.26 – Difference between zones with web shear crack and flexural shear cracks

In Fig. 3.26, zone A represents the zone in which the prestress forces are not yet fully developed. However, in this end zone of the prestressed beams, the web is often wider and shear cracks will not develop. In zone B, web shear cracks are likely to occur prior to flexural cracks. In zone C, flexural cracks are likely to occur and for zones with relatively high shear forces, the flexural cracks become shear critical cracks.

According to ACI 318-11 [41], the concrete shear capacity shall be taken as the lowest value of V_c determined by means of the following equations:

$$V_c = \min\begin{cases} V_{ci} = \dfrac{\sqrt{fcm}}{20} b_w d + V_d + \dfrac{V_i M_{cr}}{M_u} & \text{Eq. 3.42} \\ V_{cw} = 0.3\left(\sqrt{fcm} + \sigma_{cp}\right) b_w d & \text{Eq. 3.43} \end{cases}$$

The equation for V_{ci} yields the shear capacity considered in zone C, taking into account the shear force needed to induce a flexural crack and an increment to change the flexural crack to a flexural shear crack. For zone B, the shear capacity of the web V_{cw} is evaluated by means of Eq. 3.43

According to the EC2 [30], the location of zones B and C shall be determined by the verification of tensile stresses at the bottom fibre of the cross-section. The zone C starts where the tensile stress exceeds the tensile strength of concrete in the serviceability limit state. For zones uncracked in bending, a linear elastic calculation of the principal tensile stress is conducted (Eq. 3.44).

$$V_c = \frac{Ib_w}{S}\sqrt{f_{ctm}{}^2 + \sigma_{cp} f_{ctm}} \qquad \text{Eq. 3.44}$$

In case of a load situation for which the concrete tensile strength is not reached due to the effect of shear stresses and no shear cracks are formed in the ultimate limit state, a minimum amount of web shear reinforcement has to be provided in order to meet ductility requirements.

When a cross-section is cracked in bending, the flexural shear capacity is determined by means of Eq. 3.45.

$$V_c = \left[C_R k \left(100 \rho_l f_{cm}\right)^{1/3} + C_p \sigma_{cp} \right] b_w d \qquad \text{Eq. 3.45}$$

Similar to the equation for sections in zone C, the beneficial effect of a prestress force is taken into account by an additional term which represents the increase of external loading to induce flexural cracking. In its original form [42], the value of C_p has been assumed to be equal to

$$C_p = 0.096 \frac{A_c}{b_w d} \sigma_{cp} \qquad \text{Eq. 3.46}$$

Typically, for T- or I-shaped prestressed girders, the ratio of gross concrete section to the product of effective depth and web width is equal to 2 and the value of C_p has been taken as 0.2 which was later reduced to 0.15

3.2 Shear strength models for SFRC

3.2.1 Historical development

One of the first reports in literature regarding the shear strength of fibre reinforced concrete beams has been done by Batson et al. in 1972 [43]. At that time, it was still believed that the concrete tensile strength could be increased by adding high percentages of short fibres. Based on their experimental investigation, it was concluded that adding fibres to concrete altered the failure mode for FRC beams from bending to shear.

From then, research efforts in the field of shear strength of FRC elements have evolved together with the development of other types of fibres and concrete. During the past decades, the most relevant investigations towards the shear capacity of reinforced SFRC beams were done by Swamy (1985) [44], Mansur (1986) [45], Al Ta'an & Al Feel (1990) [46], Ashour (1992) [47], Imam (1995) [48, 49], Casanova (1997) , Khuntia (1999) [50], Gustaffson (1999) [51], Kwak (2002) [52]; Nogabai (2000) [53], Rosenbusch & Teutsch (2003) [54],Cucchiara (2004) [55], Greenough, (2008) [56], Cho (2009) [57], Dinh (2010) [58], Aoude (2012) [59], Parmentier (2012) [60], Ding (2012) [61], Conforti (2014) [62].

One of the main drawbacks of all of these studies is that the size of test specimen is relatively small with respect to real practical situations. Furthermore, the majority of these investigations and inherent shear strength models for SFRC are not dealing with the presence of a prestressing force. One of the first experimental investigations for the shear strength of prestressed SFRC elements has been conducted by Narayanan & Darwish in 1987 [63]. More recently, a significant step in research towards the influence of fibre reinforcement on the shear strength of full-scale precast girders has been undertaken by Minelli (2005) [64], Voo (2006) [65], De Pauw (2008) [66] and Cuenca (2012) [67].

Given the current approaches to characterise the post-cracking tensile strength of SFRC, several of these models can be considered as outdated. One of the first shear strength models taking into account the residual flexural parameters as derived by the standard bending test according to EN 14651, has been proposed by Minelli [64]. Based on the shear tests of both reinforced and prestressed SFRC beams, the existing shear strength equation for concrete cracked in bending was modified. Eventually, this model has been included in the Model Code 2010 [68] chapter 7 dealing with the design of SFRC.

As a general remark regarding the available shear strength models it should be mentioned that the majority of them are not taking into account the effect of prestress on the shear capacity.

With respect to the way in which the beneficial effect of fibres is considered into the shear strength equations, the developed models can be divided in basically two groups:

(1) A first group takes into account the effect of fibres by means of a fibre factor (i.e. direct method). One of the first design guidelines concerning the shear strength based on a direct approach has been suggested in:

- DRAMIX guideline (1995)

(2) The second group explicitly takes into account the post-cracking behaviour as derived from material testing (i.e. the indirect method). The latter is now recognized to be the best approach to design the shear strength since the post-cracking flexural parameters reflect the scatter of SFRC mix and as a consequence will yield a safe design. Based on the experimental work conducted over the past five decades, recent international codes have implemented design equations for the shear design of FRC beams. The most relevant design guidelines for the shear strength of SFRC elements are chronologically ordered and discussed below:

- RILEM (2003)
- CNR-DT (2006)
- ACI (2008)
- MC2010 (2012)

3.2.2 Models based on direct methods

3.2.2.1 Empirically based

The majority of developed strength models is based on experimental calibration, in which the shear strength component due to the presence of fibres is superposed to the shear strength of the plain concrete. The total shear capacity is then expressed as:

$$V_u = V_c + V_{fibres} \qquad \text{Eq. 3.47}$$

In which V_c and V_F are the concrete and fibre contribution respectively. The concrete contribution term has been explained in more detail in Section 3.1. For the additional shear strength due to the presence of fibres, V_F is calculated by taking into account the post-cracking residual stress. This has been proposed first by Mansur [45] in 1986 and was further improved for other combinations of concrete and fibres, fibre type and dosage by the investigations of Narayanan [69], Al Ta'an & Al Feel [46], Ashour [47], Imam [48, 49], Khuntia [50], Kwak [52], Choi [70] and Greenough [56].

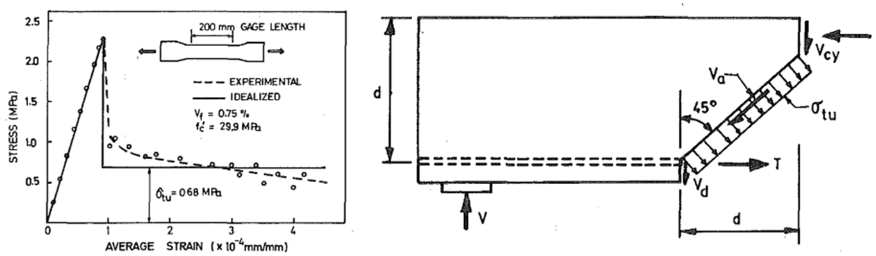

Fig. 3.27 – Determination of post-cracking tensile strength and the shear strength model as proposed by Mansur [45].

Taking into account the model of Fig. 3.27 in which a crack plane inclination angle is assumed equal to 45°, the general expression Eq. 3.47 can be rewritten as:

$$V_u = V_c + \sigma_{tu} bd \qquad \text{Eq. 3.48}$$

In order to adopt a correct value of σ_{tu}, tensile tests have to be performed or values can be estimated by means of indirect methods as described in Section 2.3.4. Alternatively, and as often applied in the available literature, the post-cracking tensile strength of SFRC is calculated taking into account the sum of single fibre contributions σ_f, and the general formulation adopted to evaluate the additional strength can be written as

$$\sigma_{tu} = \frac{N_f}{A_{cr}} \sigma_f \qquad \text{Eq. 3.49}$$

The number of fibres crossing a unit crack plane is given by

$$\frac{N_f}{A_{cr}} = \alpha_e \frac{V_f}{\pi r_f^2} \qquad \text{Eq. 3.50}$$

In which α_θ is the effectiveness factor due to the oriention of fibres. Assuming all fibres being randomly distributed [71], the effectiveness factor α_e is calculated as follows: for N fibres with a length L_f, the average fibre length projected on the x-axis (Fig. 3.28) is given by:

$$\frac{N \int_0^{\frac{\pi}{2}} \int_0^{\frac{\pi}{2}} \cos\phi \cos\vartheta \, d\phi \, d\vartheta}{N \left(\frac{\pi}{2}\right)^2} = 0.4053 L_f \qquad \text{Eq. 3.51}$$

Eq. 3.51 shows that only 41 percent of the fibre volume is effectively contributing to the post-cracking tensile capacity of the FRC.

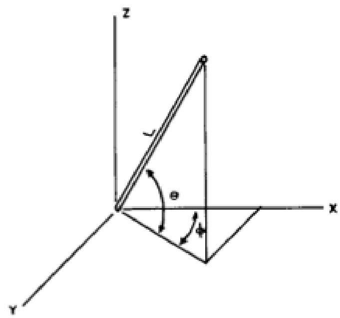

Fig. 3.28 – Projection of fibre length on the x-axis

Assuming a constant bond stress τ_b along a fibre and an averaged embedded length of $L_f/4$, the average pull-out force of a fibre σ_f is given by

$$\sigma_f = \tau_b \frac{\pi d_f L_f}{4} \qquad \text{Eq. 3.52}$$

Combining Eq. 3.49 and Eq. 3.50, the post-cracking tensile strength can be estimated by

$$\sigma_{tu} = \alpha_e \tau_b F \qquad \text{Eq. 3.53}$$

In which F is the fibre factor given by

$$F = V_f \frac{L_f}{d_f} \qquad \text{Eq. 3.54}$$

For a given cross-section , the fibre factor represents the relative amount of fibres in terms of fibre dosage and slenderness of fibres.

In literature, different values for τ_b and α_e are suggested based on experimental observations. Hence, the method is inherent to a specific combination of concrete and fibre type and is not generally applicable. In order to overcome this issue, a bond efficiency factor η has been introduced to take into account the fibre anchorage capactiy as a function of fibre shape. As a result, the general equation for the estimation of post-cracking tensile strength of SFRC is given by

$$\sigma_{tu} = \eta_b \alpha_e \tau_b F \qquad \text{Eq. 3.55}$$

Al Ta'an [72] suggested a bond efficiency factor for hooked and crimped fibres equal to 1.2 and 1.3 respectively. According to Khuntia [50], a bond efficiency factor of 1 was taken into account for the case of hooked-end steel fibres. It is suggested to apply a reduction factor of 0.67 for plain round fibres in combination with normal strength concrete and 0.75 for hooked and crimped fibres in a light-weight concrete matrix.

Regarding the value of the anchorage bond stress (Eq. 3.55), different values have been proposed in literature. The most important references are listed in Table 3.2.

Table 3.2 – Expression for the average anchorage bond stress according to several researchers

Researcher	Bond stress [N/mm²]
Narayanan & Darwish [69]	4.15
Swamy[44]	5.12
Lim [73]	6.80
Khuntia [50]	$0.68\sqrt{f_{cm}}$
Marti [74]	$0.60 f_{cm}^{2/3}$
Voo & Foster [75]	Hooked $\sqrt{f_{cm}}$ Straight $0.60\sqrt{f_{cm}}$

All of the proposed expressions for the anchorage bond stress of fibres are also visualised as a function of concrete compressive strength in Fig. 3.29.

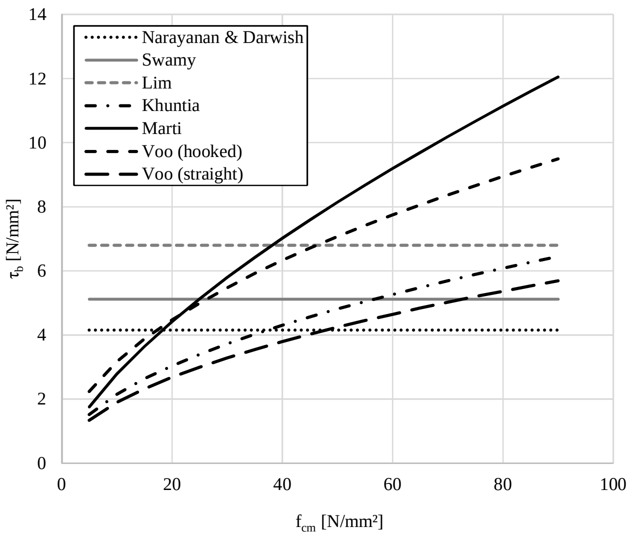

Fig. 3.29 – Comparison of different equations for the anchorage bond stress

It is clear form Table 3.2 and Fig. 3.29 that the assumption of a correct value of the bond stress is difficult and has been determined for specific fibre and concrete types which leads inevitable to an increase of model uncertainty for the considered shear strength models. Furthermore, a huge drawback of these methods is that the real pull-out behaviour of fibres is ignored and the composite behaviour is not taken into account by means of material testing.

3.2.2.2 Models based on the MCFT

Two different models based on the constitutive and equilibrium conditions as described in the modified compression field theory, are developed by Kim et al. [76] and by Ding et al. [61]. Both of the models take into account the beneficial effect of fibres by relating the principal tensile stress of concrete after cracking to the fibre dosage (see Fig. 3.30).

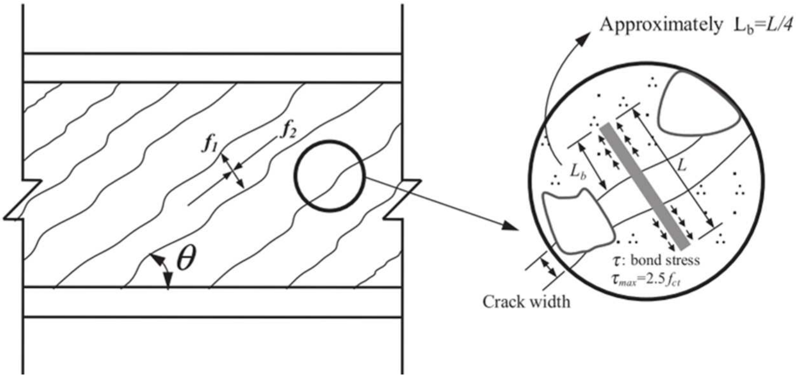

Fig. 3.30 – Concept of fibres providing post-cracking strength to a cracked thin web subjected to shear (from [76])

However in doing so, an outdated (as discussed earlier in Section 3.2.1) approach is adopted i.e. lumping the average bond stress for all fibres crossing the crack plane. An example of the error made when assuming an idealised bond strength in stead of the real pull-out behaviour of a fibre is shown in Fig. 3.31.

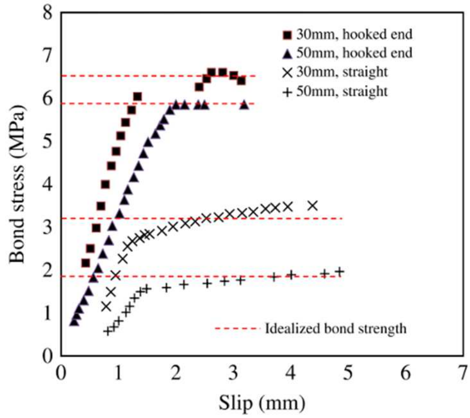

Fig. 3.31 – Comparison between idealised and experimentally obtained bond strength capacity (from [76])

In the model proposed by Ding, the principal tensile stresses in between the concrete compressive struts are taken as the sum of both the residual tensile stress due to tension softening and the post-cracking tensile strength related to the fibre pull-out mechanism.

However, when only fibres are used as shear reinforcement, the tension stiffening effect will be vanished. It can be concluded that the new concept of taking into account fibres into the calculation procedures of the MCFT is an improvement but that the implementation should be further optimized and evaluated.

3.2.2.3 DRAMIX Guideline (1995)

In 1992, it was decided by the Belgian fibre manufacturing company Bekaert to provide a guideline for the shear design of SFRC with or without traditional reinforcement based on a survey of the state-of-the-art research. In order to fulfil this task, a scientific committee was assembled in 1993 whose efforts resulted into the DRAMIX guideline [77] which was aimed to serve as a possible draft to be implemented in the new version of the Eurocode 2 about that time.

In general, the design shear strength of steel fibre concrete beams is calculated as the sum of a concrete contribution V_c and a fibre contribution V_F:

$$V_{Rd} = V_{cd} + V_{Fd} \qquad \text{Eq. 3.56}$$

The concrete contribution is similarly calculated as in Model Code 1990 (MC90) or the current European standard EN 1992-1-1 (Eurocode 2):

$$V_{cd} = \left(\frac{0.18}{\gamma_c} \cdot k \cdot \left[100 \cdot \rho_l \cdot f_{ck}\right]^{1/3} + 0.15 \cdot \sigma_{cp} \right) \cdot b_w \cdot d \qquad \text{Eq. 3.57}$$

In which k is a size effect factor to reduce the average ultimate shear stress as a function of increasing depth of members, given by

$$k = 1 + \sqrt{\frac{200}{d}} \qquad \text{Eq. 3.58}$$

The average compressive stress σ_{cp} acting in the member caused by a prestressing force is calculated by means of Eq. 3.59.

$$\sigma_{cp} = \frac{\eta f_{p0} \left(A_{p,sup} + A_{p,bot} \right)}{A_c} \qquad \text{Eq. 3.59}$$

In which f_{p0} is the initial prestress in the strands and A_c is the total area of the concrete section. The section of prestressing strands in the lower region and the upper region are denoted as $A_{p,bot}$ and $A_{p,top}$ respectively. When the prestress losses are not explicitly mentioned in literature, a loss coefficient factor η is chosen equal to 0.8.

The longitudinal reinforcement ratio ρ_l is given by

$$\rho_l = \frac{\left(A_s + A_{p,bot} \right)}{b_w d} \qquad \text{Eq. 3.60}$$

For design, the values of k, the longitudinal reinforcement ratio ρ_l and the compressive stress are limited to 2, 0.02 and 0.2 f_{cd} respectively, in order to cut off the beneficial effect of these parameters. However, for evaluation of the shear strength formulation and comparison with test results, these limitations are not applied when calculating the ultimate shear strength of steel fibre concrete beams.

For the fibre contribution $V_{F,}$ the suggested approach is similar to the shear strength equations developed based on the fibre factor. It should also be noted that the DRAMIX guideline only applies for uncoated fibres with hooked ends. The shear strength provided by the addition of fibres is calculated as follows:

$$V_{fd} = k_f \tau_{fd} b_w d \qquad \text{Eq. 3.61}$$

In which k_f is a factor taking into account the beneficial effect of flanges to the shear strength of I and T-shape cross-sections given by:

$$k_f = 1 + n\left(\frac{h_f}{b_w}\right)\left(\frac{h_f}{d}\right) \leq 1.5 \qquad \text{Eq. 3.62}$$

with

$$n = \frac{(b_f - b_w)}{h_f} \leq \begin{cases} 3 \\ 3 \times \dfrac{b_w}{h_f} \end{cases} \qquad \text{Eq. 3.63}$$

The shear strength supplement due to steel fibres τ_{fd} is calculated by:

$$\tau_{fd} = 0.54 \frac{f_{ctk,ax} R_t}{\gamma_c} \qquad \text{Eq. 3.64}$$

with $f_{ctk,ax}$, the characteristic value of the axial tensile strength of concrete and R_t, a factor used to calculate the post-cracking stress of the SFRC as a fraction of the axial tensile strength. For uncoated hooked-end steel fibres, the DRAMIX guideline suggests to derive R_t as follows:

$$R_t = 1.1\left(\frac{F}{0.459 + F}\right) \qquad \text{Eq. 3.65}$$

3.2.3 Models based on indirect methods

3.2.3.1 Plasticity model

The theory of plasticity has been developed to calculate the strength of both plain and reinforced concrete successfully in the past. With respect to shear, different equations have been proposed and validated with respect to experimental data by Thurlimann and Nielsen [33]. Since fibres are providing post-cracking ductility to concrete and tensile stresses can be transmitted up to relatively large crack widths, SFRC can be considered as a material with high plasticity. Regarding this hypothesis, it was first proposed by Voo et al. [78] to use the plasticity theory to evaluate the shear strength of steel fibre reinforced reactive powder concrete prestressed girders. In the proposed model, the effect of the flanges for T- or I-shaped section is neglected.

The upper bound solution [33] for determining the shear strength of a simply supported concrete beam with rectangular cross-section and loaded with two symmetrically positioned concentrated point loads, is given by

$$V_u = \frac{1}{2} f_c^* bh \left(\sqrt{1 + \left(\frac{x}{h}\right)^2} - \frac{x}{h} \right) \qquad \text{Eq. 3.66}$$

in which f^*_c is the effective concrete compressive strength in N/mm² given by

$$f_c^* = \nu_c f_{cm} \qquad \text{Eq. 3.67}$$

At the ultimate state of shear failure, the concrete struts are subjected to both compressive strains and tensile strains perpendicular to the strut inclination. As a result of this biaxial strain state, the compressive strength of the concrete will be significantly reduced with respect to a uniaxial compressive behaviour. This compression softening phenomena is implemented in the plasticity theory by means of empirical factors based on both material and geometrical properties. The reduction factor is given by Eq. 3.68.

$$\nu_c = 1.2\left(\frac{3.5}{\sqrt{f_{cm}}}\right)(15\rho_l + 0.58)\left[0.27\left(1 + \frac{1}{\sqrt{h}}\right)\right]\left(1 + 0.2\frac{10}{f_{cm}}\right) \qquad \text{Eq. 3.68}$$

The geometrical parameters used in Eq. 3.66, are the height of the beam h, the width of the beam b and the projected length of the critical shear crack on the horizontal axis x. A schematic figure is shown in Fig. 3.32.

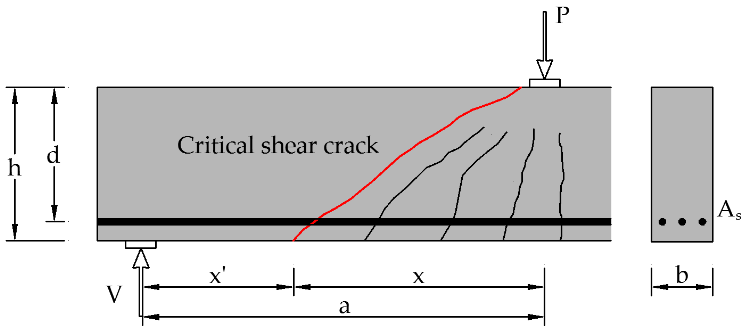

Fig. 3.32 – Geometrical parameters considered for the plasticity theory.

The plasticity theory was first used by Voo et al. [78] to investigate the shear capacity of prestressed Reactive Powder Concrete (RPC) girders by means of the Variable

Engagement Method. Zhang [79] & Voo [78] proposed to evaluate the ultimate shear strength as given by Eq. 3.69 with respect to the cracking load which is needed to exhaust the shear critical crack.

$$V_{cr} = \frac{1}{2} f_t^* b \frac{h^2 + x^2}{a} + \frac{\sum P_e d_{pi}}{a} \qquad \text{Eq. 3.69}$$

In which P_e is the resulting compressive force due to prestress, d_{pi} is the effective depth of the i^{th} prestressing strand and f_t^* is the effective post-cracking tensile capacity of SFRC. For the use of the plasticity theory in the current study it is assumed that the crack width of the shear critical crack is constant along the depth of the cross-section of the beam and is equal to 2.5 mm at failure. Furthermore, a rigid plastic model is considered in accordance to the MC2010 provisions for fibre reinforced concrete and as a result, the value of f_t^* is taken as

$$f_t^* = f_{Ftu} = \frac{f_{R3}}{3} \qquad \text{Eq. 3.70}$$

In order to find a closed solution for V_u and V_{cr}, an appropriate value of the projected crack length x is found by intersecting Eq. 3.69 and Eq. 3.66 (Fig. 3.33). Hence, the shear capacity is found by solving iteratively for a value of x. The corresponding values of both the upper bound solution V_u and the cracking load V_{cr} are taken as the shear strength of the SFRC beam.

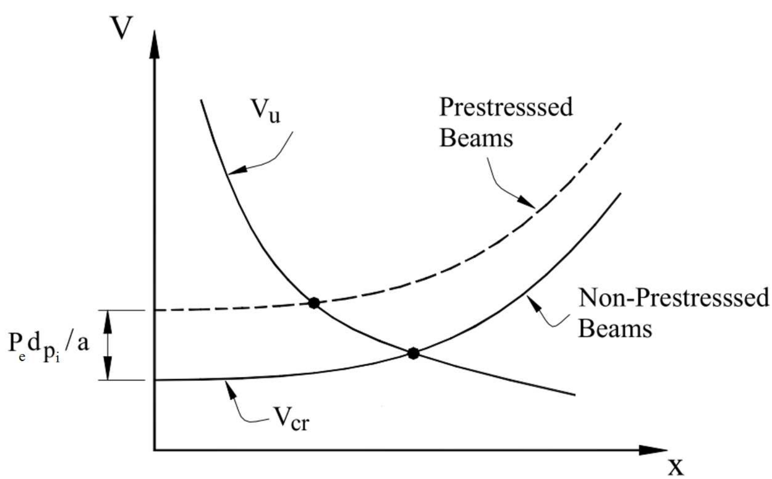

Fig. 3.33 – Equilibrium between V_u and V_{cr} as a function of x

As can be seen from Fig. 3.33, the application of a prestressing force causes the V_{cr} curve to shift upwards with a constant term. As a result, the value of x' (i.e. equal to a-x, Fig. 3.29) at which equilibrium is found decreases and the critical shear crack will be steeper.

3.2.3.2 RILEM (2003)

As a result of the work of the RILEM Technical Committee TC 162-TDF, a more comprehensive approach is suggested to calculate a design shear strength for FRC. Based on the work of RILEM TC 162 TDF (Technical Committee 162 ‘Test and design methods for fibre reinforced concrete’), final recommendations [29] were formulated in 2003 concerning the design of FRC members. This document can be considered as a first step towards code integration of structural design of FRC.

The additional term taking into account the contribution of fibres to the design shear strength of FRC is given by

$$V_{fd} = k_f k_1 \tau_{fd} \cdot b_w \cdot d \qquad \text{Eq. 3.71}$$

In which an extra term k_1 has been added equal to:

$$k_1 = \frac{1600 - h}{1600} \qquad \text{Eq. 3.72}$$

In contrast to the DRAMIX guideline, in the RILEM final recommendations it is emphasised that the material properties of the FRC composite used for design, have to be measured by standardised bending tests on small prims (see Section 2.3). Similar to the DRAMIX guideline model, the effect of cross-section shape is taken into account.

3.2.3.3 CNR-DT 204/2006 (2006)

The shear strength equation implemented in the Italian guidelines of the National Research Council, was first published in the thesis of Minelli [64]. Based on his study, it was assumed that the fibres act as a distributed longitudinal reinforcement enhancing the effect of aggregate interlock caused by smaller crack width. Hence, the shear strength equation for plain concrete from EC2 has been adapted by a factor increasing the longitudinal reinforcement ratio as a function of the residual stress of the FRC.

$$V_{Rd} = \left(\frac{0.18}{\gamma_c} \cdot k \cdot \left[100 \cdot \rho_l \left(1 + 7.5 \cdot \frac{f_{Ftuk}}{f_{ctk}} \right) \cdot f_{ck} \right]^{1/3} + 0.15 \cdot \sigma_{cp} \right) \cdot b_w \cdot d \qquad \text{Eq. 3.73}$$

3.2.3.4 ACI (2008)

Despite the increasing evidence from research results, the American Concrete Institute did not allow SFRC as an alternative for conventional shear reinforcement (i.e. steel stirrups) before 2008. For the use of steel fibres as minimum shear reinforcement in both prestressed and non-prestressed members, the ACI requires a minimum flexural performance based on ASTM C1609 four-point bending tests. According to the ACI Code, the residual flexural strength at midspan deflections 1/300 and 1/150 of the span length should be respectively higher than 90% and 75% of the first cracking stress. Furthermore, the fibre dosage shall not be lower than 0.75% and the concrete compressive strength have to be lower than 41.4 MPa (6 ksi).

Two main drawbacks are inherent to the ACI 318 code provisions: first, when reaching the flexural strength for fibre dosages lower than 0.75%, the use of fibres is not economic and second, for prestressed concrete elements, the concrete compressive stress will be traditionally higher than 41 MPa. As a result, current ACI design guideline is holding back the use of fibres as shear reinforcement for daily practice.

3.2.3.5 Model Code 2010 (2012)

A more recent model has been implemented in Model Code 2010 (chapter 7.7, section 7.7.3). This approach is in line with the recent adaptations to the shear design provisions in the latest version of EC2. The shear strength of fibre reinforced section can be obtained as follows:

$$V_{Rd} = \frac{1}{\gamma_F}\left[k_v f_{cm} + k_f f_{Ftuk} \cot\theta\right] b_w z \qquad \text{Eq. 3.74}$$

Where f_{Ftuk} is the characteristic post-cracking tensile strength of SFRC determined from axial tensile tests or indirectly from standard three-point bending test results. The crack width at which the post-cracking strength is considered shall be taken as:

$$w_u = 0.2 + 1000\varepsilon_x \geq 0.125\text{mm} \qquad \text{Eq. 3.75}$$

In which the strain at mid-depth for prestressed members is obtained by

$$\varepsilon_x = \frac{\left(\frac{M_{Ed}}{z} + V_{Ed} + N_{Ed}\frac{\left(z_p - e_p\right)}{z}\right)}{2\left(\frac{z_s}{z}E_s A_s + \frac{z_p}{z}E_p A_p\right)} \qquad \text{Eq. 3.76}$$

In which M_{Ed}, V_{Ed} are taken as positive quantities and N_{Ed} is negative for compression. The considered cross-section for design is shown in Fig. 3.34. In case ε_x is negative, it shall be taken as zero.

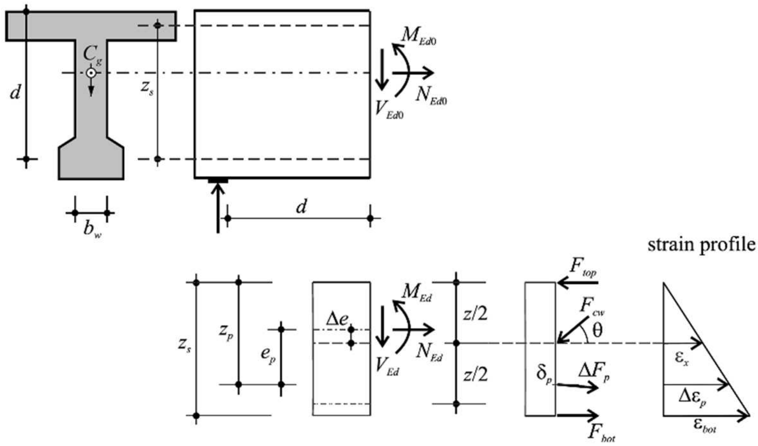

Fig. 3.34 – Definition of cross-sectional parameters, internal loads and strain profile according to MC2010.

k_f is a reduction factor taking into account the variation of fibre dispersion and inherent post-cracking performance between three-point bending test specimen and the actual elements for which the shear design is conducted. This value is proposed to be equal to 0.8, without further comments provided in MC2010.

The factor k_v takes into account both the strain and size effect. As a result, this factor is computed as follows:

$$k_v = \frac{0.4}{1+1500\varepsilon_x}\frac{1300}{1000+k_{dg}z} \qquad \text{Eq. 3.77}$$

with the aggregate size parameter given by

$$k_{dg} = \frac{32}{16+d_g} \geq 0.75 \qquad \text{Eq. 3.78}$$

If the particle size is less than 16 mm, it is suggested to take the value of k_{dg} equal to 1.

According to the variable inclination angle method, the inclination of shear critical cracks can be chosen between the following limits:

$$29° + 7000\varepsilon_x \leq \theta \leq 45° \qquad \text{Eq. 3.79}$$

More detailed background information has been provided in Section 3.2.2.2.

3.3 Conclusions

Regarding the investigations on the shear capacity of SFRC elements, the majority of all tests have been conducted on non-prestressed and relatively small elements. Over the past three decades, the experimental work has led to the development of different semi-analytical shear strength equations or design methods. Despite the large number of investigations, only a few models deal inherently with the presence of a prestressing force and apply the currently widely established residual flexural parameters, determined by standardised three-point bending tests.

3.4 References

[1] Ritter, W. (1899). "Die Bauweise Hennebique". *Schweizerische Bauzeitung*, Vol. February, pp. 41-61.

[2] Morsch, E. (1902) "*Der Eisenbetonbau, seine Anwendung und Theorie*". Neustadt a.d. Haardt: Technischer Leiter der Wayss & Freytag AG.

[3] Collins, M. P., Mitchell, D. (1991) "*Prestressed Concrete Structures*". Englewood Cliffs, New Jersey: Prentice-Hall, p. 766.

[4] fib. (2012) "*Bulletin No. 62: Structural Concrete Textbook on behaviour, design and performance, Second edition Volume 5: Through-life care and management of concrete structures - Assessment, protection, repair and strengthening*". Lausanne, Switzerland: fédération internationale du béton.

[5] ACI. (1999). "445R-99: Recent approaches to Shear Design of Structural Concrete".

[6] Shepherd, R., Frost, J. (1995) "*Failures in civil engineering: Structural, foundation, and geoenvironmental case studies*". New York: ASCE.

[7] Lubell, A., Sherwood, T., Bentz, E. C., Collins, M. P. (2004). "Safe Shear Design of Large, Wide Beams". *Concrete International*, Vol. January(26), pp. 66-78.

[8] Collins, M. P., Kuchma, D. (1999). "How safe are our large, lightly reinforced concrete beams, slabs and footings". *ACI Structural Journal*, Vol. 96(4), pp. 482-490.

[9] Feld, J., Carper, K. L. (1997) "*Construction Failure*". John Wiley & Sons.

[10] Taylor, H. P. J. (1974). "*The Fundamental Behavior of Reinforced Concrete Beams in Bending and Shear*". In: ACI SP-42: Shear in Reinforced Concrete. Detroitpp. 43-77.

[11] Taylor, H. P. J. (1970). "Investigation of the forces carried across cracks in reinforced concrete beams in shear by interlock of aggregate, Technical report 42.447". London.

[12] Taylor, H. P. J. (1970). "Further tests to determine shear stresses in reinforced concrete beams, Technical report TRA 438". London.

[13] Sarkar, S., Adwan, O., Bose, B. (1999). "Shear stress contributions and failure mechanisms of high strength reinforced concrete beams". *Materials and Structures*, Vol. 32(March), pp. 112-116.

[14] ASCE-ACI-Committee-426. (1973). "The Shear Strength of Reinforced Concrete Members". *Journal of structural Division (ASCE)*, Vol. 99(6), pp. 1091-1187.

[15] Kupfer, H., Hulsdorf, H. K., Rusch, H. (1969). "Behavior of Concrete Under Biaxial Stresses". *ACI Journal*, Vol. 66(8), pp. 656-666.

[16] Walraven, J. (1980). "*Aggregate Interlock - A theoretical and experimental analysis*" (PhD-thesis), Delft University of Technology.

[17] Walraven, J., Reinhardt, H. W. (1981). "Theory and Experiments on the Mechanical Behavior of Cracks in Plain and Reinforced Concrete Subjected To Shear Loading". *HERON*, Vol. 26, pp. 1-68.

[18] Gambarova, P. G., Karakoç, C. (1983). "A new approach to the analysis of the confinement role in regularly cracking concrete elements.". *7th International Conference on Structural Mechanics in Reactor Technology, Chicago, USA*, pp. 251-261.

[19] Li, N., Maekawa, L., Okamura, H. (1989). "Contact density model for stress transfer across cracks in concrete". *Journal of the Faculty of Engineering, University of Tokyo*, Vol. 40(1), pp. 9-52.

[20] Maekawa, K., Pimanmas, A., Okamura, H. (2003) "*Nonlinear Mechanics of Reinforced Concrete*". London: Spon Press.

[21] Bentz, E. C., Vecchio, F. J., Collins, M. P. (2006). "Simplified Modified Compression Field Theory for Calculating Shear Strength of Reinforced Concrete Elements". *ACI Structural Journal*, Vol. 103(4), pp. 614-624.

[22] Dei Poli, S., di Prisco, M., Gambarova, P. G. (1990). "Stress Field in Web of RC Thin-webbed Beams Failing in Shear". *Journal of Structural Engineering (ASCE)*, Vol. 116(9), pp. 2496-2515.

[23] Fenwick, R. C., Paulay, T. (1968). "Mechanisms of shear Resistance of Concrete Beams". *Journal Structural Division ASCE*, Vol. 94(10), pp. 2325-2350.

[24] Park, R., T., P. (1975) "*Reinforced Concrete Structures*". New York: Wiley-Interscience Publication.

[25] Kani, G. N. J. (1964). "The Riddle of Shear Failure and Its Solution ". *Journal of the American Concrete Institute*, Vol. 61(4), pp. 441-468.

[26] Shioya, T., Iguro, M., Nojiri, Y., Akiyama, H., Okada, T. (1990). "ACI SP 118: Shear Strength of Large Reinforced Concrete Beams".

[27] Frosch, R. J. (2000). "Behavior of Large-Scale Reinforced Concrete Beams with Minimum Shear Reinforcement". *ACI Structural Journal*, Vol. 97(6), pp. 814-820.

[28] Bazant, Z. P., Kim, J. K. (1984). "Size effect in shear failure of longitudinally reinforced beams". *ACI Journal*, Vol. 81(5), pp. 456-468.

[29] RILEM. (2003). "Final Recommendation of RILEM TC 162-TDF: Test and design methods for steel fibre reinforced concrete sigma-epsilon-design method". *Materials and Structures*, Vol. 36(262), pp. 560-567.

[30] CEN. (2004). "EN1992-1-1:2004 - Eurocode 2: Design of concrete structures - Part 1-1: General rules and rules for buildings". Brussels, Belgium.

[31] Kordina, K., Blume, F. (1985). "Empirische Zusammenhänge zur Ermittlung der Schubtragfähigkeit stabförmiger Stahlbetonelemente". Berlin, Sohn Eu.

[32] MacGragor, J. G. (1992) "*Reinforced Concrete: Mechanics and Design*". Englewood Cliffs, New Jersey: Prentice Hall.

[33] Nielsen, M. P. (1999) "*Limit Analysis and Concrete Plasticity*". CRC Press.

[34] Wagner, H. (1929). "Ebene Blechwandträger mit sehr Dünnem Stegblech". *Zeitschr Flugtechnik und Motorluftschiffahrt*.

[35] Vecchio, F. J., Collins, M. P. (1986). "The Modified Compression-Field Theory for Reinforced Concrete Elements Subjected to Shear". *ACI Journal*, Vol. 83(22), pp. 219-231.

[36] Bentz, E. C. (2000). "*Sectional Analysis of Reinforced Concrete Members*" (PhD-thesis), University of Toronto, Department of Civil Engineering.

[37] Collins, M. P., Mitchell, D., Adebar, P., Vecchio, F. J. (1996). "A general shear design method". *ACI Structural Journal*, Vol. 93(1), pp. 36-45.

[38] Zsutty, T. C. (1968). "Beam Shear Strength Prediction by Analysis of Existing Data ". *ACI Journal*, Vol. 65(11), pp. 943.

[39] Hedman, O., Losberg, A. (1978). "Design of concrete structures with regards to shear forces". *CEB Bulletin 126*, pp. 186-206.

[40] Remmel, G. (1992). "*Zum Zugtragverhalten hochfester Betone und seinem Einfluss auf die Querkrafttragfahigkeit von schlanken Bauteilen ohne Schubbewehrung*", Technische Hochschule Darmstadt.

[41] ACI. (2011). "ACI 318-11: Building Code Requirements for Structural Concrete and Commentary". Farmington Hills, USA.

[42] CEB-FIP. (1987). "Shear in Prestressed Concrete Members - State-of-the-Art Report (Bulletin 180)". Lausanne, Switzerland.

[43] Batson, G. B., Jenkins, E., Spatney, R. (1972). "Steel Fibers as Shear Reinforcement in Beams". *ACI Journal*, Vol. 69(10), pp. 640-644.

[44] Swamy, R. N., Bahia, H. M. (1985). "The effectiveness of steel fibers as shear reinforcement". *Concrete International*, Vol. March, pp. 35-40.

[45] Mansur, M. A., Ong, K. C. G., Paramasivam, P. (1986). "Shear Strength of Fibrous Concrete Beams without Stirrups". *Journal of Structural Engineering (ASCE)*, Vol. 112(9), pp. 2066-2079.

[46] Al-Ta'an, S. A., Al-Feel, J. R. (1990). "Evaluation of shear strength of fiber reinforced concrete beams". *Cement and Concrete Composites*, Vol. 12, pp. 87-94.

[47] Ashour, S. A., Hasanain, G. S., Wafa, F. F. (1992). "Shear behaviour of high strength fiber reinforced concrete". *ACI Structural Journal*, Vol. 89(2), pp. 176-184.

[48] Imam, M., Vandewalle, L., Mortelmans, F., Van Gemert, D. (1997). "Shear domain of fibre-reinforced high-strength cocnrete beams". *Engineering Structures*, Vol. 19(9), pp. 738-747.

[49] Imam, M., Vandewalle, L., Mortelmans, F. (1998). "Shear-moment analysis of reinforced high strength concrete beams containg steel fibers". *Canadian Journal of Civil Engineering*, Vol. 22, pp. 462-470.

[50] Khuntia, M., Stojadinovic, B., Subhash, C. G. (1999). "Shear strength of normal and high-strength fiber reinforced concrete beams without stirrups". *ACI Structural Journal*, Vol. 96(2), pp. 282-289.

[51] Gustafsson, J., Noghabai, K. (1999). "Steel fibers as shear reinforcement in high strength cocnrete beams". *Bi annual report - Nordic Concrete Research (NCR)*, Vol. 1, pp. 1-18.

[52] Kwak, Y. K., Eberhard, M. O., Kim, W. S., Kim, J. (2002). "Shear strength of steel fiber-reinforced concrete beams without stirrups". *ACI Structural Journal*, Vol. 99(4), pp. 530-538.

[53] Noghabai, K. (2000). "Beams of Fibrous Concrete in Shear and Bending: Experiment and Model". *Journal of Structural Engineering*, Vol. 126(2), pp. 243-251.

[54] Rosenbusch, J., Teutsch, M. (2003). "Shear Design with σ-ε Method". *RILEM TC 162-TDF Workshop, Bochum, Germany*.

[55] Cucchiara, C., La Mendola, L., Papia, M. (2004). "Effectiveness of stirrups and steel fibres as shear reinforcement". *Cement and Concrete Composites*, Vol. 26(7), pp. 777-786.

[56] Greenough, T., Nehdi, M. (2009). "Shear Behavior of Fiber-Reinforced Self-Consolidating Concrete Slender Beams". *Environmental Engineering*.

[57] Cho, J.-S., Lundy, J., Chao, S.-H. (2009). "Shear Strength of Steel Fiber Reinforced Prestressed Concrete Beams". *Structures Congress 2009: Don't Mess with Structural Engineers, Austin, Texas*, pp. 1058-1066.

[58] Dinh, H. H., Parra-Montesinos, G. J., Wight, J. K. (2010). "Shear behavior of steel fiber reinforced concrete beams without stirrup reinforcement". *ACI Structural Journal*, Vol. 107(5), pp. 597-606.

[59] Aoude, H., Mehdi, B., Cook, W. D., Mitchell, D. (2012). "Response of Steel Fiber-Reinforced Concrete Beams with and without Stirrups". *ACI Structural Journal*, Vol. 109(3), pp. 359-367.

[60] Parmentier, B., Cauberg, N., Vandewalle, L. (2012). "Shear resistance of macro-synthetic and steel fibre reinforced concrete beams without stirrups". *BEFIB 2012, Guimaraes*.

[61] Ding, Y., Zhang, F., Torgal, F., Zhang, Y. (2012). "Shear behaviour of steel fibre reinforced self-consolidating concrete beams based on the modified compression field theory". *Composite Structures*, Vol. 94(8), pp. 2440-2449.

[62] Conforti, A., Tinini, A., Minelli, F., Plizzari, G., Moro, S. (2014). "Structural applicability of polypropylene fibres: deep and wide-shallow beams subjected to shear". *FRC 2014 Joint ACI-fib International Workshop - Fibre Reinforced Concrete: from Design to Structural Applications, Montréal, Canada*, pp. 341-355.

[63] Narayanan, R., Darwish, I. Y. S. (1987). "Shear in prestressed concrete beams containing steel fibres". *The International Journal of Cement Composites and Lightweight Concrete*, Vol. 9(2), pp. 81-90.

[64] Minelli, F. (2005). "*Plain and Fibre Reinforced Concrete Beams under Shear Loading: Structural Behaviour and Design Aspects*" (PhD-thesis). Brescia, University of Brescia.

[65] Voo, Y. L., Foster, S. J. (2008). "Shear strength of steel fiber reinforced ultra-high performance concrete beams without stirrups". *5th international Specialty Conference on Fibre Reinforced Materials*, pp. 177-184.

[66] De Pauw, P., Taerwe, L., Van den Buverie, N., Moerman, W. (2008). "Steel fibre concrete as an alternative for traditional shear reinforcement in pretensioned concrete beams". *7^{th} international RILEM symposium on fibre reinforced concrete: design and applications (BEFIB 2008)*, pp. 887-898.

[67] Cuenca, E., Serna, P. (2013). "Shear behavior of prestressed precast beams made of self-compacting fiber reinforced concrete". *Construction and Building Materials*, Vol. 45(August 2013), pp. 145–156.

[68] fib. (2010). "Model Code for Concrete Structures 2010". Lausanne, Switzerland, fédération internationale du béton.

[69] Narayanan, R., Kareen-Palanjian, A. S. (1986). "Factors Influencing the Strength of Steel Fibre Reinforced Concrete". *Third International Rilem Symposium*.

[70] Choi, C. K., Kwak, H. G. (1990). "The effect of finite element mesh size in nonlinear analysis of reinforced concrete structures". *Computers & Structures*, Vol. 36(5), pp. 807-815.

[71] Romualdi, J. P., Mandel, J. A. (1964). "Tensile strength of concrete affected by uniformly dispersed and closely spaced short lengths of wire reinforcement". *Journal of the American Concrete Institute* Vol. 61(6), pp. 657-672.

[72] Al-Ta'an, S. A., Al-Saffar, N. S. (2008). "Nonlinear Finite Element Analysis of Fibrous Reinforced Concrete Beam-Column Joints". *Al-Rafidain Engineering*, Vol. 16(5), pp. 57-69.

[73] Lim, T. Y., Paramasivam, P., Lee, S. L. (1987). "Analytical Model for Tensile Behaviour of Steel-Fiber Concrete". *ACI Materials Journal*, Vol. 84(4), pp. 286-298.

[74] Marti, P., Pfyl, T., Sigrist, V., Ulaga, T. (1999). "Harmonized Test Procedures for Steel Fiber-Reinforced Concrete". *ACI Materials Journal*, Vol. 96(6), pp. 676-686.

[75] Voo, J. Y., Foster, S. J. (2004). "Tensile-fracture of Fibre-Reinforced Concrete: Variable Engagement Model". *6th RILEM Symposium on Fibre-Reinforced Concretes (FRC) - BEFIB 2004, Varenna, Italy*, pp. 875-884.

[76] Lee, D. H., Hwang, J.-H., Ju, H., Kim, K. S., Kuchma, D. A. (2012). "Nonlinear finite element analysis of steel fiber-reinforced concrete members using direct tension force transfer model". *Finite Elements in Analysis and Design*, Vol. 50, pp. 266-286.

[77] Nemegeer, D., Vandewalle, L., Van Nieuwenburg, D., Van Gysel, A., Vyncke, J., Deforche, E. (1995). "Dramix guideline: Design of concrete structures - Steel wire fibre reinforced concrete structures with or without ordinary reinforcement". *Infrastructuur in het leefmilieu 4*, pp. 227-239.

[78] Voo, Y. L., Foster, S. J., Gilbert, R. I. (2006). "Shear Strength of Fiber Reinforced Reactive powder Concrete Prestressed Girders without Stirrups". *Journal of Advanced Concrete Technology*, Vol. 4(1), pp. 123-132.

[79] Zhang, J.-P. (1994) "*Strengh of cracked concreet, Part 1 - Shear strength of conventional reinforced concrete beams, deep beams, corbels, and prestressed reinforced beams without shear reinfrocement*". Lyngby, Denmark: Danmarks Tekniske Univ.

4 POST-CRACKING BEHAVIOUR OF SFRC

4.1 General

In this chapter, research results are reported concerning the post-cracking behaviour of SFRC. The post-cracking behaviour of SFRC is investigated on both the micro-scale (fibre level) and the meso-scale level (composite level) to evaluate the crack bridging ability of fibres when subjected to a pure Mode I (opening) and a combined Mode I and Mode II (mixed mode) crack propagation.

In a way to understand the mechanisms influencing the post-cracking tensile strength capacity of SFRC, research has been carried out to investigate the crack-bridging ability for SFRC subjected to bending. Based on the experimental observations from the bending tests, different modelling techniques are proposed. All of the models provide rational approaches to analyse and to evaluate the constitute law of SFRC in tension by taking into account the pull-out behaviour of fibres. Therefore, existing pull-out models of a single fibre [1-4] have been revised and further optimized.

In order to investigate the response of a single fibre subjected to pull-out conditions inherent to a transverse displacement of the crack plane, a micro scale test method has been developed and used to investigate the transverse pull-out response of hooked-end steel fibres. The experimental observations were then used in combination with the revised analytical pull-out models to be implemented into an analytical model to simulate the experimentally obtained direct shear behaviour of SFRC.

In this doctoral study, short (30 mm) and long (60 mm) hooked-end fibres are used. The used fibres are manufactured by Bekaert and commercially known as DRAMIX® RC-80/30-CP, RC-80/60-BP and RC-80/60-BN.

4.2 Bending behaviour

4.2.1 Introduction

Recent evolutions in the application fields of SFRC are focused on the replacement of conventional reinforcement by hooked-end steel fibres in concrete members where minimum reinforcement is required, and so to provide a concrete element the necessary post-cracking strength [5-7]. In this case it is important to know how many fibres have to be added to the concrete mix in order to meet specific design criteria such as maximum deflection and crack width when subjecting the concrete member to the desired design load.

To characterize steel fibre reinforced concrete, prisms with standard dimensions of 150 mm x 150 mm x 600 mm are used to derive residual flexural parameters by means of three- or four-point bending tests [8, 9]. In this way, a performance classification of the SFRC can be done and a Mode I crack opening constitutive law for SFRC can be derived for structural design purposes. For the latter, the Model Code 2010 (MC2010) provides both a simplified rigid-plastic model and a more detailed bi-linear constitutive model in which a distinction can be made between strain-hardening and strain-softening. An example is given in Fig. 4.1.

Although the current approach is widely accepted, some drawbacks are inherent to the procedure that has to be followed before a design can be performed. First, a minimum amount of bending tests have to be performed to get an insight into the scatter of the flexural load-deflection response and to deduct characteristic values of residual flexural parameters. It is assumed that the observed scatter from bending tests is mainly a consequence of variability of the total amount of fibres crossing the crack plane, the orientation profile of fibres, the difference in fibre embedded length, concrete strength and fibre shape [10-12]. Moreover, it is a time consuming job to cast and to prepare specimens and to conduct laboratory tests.

Secondly, the obtained load-CMOD (Crack Mouth Opening Displacement) curves for SFRC are, according to MC2010 turned into pure strain-hardening or -softening constitutive laws which have two discontinuities (Fig. 4.1 - Rigid plastic or Bi-linear): (1)

just after cracking, when the concrete stress drops from the tensile strength to a lower residual stress and (2) at the assumed ultimate crack opening w_u where stresses drop from a residual stress to zero. In reality however, stresses are more continuous as a function of crack opening and related to the pull-out conditions of fibres.

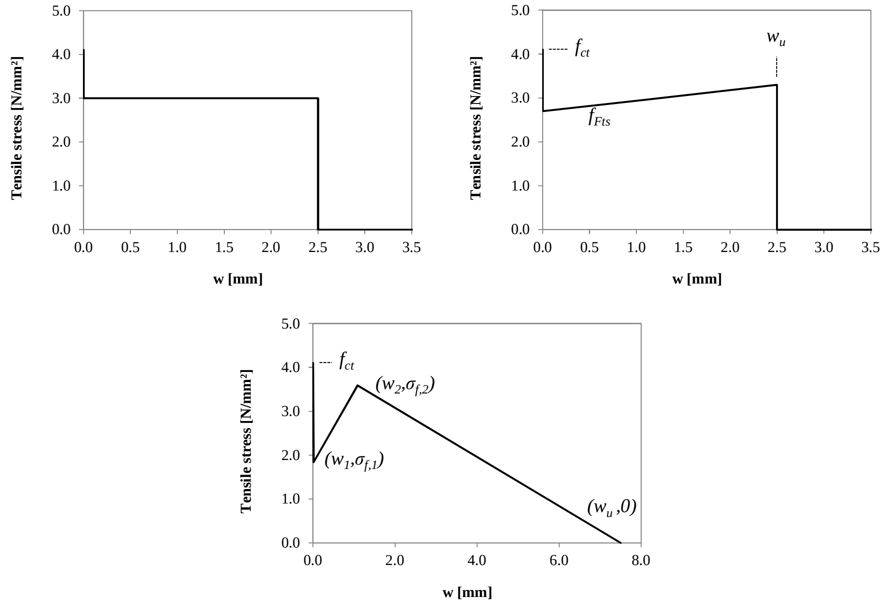

Fig. 4.1 - Example of different post-cracking constitutive laws for SFRC with f_{ct}=4.1 N/mm², f_{R1} = 6 N/mm² and f_{R3} = 9 N/mm²

In this work, two modelling variants for the Mode I behaviour of SFRC are proposed, which allow to also consider pseudo-hardening behaviour of SFRC.

A standard three-point bending test according to the European standard NBN EN 14651 [9] is used to determine the residual flexural parameters of SFRC mixes and by means of inverse analysis [13-15] (see Section 2.3.4) an estimation of the Mode I constitutive law is obtained. However, since any found solution is considered to be non-unique, a certain model error has to be dealt with. In this chapter, a tri-linear crack opening law is adopted in order to catch both the softening and hardening (and combination of both) behaviour of SFRC (Fig. 4.1).

In addition to the discussion about the uniqueness of solutions found through inverse analysis, another model is developed to calculate the axial crack bridging ability of SFRC based on the single fibre pull-out response of hooked-end steel fibres. The fibre pull-out response of a steel fibre, both straight and deformed, embedded in a concrete matrix has been widely investigated in the past [1, 3, 4, 16-21] (see section 2.2.3). Thereby, attention is given to the influence of the type of fibre, the concrete strength and the inclination of the pull-out force. The developed analytical tool implements an accurate axial pull-out model developed by Van Gysel [1, 2] and takes into account the matrix compressive strength, fibre tensile strength, geometry, orientation, spatial distribution and embedded length of a fibre.

In addition, a third modelling technique is presented which can be used to characterize the non-linear behaviour of steel fibre reinforced concrete subjected to bending and to estimate the scatter of flexural response by means of finite element modelling (FEM). The composite material is considered to be a two-phased model where the concrete matrix and the individual fibres are modelled separately. Thereby, the fibres are considered as frictionless cable elements [22, 23]. In order to verify the FEM-analysis, four-point bending tests have been performed and compared with the simulated curves.

The relationship between all the proposed modelling techniques is schematically visualized in Fig. 4.2.

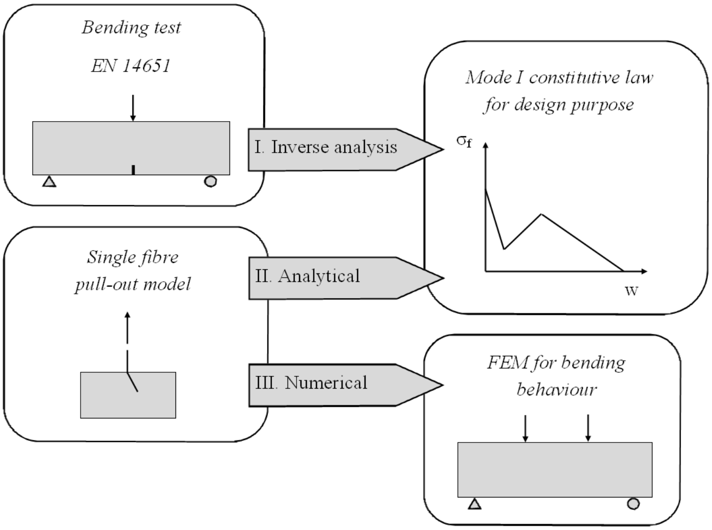

Fig. 4.2 - Schematic overview of proposed modelling techniques

4.2.2 Experimental investigation

A total of 42 bending tests have been conducted on SFRC prisms with nominal dimensions 150 x 150 x 600 mm. The test matrix is given in Table 4.1 and comprised both three- and four-point bending tests. Test parameters include fibre dosage, fibre type and concrete type. For each of the test series, three specimens (six specimens for series LH20, LH40) are casted and cured in a room with a constant RH of 90% and temperature of 20°C. Specimens are tested in a displacement controlled way at 28 days. For the three-point bending tests (3P), concrete mix SFRC-1 (mean compressive strength $f_{cm,cub}$ = 68.7 N/mm²) is used in combination with high strength fibres with a length equal to 30 mm (SH) or 60 mm (LH). For the four-point bending test series (4P), concrete mix SFRC-2 ($f_{cm,cub}$ =

57.4 N/mm²) is used in combination with 60 mm long fibres with a high (LH) and normal strength (LN). All fibre properties such as wire strength (f_t), diameter (d_f), length (L_f) and fibre weight (M_f) are summarized in Table 4.2. The applied fibre dosages (V_f) for all SFRC batches ranged between 20 and 60 kg/m³. The concrete composition and average cube (side length 150 mm) compressive strength is shown in Table 4.3. In general, the workability varied in between an acceptable range for both mixes. The observed air-content for series 3P-SH-60 and SP-LH-60 is significantly higher with respect to the average air-content of about 2.0 % for the other specimens.

All of the fibres are made of bare steel, except for fibre type SH, which is a zinc-coated fibre. To eliminate the negative effects on the concrete quality by the hydrogen gas formed by a chemical reaction between the zinc coating and the alkalis in the fresh concrete [24], these fibres are manufactured with a protective reaction inhibitor. The zinc-coated steel fibres are passivated by means of a chromium based compound which guarantees the good bond between fibre and surrounding concrete in the hardened state.

Table 4.1 - Test matrix for all bending tests

Designation	Concrete Mix	Fibre type	V_f [kg/m³]	$f_{cm,cub}$ [N/mm²]	# tests
3P-SH-20	SFRC-1	SH	20	71.8	3
3P-SH-40			40	68.4	3
3P-SH-60			60	65.1	3
3P-LH-20		LH	20	68.8	6
3P-LH-40			40	73.2	6
3P-LH-60			60	64.7	3
4P-LN-20	SFRC-2	LN	20	51.4	3
4P-LN-40			40	58.8	3
4P-LN-60			60	56.5	3
4P-LH-20		LH	20	59.7	3
4P-LH-40			40	61.0	3
4P-LH-60			60	56.8	3

Table 4.2 - Overview of used fibres

Fibre type	Fibre name	f_t [N/mm²]	L_f [mm]	d_f [-]	M_f [g]
RC-80/60-BN	LN	1236	60	0.75	2.19E-01
RC-80/60-BP	LH	2520	60	0.71	1.96E-01
RC-80/30-CP	SH	3096	30	0.38	2.69E-02

Table 4.3 – Constituents of used concrete mixes [kg/m³]

Mix	SFRC-1	SFRC-2
Cement CEM I 52,5 N	-	390
Cement CEM I 52,5 R	390	-
Crushed aggregate 2/7	257	150
Crushed aggregate 7/14	566	850
Sand 0/1	202	-
Sand 0/4	674	805
Fly ash	60	-
Superplasticiser (Glenium 51)	2.61	2.20
Water	190	188
W/C	0.46	0.48
W/P	0.42	0.48
$f_{cm,cub}$ [N/mm²]	68.7	57.4
CoV [%]	5.0	5.9

4.2.2.1 Three-point bending tests

Three point-bending tests on notched prisms are conducted according to the European standard EN14651 (see also section 2.3.4). In order to capture the post-peak behaviour of both plain concrete and fibre reinforced concrete specimens, the testing procedure is controlled by a monotonic increase of the crack mouth opening displacement (CMOD). Until a crack opening of 0.1 mm is reached, the opening rate is kept constant at 0.05 mm/min after which the crack opening displacement rate is increased up to 0.2 mm/min. The tests are conducted until reaching a CMOD of at least 4 mm. For all three-point bending test series, the complete stress-CMOD curves are shown in Fig. 4.3.

Due to the overall dispersion and different orientation of fibres within a concrete matrix, it should be noted that fibre dosage as such cannot only be used as a parameter to quantify the performance of a fibre reinforced concrete. As defined in MC2010 [25], a classification of FRC performance shall be done based on the residual flexural stresses, obtained from three-point bending tests on notched prisms (EN 14651 [9]), at defined crack mouth opening displacement (CMOD) values:

$$f_{Ri} = \frac{3F_{Ri}L}{2bh_{sp}^2} \qquad \text{Eq. 4.1}$$

With i=1..4, respectively for CMOD values 0.5, 1.5, 2.5 and 3.5 mm and in which F_{Ri} is the applied load at CMOD = i, L the span length (i. e. 500 mm), b the width of the prism and h_{sp} the height of the prism above the notch in mm. The experimentally obtained average values of f_{R1} and f_{R3} are summarized in Table 4.4. As expected, the residual stresses increased for higher fibre dosages. Regarding the values for f_{R3}, short fibres provided lower stresses than long fibres. All residual stresses are between 2.81 and 10.70 N/mm². The coefficient of variation for all tested series ranged between 10 and 33 %. No clear relationship between coefficient of variation and fibre type and dosage is found.

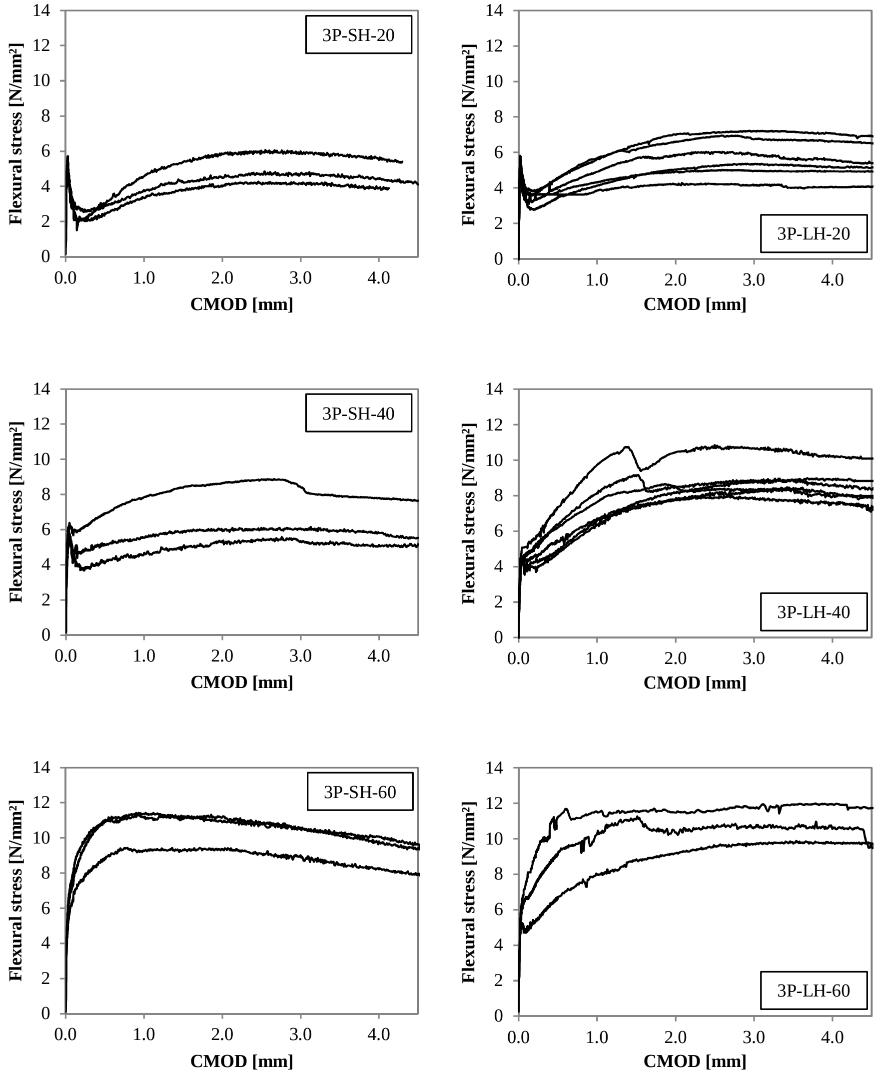

Fig. 4.3 - Three-point bending test results for series 3P-SH (left) and 3P-LH (right)

Table 4.4 - Average values and CoV of f_{R1} and f_{R3}.

	f_{R1} [N/mm²]		f_{R3} [N/mm²]	
Series	Average	COV	Average	COV
3P-SH-20	2.81	11%	4.95	19%
3P-LH-20	3.98	12%	5.75	20%
3P-SH-40	5.41	26%	7.06	33%
3P-LH-40	5.81	17%	8.73	12%
3P-SH-60	10.25	12%	10.26	10%
3P-LH-60	9.01	25%	10.71	10%

It has been reported that for SFRC with high dosages of fibres, due to the density of fibres, interaction will occur and lead to less effectiveness [26, 27] (see Section 2.2.2). As a consequence, the increase of residual stresses f_{R3} is less than proportional with respect to the increase of added fibre content. This trend can also be observed in the three-point bending test results (see Table 4.4).

4.2.2.2 Four-point bending tests

While the three point bending test is carried out to derive discrete crack-opening stress relationships, another series of bending tests has been performed in order to investigate the bending behaviour of SFRC for prisms without a notch and hence with the possibility of multiple cracking. Therefore, four-point bending tests based on the Belgian Standard NBN-B15-238 [28], are conducted (see Section 2.3.2). The span length is equal to 450 mm and the distance between the two loads and the loads and both supports is equal to 150 mm. During testing, the deflection is measured by means of a linear variable displacement transducer (LVDT), attached to a brace which is fixed to the prism by a hinge at one support and free to slide at the other support. Testing is performed displacement-controlled at a deflection rate of 0.05 mm/min until reaching a midspan deflection of at least 4 mm. The obtained flexural stress-deflection curves for series 4P-LN and 4P-LH are shown in Fig. 4.4.

According to NBN-B15-238, the ductility of SFRC can be expressed in two ways. The first method defines toughness as the ratio between applied load at prescribed deflections and the first cracking load. For the second method, a toughness parameter is proposed as a conventional flexural strength given by

$$f_{f,n} = \frac{B_n n}{bh^2} \qquad \text{Eq. 4.2}$$

In which B_n is the area under the load-deflection curve up to a deflection equal to the span length divided by n. Typically, these conventional flexural stresses are calculated at a deflection of 1.5 mm (n = 300) and 3 mm (n = 150). An overview of all obtained values for $f_{f,300}$ and $f_{f,150}$ is given in Table 4.5. and Table 4.6.

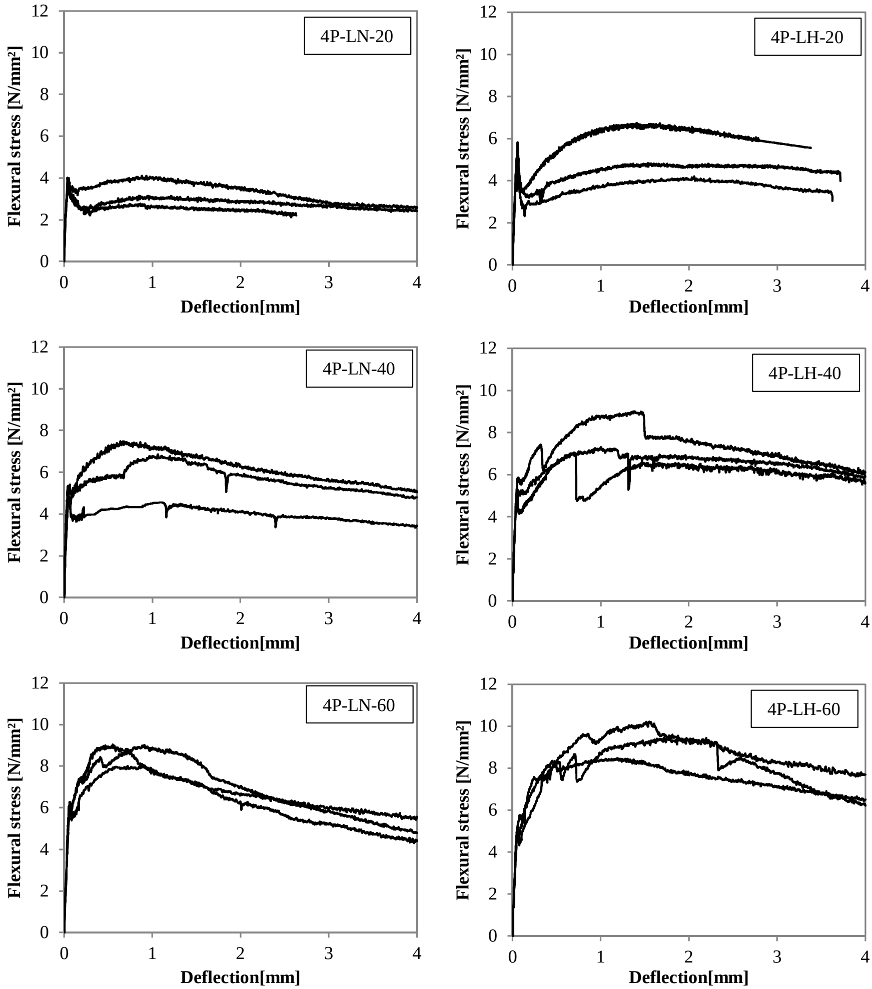

Fig. 4.4 - Four-point bending test results for series 4P-LN (left) and 4P-LH (right)

Table 4.5 - Average values and CoV of $f_{f,300}$ and $f_{f,150}$ (series LN)

n	Series	Average $f_{f,n}$ [N/mm²]	COV [%]
	4P-LN-20	3.09	19%
300	4P-LN-40	5.65	23%
	4P-LN-60	6.91	5%
	4P-LN-20	2.96	18%
150	4P-LN-40	5.46	22%
	4P-LN-60	6.32	5%

Table 4.6 - Average values and CoV of $f_{f,300}$ and $f_{f,150}$ (series LH).

n	Series	Average $f_{f,n}$ [N/mm²]	COV [%]
300	4P-LH-20	4.42	25%
	4P-LH-40	6.63	15%
	4P-LH-60	8.00	6%
150	4P-LH-20	4.70	24%
	4P-LH-40	6.72	12%
	4P-LH-60	8.24	7%

4.2.3 Inverse analysis

Since the described approach herein is used to find the relationship between a given crack opening and corresponding tensile stress, a fictitious length method [13] (see also section 2.3.4.4) is used in order to transform a given crack opening to an equivalent tensile strain for the tensile linear elastic phase and an equivalent strain at the top of the cross section (see Fig. 2.44, section 2.3.4.4). The fictitious length L_f only affects the stiffness of the linear behaviour (initial part of the curve), the proper fictitious length is found by fitting the linear slope of the reference three-point bending test without fibres and assuming a bilinear softening cohesive crack mode according to MC2010. A comparison for different values of L_f is given in Fig. 4.5.

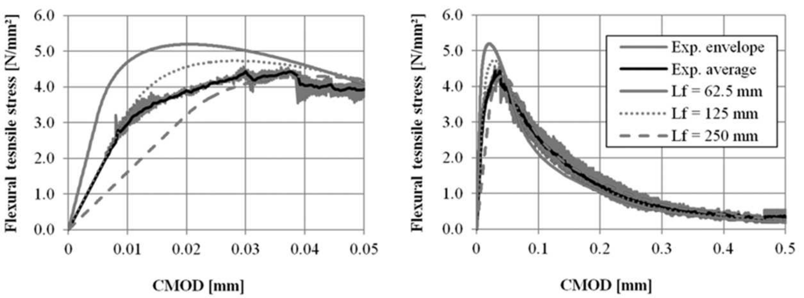

Fig. 4.5 - Influence of fictitious length on the simulated linear stiffness and bending tensile strength

Based on the described procedure, a fictitious length equal to 125 mm is chosen to perform the inverse analysis for all of the tested SFRC prisms.

In order to be able to catch the complete load-CMOD shape of the bending tests, the MC2010 bi-linear tension-softening law is changed to a tri-linear one. The overall benefit of a tri-linear stress-crack opening law (Fig. 4.1) has been proven to be successful in the past by several researchers for both numerical and analytical purposes [29, 30]. However, by introducing more parameters than can be derived from the inverse analysis in order to fit the flexural response, the uniqueness of the fitted solutions may be doubtful. Therefore, some restrictions are defined with respect to the first and last point of the post-cracking law: a) the tensile strength of concrete (at a crack opening equal to zero) is a fixed parameter since it is calculated by using the compressive strength of the concrete and b) the ultimate crack opening w_u (σ_f = 0 N/mm²) shall be taken equal to $L_f/4$ since it is the theoretical average of fibre embedded length.

To apply a criteria for acceptance of the derived stress-crack opening law by the inverse analysis (IA) iteration procedure, an absolute relative error R is defined by Eq. 4.3:

$$R = \frac{|A_{EXP} - A_{IA}|}{A_{EXP}} < 1\% \qquad \text{Eq. 4.3}$$

In which A_{EXP} is the area under the experimental curve and A_{IA} the area under the load-deflection curve obtained by inverse analysis. To assure a good fit between the complete experimental and theoretical load-deflection curve, two intervals are considered: from 0.1 to 0.5 mm and from 0.5 mm to 4 mm. The assumed mode I crack opening law is accepted when the relative error is lower than 1% for both intervals at the same time. The obtained constitutive stress-crack opening laws for series 3P-SH and 3P-LH are shown in Fig. 4.6 for a crack opening range from 0 to 4.5 mm (per specimen in grey, average in black).

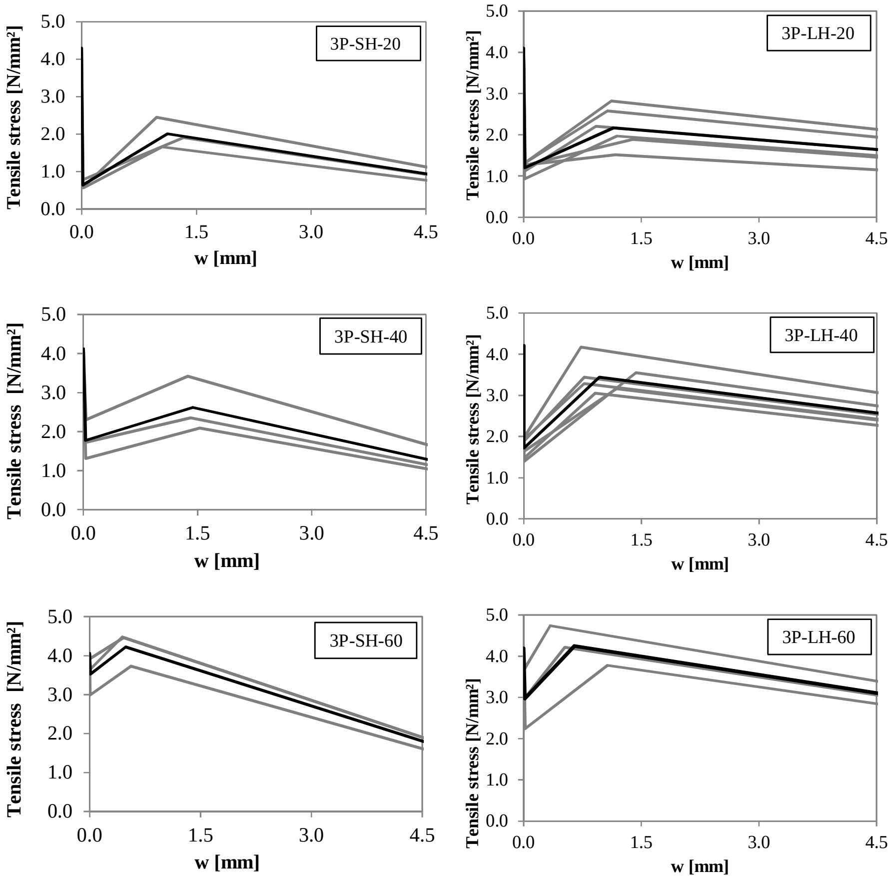

Fig. 4.6 - Tri-linear stress-crack opening curves by means of inverse analysis

Based on the obtained post-cracking residual stresses by means of three-point bending tests and the values of $\sigma_{f,1}$ and $\sigma_{f,2}$, which define the shape of the tri-linear post-cracking tensile curve, a strong correlation is found between the values of f_{R1} and $\sigma_{f,1}$ and f_{R3} and $\sigma_{f,2}$ (Fig. 4.7).

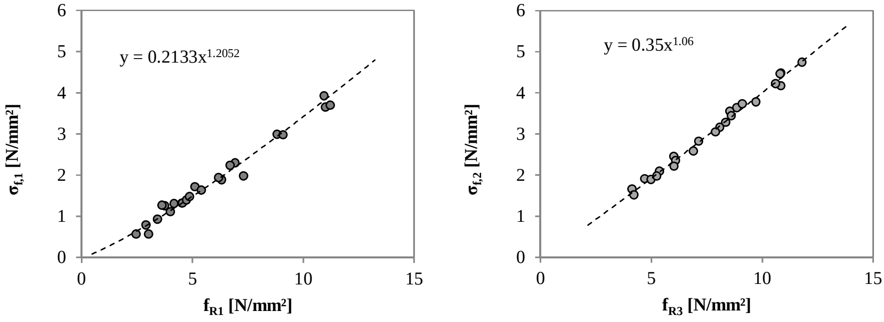

Fig. 4.7 - Relationship between stresses $\sigma_{f,1}$ and $\sigma_{f,2}$ and the residual stresses f_{R1} and f_{R3}.

Further, the crack-widths for corresponding values of both $\sigma_{f,1}$ and $\sigma_{f,2}$ should be defined. The crack width w_1 corresponding to the value of $\sigma_{f,1}$ will depend mainly on the fracture energy release rate of plain concrete and hence, being fixed as the average value obtained from the IA, which equals 0.015 mm. For the second point (w_2, $\sigma_{f,2}$), it can be seen in Fig. 4.6 that the crack-width opening related to the maximum post-cracking stress decreases for higher fibre residual stress levels. Furthermore, for increasing fibre dosages, the difference between point 1 and 2 will become smaller and the first branch of the tri-linear model will be ascending ($f_{ct} < \sigma_{f,1} < \sigma_{f,2}$), resulting in a transition between pseudo-hardening and pure hardening post-cracking composite behaviour. Fig. 4.8 shows the relation between the values of w_2 and f_{R1}.

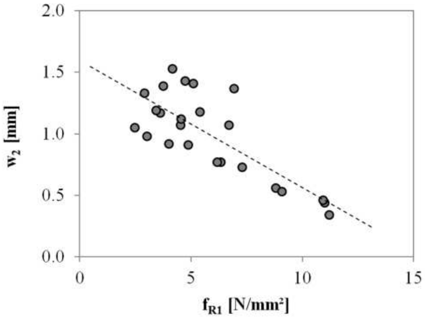

Fig. 4.8 – Relation between w_2 and f_{R1}.

Based on the observations from three-point bending tests and the inverse analysis results, the complete Mode I post-cracking curve for hooked steel fibre reinforced concrete used in this study can be defined as follows:

$$w_0 = 0 \quad \text{Eq. 4.4}$$
$$w_1 = 0.015\text{mm} \quad \text{Eq. 4.5}$$
$$w_2 = 1.6\text{mm}(1 - f_{R1} / 10\text{MPa}) \quad \text{Eq. 4.6}$$
$$w_u = L_f / 4 \quad \text{Eq. 4.7}$$

$$\sigma_{f,0} = f_{ct} \quad \text{Eq. 4.8}$$
$$\sigma_{f,1} = 0.21 f_{R1}^{1.21} \quad \text{Eq. 4.9}$$
$$\sigma_{f,2} = 0.35 f_{R3}^{1.06} \quad \text{Eq. 4.10}$$
$$\sigma_{f,u} = 0 \quad \text{Eq. 4.11}$$

When the proposed equations (Eq. 4.4 - Eq. 4.11) are applied to predict the three-point bending response based on average values of f_{R1} and f_{R3}, the expected relative error R (Eq. 4.3) is expected to increase, compared to the 1% assumed during the inverse analysis of individual specimens. Table 6 summarizes the values of R between the modelled and average experimental curve for each series in the intervals CMOD = 0.1-0.5 mm and CMOD = 0.5-4.0 mm. It can be seen that the error increases up to 7.4% for series 3P-SH-40. All of the values are in an acceptable range of accuracy and it can be concluded that for the considered series of three-point bending tests the predictive capacity of the proposed model is acceptable.

Table 4.7 - Relative error (R) in % between average experimental and predicted stress-CMOD curves.

Series	0.1 - 0.5 mm	0.5 - 4.0 mm
3P-SH-20	4.0	1.7
3P-SH-40	7.4	1.1
3P-SH-60	2.5	1.0
3P-LH-20	4.1	2.8
3P-LH-40	6.8	4.7
3P-LH-60	6.1	4.4

4.2.4 Analytical model based on fibre pull-out

An analytical model for the Mode I crack opening behaviour is developed based on the pull-out of a single fibre. The stress crack-opening law can then be obtained by lumping all fibre pull-out forces at a certain crack opening displacement and divide the force by the surface of the considered crack plane. The main influencing parameters for the fibre pull-out are implemented automatically by means of the semi-analytical pull-out model as described by Van Gysel et al. [1, 2].

4.2.4.1 Material properties

When sampling an SFRC-mix, both concrete strength and steel fibre strength variation is assumed to be described with a normal distribution function. The adopted values for all different types of fibre and for concrete in general are those as experimentally characterized (see Section, 4.2.2 in Table 4.1 and Table 4.2).

4.2.4.2 Crack-bridging capacity of a single fibre

When studying the effect of fibre inclination on the pull-out behaviour of a single fibre [1, 2, 4, 21], bridging a crack, the fibre pull-out direction is not perpendicular to the crack surface. Moreover, the pull-out direction changes in function of crack opening w and spalling length L_{sp} of the concrete at the fibre exit point. From Fig. 4.9, it is clear that the acting pull-out direction differs from the initial fibre orientation angle θ.

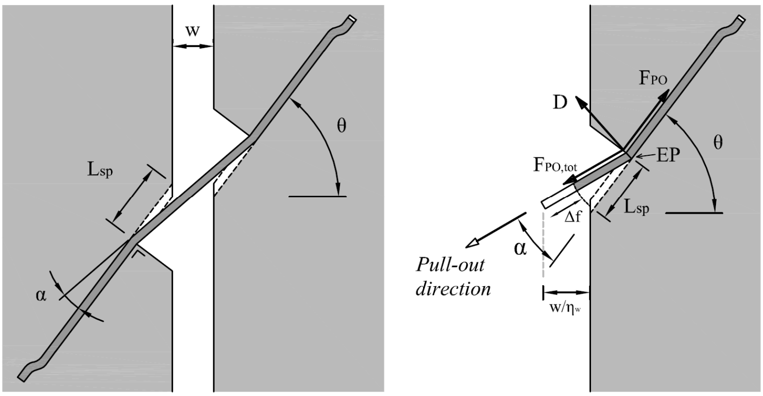

Fig. 4.9 - Schematic of the crack bridging mechanism of an inclined fibre during debonding

Due to the inclined pull-out and related spalling, a deviatoric force will occur at the fibre exit point, because the fibre deviates from its initial orientation with an angle α. The deviatoric force D is given by:

$$D = 2F_{PO} \sin\frac{\alpha}{2} \qquad \text{Eq. 4.12}$$

To account for the additional frictional force at the fibre exit point, the deviatoric force is multiplied with a friction parameter μ in order to take into account the frictional effects between fibre and concrete. For simplicity, this parameter is taken equal to 0.6 [3, 4]. The total pull-out load $F_{PO,tot}$ is then calculated by Eq. 4.13.

$$F_{PO,tot} = F_{PO} + \mu D \qquad \text{Eq. 4.13}$$

A state of equilibrium in the pull-out stage when spalling occurs is found by solving the set of Eq. 4.14 - Eq. 4.16.

$$\alpha = \arcsin\left(\frac{w\sin\theta}{2\left(\Delta f + L_{sp}\right)}\right) \qquad \text{Eq. 4.14}$$

$$\Delta f = \Delta L_a + \Delta u + \frac{F_{PO,tot} L_{sp}}{A_f E_f} \qquad \text{Eq. 4.15}$$

$$w = \eta_w \left[\sqrt{\Delta f^2 + L_{sp}{}^2 \cos^2 \theta + 2L_{sp} \Delta f} - L_{sp} \cos\theta \right] \qquad \text{Eq. 4.16}$$

In which Δf is the relative elongation of the fibre at the exit point with respect to the initial position before cracking occurs and is the sum of the debonding length ΔL_a, a pull-out distance Δu (i.e. slip) and the elastic elongation of the free fibre end. In the fibre debonding stage, both embedded fibre parts are contributing to the crack width and η is taken equal to 2 while the pull-out distance Δu is zero. When the maximum pull-out load is reached, the fibre starts to slip and only one embedded fibre part can contribute to the increased crack opening. As a result, η_f becomes equal to 1 and Δf is increased with the value of Δu. The spalling length L_{sp} is a function of the total pull-out load and hence the equilibrium state will be found iteratively. For a detailed calculation procedure, reference is made to [1] and [4].

4.2.4.3 Fibre orientation and embedded length distribution

Theoretically, the embedded length of a fibre cannot exceed half of the fibre length L_f. As a consequence, the embedded length is assumed to be uniformly distributed within the boundaries 0 and $L_f/2$. The pull-out capacity of a single fibre can only be fully reached when the tensile pull-out forces are sustained by a concrete pull-out cone. By assuming this, no fibre pull-out forces are considered when the embedded length is smaller than the minimum required embedded length to avoid a tensile failure of the concrete matrix.

Given the influence of an inclined pull-out force on the pull-out behaviour of a single fibre, it is obvious that the overall orientation of fibres in a cracked section is of great importance. Gettu [31] determined the uniaxial tensile behaviour on cylinders, drilled in standard bending prisms. Related to the place where a cylinder is drilled and the drilling direction, large differences in residual tensile strength for the same fibre content were found. The research conducted by Grunewald [32] revealed the influence of the fluidity of SFRC. When fibres were added to self-compacting concrete, fibres were more aligned to the flow direction of the concrete when pouring SFRC into the mould. Due to the presence of a large amount of aligned fibres, the flexural capacity is higher than a conventional SFRC with the same fibre content and the scatter on residual strength decreased.

Also the method of placing SFRC into the mould is affecting the overall orientation of fibres. Kang [33] found that when the material is placed in small layers which are separately compacted, the load capacity is about 50 % higher than in the case were the mould is filled transversely to the longitudinal direction of the prism. Another important aspect in the production process of SFRC elements is the applied vibration technique. External vibration applied to the formwork may induce fibre segregation and a preferential orientation of fibres to the planes of the formwork. With all these orientation-influencing aspects in mind, adding fibres to the numerical simulation model needs to be done in such a way that the real orientation of fibres is approached. Kang and Laranjeira proposed mathematical models to describe the variability of inclination of fibres with respect to the longitudinal axis of a beam. The mathematical formulation of fibre orientation, proposed by Laranjeira [34], is based on an orientation number η_θ, which is a base parameter that defines the mean value and standard deviation of all orientation angles of the individual fibres. A truncated Gaussian distribution was found to be in good agreement with the experimentally determined orientation. Furthermore, Laranjeira et al. proved that the average orientation angle itself is correlated with the spread of all orientation angles and hence, one parameter (a dimensionless value between 0 and 1 and denoted as the orientation number η_θ) can be used to determine the orientation profile of a SFRC-batch. When assuming the value of η_θ correctly, the average orientation angle θ_m and standard deviation σ_θ (both in radians) are calculated by Eq. 4.17 and Eq. 4.18.

$$\theta_m = \arccos(\eta_\theta) \qquad \text{Eq. 4.17}$$

$$\sigma_\theta = 90 \times \eta_\theta (1 - \eta_\theta) \qquad \text{Eq. 4.18}$$

Fig. 4.10 shows the difference between the orientation distribution of fibres for η_θ equal to 0.87 ($\theta_m = 30°$), 0.71 ($\theta_m = 45°$) and 0.50 ($\theta_m = 60°$).

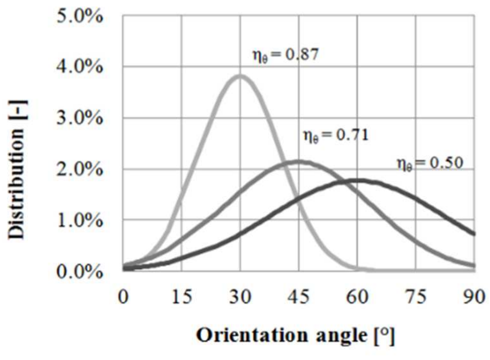

Fig. 4.10 - Orientation distributions for different values of η_θ.

Embedded length [mm] \ Orientation [°]	3	9	15	21	27	33	39	45	51	57	63	69	75	81	87
1	1	2	6	5	4	12	8	15	8	7	13	0	3	4	1
3	0	3	4	3	3	2	2	15	0	0	2	8	5	5	3
5	0	0	4	7	3	10	0	8	15	5	11	2	7	1	4
7	0	2	4	8	5	10	3	7	13	5	7	1	6	2	4
9	0	2	6	9	0	0	8	6	0	9	5	5	6	5	0
11	0	2	6	7	6	3	12	0	8	7	10	0	8	3	1
13	2	2	6	8	5	5	5	5	6	10	3	7	0	3	0
15	0	1	3	7	8	6	2	9	6	8	8	11	8	0	2
17	2	2	1	0	2	3	7	6	5	4	13	12	5	1	0
19	1	2	6	0	3	5	5	15	8	3	14	0	5	4	0
21	1	2	2	7	4	7	4	9	1	11	5	7	7	4	2
23	0	2	0	8	4	5	12	12	16	4	3	12	8	6	2
25	2	2	4	0	2	2	10	11	9	10	0	7	8	6	1
27	1	2	6	7	1	7	0	12	13	11	14	1	6	4	1
29	0	0	0	4	7	7	10	4	14	11	12	6	6	5	0
TOTAL	**10**	**26**	**58**	**80**	**57**	**84**	**88**	**134**	**122**	**105**	**120**	**79**	**88**	**53**	**21**

Fig. 4.11 - Overview of sampled distributions of fibre inclination and embedded length

In the applied method, a two sided truncated normal distribution is used to sample the inclination angle between the limits of 0° and 90°, with 0° being a fibre aligned with the crack opening direction and 90° being a fibre parallel to the crack, and hence without any crack-bridging ability. The cumulative distribution function is then used to perform Monte Carlo sampling [35].

Aiming for a balance between accuracy and calculation speed, the orientation angle and embedded length of fibres is divided into 15 equal intervals, ranging from 3° to 87° and from 0.033 to 0.966 times L_f respectively. Hence, 225 different fibre pull-out curves are computed and attributed consequently to a fibre with corresponding orientation. An example of a sampled distribution of 1125 fibres with orientation profile $\theta_m = 50°$ and a fibre length equal to 60 mm is given in Fig. 4.11.

4.2.4.4 Mode I composite behaviour

Based on the single fibre pull-out response, the Mode I composite behaviour is obtained analytically by lumping all individual fibre pull-out (F_{PO}) curves while assuming appropriate distribution of both fibre and concrete properties as well as the dispersion of fibres. The total pull-out force of all fibres is then divided by a crack surface area A_{cr}. In order to get the combined behaviour of plain concrete and fibres, a bi-linear softening law [25] for plain concrete (σ_{ct}) is also taken into account (Fig. 4.12). Hence, as a function of crack opening w, fibre orientation distribution and embedded length, concrete compressive strength f_{cm} and fibre strength f_{Fy}, the tensile response of SFRC can be expressed as:

$$\sigma_f(w) = \frac{\sum_{i=0}^{N_f} F_{PO}\left(w, \theta, f_c, f_{fy}\right)}{A_{cr}} + \sigma_{ct}(w) \qquad \text{Eq. 4.19}$$

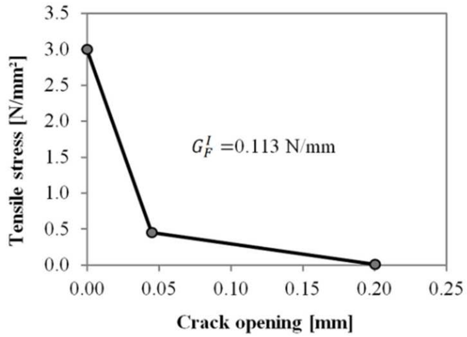

Fig. 4.12 – Bi-linear softening law adopted for plain concrete.

A typical axial stress-crack opening result obtained by means of the analytical procedure based on single-fibre pull-out behaviour is shown in Fig. 4.13.

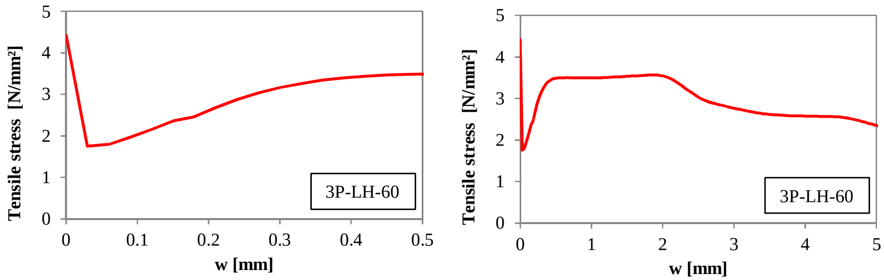

Fig. 4.13 – Modelled post-cracking tensile stress-crack width obtained from fibre pull-out: from 0 – 0.5 mm (left) and from 0 – 5 mm (right).

4.2.5 Comparison between analytical and inverse analysis model

Fig. 4.14 shows a comparison of the Mode I composite behaviour, for the pull-out based model and the inverse analysis (IA) procedure. On overall, a good agreement is found between the detailed response of the analytical model based on single-fibre behaviour, and the more simple predefined tri-linear model to be calibrated through inverse analysis or through correlation with EN 14651 SFRC performance tests. Further, it can be seen (Fig. 4.15) that the post-cracking peak stress is estimated quite well by the model.

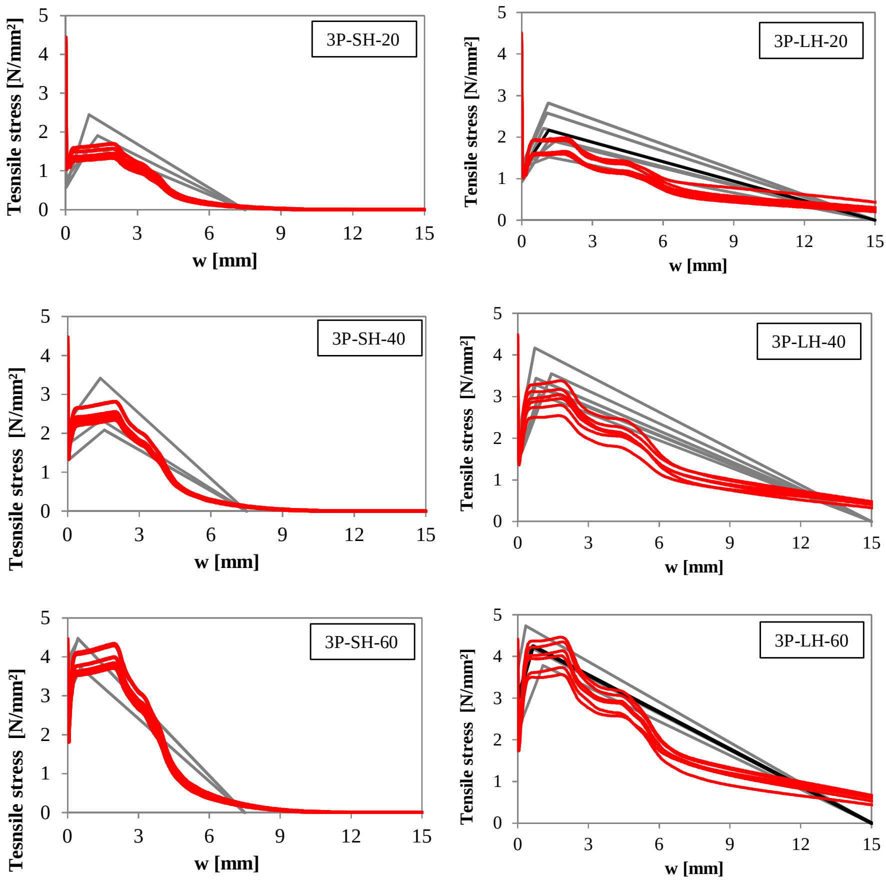

Fig. 4.14 - Comparison between modelled Mode I crack opening versus inverse analysis results

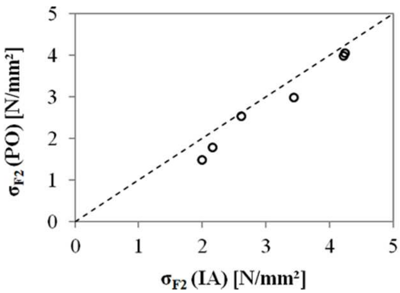

Fig. 4.15 - Comparison between modelled Mode I crack opening versus inverse analysis results

The integration of post-cracking stresses of the Mode I crack opening behaviour from zero until the ultimate crack width at which no stresses can be transmitted anymore (i.e. $w_u = L_f/2$), is herein defined as the total fracture energy (Eq. 4.20).

$$G_f^I = \int_0^{w_u} \sigma_F(w) \qquad \text{Eq. 4.20}$$

Fig. 4.16 shows good agreement between the total fracture energy as derived by the inverse analysis procedure and based on the fibre pull-out mechanism. A quantitative comparison (in terms of relative error) between the two methods is done for the Mode I fracture energy between crack width intervals 0.1 - 0.5 mm and 0.5-4.0 mm, as given in Table 4.8.

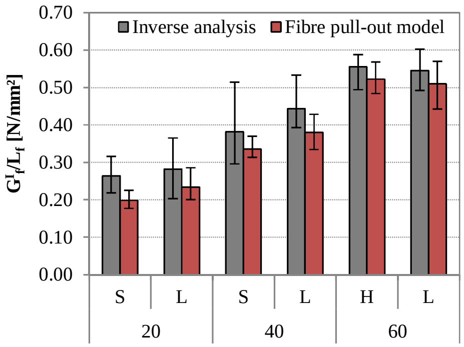

Fig. 4.16 - Mode I fracture energy based on IA and fibre pull-out.

Table 4.8 - Relative error (R) in % between the fracture energy derived by fibre pull-out (PO) and inverse analysis (IA)

Series	0.1 - 0.5 mm	0.5 - 4.0 mm
3P-SH-20	27.2	22.1
3P-SH-40	15.0	1.4
3P-SH-60	10.2	4.3
3P-LH-20	0.1	21.8
3P-LH-40	3.9	15.4
3P-LH-60	9.3	5.4

4.2.6 Finite element Model based on fibre pull-out

4.2.6.1 Modelling concept

The SFRC finite element modelling approaches proposed by Soetens [22] as well as by Cunha [29] are quite similar: firstly, a plain concrete volume is defined and fibre elements are added afterwards. The two phased model (Fig. 4.17) is then used to perform a non-linear finite element analysis. Once a concrete element is cracked, all fibres crossing that element volume will be activated and start to provide crack bridging stresses. Fibre forces are calculated by taking into account the axial post-cracking strains (converted to a fictitious pull-out displacement) and fibre inclination with respect to the longitudinal bending-axis of the analysed prism.

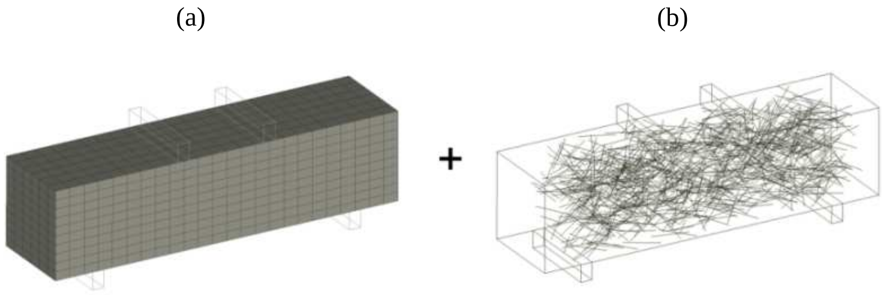

Fig. 4.17- Finite element two-phase modelling concept (a) concrete prism (b) fibres

Once a volume is defined, a Monte Carlo sampling algorithm is designed to place fibres randomly and because in reality the fibre position is affected by the presence of a formwork, the wall effect phenomenon is implemented simultaneously by a so called point-in-polygon (PIP) algorithm [36]. Consequently, all sampled fibres will lie within the boundaries of the prism volume. The randomness of fibre inclination is implemented by assuming the following conditions related to the fibre coordinates (x, y, z) in the matrix (see Fig. 4.18):

$$x_1 = x_m + \frac{L_f}{2}\cos\alpha \qquad \text{Eq. 4.21}$$

$$y_1 = y_m + \frac{L_f}{2}\sin\alpha\cos\beta \qquad \text{Eq. 4.22}$$

$$z_1 = z_m + \frac{L_f}{2}\sin\alpha\sin\beta \qquad \text{Eq. 4.23}$$

$$x_2 = 2x_m + x_1 \qquad \text{Eq. 4.24}$$

$$y_2 = 2y_m + y_1 \qquad \text{Eq. 4.25}$$

$$z_2 = 2z_m + z_1 \qquad \text{Eq. 4.26}$$

in which $x_{m,}$ y_m and z_m are the coordinates of the midsection of the fibre and the orientation angles α and β (see Fig. 4.18) are given by the following equations:

$$\alpha = F^{-1}(x)\sigma_\theta + \theta_m \qquad x \in [0,1] \qquad \text{Eq. 4.27}$$

$$\beta = 2\pi F^{-1}(x) \qquad x \in [0,1] \qquad \text{Eq. 4.28}$$

with σ_θ and θ_m given by Eq. 4.17 and Eq. 4.18.

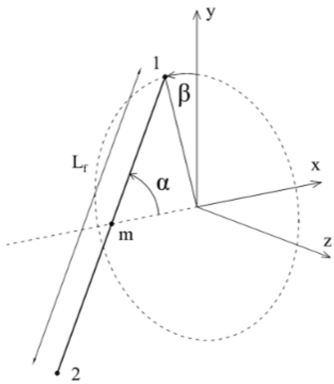

Fig. 4.18- Definition of fibre inclination angles α and β

4.2.6.2 Implementation into finite element analysis

As mentioned before, the pull-out model developed by Van Gysel [2] can provide the needed relationship between pull-out load and slip values for every different pull-out configuration (i.e. the combination of embedded length and pull-out direction). However, these load-slip curves cannot be implemented into the finite element approach directly and therefore, both pull-out load and slip values have to be converted to an equivalent stress-strain material behaviour.

When a concrete element is cracked, the crack strains are induced to all fibre elements crossing this crack. These fibres are now activated and will be able to provide the crack to sustain post-cracking tensile stresses. In case of a completely bonded cable element, strains along the cable element will only increase locally where the mother element is cracked (Fig. 4.19a), which is not representative for the fibre pull-out slip behaviour. This is solved by assuming a constant equivalent strain along the reinforcement element (Fig. 4.19b), whereby fibres are modelled as cable elements with fixed ends (i.e. the cable element is only fixed to the concrete mother elements at both ends). In this way, the fibre element is insensitive to the localisation of the cracked mother element along its length. With the equivalent material model assigned to the cable element, inherently, an embedded length is assumed and the fixed ends geometrical configuration is neglected (see also [23]).

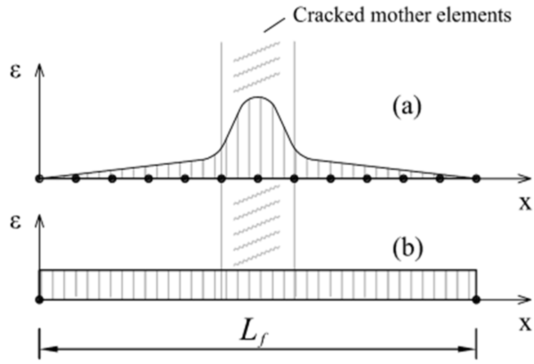

Fig. 4.19- Strain distribution over fibre length with a completely (a) and partially embedded (b) cable element

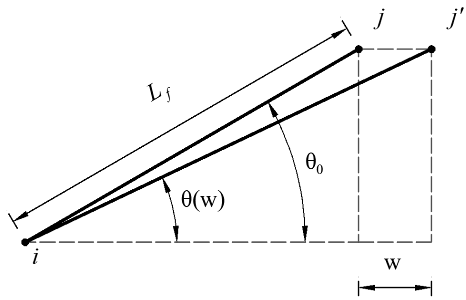

Fig. 4.20 - Original and deformed cable element geometry.

Assuming a cable element with fixed ends and a constant strain, the fibre pull-out load-slip behaviour can be transferred into an equivalent stress-strain behaviour given by Eq. 4.29 and Eq. 4.30.

$$\varepsilon_{eq} = \frac{w}{L_f}\cos\theta(w) \qquad \text{Eq. 4.29}$$

$$\sigma_{eq} = \frac{F_{PO}}{A_f}\left(\frac{1}{\cos\theta(w)}\right) \qquad \text{Eq. 4.30}$$

In which the variable pull-out direction θ(Δ) due to geometrical effects (see Fig. 4.20) is given by

$$\theta(w) = \arctan\left(\frac{L_f \sin\theta_0}{L_f \cos\theta_0 + w}\right) \qquad \text{Eq. 4.31}$$

in which θ_0 is the initial fibre inclination angle; L_f is the length of the fibre element; F_{PO} is the pull-out load; w is the crack opening and A_f is the cross-section of the fibre.

4.2.6.3 Concrete properties

To implement the non-linear behaviour of the concrete matrix, a fixed smeared crack model is adopted assuming an exponential crack opening law for the post-tensile cracking behaviour of the plain concrete [37]. Linear cubic elements are used to model the concrete prism. The average values of the modulus of elasticity and tensile strength of the concrete are calculated based on the compressive strength Table 4.3 by the equations given in Model Code 2010. For the usage of the bi-linear softening law after cracking Fig. 4.12, a fracture energy G_F^I for plain concrete is calculated by the provisions given in MC90.

4.2.6.4 Fibre properties

As mentioned before, the pull-out model developed by Van Gysel [2] can provide the needed relationship between pull-out load and slip values for every different pull-out configuration. However, these load-slip curves can't be implemented into the finite element approach directly and therefore, both pull-out load and slip values have to be converted to an equivalent stress-strain material behaviour as explained in Section 4.2.6.2).

4.2.7 Model verification

For each conducted series of experimental four-point bending test, six three-dimensional finite element models are sampled and analysed. All six numerical models were parallel calculated on a personal computer. It took about one complete day to finish one series. A typical post-processing result, including the occurrence of multiple cracking, is shown in Fig. 4.21.

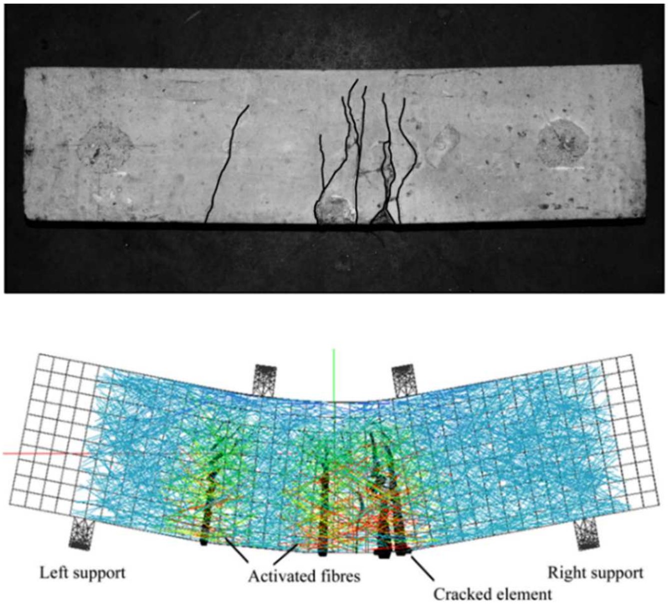

Fig. 4.21 – Activation of fibres in case of multiple cracking

Since all finite element models are unique through different fibre distribution, orientation, fibre tensile strength and concrete compression strength, scatter on the flexural response is obtained. The experimental envelope of the four-point bending tests are shown together with the envelope of modelled flexural stress-deflection curves in Fig. 4.22.

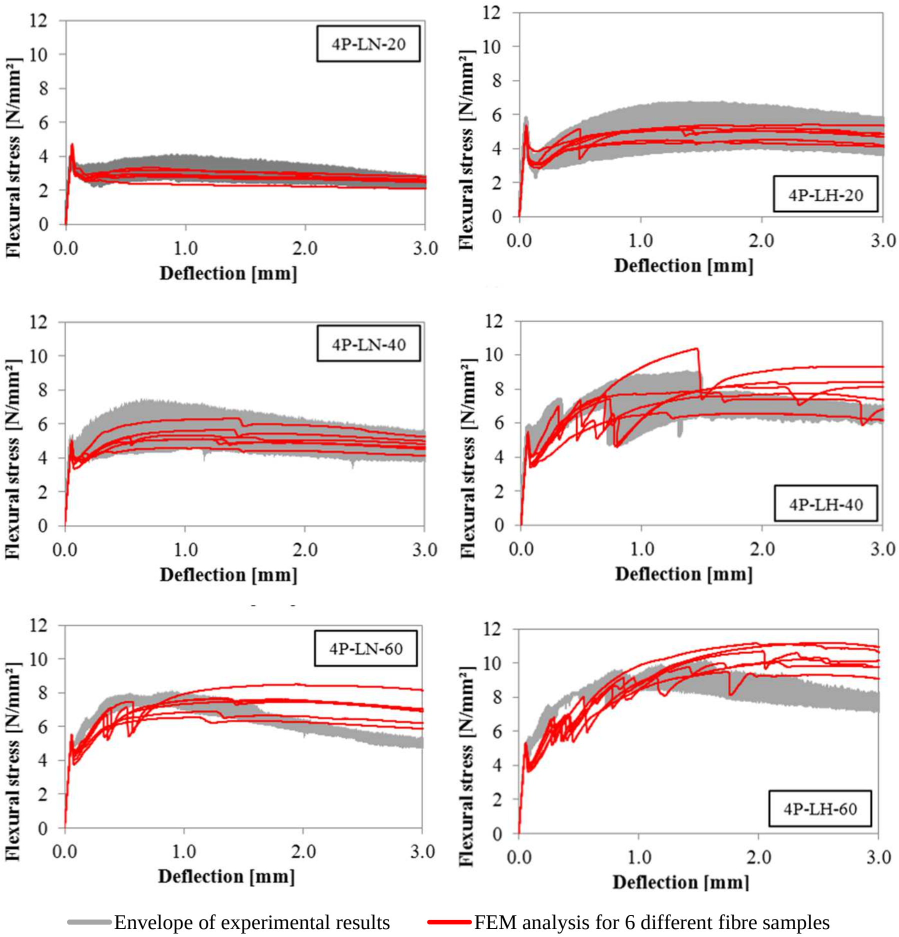

Fig. 4.22 - Comparison between the numerically and experimentally obtained flexural response of SFRC

From Fig. 4.22, it can be seen that the developed model is quite accurate in predicting both the first cracking stress as well as the overall cracking behaviour. Only for SFRC with fibre dosage equal to 60 kg/m³ at higher deflections (>1.5 mm), an overestimation of the post-cracking flexural stresses is made. This difference between the model and the experiments can be attributed to the fact that in reality fibres at higher dosages are interacting with each other in damaging the concrete matrix, resulting in a reduced post-cracking ability of the composite at higher deflections. Nevertheless, both the numerical and experimental curves have no significant increase of flexural stresses for deflections higher than 1.5-2.0 mm and the numerical curves slightly start to drop for a deflection of about 2.0 mm. The relative error between the average experimental and average modelled curves are shown in Fig. 4.23 for series 4P-LH and 4P-LN respectively. From this comparison, it can be concluded that the average error is in the range of 10-15 % for deflections between 0 and 1.5 mm. For series 4P-LH-40, 4P-LH-60 and 4P-LN-60, the model overestimates the flexural stresses for about 25-30 % when the deflections are higher than 1.5 mm.

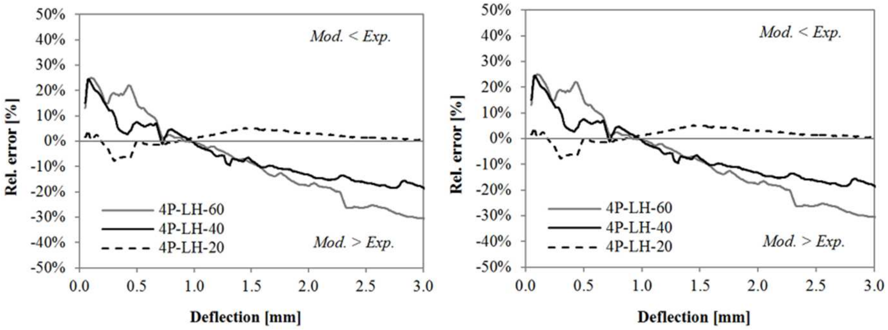

Fig. 4.23 – Relative error between modelled and experimental 4P-bending response

In Fig. 4.24, a comparison is made between the modelled and experimental conventional flexural stresses $f_{f,n}$ (Eq. 4.2), in terms of minimum, maximum and mean values for both $f_{f,300}$ and $f_{f,150}$. The values shown in Fig. 4.24 reveal a good correlation between the model and the experiments and it indicates the feasibility of the model to predict the flexural behaviour of SFRC. Moreover, the model proved to be able to predict the multiple cracking behaviour (Fig. 4.24) as experimentally observed during the four-point bending tests. Regarding the overall similarity between finite element simulations and experimental tests, the proposed method can be useful to gain a quick insight into the flexural behaviour of SFRC prior to testing.

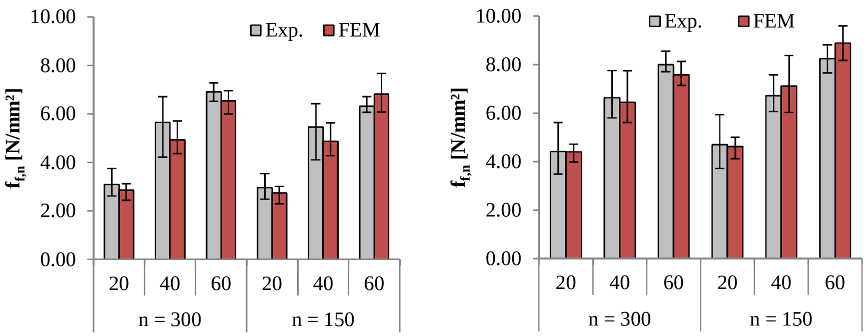

Fig. 4.24 - Comparison between the numerically and experimentally obtained values for $f_{f,300}$ and $f_{f,150}$

4.3 Transverse pull-out behaviour

4.3.1 Introduction

In contrast to the high number of investigations that link the pull-out behaviour of a single fibre to the tensile or bending behaviour of SFRC, only one study is known to the author that applies the same approach for examining the fracture of SFRC under Mode II [38]. In this study, Lee conducted a large number of push-off tests on Z-type specimens with a total of eight fibres crossing the vertical shear plane with each of them fixed in a known position and orientation. Based on the experimental results, a Variable Engagement Model (VEM) was developed to predict the direct shear capacity of SFRC. For the testing of the transversal pull-out, different test configurations can be adopted as discussed in Section 2.3.5. In this work, the modified (small-scale) JSCE SF4 push-through test [39, 40] is used.

4.3.2 Materials and methods

Based on the push-through tests on standardized prisms (150 mm x 150 mm x 500 mm), which was firstly developed by the JSCE [40] and modified by Banthia [39] afterwards, a similar test setup was adopted to investigate the transversal pull-out response of a single hooked-end steel fibre. In total, for each different fibre orientation angle θ (+60°, +30°, 0°, -30° and -60°), five series of mortar prisms (290 mm x 70 mm x 40 mm) were casted. Therefore, a casting procedure was followed which consists out of two phases. In the first phase (Fig. 4.25), the central part of the prism was replaced by two wooden blocks with a thickness of 20 mm. Between these wooden plates, two fibres were clamped symmetrically and hence, their orientation and position were fixed. Then, the empty right and left part of the mould were filled with mortar and they were compacted by allowing the mould to fall through a controlled height (20 mm), at the rate of 60 jolts per min. One day later, the first phase mortar pieces were demoulded and the wooden blocks were removed. The position and orientation of the fibres is then fixed by the hardened right and left mortar blocks. To avoid bond between the first and second phase mortar, a plastic foil was placed between them and finally, the second phase mortar (Fig. 4.26) was poured and compacted. Immediately after casting, the mortar prisms were stored at 20 °C and 95 % of relative humidity.

The used mortar contained 1310 kg/m³ of sand 0/5 and 655 kg/m³ of cement type CEM I 52,5 N with a W/C ratio equal to 0.45. The fibres used in this study are hooked-end steel fibres (DRAMIX RC-80/60-BP) with a length of 60 mm and a diameter of 0.75 mm and a tensile yield strength equal to 2000 N/mm². For each test series, standard mortar prisms (40 mm x 40 mm x 160 mm) were casted and used to determine both flexural ($f_{ct,fl}$) and compressive strength (f_c) of the used mortar at the testing age of 28 days. For each orientation, all measured values are listed in Table 4.9.

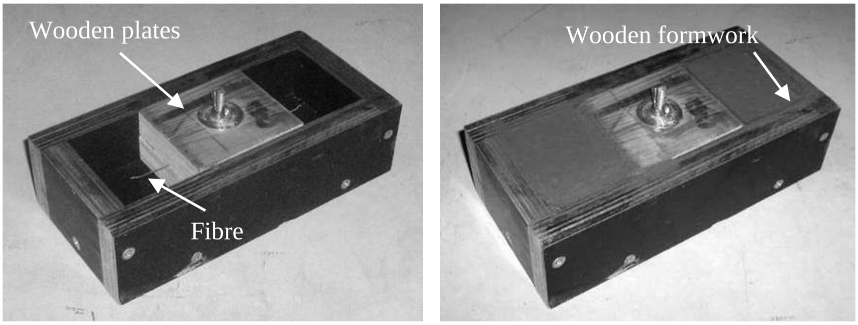

Fig. 4.25 - First moulding phase

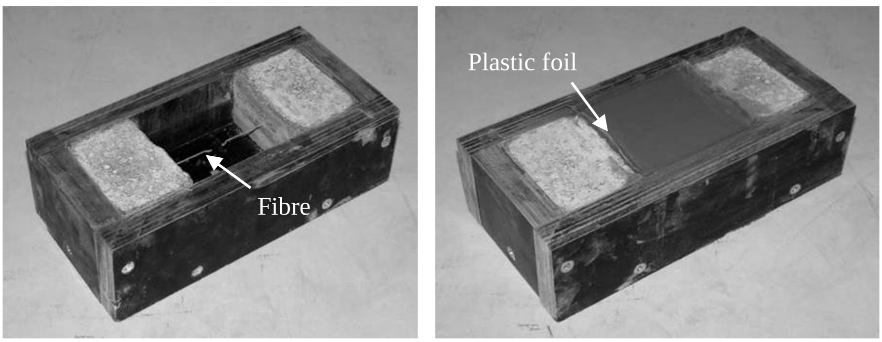

Fig. 4.26 - Second moulding phase

Table 4.9 - Mortar properties at 28 days

Test series	$f_{ct,fl}$ [N/mm²]	f_c [N/mm²]	
+60°	8.1	69.3	69.9
	8.4	73.5	72.9
+30°	7.0	67.8	68.9
	7.3	68.2	71.4
+0°	9.0	72.3	75.0
	6.9	69.5	67.9
-30°	7.7	73.3	75.0
	8.4	71.5	70.2
-60°	7.3	65.0	71.0
	6.8	72.7	69.6
Average	7.7	70.7	
St. Dev.	0.8	2.6	
CoV	9.8 %	3.7 %	

A displacement controlled load was applied with an initial rate of 0.0025 mm/s until a peak load was reached. The rate was then increased to 0.01 mm/s until fibres were completely pulled out on both sides or fibre rupture occurred at one side. The relative vertical displacement Δ was continuously measured by means of a linear variable displacement transducer (LVDT) with a nominal range of 50 mm. The applied compression load was measured by means of a load cell, placed between the specimen central part and the loading equipment. Due to the symmetry of the test setup, the measured vertical load is equal to the sum of pull-out forces of the two fibres crossing the vertical sliding plane and thus, to derive the pull-out load of a single fibre, the total load has to be divided by two. A schematic of the test setup is shown in Fig. 4.27.

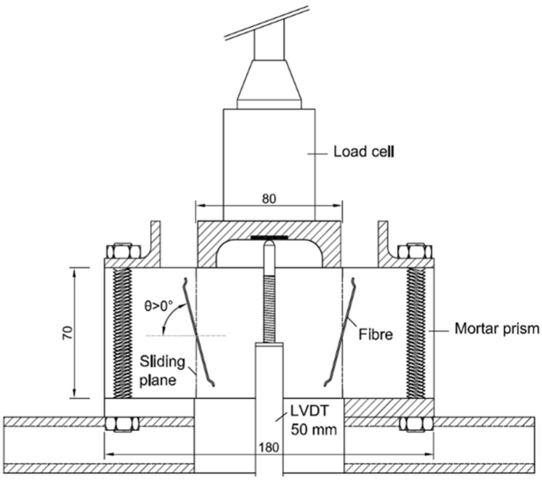

Fig. 4.27 - Single fibre push-through test setup

4.3.3 Test results and discussion

For each different orientation angle, the load per fibre (averaged over two fibres) as a function of shear slip Δ is plotted in Fig. 4.28 to Fig. 4.33. To have a clear view on the difference in pull-out behaviour due to the variation of the orientation angle, the maximum axis value of both vertical displacement (40 mm) and pull-out load (1 kN) is kept constant for all graphs. The grey lines are representing the individual experimental test results, while the black curve and the dotted grey line are respectively the mean value and the standard deviation of the pull-out load during the pull-out process.

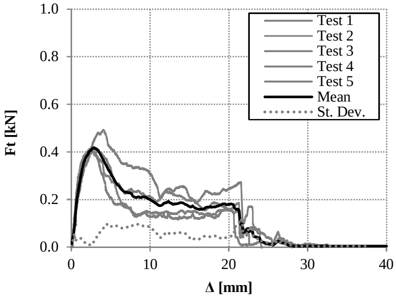

Fig. 4.28 - Pull-out force vs. Δ [+60°]

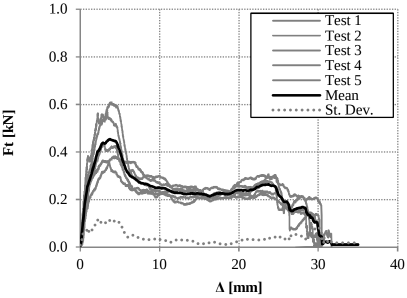

Fig. 4.29 - Pull-out force vs. Δ [+30°]

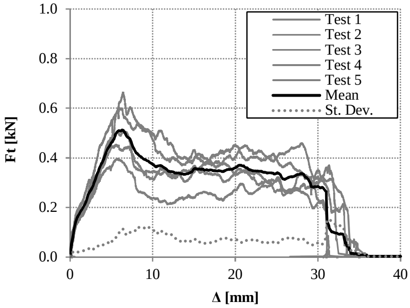

Fig. 4.30 - Pull-out force vs. Δ [0°]

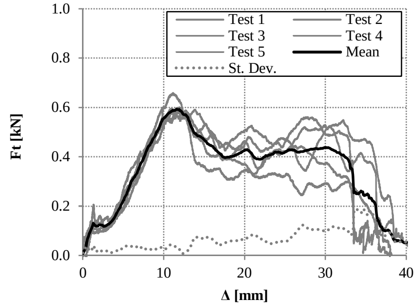

Fig. 4.31 - Pull-out force vs. Δ [-30°]

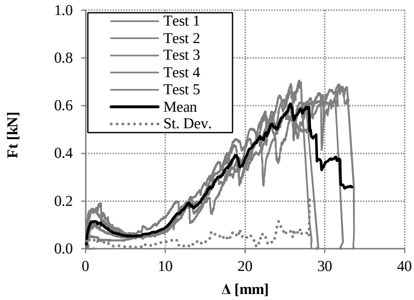

Fig. 4.32 - Pull-out force vs. Δ [-60°]

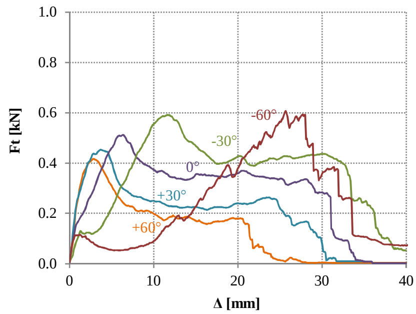

Fig. 4.33 - Average pull-out curves

Generally, two types of failure were observed as a function of initial fibre orientation angle θ: in case of an aligned transversal pull-out (θ > 0), the pull-out behaviour is highly similar to the axial pull-out and the fibre is completely pulled out of the surrounding matrix on at least one sliding plane. Hence, fibres being transversally pulled out aligned with their orientation will lead to a ductile failure behaviour of SFRC failing in shear. A positive orientation angle of the fibre leads to a direct tensile loading of the fibre and debonding starts taking place immediately. When the fibre is completely debonded, the fibre starts to slip and the pull-out load decreases until a quasi-horizontal branch (i.e. the residual pull-out strength) is reached. The average residual transversal pull-out force increases linearly with decreasing values of θ (Fig. 4.34). This increase can be attributed to the additional friction forces, acting on the fibre exit point.

In contrast to this relatively ductile pull-out behaviour, a more brittle rupture of fibres was observed for the case of an initial orientation of fibres opposite to the pull-out direction (i.e. θ < 0). For negative values of θ, the effect of snubbing takes place (cf. [38]) and higher values of Δ at the peak pull-out load are observed. Due to the snubbing effect, initially the fibre is subjected to compression and bending, considerably higher frictional forces act on the fibre during the debonding phase and may lead to the rupture of the fibre before it starts to slip significantly. For decreasing values of θ, the peak pull-out load increases linearly (see Fig. 4.35)

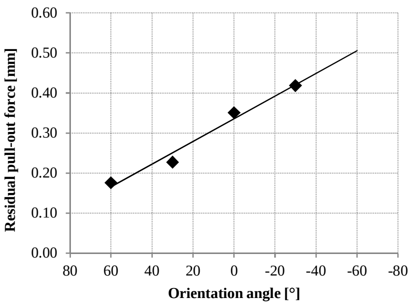

Fig. 4.34 - Residual pull-out force vs. θ

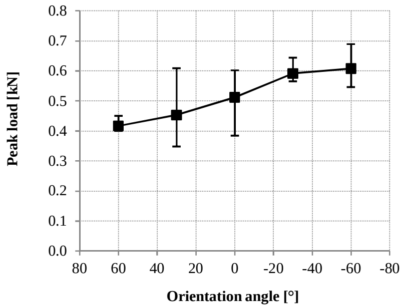

Fig. 4.35 - Peak load vs. θ

Further analysis of the experimental data has been done with respect to the observed slip at peak load and the total work needed to require a complete pull-out failure of a fibre. The relationship between orientation angle and slip at peak load is shown in Fig. 4.36 and the average pull-out work as a function of initial inclination angle is shown in Fig. 4.37.

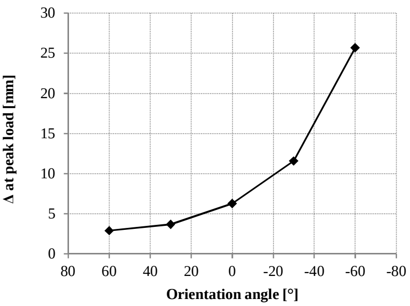

Fig. 4.36 – Shear slip displacement at peak load as a function of fibre inclination

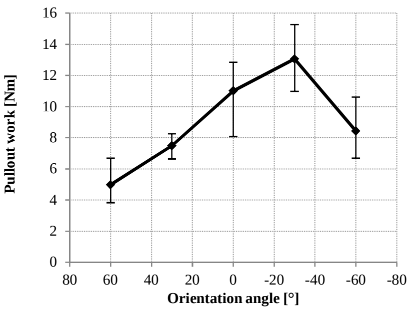

Fig. 4.37 – Total pull-out work as a function of fibre inclination

From Fig. 4.36, it can be seen that the snubbing effect is exponentially increasing for higher opposite pull-out direction. Hence, for these pull-out conditions, the fibre deformation at the exit point will first cause significant damage to the surrounding matrix prior to develop tensile forces in the fibre itself.

For initial fibre orientations between +60° and -30°, the required total pull-out work (Fig. 4.37) is increasing linearly. This can be attributed to the existence of a residual branch after debonding takes place during the pull-out process. However, for orientations equal to -60°, it is found that the mechanical anchorage due to friction at the fibre exit point leads to fibre rupture and no residual pull-out forces can be developed. As a result, the total pull-out work (as a measure for ductility) decreases.

4.4 Direct Shear Behaviour

4.4.1 Introduction

Whereas in Section 4.3 the transverse pull-out behaviour at single fibre level is discussed, in this section, the direct shear behaviour of SFRC is considered. The experimental study makes use of the modified JSCE SF6 test method (Section 2.3.5), extending on the single fibre experiments of Section 4.3.

Based on the observed direct shear behaviour and test results reported in literature, a new modelling approach for the direct shear capacity of SFRC is presented herein. Starting from existing aggregate interlock models [41-43], the beneficial effect of fibres and confining forces towards the shear friction behaviour are integrated into a semi-analytical calculation tool which takes into account the effect of crack propagation.

In this way, the model can not only estimate the interface shear strength of a crack in SFRC, but it can also be used to simulate the complete shear stress – slip response. Comparison between the test results and the calculated response demonstrates the feasibility of the proposed semi-analytical model.

4.4.2 Materials & methods

4.4.2.1 Mix composition and test programme

A test programme, comprising 69 direct shear tests, is carried out in order to investigate the influence of fibre dosage, fibre type, concrete type and normal stresses on the direct shear behaviour of SFRC. The used steel fibre reinforced concrete grade is C50/60 and contains hooked-end DRAMIX cold drawn wire high strength steel fibres (f_{Ft} > 2000 N/mm²). Two different fibres with a length equal to 60 mm (L) and 30 mm (S) are used in combination with a self-compacting concrete (SCC) and a traditional concrete (TC) with a slump between 160-210 mm (i.e. consistency class S4 according to the European Standard EN 206-1:2000). The following mixing procedure is adopted: the concrete constituents (see Table 4.10) are first mixed without the cement and with half of the water volume for one minute. Then the fibres, cement and the other half of mixing water are added and the concrete is mixed an additional two minutes while adding the superplasticizer. Since the use of a superplasticizer can increase the inclusion of air during mixing, the air-content is measured according to the European Standard NBN EN 12350-7 immediately after mixing. Because a high air-content can decrease the fibre-matrix interaction mechanisms, the air-content of SFRC-mixes should be kept lower than 4 % [44]. Specimens in traditional concrete are compacted on the vibrating table during one minute. In this way, heavy compaction is avoided which can cause fibre segregation or bad dispersion of fibres in general.

For material characterisation of each steel fibre reinforced concrete batch, standard prisms sized 150 mm x 150 mm x 600 mm and standard cylinders of 150 mm x 300 mm

[45] are cast and stored under wet conditions (R.H. > 95%) for 28 days. An overview of all test series and the obtained SFRC properties for the fresh and hardened state are summarized in Table 4.11.

Table 4.10 - SFRC mix constituents [kg/m³]

Constituent	TC	SCC
Sand 0/1	202	-
Sand 0/4	674	816
Crushed limestone 2/7	257	346
Crushed limestone 7/14	566	388
Cement CEM 52.5 (N/R)	390 (R)	360 (N)
Limestone filler	-	240
Superplasticizer	2.2	3.5
Fibres 30 / 60 mm	20-60	20-60
Water	190	165
W/C	0.49	0.46

Table 4.11 – Fresh and hardened properties for all SFRC-batches

Designation	fc,cyl [N/mm²]	Air [%]	Slump [mm]	Flow [mm]	No. of tests	Fibre content [kg/m³]	Confining pressure [N/mm²]
TC-0-0	57.8	-	160	-	3	0	0
TC-20S-0	65.9	2.5	210	-	3	20	0
TC-40S-0	59.9	2.9	210	-	3	40	0
TC-60S-0	57.7	5.9	180	-	3	60	0
SCC-0-0	65.1	1.0	-	825	3	0	0
SCC-20L-0	63.6	1.5	-	745	3	20	0
SCC-40L-0	62.7	2.0	-	805	3	40	0
SCC-60L-0	60.0	2.0	-	825	6	60	0
SCC-20S-0	64.3	2.2	-	740	6	20	0
SCC-40S-0	58.3	1.8	-	770	6	40	0
SCC-60S-0	60.5	2.8	-	650	6	60	0
SCC-20L-5	65.1	1.8	-	705	3	20	5
SCC-20L-10	65.1	1.8	-	705	3	20	10
SCC-40L-5	70.4	2.3	-	725	6	40	5
SCC-40L-10	70.9	2.3	-	656	6	40	10
SCC-40L-25	72.1	0.9	-	790	6	40	25

4.4.2.2 Direct shear test specimen and setup

All shear tests are done by means of the modified JSCE direct shear test [40]. A schematic of the test setup is shown in Fig. 4.38 (left). In order to obtain predefined crack planes, 30 mm deep notches are sawn vertically at both sides of the standard prisms (Fig. 4.38, right). Hence, the shear plane is equal to 90x150 mm².

During testing, linear variable displacement transducers (LVDT's) are used to measure the relative vertical displacement (slip). Simultaneously, the crack dilation is monitored by means of horizontally placed extensometers (Fig. 4.38, left). The vertical load is applied displacement controlled by means of a hydraulic jack at a load-displacement rate equal to 0.02 mm/min until a maximum load is reached and increased to 0.1 mm/min afterwards.

In order to investigate the effect of confining pressure, further modifications are made to the test setup (Fig. 4.39). A horizontal compression load is applied by a horizontal jack. By means of a load cell this compression force is monitored and kept constant (manually controlled). The reaction forces are balanced by symmetrically positioned steel beams connected by threaded bars (Fig. 4.39).

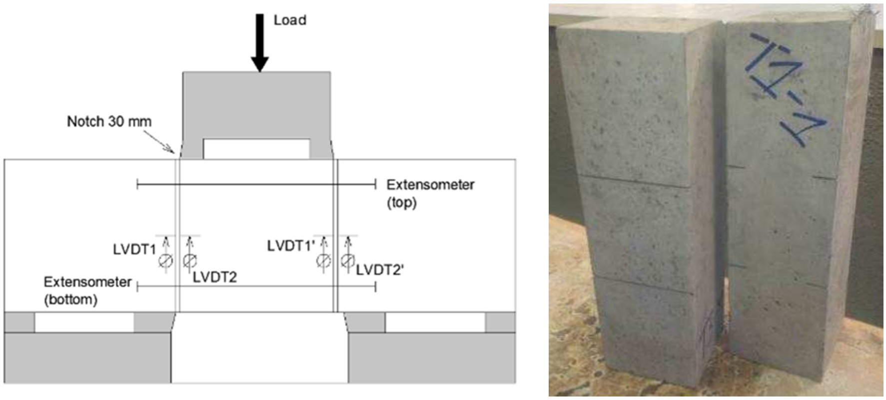

Fig. 4.38 - Schematic of the test setup (left) and double-notched specimens (right)

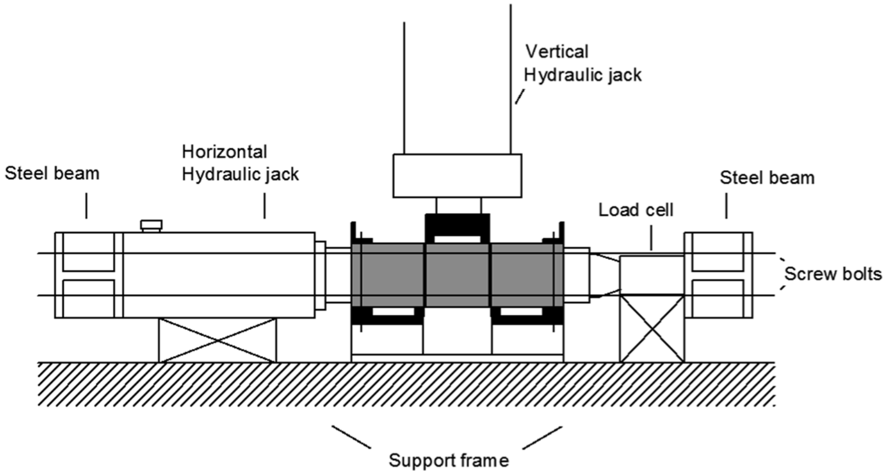

Fig. 4.39 - Schematic of the confined test setup.

The confined pressure is transferred to the shear interface by the rigid outer parts of the test specimen. In this way, the complete loading system as depicted in Fig. 4.39 is fixed, except for the vertical hydraulic jack and the central part which moves downwards between the two outer parts.

4.4.3 Direct shear behaviour

During testing, all specimen failed by shearing at the notched interface. In a first stage of the test, a linear elastic behaviour is observed until a first crack is induced in both shear planes near the bottom of the specimen. While increasing the load, this crack propagates towards the upper side of the specimen until a maximum or peak load is reached. This behaviour reveals secondary effects, in which partially bending occurred prior in reaching the ultimate shear stress at the interface and hence, undesirable compressive stresses are acting in the upper region of the shear interface. As a consequence, the adopted test setup did not fully result in the desired pure shear failure. Fig. 4.40 shows the difference between the shear stress-crack width relationship for the upper and lower extensometer.

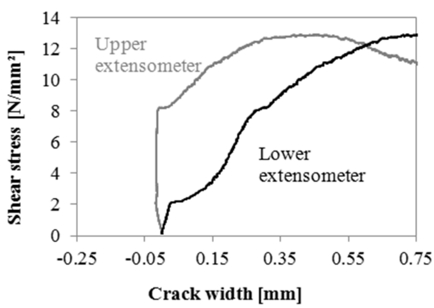

Fig. 4.40 - Difference between horizontal crack width propagation near top and bottom of the specimen.

Important slipping (vertical crack displacement) occurs at the shear interface after the upper region of the specimen is cracked and a strong non-linear response is observed. After the peak shear stress, an exponential decay of shear stress is observed reaching a quasi-horizontal branch at a slip of about 8 mm and crack opening ranging between 1.5 and 2 mm.

When analysing the cracked surface after testing, it can be observed that the aggregates are broken and crushing of local asperities damaged the shear interface. The post-cracking strength is provided by friction and pull-out of fibres.

In Fig. 4.41 till Fig. 4.44, the experimentally obtained direct shear behaviour is given for all tested series, showing the individual tests results as well as the average curve (black line).

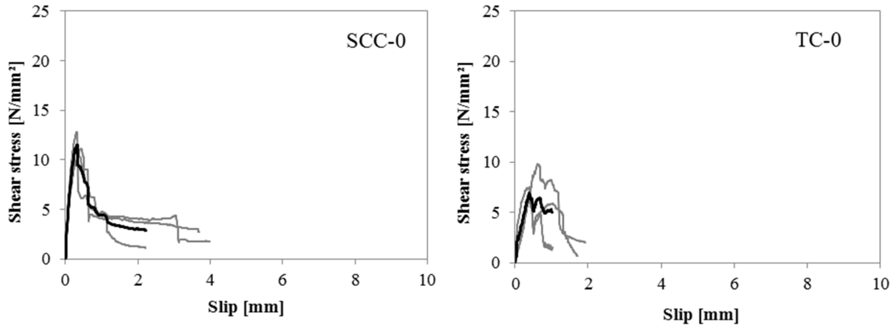

Fig. 4.41 - Shear stress-slip behaviour for plain concrete series SC-0 and T-0

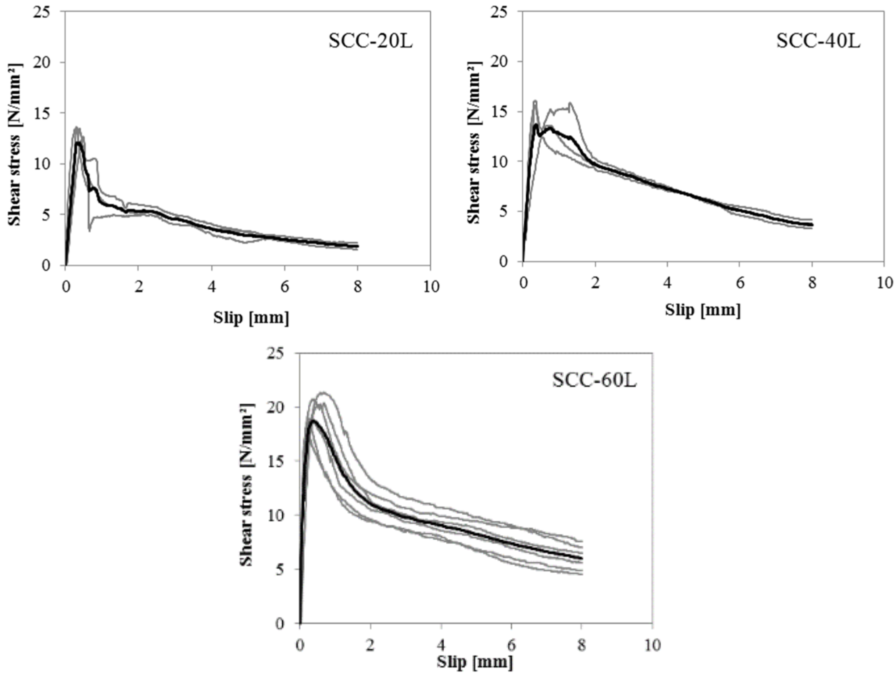

Fig. 4.42 - Shear stress-slip behaviour for series SCC-L

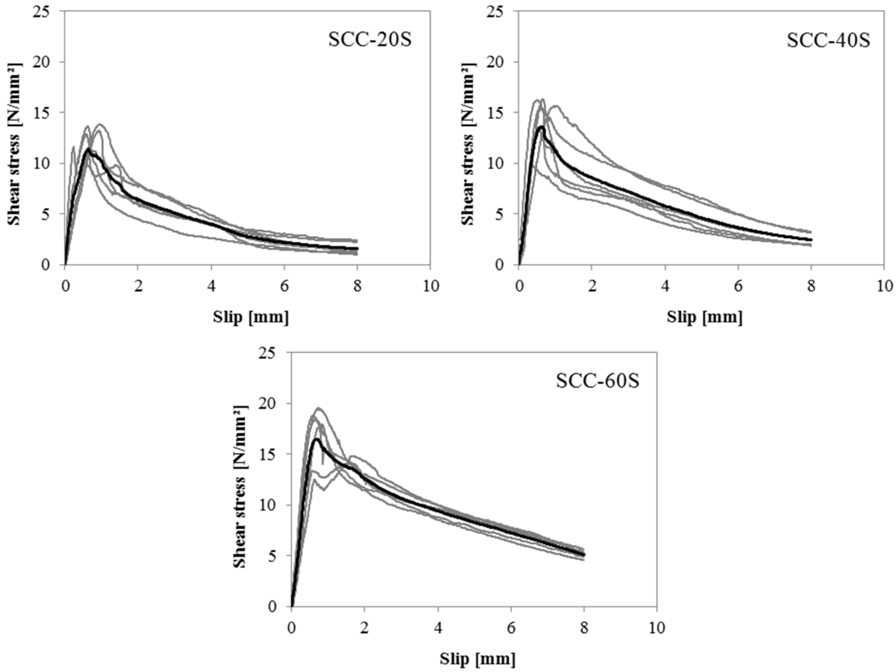

Fig. 4.43 - Shear stress-slip behaviour for series SCC-S

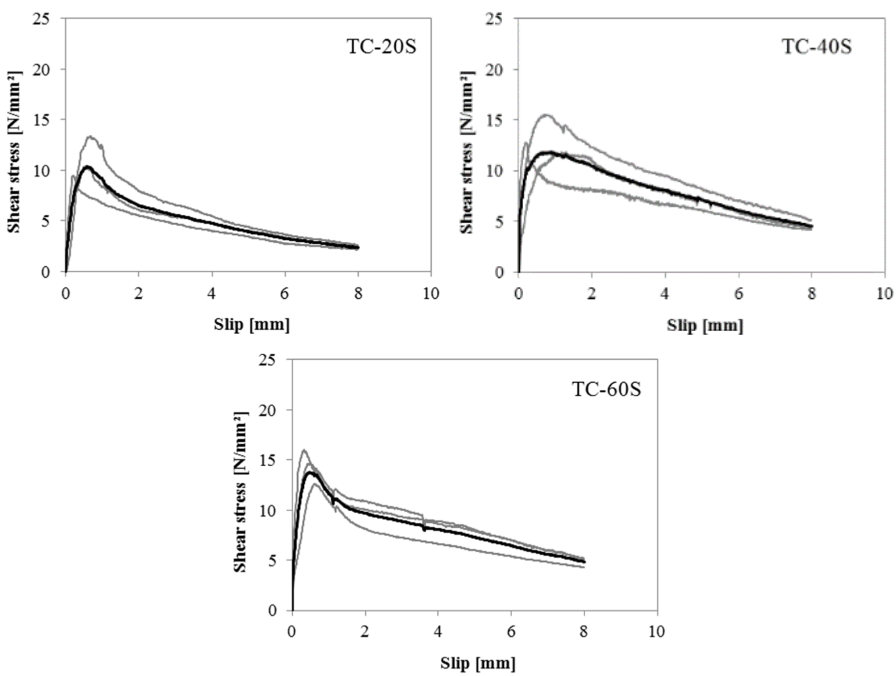

Fig. 4.44 - Shear stress-slip behaviour for series TC-S

4.4.3.1 Influence of fibre dosage and type

The maximum shear stress of cracked fibre reinforced concrete τ_{SFRC} increases for higher fibre dosages. Table 4.12 summarizes $\tau_{SFRC,max}$ in terms of average ($\tau^{avg}_{SFRC,max}$), minimum ($\tau^{lo}_{SFRC,max}$) and maximum ($\tau^{up}_{SFRC,max}$) values, normalized by the square root of the compressive strength for each series. $\tau^{avg}_{SFRC,max}$ as a function of fibre dosage V_f is also shown in Fig. 4.45.

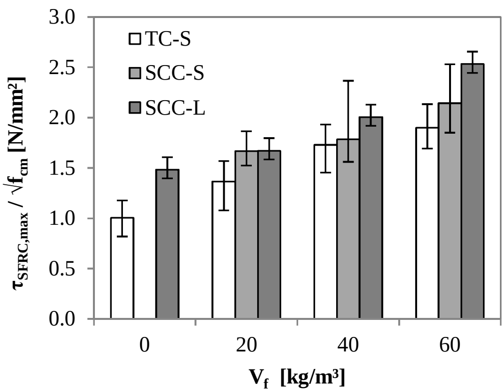

Fig. 4.45 - Normalized maximum direct shear strength as a function of fibre dosage.

For test series TC, the average increase of shear stress with respect to the plain concrete series is equal to 45%, 75% and 88% for fibre dosages of 20, 40 and 60 kg/m³ respectively. This clearly indicates that for series TC the increase rate of shear strength is less than proportional with the fibre dosage. For series SCC, the increase of shear strength is more than proportional with added fibre content. Regarding the influence of fibre type for series SCC-S and SSC-L, the increase of direct shear strength is larger for longer fibres than for shorter fibres with a same fibre aspect-ratio. For the series with the shorter fibres, the coefficient of variation (CoV) is in the range between 8-20 % while for the series with long fibres the CoV is between 1 and 8 %. All values are summarised in Table 4.12.

Table 4.12 - Maximum shear stress for all tested series

Test series	$\tau^{avg}_{SFRC,max}$ [N/mm²]	$\tau^{lo}_{SFRC,max}$ [N/mm²]	$\tau^{up}_{SFRC,max}$ [N/mm²]	CoV [%]
TC-0-0	7.64	6.34	9.06	17.9%
TC-20S-0	11.1	9.4	13.4	18.8%
TC-40S-0	13.4	11.8	15.5	14.3%
TC-60S-0	14.4	12.6	16.0	11.7%
SCC-0-0	11.9	11.2	12.9	7.4%
SCC-20L-0	13.3	12.7	13.8	4.0%
SCC-40L-0	15.9	15.7	16.1	1.4%
SCC-60L-0	19.6	17.3	21.3	7.5%
SCC-20S-0	12.8	11.2	13.9	8.4%
SCC-40S-0	14.5	9.8	16.4	17.4%
SCC-60S-0	17.2	14.1	19.6	12.9%

4.4.3.2 Crack propagation

For all of the direct shear tests, the average crack opening (i.e. the average of measured crack width near top and bottom of the test specimen) is shown as a function of the relative vertical displacement or slip, in Fig. 4.46 till Fig. 4.48. The individual crack propagation curves are shown as a solid grey line and the average for each series as a solid black line. The observed crack propagation behaviour has the same shape for all tested series with steel fibres. In the initial branch of the crack width-slip curve (corresponding with the pre-peak branch in the shear stress-slip curves), the ratio of crack widening to sliding is larger than for the branch at higher slip values (corresponding with the post-peak branch in the shear stress-slip curves). Hence, after reaching the maximum shear stress, crack sliding becomes more important with respect to crack widening.

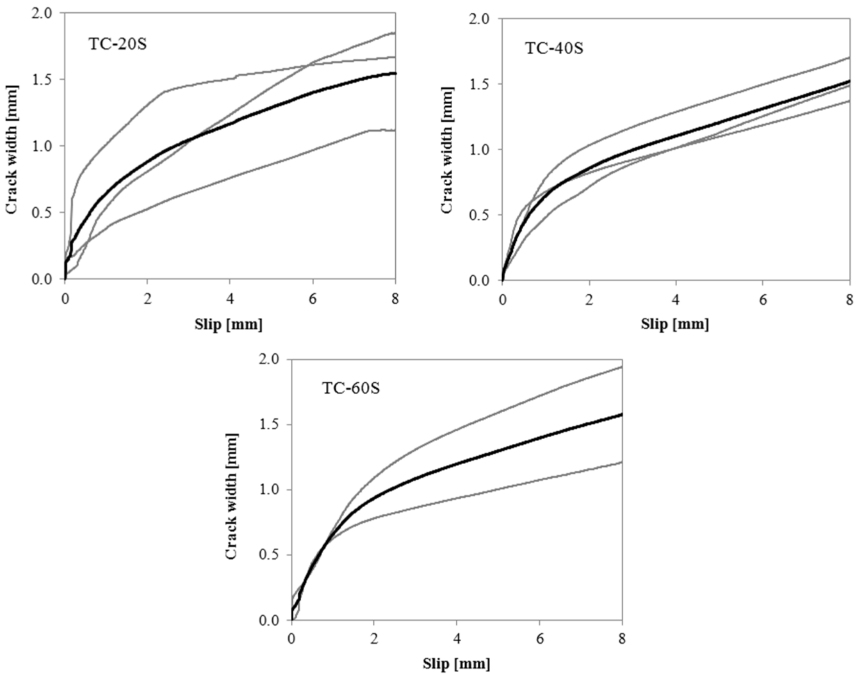

Fig. 4.46 - Crack propagation curves for test series TC-S

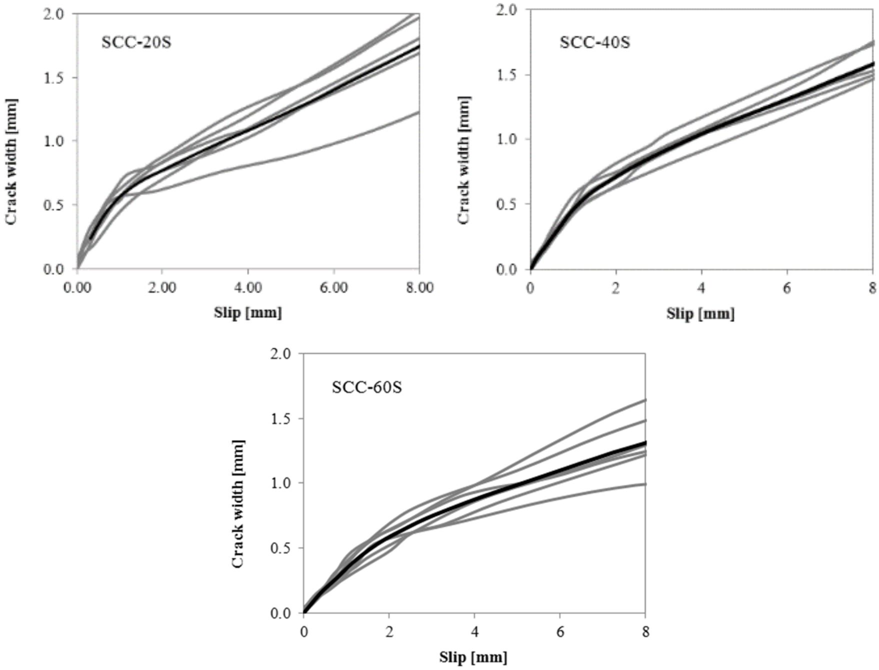

Fig. 4.47 - Crack propagation curves for test series SCC-S

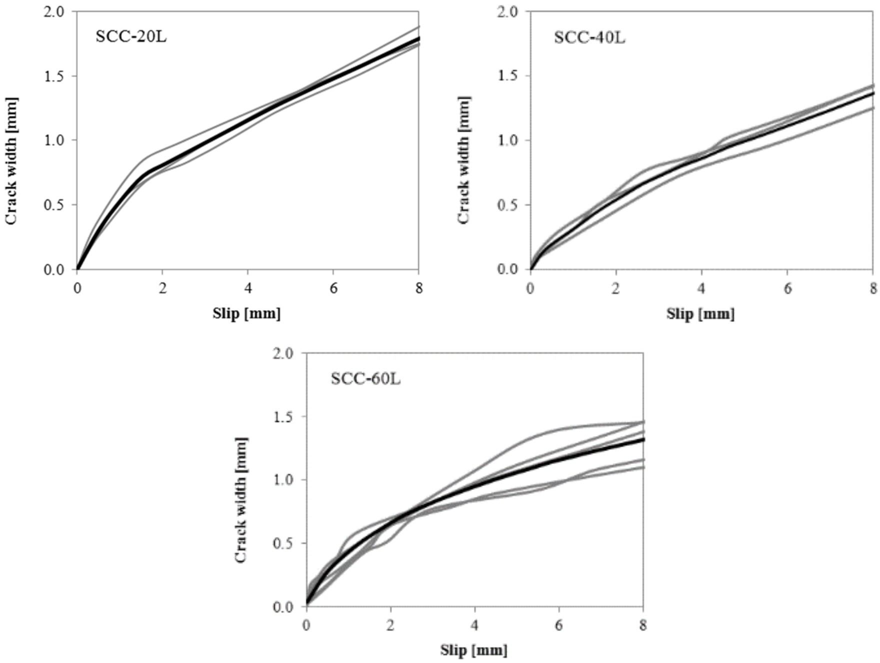

Fig. 4.48 - Crack propagation curves for test series SCC-L

From the curves of Fig. 4.46 till Fig. 4.48, no significant effect of fibre dosage and type can be observed on the crack propagation behaviour. This indicates that the crack dilatation is likely inherent to the adopted test setup. As a consequence, the shear crack propagation is of key importance to be able to compare different test results obtained from different kinds of direct shear tests.

4.4.3.3 Influence of confining pressure

According to the Coulomb friction law, the maximum stresses that can be transferred through the shear interface will increase with higher confining stresses. Fig. 4.49 shows the obtained shear stress-slip curves for series 20-S and 40-S as a function of applied stress normal to the shear crack interface.

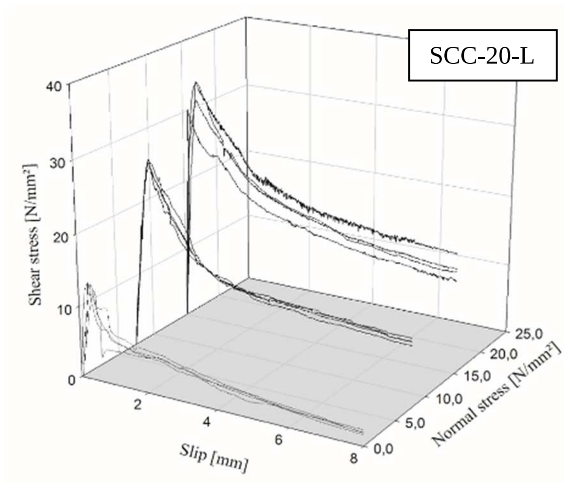

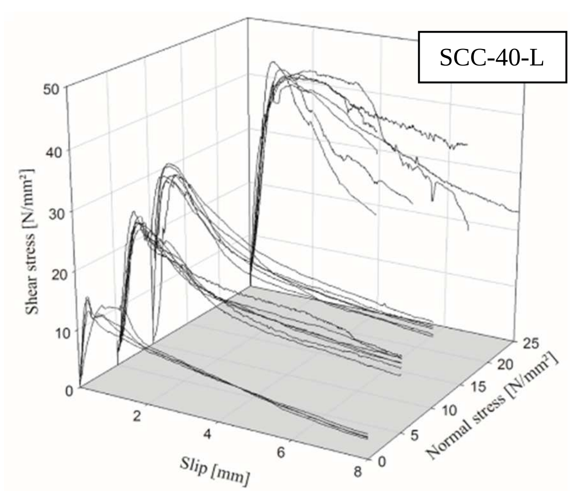

Fig. 4.49 - Shear stress -slip curves as a function of confining stress for series SCC-20-L (upper) and SCC-40-L (lower)

From Fig. 4.49, a shear stress increase can be observed with higher normal stresses over the complete range of slip considered (0-8 mm). For test series SCC-40-L however, the biaxial stress state, for a confining stress equal to 25 N/mm², caused a compressive failure after reaching the peak shear stress. In order to know the effect of slip on the increase of shear stresses, the shear stresses observed at the peak and at a slip value of 4 mm are shown in Fig. 4.50.

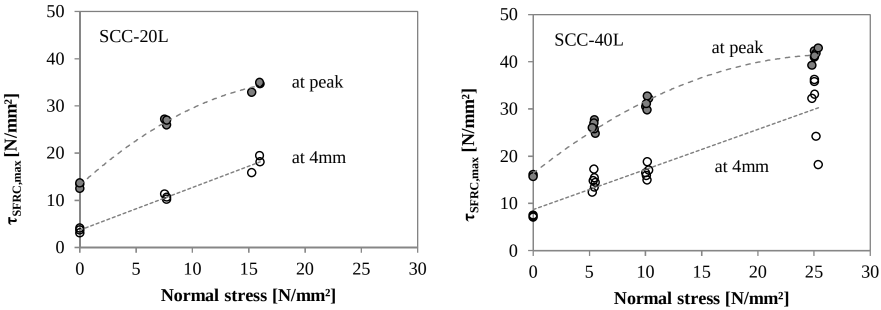

Fig. 4.50 - Shear stress -slip curves as a function of confining stress for series SCC-20L and SCC-40L at peak and a slip of 4 mm.

For the shear stresses at peak, the increase is less than proportional with the stress applied normal to the shear interface. This can be attributed to severe damage and crushing of aggregates due to the confined stress at small crack openings. Further, it can be seen that for normal stresses in the range of 0 to 5 N/mm² the ratio of normal to transversal stress decreases for larger slip values and hence for smaller ratios of crack width to slip. This indicates that the frictional effects are dependent on the crack propagation behaviour.

4.4.4 Shear friction models for SFRC

Most of the direct shear models for SFRC found in literature [39, 46-48] (see Chapter 2, Section 2.3.5) focus on the maximum shear stress observed during testing rather than the overall shear behaviour. Therefore, a distinction is made between two types of modelling concepts namely the direct shear strength models and the direct shear behaviour models.

4.4.4.1 Direct shear strength

<u>*Unconfined shear strength*</u>

A validation of the empirical models found in literature (see Section 2.3.5, Table 2.3) is performed by looking into both the shear strength provided by the plain concrete τ_c and by the addition of fibres τ_f (see also Section 2.3.5, Eq. 2.3). Starting with the plain concrete component τ_c, in Fig. 4.51 a comparison is given between a dataset of direct shear test results and the available models. The dataset considers results for plain concrete found in literature [39, 46-54] and the reference specimens of this study. Two criteria were used in order to select proper data: 1) the used test setup is either the modified JSCE method or the

Z-type specimens method and 2) all specimens are uncracked prior to testing. In total, 32 different test results ranging from 20-80 N/mm² cylinder compression strength are included in the database.

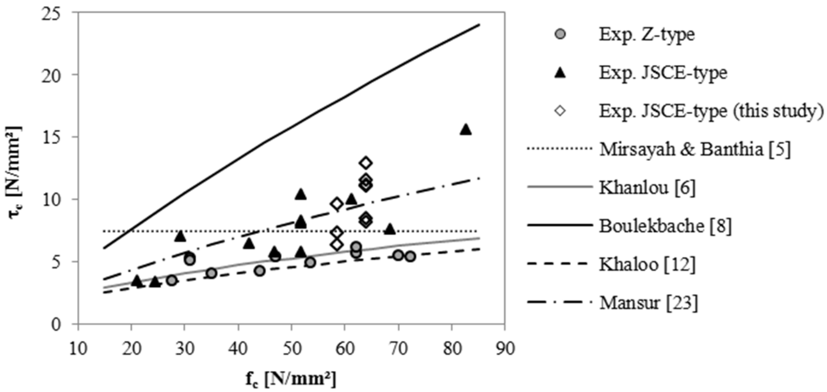

Fig. 4.51 - Comparison between experimentally observed plain concrete (PC) direct shear strength and proposed models

As can be seen in Fig. 4.51, both the equations of Khanlou and Khaloo show a good correlation for the maximum shear capacity derived by means of Z-type push-off tests. The plain concrete contribution as suggested by Boulekbache is systematically overestimating the shear strength of plain concrete for concrete strengths between 20 and 80 N/mm². The equation proposed by Mirsaya and Banthia does not take into account the effect of concrete compressive strength although there is a clear correlation found through experimental testing. The model by Mansur is more in agreement with the shear strength derived for plain concrete by means of the JSCE test setup.

Further, it can be noticed that when the shear capacity is determined by means of the modified JSCE test, higher shear stresses are observed compared to the tests for which the Z-type specimens are used. This can be attributed to a difference in shear crack propagation and failure aspects. To evaluate this, more detailed information is needed with respect to the slip and crack opening displacement for the shear tests, which is not reported by the authors.

In order to evaluate the existing empirical formulations which take into account the effect of fibre dosage (see Section 2.3.5, Table 2.3)), the experimentally observed maximum shear strength is plotted as a function of fibre dosage for both series TC-S and SCC-L (see Fig. 4.52).

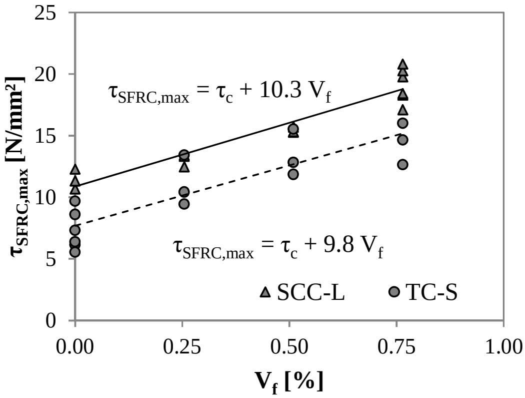

Fig. 4.52 - Influence of fibre content on the maximum direct shear capacity for series TC-S and SCC-L

Given the available shear strength models (see Section 2.3.5, Table 2.3), the fibre effect τ_f can be written in the following general form:

$$\tau_f = AV_f^{B} \qquad \text{Eq. 4.32}$$

In which A and B are constant values, defining the incremental effect of fibres on the maximum shear capacity of the concrete. Based on the observed direct shear behaviour for series TC-S and SCC-L, a regression analysis yields a linear relationship (i.e. B = 1) between fibre dosage and shear stress increase (Fig. 4.52) leading to the values of A equal to 10.3 and 9.8, respectively. The value of A as proposed by Boulekbache (A = 6.4 for L_f/d_f = 80) is underestimating the fibre contribution. The same conclusion can be drawn when considering the proposed equation by Khanlou (A = 4). Since the used fibres in this study have hooked ends, a comparison with the models of Khaloo [52] and Mirsayah & Banthia [39] is not made.

Furthermore, the experimental tests of series TC-S and SCC-L indicate that the equations proposed by Boulekbache and Khanlou are only applicable for SFRC made of low-strength steel fibre (i.e. with a tensile strength equal to 1100 N/mm²) and that the proposed equations do not take into account the complete fibre-matrix interaction (i.e. fibre pull-out mechanism as a function of matrix strength and fibre type). From the test results, it can be observed that the increase of shear friction capacity is higher when high-strength fibres (with a tensile strength of at least 2200 N/mm²) are combined with a concrete grade C50/60.

Confined shear strength

As suggested by Loov [55], the increase of the maximum direct shear capacity of cracked concrete with traditional reinforcement bars crossing the shear interface perpendicularly is related to concrete compressive strength and normal confining stress due to yielding of the reinforcement bridging the crack. This additional effect τ_{conf} can be written as follows:

$$\tau_{conf} = k\sqrt{f_c \rho f_y} \qquad \text{Eq. 4.33}$$

in which f_c is the cylinder compressive strength in N/mm², ρ is the geometrical reinforcement ratio, f_y is the yield stress of reinforcement in N/mm² and k is a proportionally constant which is determined by Wong [56] to be equal to 0.46 and 0.57 for initially uncracked and cracked specimens respectively. These values of k are obtained from push-off tests on concrete specimens with a compressive strength between 16 and 31 N/mm² and a confining pressure not higher than 10 N/mm².

When the confining pressure is a result of an externally applied force, Eq. 4.33 can be rewritten as

$$\tau_{conf} = k\sqrt{f_c \sigma_{cp}} \qquad \text{Eq. 4.34}$$

in which σ_{cp} is the externally applied confining stress perpendicular to the crack plane.

The increase of $\tau_{SFRC,max}$ with respect to $\sqrt{f_c \sigma_{cp}}$ is shown in Fig. 4.53 for confined test series SCC-20L (left) and SCC-40L (right).

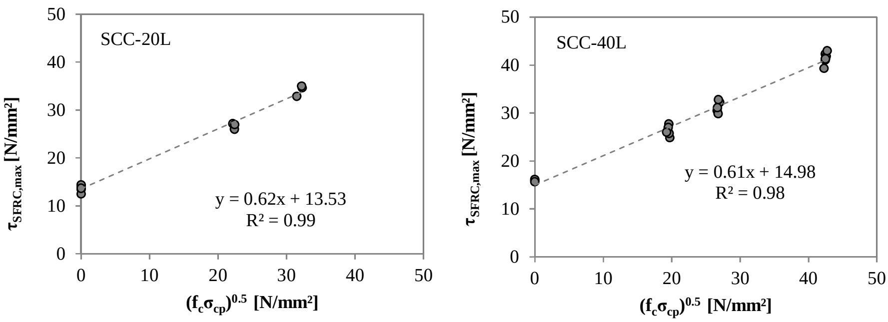

Fig. 4.53 - Correlation between confining pressure, concrete compressive strength and the maximum direct shear strength for series SCC-20L (left) and SCC-40L (right).

From Fig. 4.53, it can be concluded that for higher concrete strengths (60-70 N/mm²) and normal confining stresses (5-25 N/mm²) the value of k in Eq. 4.34 is equal to 0.62 and 0.61 for series SCC-20L and SCC-40L respectively. This behaviour implies that the shear friction capacity is not a linear function of the confining pressure and the coulomb friction law cannot be applied straightforward. For higher normal confining stresses, the frictional stresses do not increase proportionally.

4.4.4.2 Direct shear behaviour

In order to consider SFRC properties and crack propagation into more detail, a more fundamental model is proposed based on the experimental data derived from the direct shear tests. The shear design equation of an interface intersected by dowels or reinforcement bars according to the Model Code 2010 [25] or the similar expression in ACI 318-11 [57], is used as a basis for further development of a SFRC shear stress transfer model. Similar attempts to model the direct shear behaviour of fibre reinforced mortar were made in the past by Lee [38] and Ng [58] based on the Variable Engagement Model (VEM) developed by Foster et al. [59].

It is considered that the shear friction capacity of cracked fibre reinforced concrete is attributed to:

- Transversal fibre pull-out mechanism of all fibres.
- Aggregate interlock of the rough interface.
- The normal stress component (σ_{cp}), which can be attributed to yielding of the reinforcement or a physically applied normal stress field.

The proposed model neglects the bending stiffness of individual fibres and it is further assumed that dowel action does not contribute to the shear strength of the cracked interface. This assumption is made based on the observed shear crack opening behaviour. Since the opening of the crack is primarily more important than the shear slip, the fibre will be bended rather than sheared. As a result, the shear strength interface equation can be written in the following general form:

$$\tau_{SFRC} = \tau_{agg} + \mu\sigma_{cp} + \sum_{i=1}^{N_f} \frac{F_{PO,i}\left(\cos\theta_{f,i} + \mu\sin\theta_{f,i}\right)}{A_c} \qquad \text{Eq. 4.35}$$

In which τ_{agg} is the aggregate interlock component, μ is a friction coefficient, N_f is the total amount of fibres crossing the shear crack, $F_{PO,i}$ is the pull-out force of the i^{th} fibre with pull-out direction angle $\theta_{f,i}$ and A_c is the shear crack area.

<u>*Aggregate interlock*</u>

During the 1980's, several aggregate interlock models have been proposed based on the outcome of extensive experimental testing of the shear transfer mechanism in cracked concrete. As a consequence, available models for aggregate interlock generally have a pronounced empirical basis and for each model, the applicability is inherent to specific boundary conditions of the research programme for which a curve fit is applied. Attempts to provide a more physical modelling of aggregate interlocking has been done by Walraven [42] and Li [43], by assuming a distribution of particles at a cracked interface and considering mechanical effects on the micro-level of the rough interface. Although these models have a more physical basis and are able to model the aggregate interlock quite well, their simplified forms are more often applied. Another established yet fully empirical model was developed by Bazant and Gambarova [41] based on the experimental work of Paulay and Loeber [60] and improved by Gambarova and Karakoç [61]. A detailed description of the two-phase model, the rough crack model and the contact density model can be found in Chapter 3, Section 3.1.3.

Aggregate interlocking is strongly influenced by the crack propagation behaviour which is a combination of both opening and sliding. Thereby, it is assumed that crack opening and sliding increase simultaneously after cracking of the concrete. According to Model Code 1990 [62], the crack-width opening relationship can be written as:

$$w = As^{B} \qquad \text{Eq. 4.36}$$

in which w is the crack width perpendicular to the crack plane (horizontal), s is the vertical displacement of the sliding crack planes and the parameters A en B are empirically determined constant values. From the obtained experimental data, it is found that these constants are mainly dependent on the boundary conditions of the adopted direct shear test setup. A regression analysis of the average experimental crack propagation curves (see Fig. 4.46 till Fig. 4.48) resulted into crack propagation parameters A en B for each series (see Table 4.13).

Table 4.13 - Crack propagation parameters A en B.

Test series	A	B
TC-20S	0.63	0.45
TC-40S	0.62	0.42
TC-60S	0.60	0.41
SCC-20L	0.51	0.60
SCC-40L	0.34	0.67
SCC-60L	0.46	0.51
SCC-20S	0.50	0.58
SCC-40S	0.45	0.60
SCC-60S	0.37	0.61

A comparison between the simplified aggregate interlocking models as suggested by Walraven & Reinhardt [42], Li & Maekawa [43] and Gamabarova & Karakoç [61] is shown in Fig. 4.54, for a concrete compressive strength of 60 N/mm², D_{max} = 7 mm and a shear crack propagation law according to Eq. 4.36 with A and B taken equal to 0.6.

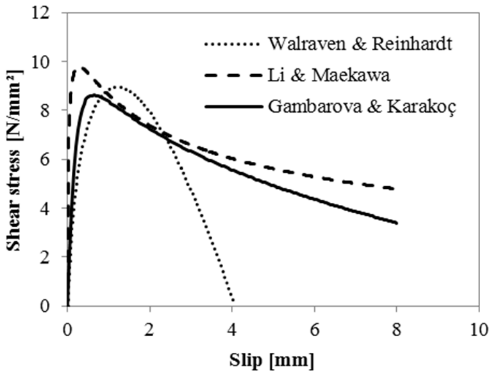

Fig. 4.54 - Comparison between existing simplified aggregate interlock models.

Based on the overall shape of the shear stress slip curves obtained experimentally, the model as proposed by Gambarova and Karakoç [61] is chosen for the τ_{agg} term in Eq. 4.36. In order to deal with the observation that the shear crack goes through the aggregates rather than around them, a lower roughness of the interface needs to be considered. Since, this interface roughness is mainly dependent on the particle size distribution of the concrete matrix, the maximum aggregate particle size D_{max} is replaced by half of its value.

Fibre pull-out

For traditionally reinforced concrete, the effect of reinforcement inclination with respect to the sliding plane is investigated by Walraven & Reinhardt [63] and Mattock [64]. It was found that rebars with an orientation opposed to the sliding direction resulted in a significant decrease of ultimate shear friction capacity. For rebars oriented in the same direction as the sliding occurs, a maximum shear capacity is reached for an orientation angle equal to 45°.

In Section 4.3, the influence of fibre orientation on the transverse pull-out behaviour has been investigated. It was found that fibres with an opposed fibre inclination with respect to the sliding plane caused increased damage at the fibre exit point and bending occurred prior to fibre pull-out. Due to the increased curvature of the fibre at the exit point, high coulomb friction is developed locally and fibres tend to break. When fibres are orientated in line with the sliding direction, the pull-out mechanism is more similar to pure axial pull-out behaviour.

However, the experimental investigation of transverse pull-out behaviour has been done in a two-dimensional situation without taking into account the effects of aggregate interlock and inherent crack dilatation. In contrast to the individual fibre tests, fibre pull-out in a composite situation will be fundamentally different: all fibres are randomly distributed in a 3D-space and the crack dilatation state governs the fibre pull-out condition. Since the proposed model herein will deal with a three-dimensional approach to implement the transversal fibre pull-out, assumptions as discussed in the following are made in order to define the geometrical conditions of fibres crossing a crack sliding plane. A schematic of a single fibre positioned arbitrarily at the shear interface is shown in Fig. 4.55.

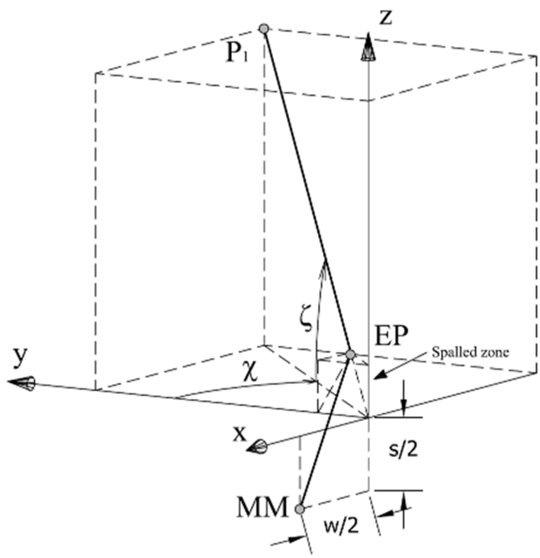

Fig. 4.55 - Influence of fibre inclination towards the direct shear pull-out behaviour of a single fibre [65]

During the debonding phase, the fibre pull-out midpoint (MM) follows the crack dilatation path defined by a crack width and slip displacement. During the pull-out process spalling will occur at the fibre exit point (EP) which is defined based on the spalling criterion as proposed by Laranjeira [3, 4]. Further, the initial position of the fibre with respect to the shear plane is defined by the angles χ and ζ and the location of point P_1. Based on the fibre dosage and orientation profile, the position of all fibres along the shear crack interface can be defined by means of a Monte Carlo sampling algorithm [22, 35]. Thereby, the angles χ and ζ are randomly distributed in the following ranges:

$$\chi \in \left[0, \frac{\pi}{2}\right[\qquad \text{Eq. 4.37}$$

$$\zeta \in \left[-\frac{\pi}{2}, \frac{\pi}{2}\right[\qquad \text{Eq. 4.38}$$

During the pull-out of a fibre, four different situations can be considered. Fig. 4.56 shows a two-dimensional view of these theoretical configurations.

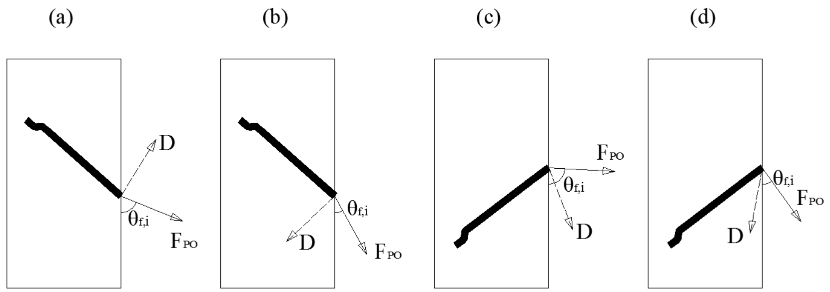

Fig. 4.56 - Different pull-out conditions considered for direct shear.

The situations as shown in Fig. 4.56 are a combination of angle ζ, which can be either positive (Fig. 4.56a and Fig. 4.56b) or negative (Fig. 4.56c and Fig. 4.56d), and the direction of the deviatoric force D, which can be oriented to the right (Fig. 4.56a and Fig. 4.56c) or to the left (Fig. 4.56b and Fig. 4.56d).

In the 3D-space, the fibre pull-out behaviour is calculated in the plane defined by the three points P_1, EP and MM. During the pull-out process, the location of MM is defined by the crack propagation behaviour of the shear crack interface while the position of EP depends on the spalling of concrete at the fibre exit point. A solution algorithm is developed which calculates the complete fibre pull-out behaviour as a function of crack width and inherent slip according to the pull-out model developed by Van Gysel [1, 2, 66]. The contribution of all individual fibres is given by the last term of Eq. 4.35 and depends on the friction coefficient μ.

In literature, different shear friction coefficients for concrete to concrete sliding can be found, ranging between the values 0.35 and 1.4, dependent on the type of concrete and roughness of the crack surface [25, 67]. According to Wong [56], a distinction should be made between the coefficient of static friction, which depends only on the concrete constituents, and the effect of shear dilation. To implement the effect of crack dilation, Wong [56] proposed the following relationship between transversal and axial loads:

$$\frac{F_s}{F_n} = \tan(\varphi + i) \qquad \text{Eq. 4.39}$$

in which

$$\phi = \tan^{-1}\mu \qquad \text{Eq. 4.40}$$

$$i = \frac{dw}{ds} = ABs^{B-1} \qquad \text{Eq. 4.41}$$

In order to obtain a suitable value of μ, the experimental observations from the confined push-off tests are used in combination with the observed crack propagation behaviour (Fig. 4.46 - Fig. 4.48).

4.4.5 Model verification

In order to verify the proposed simulation model, the experimental envelope is compared with respect to the simulated shear stress-slip curves for the nine tested series. In Fig. 4.57 - Fig. 4.59, the comparison of all tested series with respect to the modelled curves are shown.

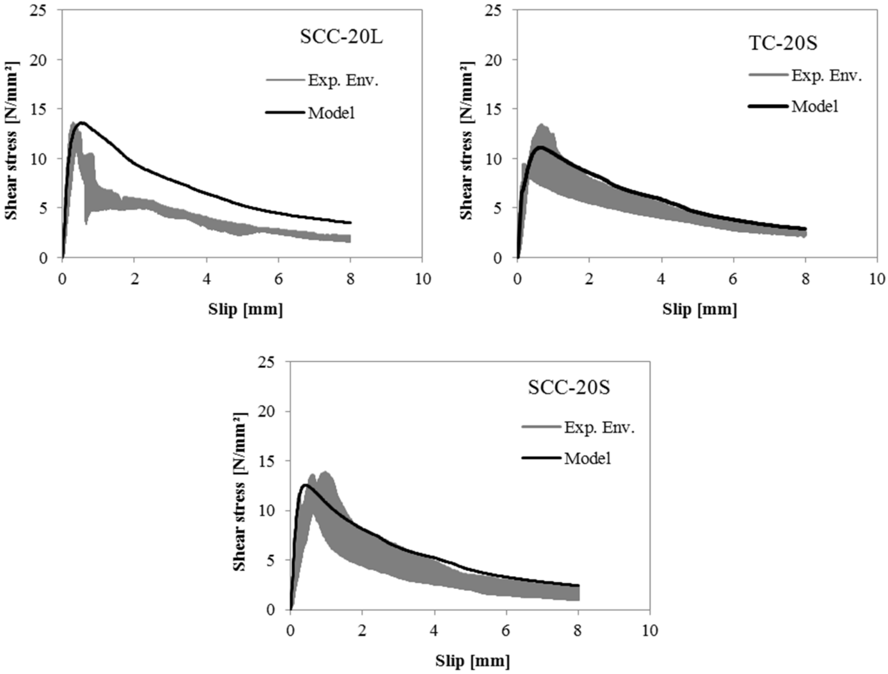

Fig. 4.57 – Model verification for a fibre dosage equal to 20kg/m³

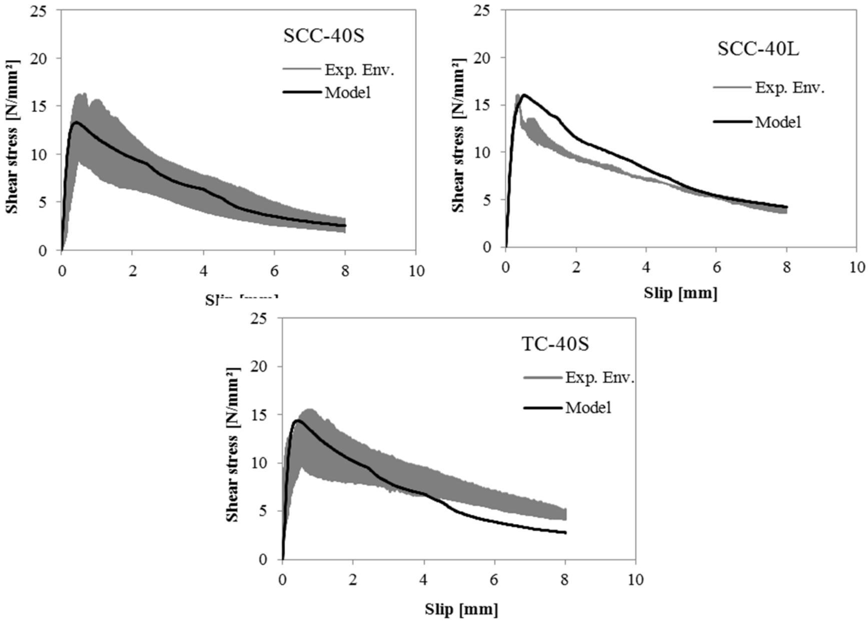

Fig. 4.58 – Model verification for a fibre dosage equal to 40kg/m³

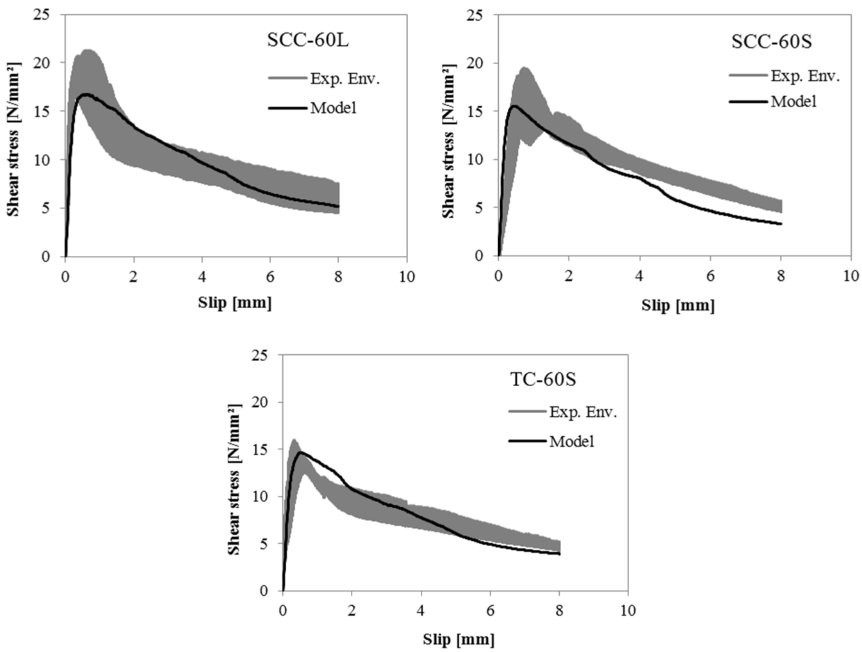

Fig. 4.59 – Model verification for a fibre dosage equal to 60kg/m³

It can be seen form Fig. 4.57 - Fig. 4.59 that the simulated curves fit quite well with the observed direct shear behaviour. Hence, the proposed model is not only able to simulate the interface peak shear stress but also the complete non-linear branch for larger slip values. Fig. 4.60 shows a comparison between both the average simulated and experimentally obtained peak shear stresses.

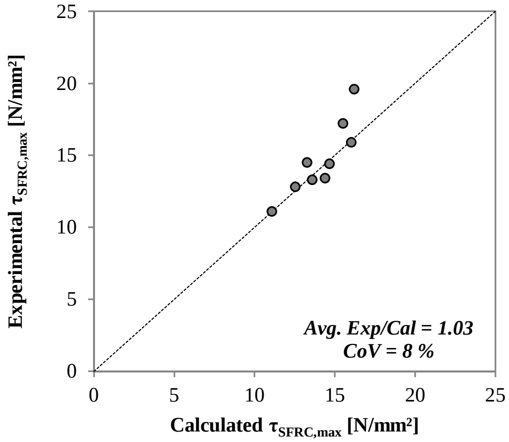

Fig. 4.60 - Parity diagram for the maximum interface shear strength of SFRC

4.5 Conclusions

4.5.1 Axial fibre pull-out and related behaviour in bending

Three point bending tests according to the current European Standard EN 14651 are conducted in order to obtain residual flexural parameters for SFRC. Based on the results of an inverse analysis procedure, a tri-linear post-cracking behaviour is proposed for the Mode I constitutive model. The model parameters have been defined as a function of the standard residual flexural parameters f_{R1} and $f_{R3,}$ following EN 14651. The advantage of the new model with respect to the linear model proposed in the MC2010 is the possibility to model a pseudo-hardening behaviour instead of pure softening or hardening.

Alternative to the tri-linear Mode I constitutive model, an analytical model based on single fibre pull-out is developed and found to be feasible to simulate the uni-axial post-cracking constitutive law of hooked-end SFRC. A good match is found between the Mode I constitutive law derived by inversed analysis and the fibre pull-out approach. This proves the validity of the performed inversed analysis and confirms its physical meaning. Regarding the numerical simulations of four-point bending behaviour of SFRC prisms, it can be concluded that with modern computer technology and finite element modelling, experimental results can be simulated successfully and can be used to estimate the post-cracking response of SFRC prisms subjected to four-point bending. Hereby, the proposed finite element approach takes into account the variability of concrete and fibre properties as well as the spatial distribution and global orientation of fibres. However, since a lot of other parameters (which are inherent to the production process of the SFRC mix) are not feasible to be implemented in these modelling techniques, these methods should never be used to obtain design parameters.

For fibre dosages higher than 40 kg/m³, mutual fibre interaction will become important and local damage of concrete matrix will reduce fibre efficiency at larger crack openings. Further research is needed in order to define a mutual fibre interaction damage factor as a function of crack opening and the amount of fibres bridging the crack. To confirm or improve the proposed models and its applicability, further assessment against larger data sets is necessary.

4.5.2 Transverse fibre pull-out

A newly developed test method, inspired by the JSCE push-through test on larger SFRC prisms, was used to characterize the transversal pull-out behaviour of a single hooked-end steel fibre. Although the experimental testing was quite easy to conduct and test results could be obtained relatively fast, a better casting procedure should be developed to decrease the undesirable influence of the vertical shear crack widening and hence, to reduce scatter and increase the reproducibility of test results.

The observed transversal pull-out behaviour is highly dependent on the initial orientation of the fibre with respect to the crack sliding direction. In case of an aligned orientation, the pull-out behaviour is quite similar to the axial pull-out. However, for fibres crossing the shear crack plane with an orientation perpendicular or opposite to the shear crack slip direction, the fibres are first bent at the crack interface causing damage at the fibre exit point. As a result, the anchorage capacity increases due to the higher frictional forces and for an initial fibre orientation angle equal to -60° (i.e. opposite to the slip direction oriented at 60°), the mechanical anchorage capacity will induce brittle failure due to fibre rupture.

Although the obtained test results provide better insight into the crack-bridging mechanism of cracked SFRC subjected to shear, it must be noted that the conducted tests on single fibres and inherent pull-out behaviour do not reflect the real composite behaviour of the SFRC. Hence, in a crack, the fibre pull-out conditions will be defined by means of the crack opening propagation due to the roughness of the crack surface.

4.5.3 Shear friction

The modified JSCE test setup can be used to investigate the direct shear behaviour of plain and steel fibre reinforced concrete. However, the following remarks should be made:

- The observed relatively low crack width to slip ratio leads to high shear stresses due to aggregate interlock and shear friction. The crack dilatation is inherent to the adopted test setup and is not clearly affected by either fibre type or dosage.

This should be considered when comparing direct shear tests results obtained by means of other types of test setups.

- A linear increase of direct shear stresses is observed as a function of fibre content. The direct shear capacity of SFRC is clearly related to the amount of fibres crossing the shear crack interface.

- A widely accepted standardized test method should be developed in order to reduce experimental scatter and increase the reproducibility of test results. Thereby, the following remarks should be made: 1) asymmetric failure is more likely to occur for low reinforcement ratios ($V_f < 20$ kg/m³) and 2) for higher fibre dosages, the shear strength of SFRC increases and compression failure at the supports is possible and an adaptation of the notch depth is needed.

Similar to the approach applied for the Mode I analytical model based on single fibre pull-out, a direct shear analytical model for SFRC has been developed making use of single fibre transverse pull-out. It can be concluded that the developed model is able to simulate the direct shear behaviour by taking into account a combination of fibre pull-out, coulomb friction and aggregate interlock. In this way, the concept of a cohesion plus friction shear stress transfer model is extended to the application of steel fibre reinforced concrete. The strength of the model follows from the integration of fibre pull-out mechanisms by means of a semi-analytical transverse pull-out model which is able to deal with different strengths of both fibres and concrete, fibre dosage and fibre shape.

4.6 References

[1] Soetens, T., Van Gysel, A., Matthys, S., Taerwe, L. (2013). "A semi-analytical model to predict the pull-out behaviour of inclined hooked-end steel fibres". *Construction and Building Materials*, Vol. 43, pp. 253-265.

[2] Van Gysel, A. (2000). "*Studie van het uittrekgedrag van staalvezels ingebed in een cementgebonden matrix met toepassing op staalvezelbeton onderworpen aan buiging (in dutch)*" (PhD-thesis). Ghent, Ghent University.

[3] Laranjeira, F., Aguado, A., Molins, C. (2010). "Predicting the pullout response of inclined straight steel fibres". *Materials and Structures*, Vol. 43(6), pp. 875-895.

[4] Laranjeira, F., Molins, C., Aguado, A. (2010). "Predicting the pullout response of inclined hooked steel fibers". *Cement and Concrete Research*, Vol. 40(10), pp. 1471-1487.

[5] Foster, S. J. (2009). "The application of steel-fibres as concrete reinforcement in Australia: from material to structure". *Materials and Structures*, Vol. 42, pp. 1209-1220.

[6] Brandt, A. M. (2008). "Fibre reinforced cement-based (FRC) composites after over 40 years of development in building and civil engineering". *Composite Structures*, Vol. 86(1-3), pp. 3-9.

[7] Walraven, J. (2009). "High performance fiber reinforced cocnrete: progress in knowledge and design codes". *Materials and Structures*, Vol. 42, pp. 1247-1260.

[8] RILEM. (2002). "Recommendations of RILEM TC 162-TDF: Test and design methods for steel fibre reinforced concrete; Design of steel fibre reinforced concrete using the sigma-epsilon method: principals and applications". *Materials and Structures*, Vol. 35, pp. 262-278.

[9] CEN. (2005). "EN 14651 - Test method for metallic fibered concrete - measuring the flexural tensile strength". Brussels, Belgium, CEN.

[10] Parmentier, B., Vandewalle, L., Van Rickstal, F. (2008). "Evaluation of the scatter of the postpeak behaviour of fibre reinforced concrete in bending: a step towards reliability". *7th international RILEM symposium on Fibre Reinforced Concrete, Chennai, India*, pp. 133-143.

[11] Abrishambaf, A., Barros, J. A. O., Cunha, V. M. C. F. (2013). "Relation between fibre distribution and post-cracking behaviour in steel fibre reinforced self-compacting concrete panels". *Cement and Concrete Research*, Vol. 51, pp. 57-66.

[12] Dupont, D., Vandewalle, L. (2005). "Distribution of steel fibres in rectangular sections". *Cement and Concrete Composites*, Vol. 27, pp. 391-398.

[13] Kooiman, A. G., van der Veen, C., Walraven, J. C. (2000). "Modelling the post-cracking behaviour of steel fibre reinforced concrete for structural design purposes". *HERON*, Vol. 45(4), pp. 275-307.

[14] Löfgren, I., Stang, H., Olesen, J. F. (2005). "Fracture Properties of FRC Determined through Inverse Analysis of Wedge Splitting and Three-Point Bending Tests". *Journal of Advanced Concrete Technology*, Vol. 3(3), pp. 423-434.

[15] Tlemat, H., Pilakoutas, K., Neoclous, K. (2006). "Modelling of SFRC using inverse finite element analysis". *Materials and Structures*, Vol. 39, pp. 221-233.

[16] Georgiadis-Stefanidi, K., Mistakidis, E., Pantousa, D., Zygomalas, M. (2010). "Numerical modelling of the pull-out of hooked steel fibres form high-strength cementitious matrix, supplemented by experimental results". *Construction and Building Materials*, Vol. 24, pp. 2489-2506.

[17] Robins, P., Austin, S., Jones, P. (2002). "Pull-out behaviour of hooked steel fibres". *Materials and Structures*, Vol. 35(August 2002), pp. 434-442.

[18] Ghoddousi, P., Ahmadi, R., Sharifi, M. (2010). "Fiber pullout model for aligned hooked-end steel fiber". *Canadian Journal of Civil Engineering*, Vol. 37, pp. 1179-1188.

[19] Cunha, V. M. C. F., Barros, J. A. O., Sena-Cruz, J. (2010). "Pullout behavior of steel fibers in self-compacting concrete". *Journal of Materials in Civil Engineering*, Vol. 22, pp. 1-9.

[20] Markovich, I., van Mier, J. G. M., Walraven, J. C. (2001). "Single fiber pullout from hybrid fiber reinforced concrete". *HERON*, Vol. 46(3), pp. 191-200.

[21] Lee, Y., Kang, S.-T., Kim, J.-K. (2010). "Pullout behavior of inclined steel fiber in an ultra-high strength cementitious matrix". *Construction and Building Materials*, Vol. 24(10), pp. 2030-2041.

[22] Soetens, T., Matthys, S., Taerwe, L., Van Gysel, A. (2011). "Basis of a finite-element simulation tool to predict the flexural behaviour of SFRC prisms". *High Performance Fiber Reinforced Cementitious Composites 6, Ann Arbor, USA*, pp. 91-98.

[23] Soetens, T., Matthys, S. (2012). "Implementation of fibre pull-out behaviour in a finite element model for SFRC". *Bond in Concrete 2012 - Bond, Anchorage, Detailing, Brescia, Italy*.

[24] Bellezze, T., Fratesi, R., Failla, C. (2004). "Effect of Chemical-Physical Interaction Between Galvanized Steel Fibres and Concrete". *6th RILEM Symposium on Fibre-Reinforced Concretes (FRC) - BEFIB 2004, Varenna, Italy*, pp. 239-248.

[25] fib. (2010). "Model Code for Concrete Structures 2010". Lausanne, Switzerland, fédération internationale du béton.

[26] Markovich, I. (2006). "*High-Performance Hybrid-Fibre Concrete: Development and Uitilisation*" (PhD-thesis), Delft University of Technology, p. 211.

[27] Dupont, D. (2003). "*Modelling and experimental validation of the constitutive law (sigma-epsilon) and cracking behaviour of steel fibre reinforced concrete*". Leuven, Katholieke Universiteit Leuven.

[28] NBN. (1992). "B15-238 - Proeven op vezelversterkt beton - Buigproef op prismatische proefstukken". Brussels, Belgium, Belgian Institute for Normalisation.

[29] Cunha, V. M. C. F., Barros, J., Sena-Cruz, J. (2011). "An integrated approach for modelling the tensile behaviour of steel fibre reinforced self-compacting concrete". *Cement and Concrete Research*, Vol. 41(1), pp. 64-76.

[30] Barros, J., Gettu, R., Barragán, B. (2004). "Material Nonlinear Analysis of Steel Fibre Reinforced Concrete Beams Failing in Shear". *6th RILEM Symposium on Fibre-Reinforced Concretes (FRC) - BEFIB 2004*, pp. 711-720.

[31] Gettu, R., Gardner, D. R., Saldivar, H., Barragán, B. (2005). "Study of the distribution and orientation of fibres in SFRC specimens". *Materials and Structures*, Vol. 38(1), pp. 31-37.

[32] Grünewald, S. (2004). "*Performance-based design of self-compacting fibre reinforced concrete*" (Phd-thesis), Delft University of Technology, p. 233.

[33] Kang, S.-T., Lee, B. Y., Kim, J.-K., Kim, Y. Y. (2011). "The effect of fibre distribution characteristics on the flexural strength of steel fibre-reinforced ultra-high strength concrete". *Construction and Building Materials*, Vol. 25(5), pp. 2450-2457.

[34] Laranjeira, F., Grünewald, S., Walraven, J. C., Blom, C., Molins, C., Aguado, A. (2011). "Characterization of the orientation profile of steel fiber reinforced concrete". *Materials and Structures*, Vol. 44(6), pp. 1093-1111.

[35] Liu, J. S. (2008) "*Monte Carlo Strategies in Scientific Computing*". USA: Springer.

[36] Shimrat, M. (1962). "Algorithm 112: Position of point relative to polygon". *Commun ACM*, Vol. 5(8), pp. 434.

[37] Cervenka, V., Jendele, L., Cervenka, J. (2013). "ATENA Program Documentation Part 1: Theory". Prague, Czech Republic.

[38] Lee, G. G. (2007). "*Direct shear behaviour of steel fibres in a cementitious matrix*" (PhD-thesis). Sydney, Australia, The University of New South Wales.

[39] Mirsayah, A. A., Banthia, N. (2002). "Shear Strength of Steel Fiber-Reinforced Concrete". *ACI Materials Journal*, Vol. 99(5), pp. 473-479.

[40] JSCE. (2005). "JSCE-G 553-1999: Test method for shear strength of steel fiber reinforced concrete". Tokyo, Japan, Japan Society of Civil Engineers (JSCE).

[41] Bazant, Z. P., Gambarova, P. G. (1980). "Rough crack models in reinforced concrete". *Journal of Structural Engineering (ASCE)*, Vol. 106(4), pp. 819-842.

[42] Walraven, J. (1980). "*Aggregate Interlock - A theoretical and experimental analysis*" (PhD-thesis), Delft University of Technology.

[43] Li, N., Maekawa, L., Okamura, H. (1989). "Contact density model for stress transfer across cracks in concrete". *Journal of the Faculty of Engineering, University of Tokyo*, Vol. 40(1), pp. 9-52.

[44] ACI Committee 544. (1993). "Guide for Specifying, Proportioning, Mixing, Placing, and Finishing Steel Fiber Reinforced Concrete". *ACI Materials Journal*, Vol. 90(1), pp. 94-103.

[45] CEN. (2009). "EN 12390:2009 - Testing hardened concrete - Part 3: Compressive strength of test specimens". Brussels, CEN.

[46] Valle, M., Büyüköztürk, O. (1993). "Behavior of Fiber Reinforce High-Strength Concrete under Direct Shear". *ACI Materials Journal*, Vol. 90(2), pp. 122-133.

[47] Boulekbache, B., Hamrat, M., Chemrouk, M., Amziane, S. (2012). "Influence of yield stress and compressive strength on direct shear behaviour of steel fibre-reinforced cocnrete". *Construction and Building Materials*, Vol. 27(1), pp. 6-14.

[48] Appa Rao, G., Sreenivasa, R. (2009). "Toughness indices of steel fiber reinforced concrete under mode II loading". *Materials and Structures*, Vol. 42(9), pp. 1173-1184.

[49] Majdzadeh, F., Soleimani, S. M., Banthia, N. (2006). "Shear strength of reinforced concrete beams with a fiber concrete matrix". *Canadian Journal of Civil Engineering*, Vol. 33, pp. 726-734.

[50] Araujo, D. L., Carmo, L. C., Nunes, F. G. T., Toledo Filho, R. D. (2010). "Computational modeling of steel fiber reinforced concrete beams subjected to shear". *IBRACON Structures and Materials Journal*, Vol. 3(1), pp. 68-94.

[51] Higashiyama, H., Banthia, N. (2008). "Correlating Flexural and Shear Toughness of Lightweight Fiber-Reinforced Concrete". *ACI Materials Journal*, Vol. 105(3), pp. 251-257.

[52] Khaloo, A. R., Kim, N. (1997). "Influence of Concrete and Fiber Characteristics on Behavior of Steel Fiber Reinforced Concrete under Direct Shear". *ACI Materials Journal*, Vol. 94(6), pp. 592-601.

[53] Barragán, B., Gettu, R., Agulló, L., Zerbino, R. (2006). "Shear failure of Steel Fiber-Reinforced Concrete Based on Push-Off Tests". *ACI Materials Journals*, Vol. 103(4), pp. 251-257.

[54] Mansur, M. A., Vinayagam, T., Tan, K.-H. (2008). "Shear Transfer across a Crack in Reinforced High-Strength Concrete". *Journal of Materials in Civil Engineering*, Vol. 20(4), pp. 294-302.

[55] Loov, R. E. (1998). "Review of A23.3-94 simplified method of shear design and comparison with results using shear friction". *Canadian Journal of Civil Engineering*, Vol. 25(3), pp. 437-450.

[56] Wong, R. C. K., Ma, S. K. Y., Wong, R. H. C., Chau, K. T. (2007). "Shear strength components of concrete under direct shearing". *Cement and Concrete Research*, Vol. 37(8), pp. 1248-1256.

[57] ACI. (2011). "ACI 318-11: Building Code Requirements for Structural Concrete and Commentary". Farmington Hills, USA.

[58] Ng, T. S., Foster, S. J., Htet, M. L., Htut, T. N. S. (2014). "Mixed mode fracture behaviour of steel fibre reinforced concrete". *Materials and Structures*, Vol. 47, pp. 67-76.

[59] Foster, S. J., Lee, G. G. (2008). "*Modelling of shear-fracture of fibre-reinforced concrete*". In: Tailor Made Concrete Structures: CRC Press, pp. 493-499.

[60] Paulay, T., Loeber, P. J. (1974). "*Shear Transfer by Aggregate Interlock*". In: ACI SP-42: Shear in Reinforced Concrete. Detroit, USA: ACI, pp. 1-15.

[61] Gambarova, P. G., Karakoç, C. (1983). "A new approach to the analysis of the confinement role in regularly cracking concrete elements.". *7th International Conference on Structural Mechanics in Reactor Technology, Chicago, USA*, pp. 251-261.

[62] CEB-FIP. (1990). "Model Code 1990: Design code". Lausanne, Switzerland.

[63] Walraven, J., Reinhardt, H. W. (1981). "Theory and Experiments on the Mechanical Behavior of Cracks in Plain and Reinforced Concrete Subjected To Shear Loading". *HERON*, Vol. 26, pp. 1-68.

[64] Mattock, A. H. (1974). "Shear transfer in Concrete Having Reinforcement at an Angle to the Shear Plane, ACI Special Publication 42". pp. 17-42.

[65] Soetens, T., Matthys, S. (2012). "A semi-analytical model to simulate the direct shear pull-out behaviour of hooked-end steel fibres". *BEFIB2012, Guimaraes, Portugal*, pp. 1-12.

[66] Van Gysel, A. (1999). "A pullout model for hooked end steel fibres". *3th International RILEM Workshop on High Performance Fiber Reinforced Cement, Mainz, Germany*, pp. 351-359.

[67] Santos, P. M. D., Júlio, E. N. B. S. (2012). "A state-of-the-art review on shear-friction". *Engineering Structures*, Vol. 45, pp. 435-448.

5 FULL SCALE SHEAR TESTS

5.1 Introduction

The shear capacity of reinforced and prestressed concrete has been the subject of comprehensive research since the past century [1] (see also Chapter 3). The complex nature of shear can be attributed to a number of different parameters influencing the shear behaviour such as concrete strength, longitudinal reinforcement ratio, shear span to depth-ratio, element height, cross-section type, aggregate size, shear reinforcement ratio and load conditions. As a consequence, high scatter of test results is observed in experiments and therefore, research efforts are still undertaken to improve existing shear strength models and to better understand the shear failure mechanisms.

Since, the tailoring and placement of traditional stirrups is considered to be labour intensive by precast concrete manufacturers, alternatives to avoid traditional stirrups will be of great economic benefit. Typically, prestressed large span concrete elements, are often designed to resist high bending moments and relatively limited shear forces. In these cases where minimum required traditional shear reinforcement should be placed, as obliged by current design provisions for RC structures [2, 3], a viable solution can be found by using steel fibres [4-8].

Although the feasibility of steel fibres to replace traditional stirrups either completely or partially has been investigated and proven over the past two decades by several researchers [8-12], the number of practical applications is yet limited and engineers are not familiar with this new technique. The reasons for this are twofold. Firstly, shear test results for fibre reinforced prestressed or non-prestressed concrete elements are derived from experiments on relatively small specimens which do not match realistic dimensions of structural elements. Therefore it is necessary to extend the existing shear test database with results from full-scale tests on large span girders. A second reason is that only a few design standards [2, 13] have shear provisions for elements reinforcement with fibres. Recently, this drawback was recognized by the International Federation for Structural Concrete (fib) and in the current Model Code 2010 (MC2010) [2] two calculation methods are presented for the shear capacity of FRC elements.

In order to investigate the shear capacity of full-scale girders, prestressed elements were made by Megaton (a Flemish precast concrete company, part of the Willy Naessens Group) and tested under laboratory conditions (at Ghent University). In total, 23 shear tests have been conducted on prestressed concrete girders comparing plain concrete reference girders with SFRC girders with a fibre dosage ranging between 20 and 60 kg/m^3. This chapter provides a detailed overview and discussion of all obtained test results from the full span girders as well as the additional specimens used to determine the SFRC material properties. To allow a more thorough investigation of the crack propagation, the post-cracking shear behaviour of the girders is monitored by means of a Digital Image Correlation (DIC) technique covering the complete shear critical area and a thorough investigation of crack propagation has been done more in detail.

5.2 Materials & methods

5.2.1 Test specimens

To investigate the shear capacity of 20 m span prestressed precast SFRC girders, experimental shear tests are conducted on nine I-shaped girders manufactured by Megaton (a Flemish precast concrete company, part of the Willy Naessens Group). All girders have a constant height of 1 m. The cross-sectional dimensions and prestress strand configuration is shown in Fig. 5.1. The prestressing is achieved by means of high strength 12.5 mm strands pretensioned at an initial tensile stress equal to 1453 N/mm^2. The initial prestressing force for each strand equals 135 kN. In the girders cross-section, mild reinforcement is placed at the upper side to resist tensile stresses when the girder is loaded by its self-weight and prestress only.

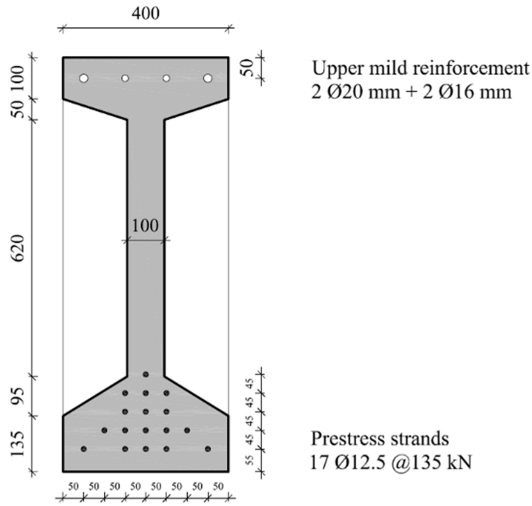

Fig. 5.1 - I-shaped cross section (dimensions in mm)

Table 5.1 – Shear reinforcement and designation for each girder

Girder	Designation	Shear Reinforcement
1	REF	Plain concrete
2	REF/ TR	Plain concrete / Traditional stirrups [(1)]
3	TR	Traditional stirrups
4	20A	20 kg/m³ RC-80/30-CP
5	20B	20 kg/m³ RC-80/30-CP
6	40A	40 kg/m³ RC-80/30-CP
7	40B	40 kg/m³ RC-80/30-CP
8	20+20	20 kg/m³ RC-80/60-BP + 20 kg/m³ RC-80/30-CP
9	60	60 kg/m³ RC-80/30-CP

[(1)] At one side of the beam, traditional transvers reinforcement is placed and the other side of the beam is plain concrete.

For all of the SFRC girders, the fibre volume varied between 20 and 60 kg/m³. In order to decrease the risk of fibre blocking due to limited free space between the prestress strands (i.e. 35 mm), it was decided to use short fibres. All used SFRC mixes contained high strength cold drawn wire hooked-end fibres (type DRAMIX RC-80/30-CP). This type of fibre has a length of 30 mm, a diameter of 0.38 mm and a wire tensile strength of at least 3000 N/mm². This high performance steel fibre is combined with a concrete strength class of C50/60. Preliminary to the casting of the girders at the precast company, the SFRC mix composition has been optimized and trial batches were mixed first in the quality control laboratories of the admixture supplier. After obtaining evidence of good mixability, workability and strength development of the mixes, the mix compostion as shown in Table 5.1 has been chosen for the production of the girders.

Table 5.2- Constituents of used concrete mix [kg/m³]

Constituent	Dosage [kg/m³]
Sand 0/1	202
Sand 0/4	674
Crushed limestone 2/6	257
Crushed limestone 6/14	566
CEM I 52.5 R/HES	390
Fly ash	60
Water	190
Superplasticizer	2.61
RC-80/30-CP	20-60

The production process of the girders consists of the following steps. The concrete without fibres is made in a ready mix plant adjacent to the precast plant and the concrete is mixed for about 2 minutes and charged in the truck-mixer. Then, the fibres are added to the concrete in the truck mixer and the concrete is mixed for an additional 5 minutes. The SFRC is then transported to the precast company and charged from the truck mixer into a concrete bucket (Fig. 5.2a) and poured into the formwork (Fig. 5.2b). Compaction of the concrete is done by means of vibrators attached to the formwork.

Fig. 5.2 - Production process: a) charging of the concrete bucket, b) filling of the formwork, c) demoulding and d) application of prestress

During casting of the girders, additional samples and specimens are cast from the same SFRC batch:

- 3 fresh concrete samples with a volume of eight litre are taken in order to determine the fibre content in the fresh state.
- 12 cubes with a side length 150 mm, for determination of the compressive strength on three cubes for the age of 2, 7, 14 and 28 days (EN 12390-3).
- 4 cylinders with a diameter equal to 150 mm and a height of 300 mm, for determination of the compressive strength at 28 days (EN 12390-3) and the modulus of elasticity (NBN B 15-203)
- 4 prisms were vertically casted to perform tests to evaluate the shrinkage (2 tests according to NBN B 15-216) and creep (2 tests NBN B 15-228).
- 3 to 6 prisms with standard dimensions 150 mm x 150 mm x 600 mm were cast in order to characterise the post-cracking tensile capacity of the SFRC mix, by means of three-point bending (EN 14651). The number of bending tests for each batch is given in Section 5.2.3 (Table 5.5).

After one day, the girders were demoulded (Fig. 5.2c) and when the cube compressive strength exceeded 50 N/mm² (at an age of about 2-3 days), the pretensioned prestressing strands are cut and the prestress is applied on the girder (Fig. 5.2d). The girders are stored in the production hall of the precast manufacturer and at the age of about 28 days, the girders are transported to the laboratory hall of Ghent University for testing.

5.2.2 Shear test programme & measurements

The test matrix of the 23 conducted shear tests is given in Table 5.3 in terms of applied test phase, shear span to depth ratio, shear reinforcement, concrete strength, age of testing and the application of the DIC-technique. The test programme involves multiple tests per girder as indicated in Fig. 5.3. In phase 1, the girder is first tested at one end (so called left shear span zone). In phase 2, the left support is moved and the girder is tested at the right shear span zone. For girders REF, 20A, 40A, 60 and TR a third phase test is conducted with a more central shear span zone. The shear span to depth ratio is kept constant for phases 1 and 3 at 2.5.

For the shear tests done in phase 2, the a/d-ratio is either 2.5 or 3.0. A schematic of all different test setups adopted in this study is shown in Fig. 5.3. As a result of these test combinations, a total of 23 different shear tests are performed on 9 precast prestressed girders.

Table 5.3- Test matrix with indication of concrete compressive strength, used test equipment, a/d and testing age.

Test Nr.	Designation	Phase	a/d	Shear reinforcement	$f_{cm,cyl}$ [N/mm²]	Age [days]	DIC
1	1-2.5-[REF]	1	2.5	REF	68.5	27	-
2	2-2.5-[REF]	2	2.5			28	Y
3	3-2.5-[REF]	3	2.5			107	-
4	1-3.0-[REF/TR]	1	3	REF	57.7	25	Y
5	2-3.0-[REF/TR]	2	3	TR	57.7	27	Y
6	1-2.5-[20A]	1	2.5	20A	41.0	29	Y
7	2-2.5-[20A]	2	2.5			30	-
8	3-2.5-[20A]	3	2.5			101	-
9	1-2.5-[20B]	1	2.5	20B	64.8	28	Y
10	2-2.5-[20B]	2	3			31	Y
11	1-2.5-[40A]	1	2.5	40A	70.4	24	Y
12	2-2.5-[40A]	2	2.5			25	-
13	3-2.5-[40A]	3	2.5			73	-
14	1-2.5-[40B]	1	2.5	40B	58.8	25	Y
15	2-3.0-[40B]	2	3			26	Y
16	1-2.5-[20+20]	1	2.5	20+20	56.1	26	Y
17	2-3.0-[20+20]	2	3			28	Y
18	1-2.5-[60]	1	2.5	60	66.5	26	Y
19	2-3.0-[60]	2	3			28	Y
20	3-2.5-[60]	3	2.5			71	Y
21	1-2.5-[TR]	1	2.5	TR	73.2	26	Y
22	2-2.5-[TR]	2	2.5			27	-
23	3-2.5-[TR]	3	2.5			67	-

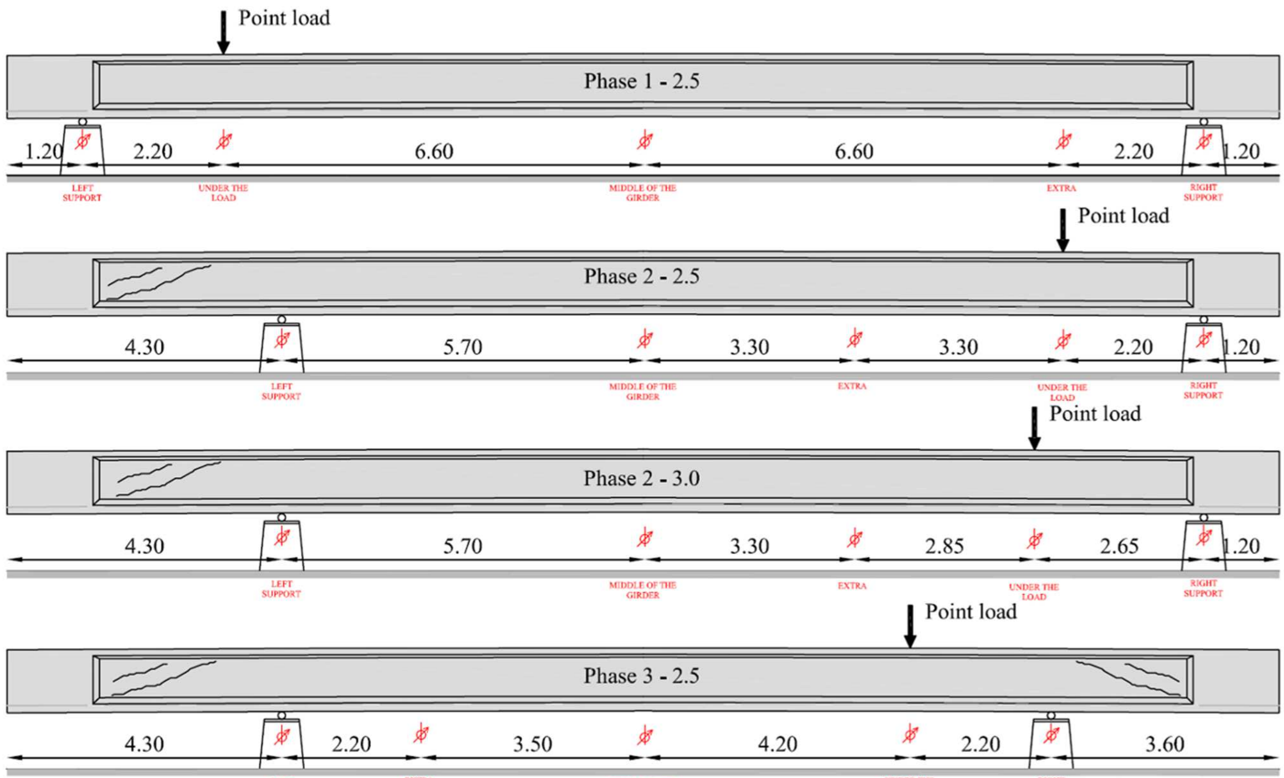

Fig. 5.3- Adopted test setups for phase 1 to 3 for both a/d equal to 2.5 and 3.0 (dimensions in m)

The girders with a height of 1000 mm have an effective depth equal to 886 mm. For the adopted shear span-depth ratios equal to 2.5 and 3.0, a concentrated load is applied at a distance of 2210 mm and 2660 mm from the support respectively. Rather than to support the beam at its physical end, the supports are placed at the beginning of the I-section zone. In this way, the shear cracks will occur only in the thin web section and the undesired beneficial effect of the rectangular end-blocks has been avoided. The point-load is applied by means of a hydraulic jack with a capacity of 1000 kN and a load pad of 400 mm by 160 mm (i.e. for the complete width of the flange). The girder is supported by means of a hinge at one end and by means of a roller at the other support. The roller support is located nearest to the point load. During testing, the applied load is manually controlled at a load rate equal to 25 kN/min. At intermediate stages, the load was kept constant in order to perform manual control measurements of the deflections and strain deformations.

During testing, displacements at the point load, at midspan, at an extra point in between the midspan and the other support and at the supports are monitored by means of linear variable displacement transducers (marked with red symbols on Fig. 5.3). For the shear critical area, the shear crack propagation is captured by means of a grid of extensometers at one side of the girder and by means of a Digital Image Correlation (DIC) technique at the other side. The position of the extensometers for each test is given in Appendix C.

The DIC-technique is fully covered in [14]. In brief terms, DIC is an optical technique which gives the displacement field that provides the best correlation between the image of a deformed surface (i.e. during testing) and a reference image of the undeformed surface. Hence, by using a DIC-technique, it is possible to monitor continuously the full-field shear deformations within a selected area of interest. This area is divided into a dense grid of analysis points. To quantify this correlation, a sum of squared differences (SSD) is calculated for every point within the grid, comparing the grey values of a square subset of pixels around the point in the reference image with the same – but transformed by an assumed displacement field – subset in the deformed image. The displacement of that point is then obtained by minimizing this SSD-function. Full-field information is obtained by interpolation between the points within the grid.

A proper DIC analysis requires images with a non-uniform high-contrast speckle pattern. This pattern was achieved by spraying a uniform white layer of paint and, after drying, projecting black paint droplets upon the specimen area of interest (a rectangle of 1100 mm by 500 mm as illustrated in Fig. 5.4). The procedure was optimized to aim for a speckle size of approximately 3 by 3 pixels as advised in [14]. This roughly corresponds with speckles of 0.5 by 0.5 mm² to 1 by 1 mm². A subset size of 21 by 21 pixels for calculating the SSD-functions was chosen. More details about the DIC test setup are explained for another case study in [15].

The covered area and DIC-test setup is shown in Fig. 5.4. Two monochromatic 5 MPx cameras were positioned next to each other and directed perpendicular towards the surface. The overlap between images of both cameras is 100 mm, allowing to combine the images of both cameras into a composite analysis, and thus covering the total area of interest. Two diffuse light sources were adopted. Their position was empirically optimized with the aim to provide a uniform light intensity over the entire area of interest. The DIC analysis was performed using proprietary VIC3D-software (version 2009).

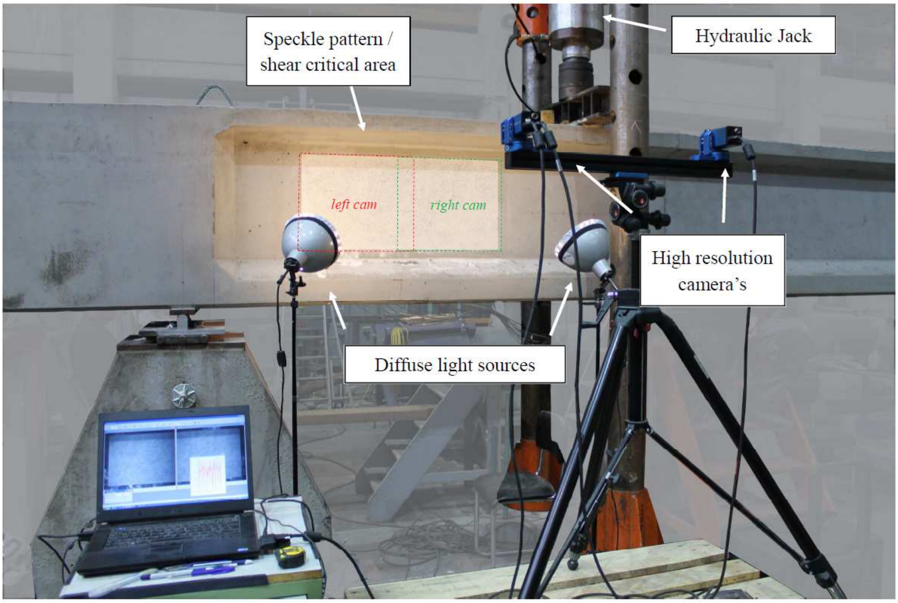

Fig. 5.4 – Test setup adopted for the DIC - measurements

The measuring accuracy for all tests conducted with DIC, obtained from the scatter observed when correlating two images of an unloaded specimen, is given in Table 5.4.

Table 5.4 – Maximum DIC measurement error for all monitored test series

Test	Maximum measurement error [mm]
2-2.5-[REF]	0.020
1-2.5-[20A]	0.047
1-2.5-[40A]	0.028
1-2.5-[20B]	0.066
2-2.5-[20B]	0.030
1-2.5-[40B]	0.084
2-3.0-[40B]	0.041
1-3.0-[REF/TR]	0.031
2-3.0-[REF/TR]	0.023
1-2.5-[TR]	0.024
1-2.5-[20+20]	0.031
2-3.0-[20+20]	0.019
1-2.5-[60]	0.018
2-3.0-[60]	0.023
3-2.5-[60]	0.020
Min.	0.018
Max.	0.084
Avg.	0.034

As can be seen in Table 5.4, the accuracy of the DIC technique is around 0.034 mm at average. This is acceptable as it corresponds with 0.007% of the shortest side of the DIC measurement zone.

5.2.3 SFRC properties

5.2.3.1 Bending tests

The post-cracking behaviour of all SFRC-batches is determined by means of three-point bending tests according to NBN EN 14651. Fig. 5.5 shows the obtained post-cracking behaviour in terms of the average residual stress plotted as a function of crack mouth opening displacement (CMOD). The individual test results can be found in Appendix B.

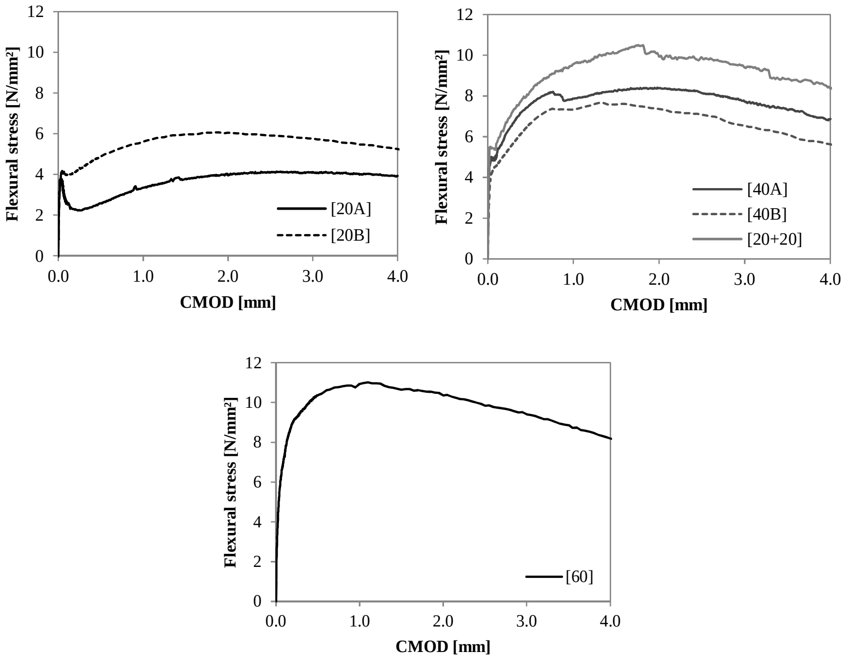

Fig. 5.5 – Average flexural stress-CMOD curves for girders 20A, 20B, 40A, 40B, 20+20 and 60.

Regarding the post-cracking behaviour of all concrete mixes, it can be concluded that even for relatively low amount of fibres (e.g. girder 20B) the residual flexural stress increases significantly. However, for girder 20A, the residual stresses immediately after cracking are only 50% of the cracking stress. For SFRC mixes with fibre dosages of 40 or 60 kg/m³, the flexural stresses increase directly after cracking. The SFRC-mix with 60 kg/m³ of fibres revealed pure hardening behaviour with a maximum stress around 11 N/mm² at a crack opening of about 1 mm.

In order to characterise the post-cracking performance, the residual flexural stresses at defined crack opening displacement (CMOD) values are considered (Eq. 5.1).

$$f_{R,i} = \frac{3F_{R,i}l}{2bh_{sp}^2}$$ Eq. 5.1

with i=1..4, respectively for CMOD values 0.5, 1.5, 2.5 and 3.5 mm and in which $F_{R,i}$ is the applied load at CMOD = i, l the span length (i.e. 500 mm), b the width of the prism and h_{sp} the height of the prism above the notch. The bending tensile strength or Limit of Proportionality (LOP) is calculated as

$$f_{ct,L}^{f} = \frac{3F_L l}{2bh_{sp}^2}$$ Eq. 5.2

In which F_L is the load corresponding to the LOP defined as the highest load in the CMOD-interval 0-0.05 mm.

The average values of f_{R1} and f_{R3} and their corresponding characteristic values are summarized in Table 5.5. The relationship between both residual stresses f_{R1} and f_{R3} and nominal fibre content is shown in Fig. 5.6.

Table 5.5 - SFRC properties

Girder	# tests (k)	V_f [kg/m³]	f_{Lm} [N/mm²]	f_{Lk} [N/mm²]	$f_{R1,m}$ [N/mm²]	$f_{R1,k}$ [N/mm²]	$f_{R3,m}$ [N/mm²]	$f_{R3,k}$ [N/mm²]
20A	3 (1.91)	20	3.76	3.59	2.59	1.73	4.09	2.84
20B	6 (1.71)	20	4.17	3.89	4.88	4.37	5.91	5.39
40A	3 (1.91)	40	5.00	4.44	7.59	5.61	8.15	5.64
40B	6 (1.71)	40	4.25	3.68	6.66	3.07	7.08	3.41
20+20*	5 (1.78)	40*	5.50	4.36	8.24	4.54	9.89	6.58
60	5 (1.78)	60	5.90	4.80	10.37	8.00	9.85	6.64

[*] 20 kg/m³ of short fibres and 20 kg/m3 of long fibres.

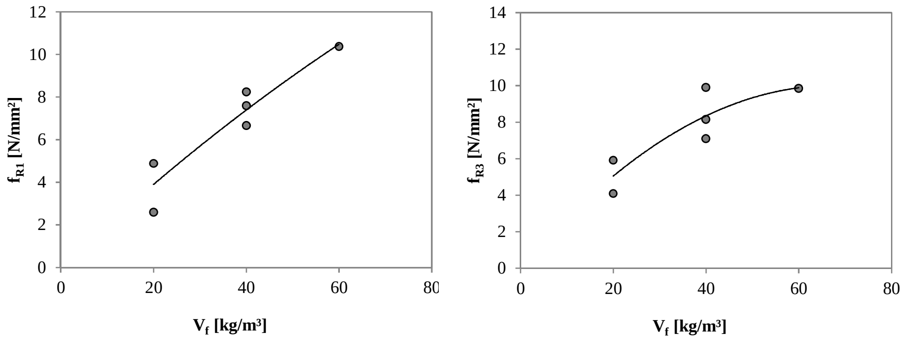

Fig. 5.6 – Average and characteristic values of f_{R1} and f_{R3} for all of the SFRC mixes

From Fig. 5.6 (left), it can be concluded that for low crack openings (cf. CMOD = 0.5 mm), the increase of post-cracking strength is an almost linear function of fibre content. For higher crack widths (cf. CMOD = 2.5 mm), the mutual interaction of fibres (see Section

2.2.2) will cause lower increase of residual stresses as a function of V_f. This mutual fibre interaction is related to the fibre density and spalling at the crack interface due to inclined fibre pull-out [16-18] (see Section 2.2.2). Given the observed trend of f_{R3} as a function of fibre content, it can be expected that for fibre dosages higher than 60 kg/m³ the residual flexural stress $f_{R,3}$ will not increase significantly.

Besides the average values for f_{R1} and f_{R3}, attention should be given towards the scatter of test results which will be of great importance with respect to the economical use of fibres, where characteristic values have to be implemented in shear design equations. The observed scatter for all f_R-values, in terms of Coefficient of Variation (CoV), is shown in Fig. 5.7.

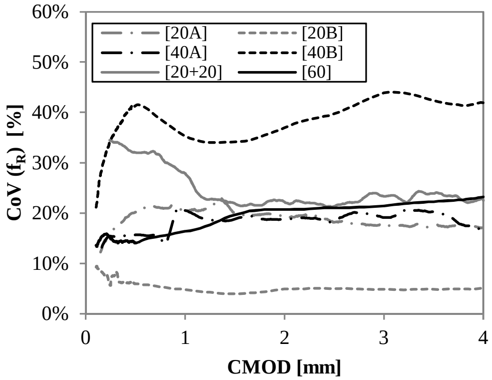

Fig. 5.7 – CoV for the residual stresses f_R as a function of CMOD for all of the SFRC mixes

For all different values of residual stresses, the coefficient of variation (CoV) ranges from 5 to 37 %. The average values of CoV for f_{R1} and f_{R3} are equal to 21 % and 18 % respectively. In literature, typical values for the CoV can be found around 15-20 % for laboratory conditions and up to 30-35 % for in-situ production conditions [19, 20]. Based on the observed values of CoV for each series, corresponding characteristic values for the residual stresses $f_{Ri,k}$ are calculated as follows:

$$f_{Rk} = f_{Rm}\left[1 - k\left(CoV\right)\right] \qquad \text{Eq. 5.3}$$

In which k [21] is a constant value as a function of the number of tests (see Table 5.5).

Due to a high scatter of test results for girder 40B, lower characteristic residual stresses are obtained for this SFRC mix compared to the mix of girder 20B. The higher CoV of f_R for girder 40B and 20+20, can be attributed to a bad dispersion of fibres. After testing, a study of the crack plane revealed that fibres initially glued together did not fully dissolve during mixing (see Fig. 5.8). Therefore, proper mixing and quality control is needed for production environments in order to guarantee an economic use of steel fibres.

Fig. 5.8 – Incomplete dispersion of fibres for girders 40B

In Model Code 2010 [2], the residual flexural stress values have to meet specific demands in order to guarantee the mechanical performance of SFRC and in order to use steel fibres as structural reinforcement for concrete elements. Fibres can either partially or completely replace conventional reinforcement when the following conditions are met:

$$f_{R1k} > 0.4 f_{Lk} \qquad \text{Eq. 5.4}$$

$$f_{R3k} > 0.5 f_{R1k} \qquad \text{Eq. 5.5}$$

The first requirement (Eq. 5.4) has to be fulfilled in order to provide the SFRC sufficient capacity to arrest the occurrence of a first crack. Eq. 5.5 requires that the post-cracking tensile stresses for higher crack widths are high enough and sufficient ductility is provided to the SFRC. Additionally, MC2010 suggests that the minimum shear reinforcement can be replaced by fibres when the residual post cracking stresses of the SFRC are high enough. In general, sufficient post-cracking member ductility is expected when the following condition is fulfilled:

$$f_{Ftuk} \geq 0.08\sqrt{f_{ck}} \qquad \text{Eq. 5.6}$$

Taking into account the values of Table 5.4 and Table 5.3, the conditions of Eq. 5.4, Eq. 5.5 and Eq. 5.6 are fulfilled for all of the girders (see Table 5.6).

Table 5.6 - Verification of SFRC performance according to MC2010

Girder	$f_{R1k}/f_{Lk} > 0.4$	$f_{R3k}/f_{R1k} > 0.5$	$f_{Ftuk} / \sqrt{f_{ck}} > 0.08$
20A	0.48	1.64	0.15
20B	1.12	1.23	0.24
40A	1.26	1.01	0.23
40B	0.83	1.11	0.16
20+20	1.04	1.45	0.32
60	1.67	0.83	0.31

5.2.3.2 Fibre content in fresh and hardened state

Fresh state

During the casting process of the girders (except for the girders 20A and 40A), the amount of fibres in the fresh concrete are determined. At three different times: at the start of the casting (T1), halfway the casting process (T2) and at the end of the casting process (T3), recipients with a fixed volume of eight litres are filled with concrete and fibres are washed out immediately. Then, the fibres are extracted by means of a magnet and weighed and expressed as the mass of fibres per unit volume. All results are summarized in Table 5.7.

Table 5.7 - Verification of SFRC performance according to MC2010

Girder	T1 [kg/m³]	T2 [kg/m³]	T3 [kg/m³]	Avg. $V_{f,exp}$ [kg/m³]	$V_{f,exp}$ / $V_{f,nom}$ [-]	St. Dev. [kg/m³]	CoV
20A	-	-	-	-	-	-	-
40A	-	-	-	-	-	-	-
20B	20.6	21	18.1	20.0	1.00	1.6	8.0%
40B	32.7	38	35.5	35.5	0.89	2.9	8.0%
20+20	57.1	43	48.6	49.5	1.24	7.2	14.5%
60	63.3	63	65.9	64.2	1.07	1.5	2.3%

As can be seen from the values reported in Table 5.7, the measured fibre contents are different from the nominal fibre content: for mixes 20B, 40B and 60, the deviation of the nominal fibre content is in an acceptable range of 15 % [22, 23]. For mix 20+20, the measured fibre content is 24% higher with respect to the nominal fibre content on average. At time T1, the measured fibre content is 43% higher than expected.

Hardened state

The fibre content in hardened state is measured by using cores, extracted from the web of the girders. For each test shear zone, the fibre content in the shear critical area is determined on six individual cores of which the positions are shown in Fig. 5.9. After drilling, the cores are crushed in a hydraulic press after determining the core volume and weight. Then the obtained concrete pieces containing fibres are further crushed manually and fibres are extracted with a strong magnet, cleaned and weighed. For all of the tested girders, the obtained average, minimum and maximum fibre dosages are shown in Fig. 5.10. A complete overview of fibre dosages per core is given in Appendix C.

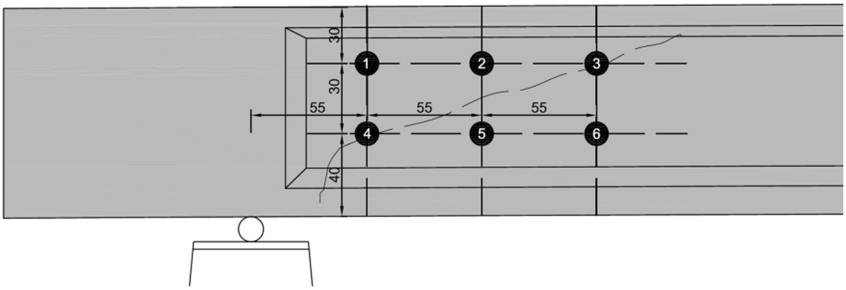

Fig. 5.9 – Location of cores for each shear critical zone

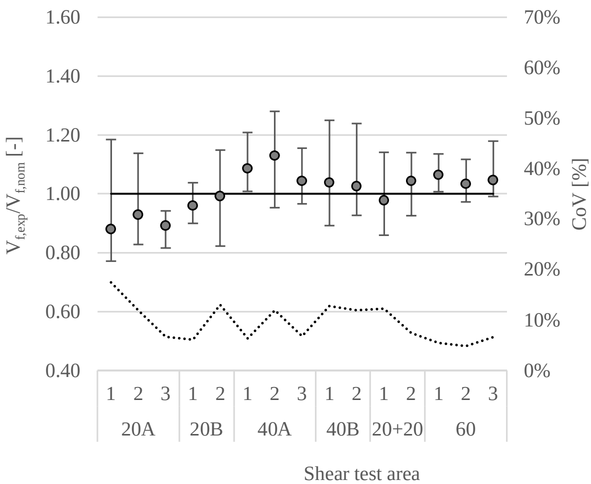

Fig. 5.10 – Average, minimum, maximum and CoV (dotted line) for the ratio between counted and nominal fibre dosage per tested area.

As can be seen from Fig. 5.10, the measured fibre content based on core-drilling is ranging between +/- 20% of the nominal fibre content, which is higher than the values obtained from the fresh concrete tests. When comparing the experimentally obtained fibre content from both fresh and hardened concrete, no clear correlation can be found. Only for the mix containing 60 kg/m³ of fibres, both methods yield an experimental fibre content which is about 5 to 10 % higher than the nominal fibre content.

5.2.3.3 Fibre reinforcement ratio

Since the flexural response of the tested SFRC prisms is inherent to number of fibres crossing the crack-plane, an additional investigation towards the amount of fibres in a cross-section has been conducted. After conducting the flexural tests, a 10 mm thin slice has been cut out mechanically near the notched cross-section. The obtained surfaces were then grinded and coloured black in order to obtain a good contrast between concrete and fibres. By means of a flat-bed scanner, the cross-sections were scanned and fibres were counted in a drawing software program. In this way, the fibre location and the total number of fibres present in the cross-section are determined. An example is shown in Fig. 5.11.

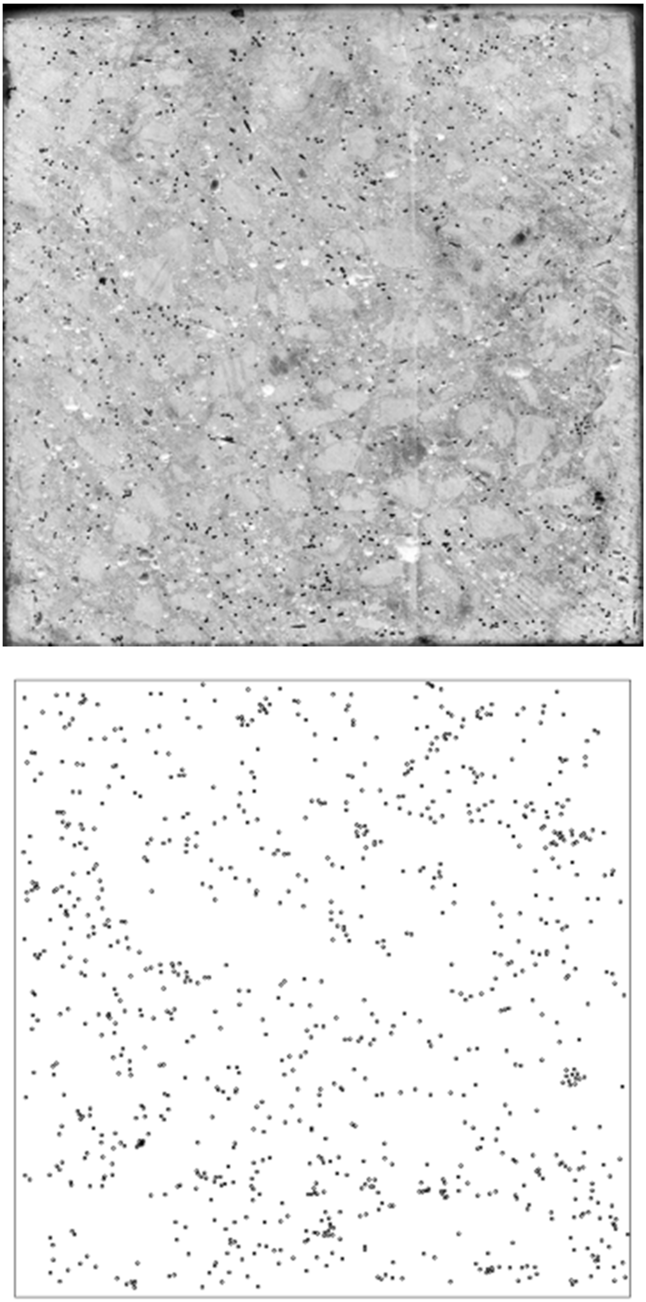

Fig. 5.11 – Scanned image and corresponding digitalisation (SFRC mix containing 60 kg/m³)

In order to compare cross-sections of SFRC containing different types of fibres, the amount of fibres is expressed as a fibre reinforcement ratio ρ_f given by

$$\rho_f = \frac{\sum_{i=0}^{N_f} A_{f,i}}{A_{c,tot}} \qquad \text{Eq. 5.7}$$

In which N_f is the amount of fibres in the cross-section, A_f is the fibre cross sectional area and $A_{c,tot}$ is the total (concrete and fibres) surface area considered.

The relationship between the observed fibre reinforcement ratios and corresponding nominal fibre content is shown in Fig. 5.12.

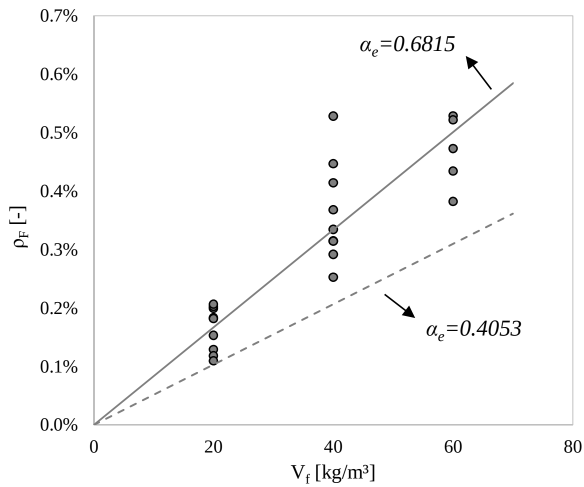

Fig. 5.12 – Fibre reinforcement ratio as a function of nominal fibre dosage

As can be seen from Fig. 5.12, the number of fibres in the analysed cross-sections is higher than expected when assuming a full random distribution (cf. Eq. 3.51). Based on a linear regression analysis of the experimental results, a value of 0.6815 for the orientation parameter α_e is obtained.

Considering only series 20A, 20B, 40A, 40B and 60, the average number of fibres and inherent CoV (between brackets) crossing a vertical plane is equal to 336 (23%), 739 (24%) and 953 (13%) for fibre dosages equal to 20, 40 and 60 kg/m³. As can be seen, the observed scatter of the number of fibres is in a cross-section is of the same order of magnitude than the scatter observed for the residual flexural stress parameters f_{Ri}. The relationship between the fibre reinforcement ratio and corresponding values of f_{Ri} are shown in Fig. 5.13

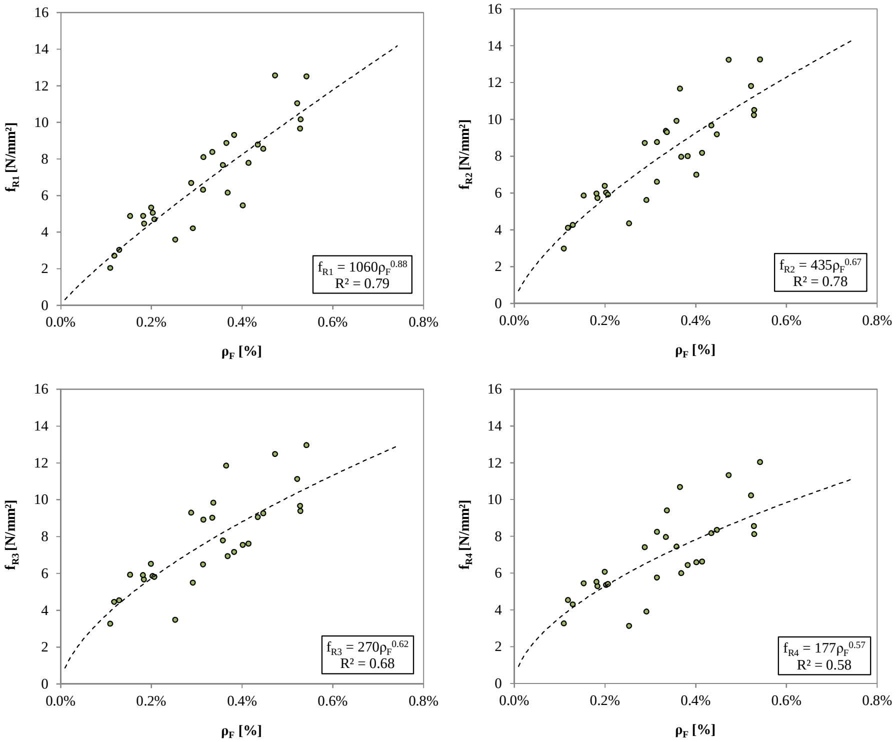

Fig. 5.13 – f_R-values as a function of fibre reinforcement ratio ρ_f

From Fig. 5.13, the relationship between the amount of fibres and the residual flexural stress at a CMOD of 0.5 mm is quasi linear. Hence, at low values of CMOD, the post-cracking tensile stress can be expressed as the product of the number of fibres and an average bond stress. For increasing CMOD, the quasi-linear relationship changes to a non-linear relationships and the increase of post-cracking stress is less than proportional to the amount of fibres. This implies that for higher fibre dosages, the anchorage capacity of fibres decreases due to mutual interaction and damage of the concrete matrix. This phenomenon is described in Chapter 2.

5.2.4 Prestress losses due to creep and shrinkage

For prestressed girders, the time dependent effects such as shrinkage and creep will reduce the initial prestress. In order to estimate this effect, for each girder standard shrinkage and creep tests are conducted according to the Belgian standard NBN B 15-216 and NBN B15-228 respectively.

The shrinkage tests were started as early as possible (1-4 days) after casting of the girders. In order to compare the shrinkage of the different concrete batches, the relative shrinkage strain increase starting from the ages of t_0 = 4 days has been considered. The obtained test results are summarized in Fig. 5.14.

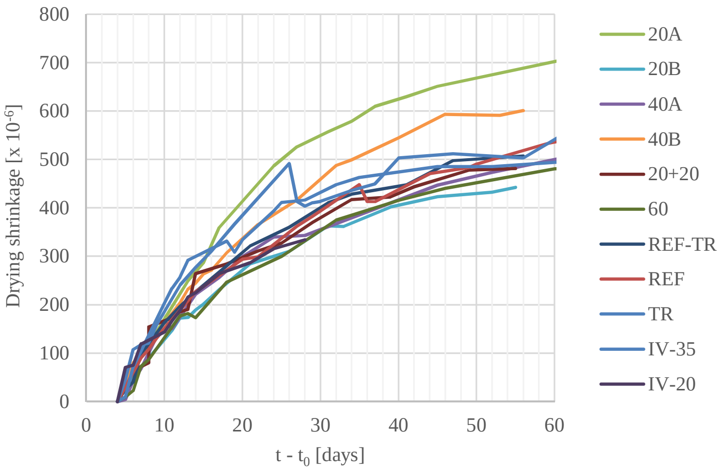

Fig. 5.14 – Drying shrinkage of prismatic test specimen.

Regarding the curves in Fig. 5.14, the relative drying shrinkage between the age of 4 and 28 days, is about 350 to 450 x 10^{-6}. For the girder 20A, a slightly higher shrinkage strain at 28 days of 550 x 10^{-6} is observed. This can be attributed to the high water to cement ratio which also caused the decrease of compressive strength.

Creep tests are conducted on concrete prisms, subjected to a fixed initial compressive stress equal to 11.5 N/mm². Since the girders are only subjected to the prestress from the moment when the concrete strength is sufficiently high (> 40 N/mm²), the creep tests are initiated between the ages of 7-12 days. All individual test results are given in Appendix B. The prestressing losses at 28 days due to the combined effects of creep and shrinkage are given in Table 5.8.

Table 5.8 – Prestressing loss for the tested girders

Girder	$\Delta\sigma_{s,s}$ [N/mm²]	$\Delta\sigma_{s,c}$ [N/mm²]	$\Delta\sigma_{s,tot}$ [N/mm²]	η [-]
REF	69	127	195	0.87
REF-TR	68	132	200	0.86
TR	79	43	122	0.92
20A	100	180	279	0.81
20B	59	73	132	0.91
40A	65	64	130	0.91
40B	79	79	158	0.89
20+20	62	80	142	0.90
60	57	61	118	0.92

From the values reported in Table 5.8, the SFRC mix 20A has the most shrinkage and creep (prestress loss η around 0.80) compared to the other SFRC mixes for which a prestress loss of about 0.90 has been observed.

Concerning these values, it has to be emphasised that the effects of creep and elastic deformation will be lower than measured on the reference prisms. For the creep tests on standard prisms, the stress is kept constant during testing, while in reality, due to creep, skrinkage and relaxation phenomena, the prestress decreases and the effects will be auto-balanced, causing a less severe creep deformation as measured on the standard prisms.

5.3 Shear behaviour of girders

5.3.1 Failure mechanisms

For the tested girders, different failure mechanisms have been observed. During testing, two stages can be distinguished: 1) a linear elastic phase and 2) a shear cracking phase, starting with the occurrence of the first diagonal crack in the thin web and with the formation of additional parallel cracks for higher load stages. Initially, due to the prestressing force, some limited vertical bending cracks are present at the top of the girder.

When increasing the shear load, a first shear crack starts to develop in the right upper corner of the thin web. These cracks further propagate and new cracks are formed parallel to these cracks for increasing shear loads (see Fig. 5.15). Due to the high level of prestress, the diagonal cracks are formed before bending cracks are visible and as a result, web-shear cracks instead of flexural shear cracks are formed up to failure of the girder.

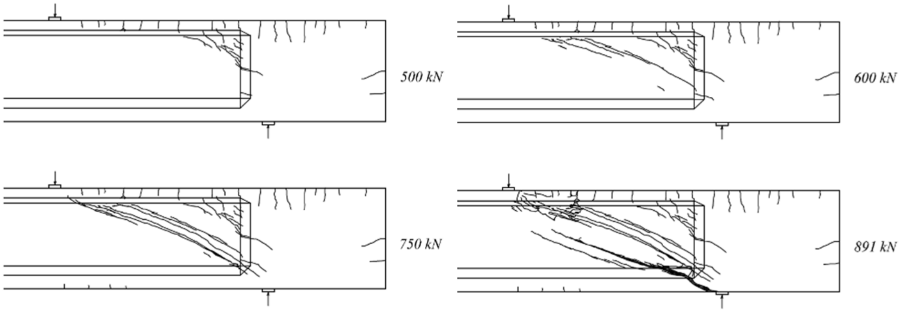

Fig. 5.15 – Typical shear crack formation observed from testing (cf. test 40B-2.5-1).

The first inclined cracks in the upper corner tend to open until relatively small crack widths of about 0.5 mm. A major diagonal shear crack is quite suddenly formed at the imaginary line between the support and the point load. The energy release is high and the crack opens directly for about several millimetres in case of lower fibre content. The load at which this first major diagonal shear crack is formed, is taken as the shear cracking load

V_{cr}. For SFRC girders with higher values of f_{R3}, the shear crack is arrested much faster and the energy release rate is significantly lower.

Further increase of the shear load will increase the shear critical crack opening until crack openings between 3 to 10 mm (see Appendix C). When reaching the ultimate shear capacity, excessive crack deformation and inherent stiffness reduction of the thin web occurs and all shear forces are transmitted directly through the compressed upper flange and (partially) decompressed lower flange. Eventually, shear failure is reached by either:

- Crushing of the web under the shear critical crack (WC)
- Failure of flanges (FL)
- Failure of interface between the lower flange and web (IL)
- Failure of interface between the upper flange and web (IU)
- A combination of above mechanisms

Examples of these main failure mechanisms are shown in Fig. 5.16 - Fig. 5.20.

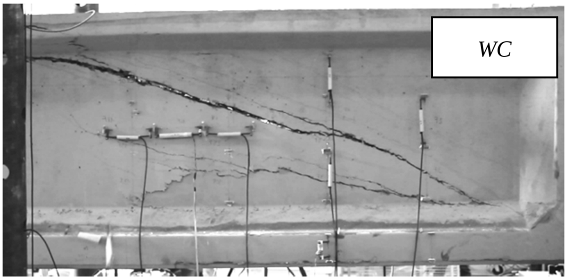

Fig. 5.16 – Web crushing failure as observed for test 40B-3.0-2

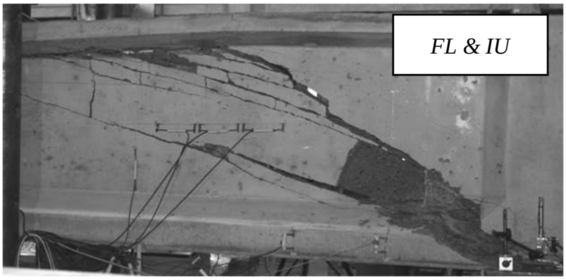

Fig. 5.17 – Failure of lower flange and interface between upper flange and web as observed for girder test REFTR-3.0-2

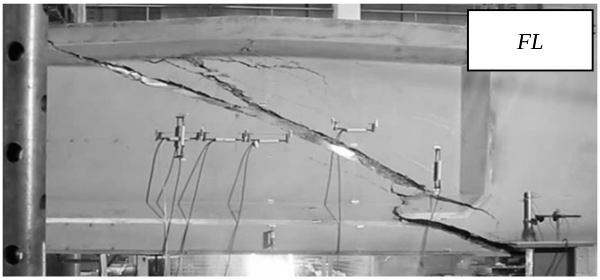

Fig. 5.18 – Failure of flanges as observed for test 20A-2.5-1

Fig. 5.19 – Failure of interface between lower flange and web as observed for test 60-3.0-2

For the girders with traditional reinforcement, the stirrups fail in tension and the energy release causes a sudden collapse of both upper and lower flanges. A still of the shear failure is shown in Fig. 5.20. For all of the tested girders containing steel fibres less explosive failures are observed with respect to the beams with traditional reinforcement.

Fig. 5.20 – Explosive failure of flanges as observed for girder test TR-2.5-1

5.3.2 Load deflection curves

An overview of all load-deflection curves is shown in Fig. 5.21.

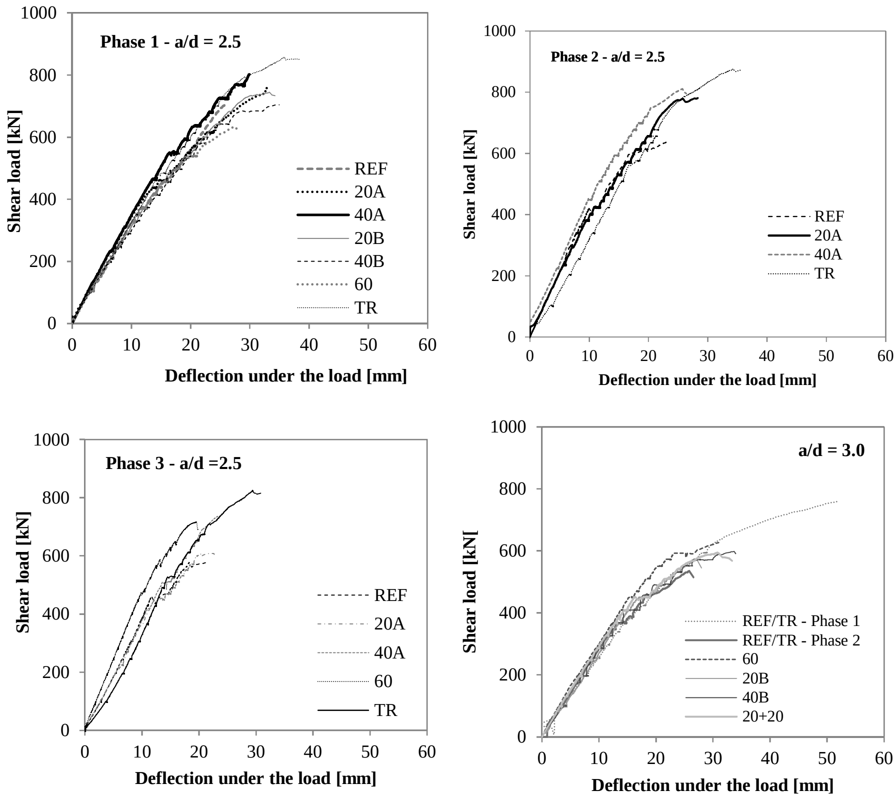

Fig. 5.21 – Load deflection curves for all of the tested girders

For girders with a/d = 2.5, it can be observed that the stiffness of the girder is slightly affected by the formation of shear cracks. Indeed, flexural cracks are only formed for shear loads close to the ultimate shear capacity. Due to the difference in span length the deflection response of all girders is stiffer for subsequent phases 1 to 3. In case of a higher shear span (a/d = 3.0), the formation of flexural cracks occurs at lower shear loads, causing an increase of deflection for load levels similar to tests with a/d =2.5.

5.3.3 Shear cracking and maximum loads

For all of the conducted shear tests, the experimentally obtained shear cracking load V_{cr}, maximum shear strength V_u and the observed inclination of compression strut θ are summarised in Table 5.9.

Table 5.9 – Overview of cracking shear load, ultimate shear load and shear cracking inclination angle for all of the tested girders.

Test Nr.	Designation	Phase	a/d	Shear reinforcement	V_{cr} [kN]	V_u [kN]	θ [°]	# cracks	Failure mechanism
1	1-2.5-[REF]	1	2.5	REF	444	702	22	1	IL
2	2-2.5-[REF]	2	2.5		415	647	19	4	WC
3	3-2.5-[REF]	3	2.5		461	578	20	2	WC & IL
4	1-3.0-[REF/TR]	1	3	REF	355	536	23	3	FL & IU
5	2-3.0-[REF/TR]	2	3	TR	387	782	23	3	FL
6	1-2.5-[20A]	1	2.5	20A	459	756	21	2	FL
7	2-2.5-[20A]	2	2.5		424	781	23	1	IL
8	3-2.5-[20A]	3	2.5		449	609	20	2	IU
9	1-2.5-[20B]	1	2.5	20B	484	786	24	3	IU & FL
10	2-3.0-[20B]	2	3		445	570	21	1	WC & IL
11	1-2.5-[40A]	1	2.5	40A	545	799	24	4	WC & IL
12	2-2.5-[40A]	2	2.5		530	809	22	2	WC & IL
13	3-2.5-[40A]	3	2.5		511	737	24	1	WC
14	1-2.5-[40B]	1	2.5	40B	434	744	27	2	IU & FL
15	2-3.0-[40B]	2	3		487	599	22	3	WC
16	1-2.5-[20+20]	1	2.5	20+20	567	696	21	2	IU & IL
17	2-3.0-[20+20]	2	3		436	595	22	2	WC
18	1-2.5-[60]	1	2.5	60	390	672	25	2	WC
19	2-3.0-[60]	2	3		452	627	26	1	IL
20	3-2.5-[60]	3	2.5		449	721	24	3	-
21	1-2.5-[TR]	1	2.5	TR	483	855	25	4	FL
22	2-2.5-[TR]	2	2.5		565	875	25	5	FL
23	3-2.5-[TR]	3	2.5		529	819	25	4	FL

In order to investigate the effect of fibres on the ultimate shear strength of FRC girders, the relationship between the shear capacity and the values of average residual stress $f_{R3,m}$ as shown in Table 5.5 is investigated. However, since the results of shear tests are prone to relatively high scattering, it should be noted that finding a correlation between the ultimate shear capacity and the f_{R3}-values can be difficult. This was evidenced by earlier research [12] from which no clear correlation between the residual flexural strength of the SFRC and the shear strength of the girders could be found. In Fig. 5.22, the ultimate shear capacity is plotted as a function of $f_{R3,m}$.

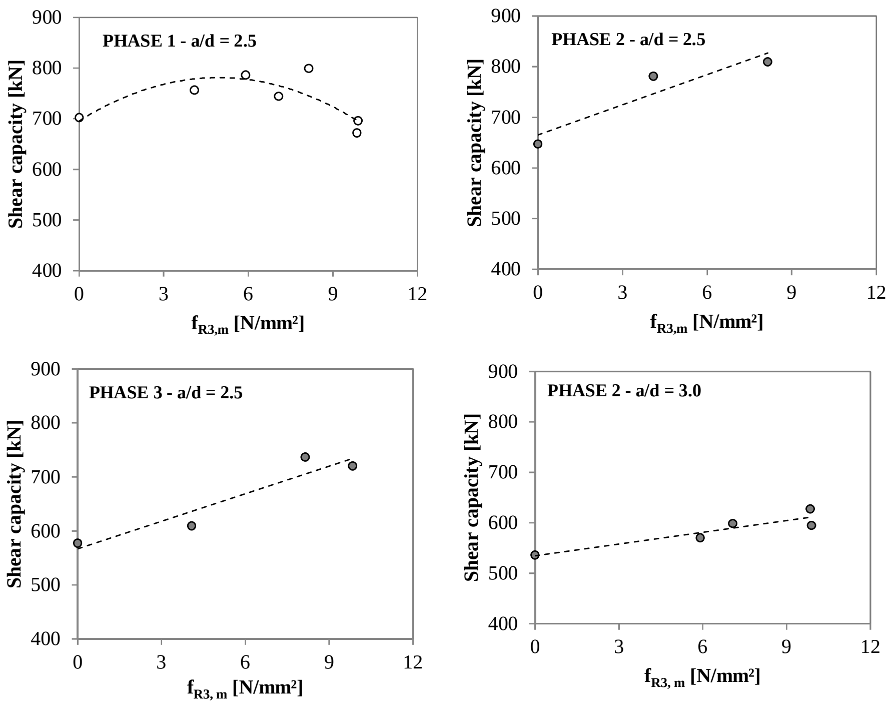

Fig. 5.22 – Ultimate shear capacity as a function of $f_{R3,m}$

For the conducted shear tests, it can be observed in Fig. 5.22 that the increase of maximum shear capacity as a function of $f_{Rm,3}$ is relatively moderate. This can be attributed to the relatively high contribution of the prestress to the shear capacity whereby the beneficial effect of fibres is less pronounced. In case of a/d equal to 2.5, a clear influence of the test phase is observed with respect to the relationship between the shear capacity and $f_{R3,m}$. For the shear tests with a/d equal to 2.5 tested in phase 1, no increase in shear strength is observed for $f_{Rm,3}$ values higher than about 7 N/mm², while this is not the case for phase 2. This indicates that an increased shear capacity is found with increasing f_{R3} (increasing fibre content), yet that for higher f_{R3}-values other shear failure mechanisms can start governing, preventing the further linear increase in shear capacity as a function of f_{R3}. This is explained in more detail at the end of this section.

In general, the shear critical area is always near the end-blocks and phase 1 and 2 will be more representative for realistic situations. However, it is found that when shear failure occurs in the absence of a rigid end-block (i.e. phase 3), it is easier for the shear critical area to deform and a lower shear capacity is observed for girders REF, 20A and 40A. Hence for phase 3, the linear increase of shear capacity as a function of $f_{Rm,3}$ is less steep.

Regarding the observed failure mechanisms, for all of the girders tested with a shear span to depth ratio equal to 2.5 and with the presence of the end block, the arching effect will become more important and loads are partially transferred directly towards the supports through the compressive zone and the end block. For the same a/d equal to 2.5 but for the tests of phase 3, the shear critical area is not confined by the rigid end block and can be deformed more easily. This results in a lower shear strength. Yet, for all of the tests done with an a/d ratio equal to 3.0, a more clear influence of fibres is observed with respect to the tests done for a/d = 2.5 in both phase 1 and 2.

A possible explanation for reaching a plateau at high post-cracking flexural stress levels as observed in phase 1 (see Fig. 5.23) can be found in the micromechanical observations at the shear crack

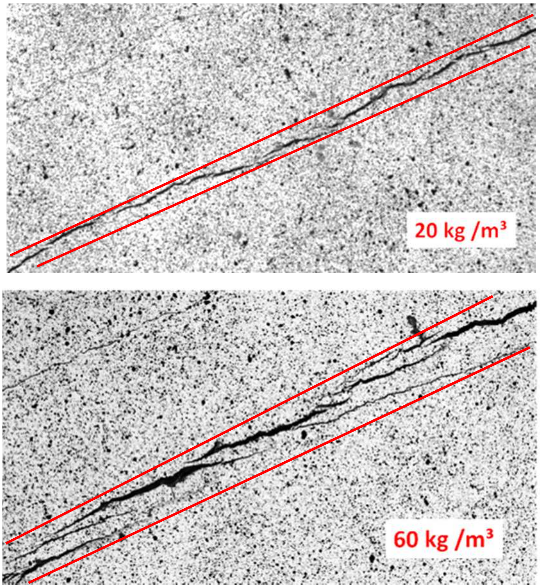

Fig. 5.23 - Difference in shear crack behaviour between low (left) and high (right) fibre dosages.

Since the compressive strut stress levels are expected to be higher for a/d = 2.5 with respect to a/d = 3, the described mechanisms are observed for tests with a/d = 2.5. The high anchorage stresses at the fibre ends and the perpendicular compressive stresses in the strut cause a biaxial state of stress in the concrete at the strut edges. Moreover, for increasing post-cracking tensile stresses, the shear capacity of the girders is expected to increase together with the compressive stresses in the struts. However, the biaxial state of stress failure envelope will cause that the concrete matrix will fail to provide sufficient anchorage capacity to the fibres and a fracture zone around the shear crack will be enlarged. Hence, with increasing fibre content, this fracture zone becomes more pronounced. This effect will cause a loss of fibre efficiency when the width of the damaged zone around the main crack is equal to the fibre length, as illustrated in Fig. 5.23.

The load at which the first shear crack will occur is mainly dependent on the concrete tensile strength, the effective prestress and the load configuration. Therefore, the ultimate shear capacities should be approached carefully. Since fibres become active after cracking, it is interesting to evaluate the influence of fibres in terms of post-cracking shear capacity (i.e. the gain of shear strength after first cracking occurs, Fig. 5.24).

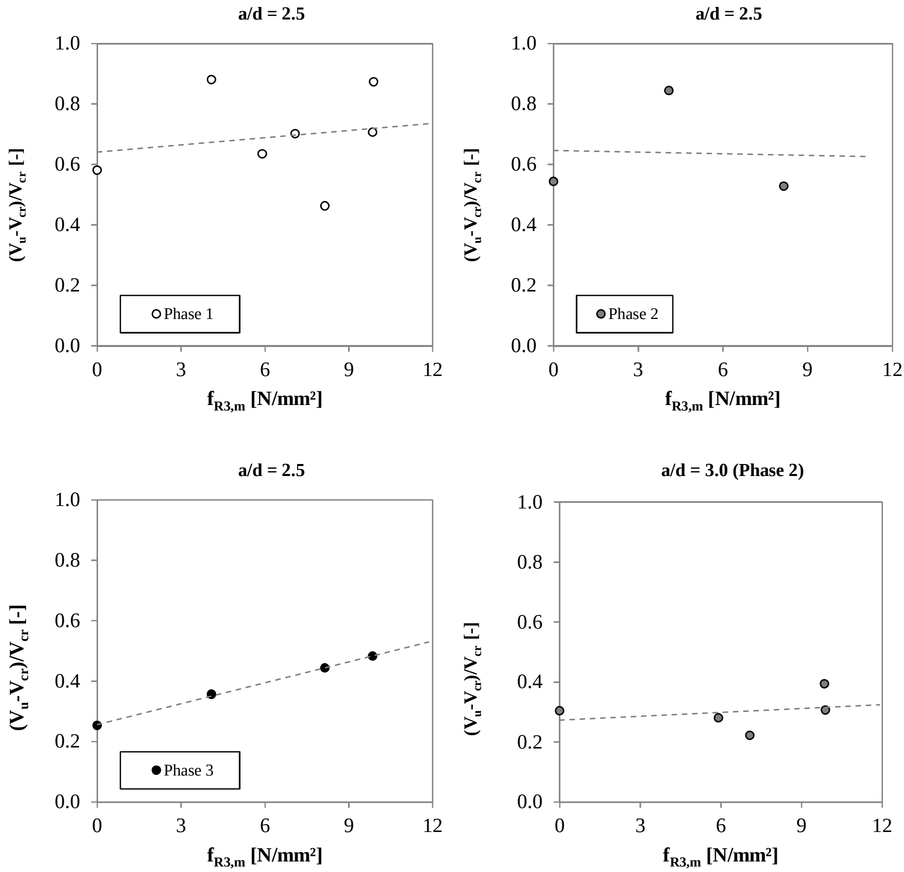

Fig. 5.24 – $(V_u\text{-}V_{cr})/V_{cr}$-ratio as a function of f_{R3m}.

When looking more into detail to the values of $(V_u\text{-}V_{cr})/V_{cr}$ obtained for the shear tests with a/d = 2.5 for phase 1 and 2, no clear correlation with respect to f_{R3} can be found, due to high scatter. Hereby, the increase in shear capacity is less clear than observed in Fig. 5.22. The high scatter of $(V_u\text{-}V_{cr})/V_{cr}$ for a/d = 2.5 for phase 1 and 2, may possibly be due to outliers in the observed values of V_{cr} (being taken as the first major shear crack observed), influenced by direct load transfer effects and the presence of the stiff end-block and whereby a significant scatter on cracking loads is typical for concrete in general. For the test conducted with a/d = 2.5 in phase 3, a more clear correlation between the shear strength increase after cracking and $f_{R3,m}$ is observed. The value of $(V_u\text{-}V_{cr})/V_{cr}$ increases linearly from 20 % to almost 50 % for the girder containing 60kg/m³ of fibres. For the girders tested in phase 2 with an a/d ratio equal to 3.0, an increase of $(V_u-V_{cr})/V_{cr}$ with respect to $f_{R3,m}$ is observed with values ranging from 20 % to 40 %. These observations are in line with Fig. 5.22.

5.3.4 Shear deformation and crack propagation

A DIC technique was used to monitor the shear crack displacements. For each state of deformation captured by the cameras, the applied shear load is known. Based on the post-processing of the DIC measurements, virtual extensometers are placed over the observed main cracks (Fig. 5.25) and as a result the relationship between shear load and crack deformation can be obtained. In Fig. 5.26, the crack width of the dominant shear cracks is given as a function of applied load. Hereby, the crack opening is considered by a virtual extensometer, positioned central over the shear crack.

For all of the conducted shear tests, the shear crack propagation has been captured by means of a grid of extensometer. Since the information obtained from the DIC is more accurate and can be used to monitor the shear crack displacement of a single crack, the obtained data from the extensometers is merely used as an additional source of information when applied in combination with the DIC measurements. For the girders tested without DIC, the data gained from the extensometers is more valuable.

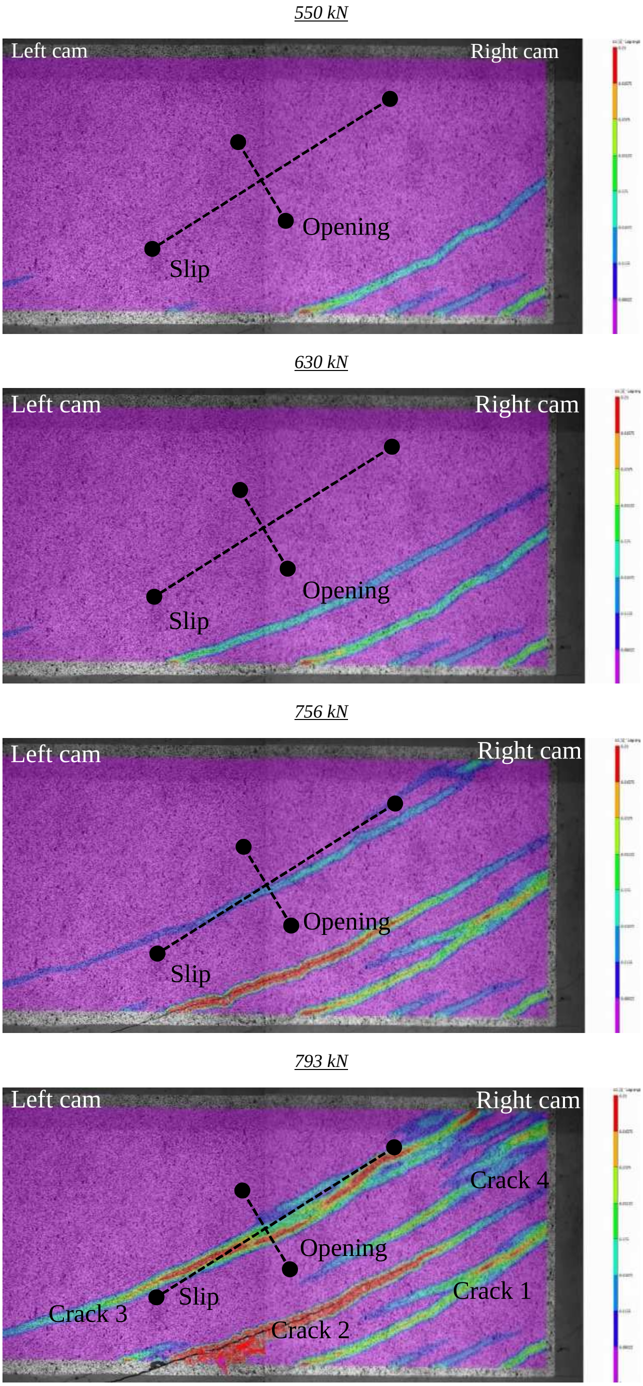

Fig. 5.25 – Principal tensile strain (range = 0 – 5 %) development for the combined regions of cam 0 and 1 (test 40A-1-2.5)

In this way, the relationship between applied shear load and measured crack opening of the dominant shear cracks is obtained for all test series (see Fig. 5.26).

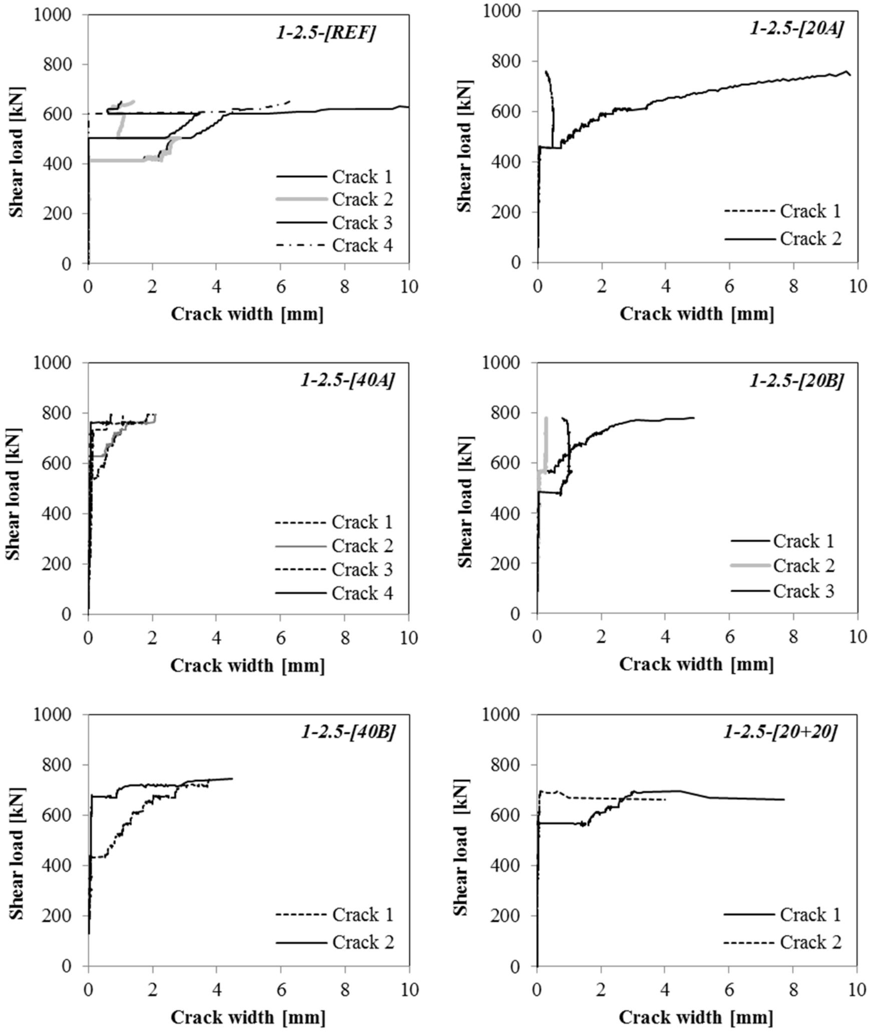

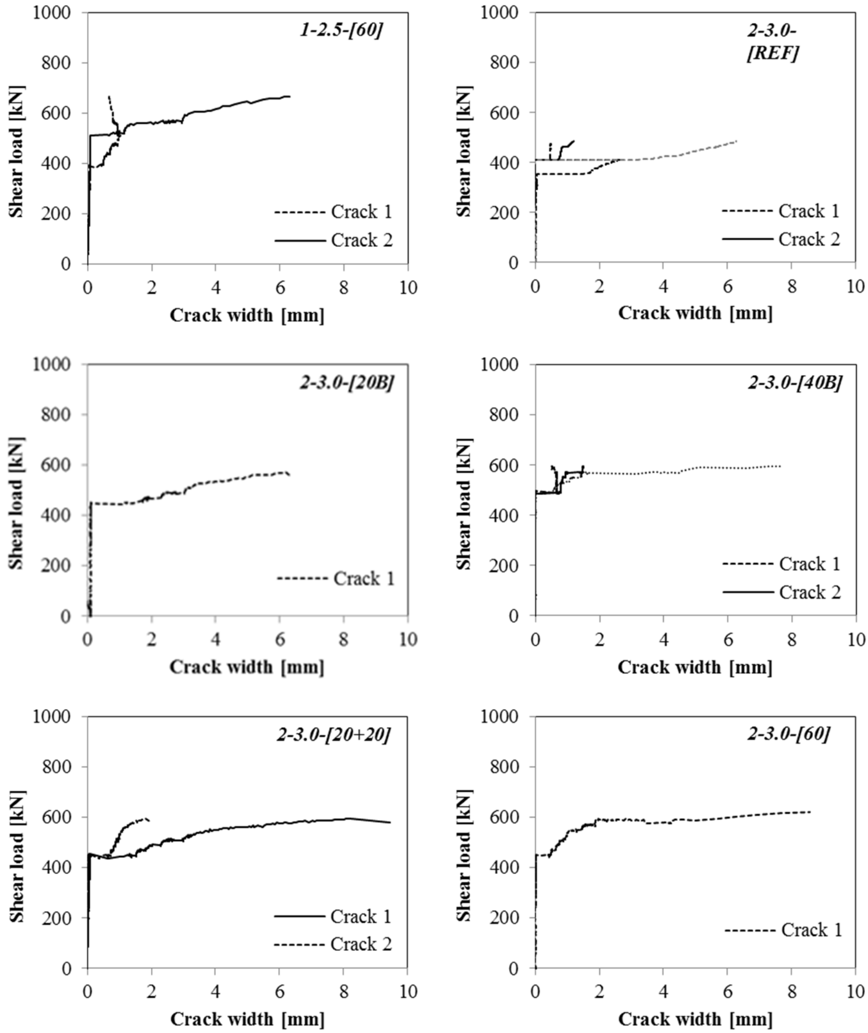

Fig. 5.26 –Shear load as a function of crack width for all considered dominant shear cracks

From Fig. 5.26, it can be observed that increasing fibre content reduces significantly the crack widths after initiation of cracking occurs. While for the girder with 60 kg/m³ of fibres the load increases after an initial crack width of 0.5 mm, the shear crack widening is dramatically higher for the plain concrete girders, where the initial shear crack propagates to at least 2 mm directly after cracking.

Hence, it can be concluded that for these prestressed SFRC girders, the effect of fibres is more important with respect to shear crack control in the thin web, compared to the increase of the ultimate shear capacity. This crack control effect diminishes near ultimate with crack widths beyond 5 to 6 mm. At this point of crack deformation, the shear loads are more similar. This is due to the fact that the ultimate limit state is governed by the presence of a compressed upper and partially decompressed lower flange. Hence, the shear crack propagation behaviour shows that shear cracks can propagate up to 10 mm, which is far beyond the ultimate limit state of reinforced structures. These results prove that the ultimate shear capacity at such high deformations is less affected by the presence of fibres, and is merely affected by the presence of the compressed flanges and therefore, the beneficial effect of fibres is also evaluated in terms of crack arresting ability. In view of these observations, an ultimate limit state can also be defined in terms of a critical crack opening rather than the ultimate load. This is done in Fig. 5.27, considering a predefined ultimate crack opening of 2.5 mm and expressing the results as a function of flexural stress $f_{R3,m}$. For the tests in which the DIC technique was not used to measure the shear crack width propagation, values measured by means of digital extensometers were used instead.

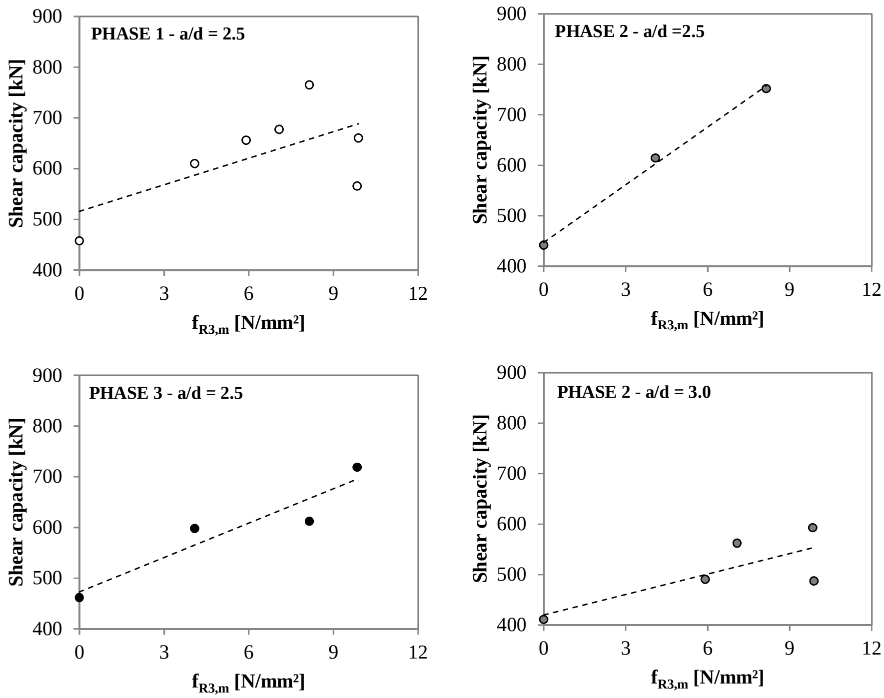

Fig. 5.27 – Shear capacity at 2.5 mm crack width as a function of f_{R3}.

Comparing Fig. 5.27 with Fig. 5.22, the same trends are observed, yet the enhancement effect of the fibres becomes more pronounced. For the tests conducted in phase 1 for a/d = 2.5, for f_{R3}-values higher than 8 N/mm², a decrease of shear strength has been observed (Fig. 5.27, top left). For the girders tested in this work, the shear capacity $V_{u,2.5}$ was increased up to about 32% and 78% ($f_{R3,m}$ equal to 9.9 N/mm²), for an a/d equal to 3.0 and 2.5 respectively.

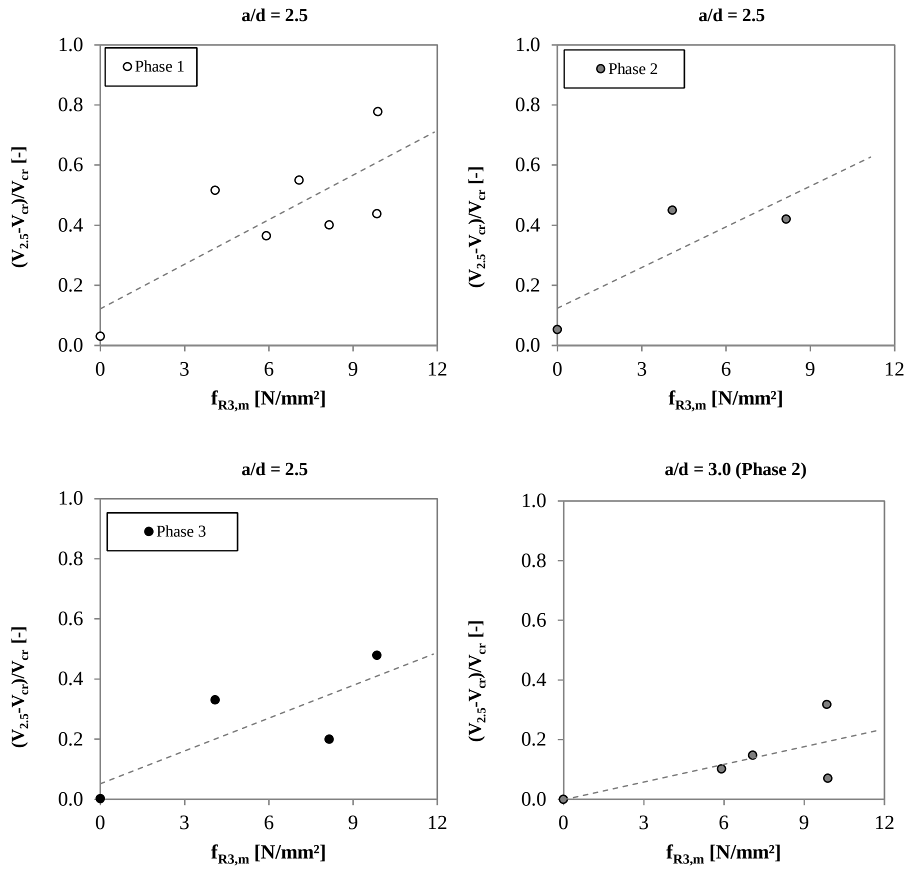

Fig. 5.28 – Ratio of $(V_{2.5} - V_{cr})/V_{cr}$ as a function of $f_{R3,m}$

When comparing Fig. 5.28 with Fig. 5.24, the beneficial effect of fibres to enhance the shear strength of prestressed concrete girders becomes more clear. For all of the girders without shear reinforcement, the cracking shear load V_{cr} and the shear load at a crack opening of 2.5 mm are almost equal. When fibres are added to the concrete (and f_{R3} increases), the post-cracking response of the web is enhanced significantly. For all of the tested SFRC girders, the ratio between $(V_{2.5}-V_{cr})/V_{cr}$ increases linearly as a function $f_{R3,m}$. The highest increase has been observed for the girder tests with an a/d equal to 2.5 (up to 80 %). For a shear span to depth ratio equal to 3.0, the increase is less pronounced up to 40 % for $f_{R3,m}$-values equal to 9.9 N/mm².

In addition to the relationship between shear load and shear crack opening (Fig. 5.26), the slip displacement behaviour of major shear cracks has been determined by means of the post-processing of the DIC-images. In Fig. 5.28, the obtained crack opening-slip relations are shown for all girders for which the DIC measurement technique is applied. Thereby, only the main critical shear cracks have been taken into account. For the majority of all tests, one or two shear cracks were dominant with respect to the crack propagation behaviour.

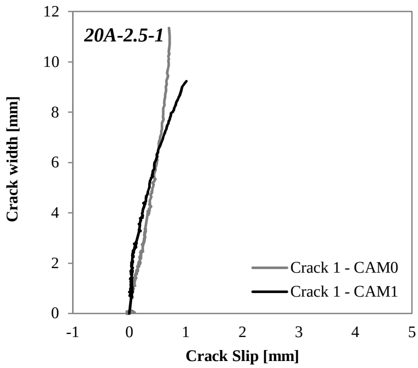

Fig. 5.29 – Shear crack propagation behaviour for girder 20A-Phase 1

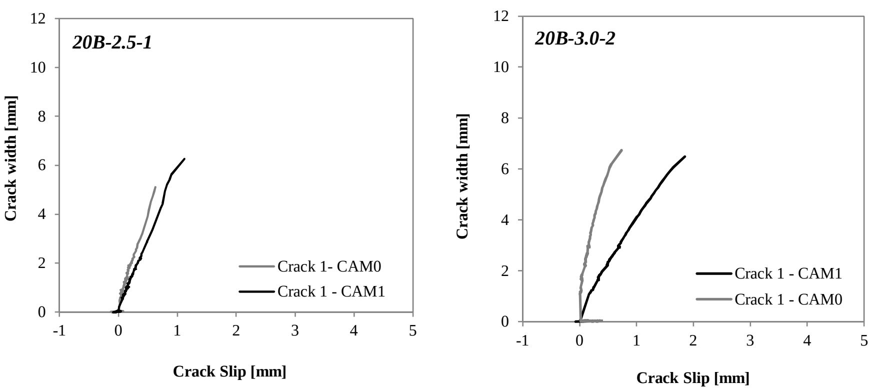

Fig. 5.30 – Shear crack propagation behaviour for girder 20B

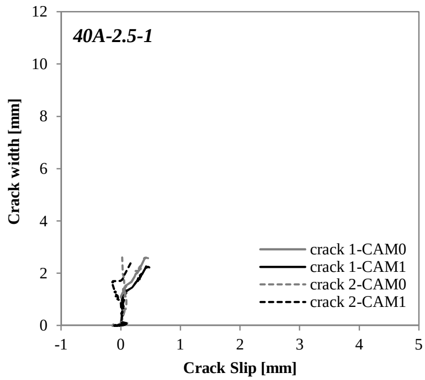

Fig. 5.31 – Shear crack propagation behaviour for girder 40A -Phase 1

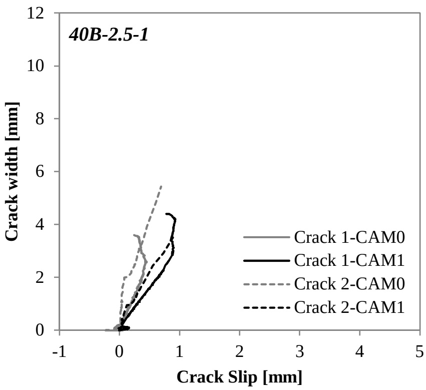

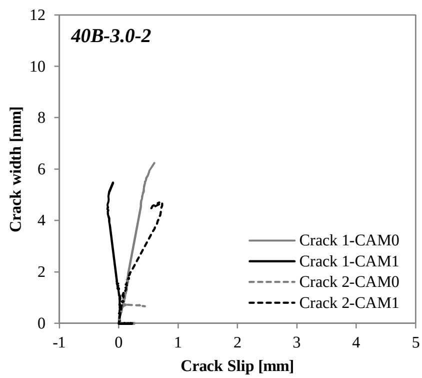

Fig. 5.32 – Shear crack propagation behaviour for girder 40B

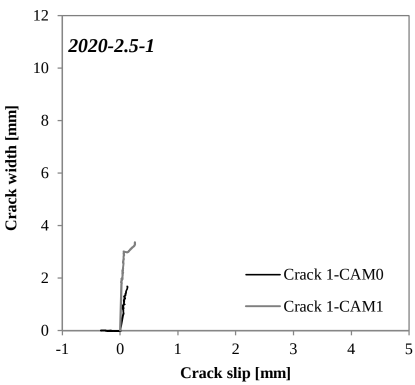

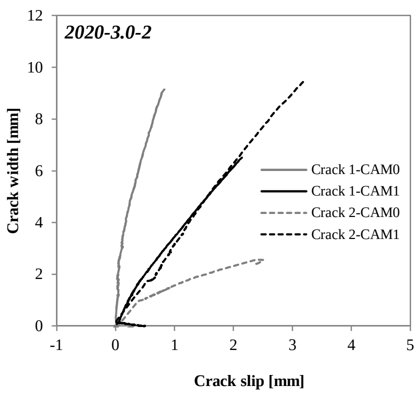

Fig. 5.33 – Shear crack propagation behaviour for girder 20+20

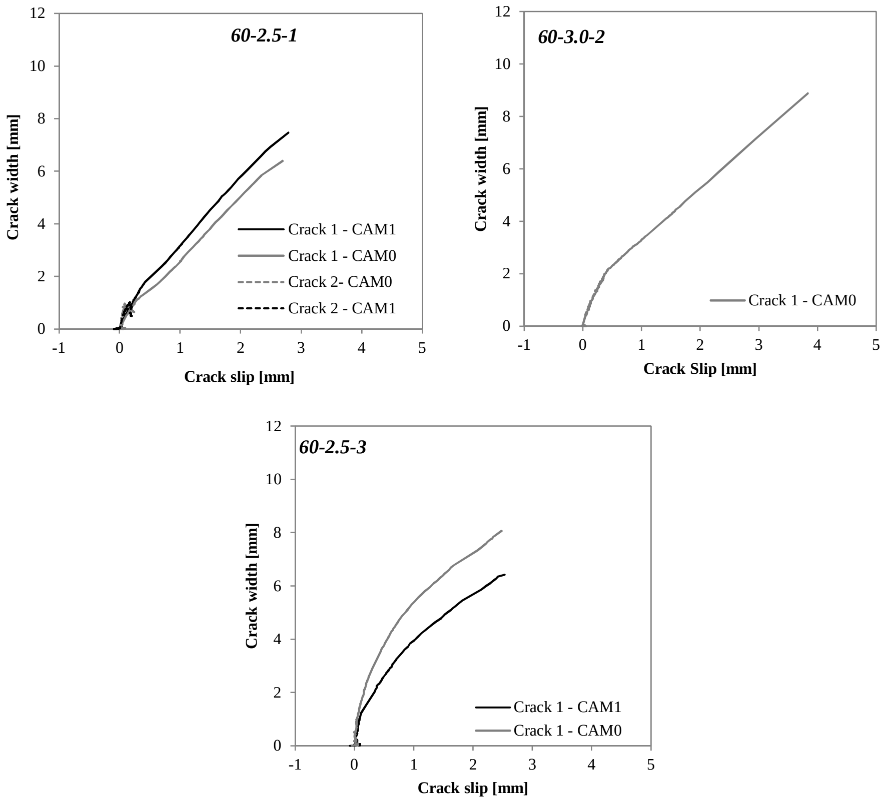

Fig. 5.34 – Shear crack propagation behaviour for girder 60

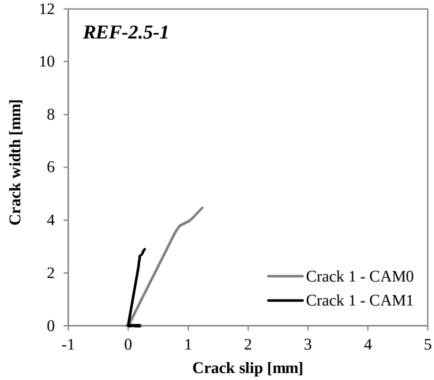

Fig. 5.35 – Shear crack propagation behaviour for girder REF

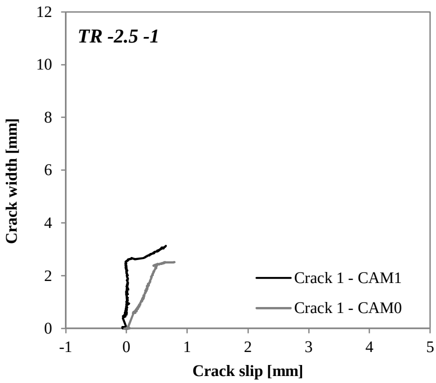

Fig. 5.36 – Shear crack propagation behaviour for girder TR

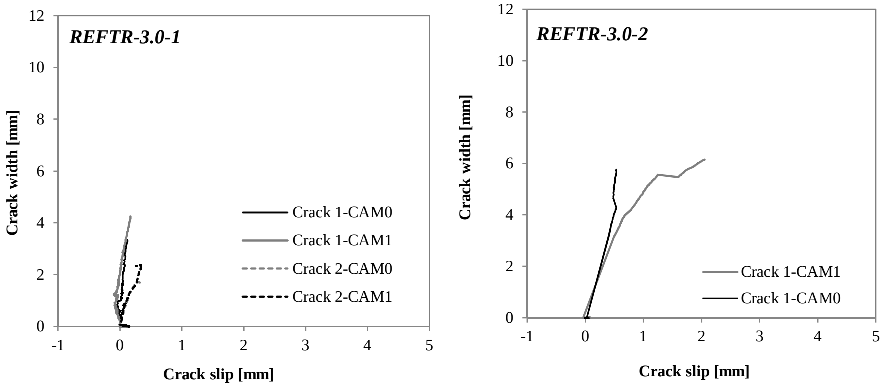

Fig. 5.37 – Shear crack propagation behaviour for girder REF/TR

Keeping in mind the analytical or empirical formulations describing the aggregate interlock mechanisms (see Chapter 2) or shear stress transfer in cracked (steel fibre) concrete (see Chapter 3), the relative increase of crack opening with respect to crack slip, is much higher for the shear cracks in the girders than for the cracks investigated at the meso-scale level on prisms by means of a direct shear test.

It is clear that the Mode I opening behaviour is dominant compared to the sliding behaviour of the crack and consequently, it can be concluded that the influence of aggregate interlock mechanisms on the observed shear capacity of all tested girders will be rather limited.

5.4 Conclusions

Based on 23 shear tests on prestressed concrete SFRC girders without shear reinforcement, it can be concluded that steel fibres can increase the shear strength of 20 m span full-scale girders. For the tested configurations (up to 60 kg/m³ of steel fibres), an increase in capacity i.e. at a crack opening equal to 2.5 mm up to about 80% is obtained with respect to plain concrete prestressed girders. The failure aspect of the girders is characterised by the development of basically one or two critical shear crack(s) in the web. By excessive deformation of the web and relatively high crack openings, the girder eventually fails in shear by a collapse of the upper and lower flanges.

It is found that the influence of fibres towards the ultimate shear strength of prestressed SFRC girders is limited for high values of f_{R3}. For this test programme, this was observed for f_{R3}-values higher than 7-8 N/mm² in case of a/d equal 2.5. This limiting effect is attributed to the biaxial stress state in the strut next to the shear cracks, causing fibres to lose anchorage capacity and effectiveness. For higher shear span to depth ratios, the beam action is more important than the arch action of the girder, which resulted in higher shear capacity for a/d equal to 2.5 versus 3.0.

Investigating the shear crack propagation by means of Digital Image Correlation, it has been observed that for thin web prestressed girders, fibres are most effective in the post-cracking stage for arresting sudden crack propagation. Due to the high prestressing level, the crack propagation of the first shear crack is sudden with crack widths up to 4 mm for girders without fibres. By adding fibres, the propagation of the first shear crack is more controlled and arrested at lower crack widths.

From production quality control tests, it is concluded that attention should be paid towards the production process of SFRC in practical environments in order to guarantee a sufficient SFRC quality level and inherent reduction of scatter for the residual stresses adopted in design.

5.5 References

[1] Duthinh, D., Carino, N. J. (1996). "NISTIR 5870: Shear Design of High-Strength Concrete Beams: A Review of the State-of-the-Art".

[2] fib. (2010). "Model Code for Concrete Structures 2010". Lausanne, Switzerland, fédération internationale du béton.

[3] CEN. (2004). "EN1992-1-1:2004 - Eurocode 2: Design of concrete structures - Part 1-1: General rules and rules for buildings". Brussels, Belgium.

[4] Li, V. C., Ward, R., Hamza, A. M. (1992). "Steel and Synthetic Fibres as Shear Reinforcement". *ACI Materials Journal*, Vol. 89(5), pp. 499-508.

[5] Minelli, F., Plizzari, G. (2013). "On the Effectiveness of Steel Fibres as Shear Reinforcement". *ACI Structural Journal*, Vol. 110(3), pp. 379-389.

[6] Cucchiara, C., La Mendola, L., Papia, M. (2004). "Effectiveness of stirrups and steel fibres as shear reinforcement". *Cement and Concrete Composites*, Vol. 26(7), pp. 777-786.

[7] Voo, Y. L., Foster, S. J., Gilbert, R. I. (2006). "Shear Strength of Fiber Reinforced Reactive powder Concrete Prestressed Girders without Stirrups". *Journal of Advanced Concrete Technology*, Vol. 4(1), pp. 123-132.

[8] Parra-Montesinos, G. J. (2006). "Shear strength of beams with deformed steel fibers". *Concrete International*, Vol. 28(11), pp. 57-61.

[9] Soetens, T., Matthys, S. (2013). "Evaluation of MC2010 models for prestressed SFRC beams subjected to shear". *7th International Conference: Fibre Concrete - Technology, Design, Application, Prague, Czech Republic*.

[10] Meda, A., Minelli, F., Plizzari, G., Riva, P. (2005). "Shear behaviour of steel fibre reinforced concrete beams". *Materials and Structures*, Vol. 38, pp. 343-351.

[11] Minelli, F. (2005). "*Plain and Fibre Reinforced Concrete Beams under Shear Loading: Structural Behaviour and Design Aspects*" (PhD-thesis). Brescia, University of Brescia.

[12] Cuenca, E., Serna, P. (2013). "Shear behavior of prestressed precast beams made of self-compacting fiber reinforced concrete". *Construction and Building Materials*, Vol. 45(August 2013), pp. 145–156.

[13] RILEM. (2003). "Final Recommendation of RILEM TC 162-TDF: Test and design methods for steel fibre reinforced concrete sigma-epsilon-design method". *Materials and Structures*, Vol. 36(262), pp. 560-567.

[14] Sutton, M. A., Orteu, J. J., Schreier, H. W. (2009) "*Image correlation for shape, motion and deformation measurements. Basic concepts, theory and applications*". Springer.

[15] Hertelé, S., De Waele, W., Denys, R., Verstraete, M. (2012). "Investigation of strain measurements in (curved) wide plate specimens using digital image correlation and finite element analysis". *Journal of Strain Analysis for Engineering Design*, Vol. 47(5), pp. 276-288.

[16] Grünewald, S. (2004). "*Performance-based design of self-compacting fibre reinforced concrete*" (Phd-thesis), Delft University of Technology, p. 233.

[17] Laranjeira, F., Molins, C., Aguado, A. (2010). "Predicting the pullout response of inclined hooked steel fibers". *Cement and Concrete Research*, Vol. 40(10), pp. 1471-1487.

[18] Markovich, I. (2006). "*High-Performance Hybrid-Fibre Concrete: Development and Uitilisation*" (PhD-thesis), Delft University of Technology, p. 211.

[19] Parmentier, B., Vandewalle, L., Van Rickstal, F. (2008). "Evaluation of the scatter of the postpeak behaviour of fibre reinforced concrete in bending: a step towards reliability". *7th international RILEM symposium on Fibre Reinforced Concrete, Chennai, India*, pp. 133-143.

[20] Parmentier, B., De Grove, E., Vandewalle, L., Van Rickstal, F. (2008). "*Dispersion of the mechanical properties of FRC investigated by different bending tests*". In: Tailor Made Concrete Structures pp. 507-512.

[21] CEN. (2002). "EN 1990 - Eurocode 0: Basis of structural design". Brussels, Belgium, CEN.

[22] CEN. (2007). "EN 14721 - Test method for metallic fibre content. Measuring the fibre content in fresh and hardened concrete". Brussels Belgium.

[23] ERMCO. (2012). "Guidance to fibre concrete: Properties, Specifications and Practice in Europe".

6 SHEAR BEHAVIOUR MODEL

6.1 Introduction

The basis of current shear design provisions goes back to the development of the Compression Field Theory (CFT), later followed by the Modified Compression Field Theory (MCFT) to introduce the influence of tension stiffening. The MCFT has been developed by Vecchio & Collins during the 1980's [1, 2]. For an overview of existing shear behaviour models, reference is made to Chapter 3.

Starting from the MCFT, and as will be further outlined in this chapter, the shear capacity of reinforced concrete members has been implemented in a sectional analysis tool in order to predict the shear capacity of reinforced (RC) and prestressed concrete (PC) elements with or without shear reinforcement, and including both traditional stirrups and/or SFRC as shear reinforcement. The model is developed based on a number of assumptions which are made based on the observations from the experimental and analytical work as described in Chapters 4 and 5. The most important difference with existing analysis tools based on the MCFT is the implementation of the post-cracking behaviour of SFRC.

Based on observations from experimental tests on full-scale prestressed SFRC girders, the model is developed with the following assumptions or considerations:

- Regarding the propagation behaviour of the critical shear crack, it has been observed for the girders in this test programme that the opening of the shear crack was dominant compared to the shear slip. As a consequence, the aggregate interlock mechanisms will be less important than the axial stress transfer between inclined cracks due to fibre pull-out.
- In the classical formulations of the MCFT, the tension stiffening effect is considered to be the main contribution to the shear strength of reinforced concrete. However, without the presence of traditional stirrups, the post-cracking residual stresses can only be transmitted due to the pull-out of fibres.
- The shear failure of SFRC girders is assumed to be governed by exhausting the pull-out capacity of all fibres crossing the crack plane for higher crack openings.
- The biaxial stress state in the web struts causes a local shear-tensile failure of the concrete matrix and the anchorage capacity in the damaged zone around the shear crack is lost. For SFRC with high values of f_{R3}, the post-cracking tensile strength cannot be fully developed and the shear capacity of the girders is not increasing proportionally with respect to the residual flexural strength as determined from standard testing of prisms.

The developed analysis tool is used to describe the shear failure behaviour in terms of applied shear load and inherent average crack width propagation and the modelled curves are compared with respect to the experimentally observed crack opening behaviour.

6.2 Model formulation

6.2.1 General

The developed sectional analysis tool is based on the strain compatibility and force equilibrium as defined in the original MCFT. Thereby, the cross-section height is divided into a finite amount of layers with a fixed height. For every layer, based on a given strain distribution, the corresponding stresses are calculated. In order to obtain the shear load acting on a girder as a function of shear deformation, equilibrium has to be obtained, both at the level of the individual layers, as well as at the level of the complete cross-section, and this applied for each deformation step.

6.2.2 Constitutive laws

6.2.2.1 SFRC in tension

In literature, different models are suggested in order to model the post-cracking stress crack opening relationship. In this study, the model proposed in Chapter 4 (section 4.2) has been taken into account. Hereby, the principal tensile stress active in a crack is only carried by the fibre pull-out forces. These stresses have to be in balance with the stresses in the concrete in between the cracks (see Fig. 6.1).

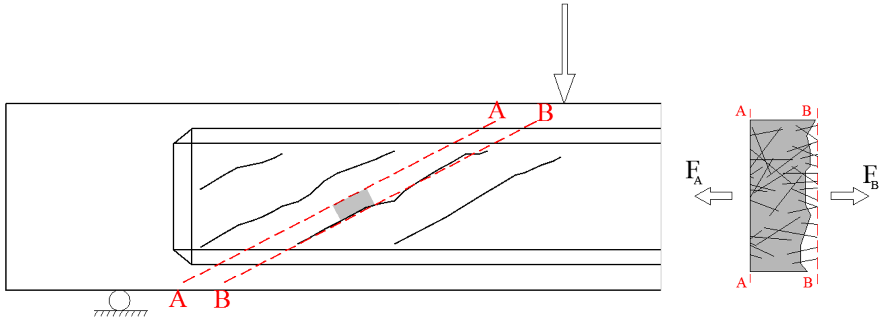

Fig. 6.1-Force equilibrium for sections in between cracks (plane A) and at the crack (plane B)

Regarding Fig. 6.1, considering two parallel planes A (in the strut) and B (in the crack), equilibrium of horizontal forces F_A and F_B is obtained when the conditions of Eq. 6.1 is met.

$$\sigma_f \sum A_{f,B} = f_{ct}\left(A_c - \sum A_{f,A}\right) + \varepsilon_1 E_f \sum A_{f,A} \qquad \text{Eq. 6.1}$$

With $A_{f,A}$ and $A_{f,B}$ the total cross-section of fibres crossing the crack and in between the cracks, respectively. E_f is the modulus of elasticity of the fibre material, ε_1 is the principal tensile strain and σ_f is the post-cracking tensile stress of SFRC at a crack opening w. Defining the geometrical percentage of fibre reinforcement as the ratio of A_f/A_c and assuming $A_{f,A}$ is equal to $A_{f,B}$, Eq. 6.1 can be rewritten as:

$$\sigma_f = f_{ct}\left(1-\rho_f\right) + \varepsilon_1 E_f \rho_f \qquad \text{Eq. 6.2}$$

Due to the presence of a principal compression stress σ_2 in the struts, the biaxial stress state will cause the concrete to rupture in tension for values of the principal tensile stress, which are lower than the uni-axial tensile stress. In order to deal with a biaxial tensile failure of concrete, a simplified reduction of the allowable axial tensile strength of concrete as a function of lateral compressive stress in the struts is adopted as given by Eq. 6.3.

$$f_{ct,max} = f_{ct}\left(1 + \frac{\sigma_2}{f_{c,cyl}}\right) \qquad \text{Eq. 6.3}$$

In which σ_2, is the compressive stress in the struts (i.e. a negative value).

The value of $\sigma_f(w)$ is calculated taking into consideration the simplified trilinear constitutive stress-crack opening law as proposed in Chapter 4, Section 4.2 (see Fig. 6.2).

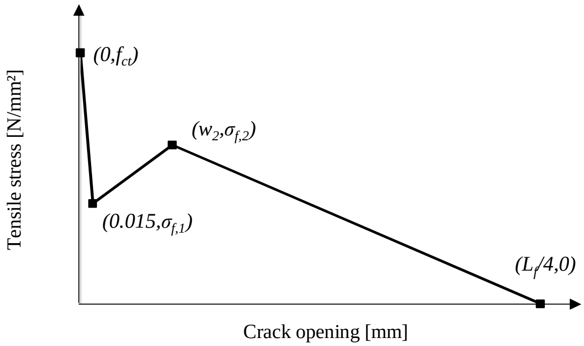

Fig. 6.2 - Schematic representation of the tri-linear stress-crack opening law for SFRC

For all of the girders, the parameters defining the post-cracking Mode I constitutive law are summarised in Table 6.1. The values given herein are obtained by applying Eq. 4.4 – Eq. 4.11 from Chapter 4, Section 4.2.3.

Table 6.1 – Values of $\sigma_{f,1}$, $\sigma_{f,2}$ and w_2 for all of the girders.

Girder	f_{ct} [N/mm²]	$\sigma_{f,1}$ [N/mm²]	$\sigma_{f,2}$ [N/mm²]	w_2 [mm]
20A	2.63	0.67	1.34	1.56
20B	2.92	1.44	1.11	2.30
40A	3.50	2.45	0.84	3.24
40B	2.98	2.10	0.93	2.79
20+20	3.85	2.71	0.78	3.97
60	4.13	3.57	0.56	3.95

By assuming the simplified tri-linear post-cracking law for SFRC, a certain error has to be dealt with. In order to estimate the inherent modelling error, the stress-CMOD curves as determined by taking into account the values of Table 6.1 are compared with respect to the average of experimentally obtained curves (Section 5.2.3).

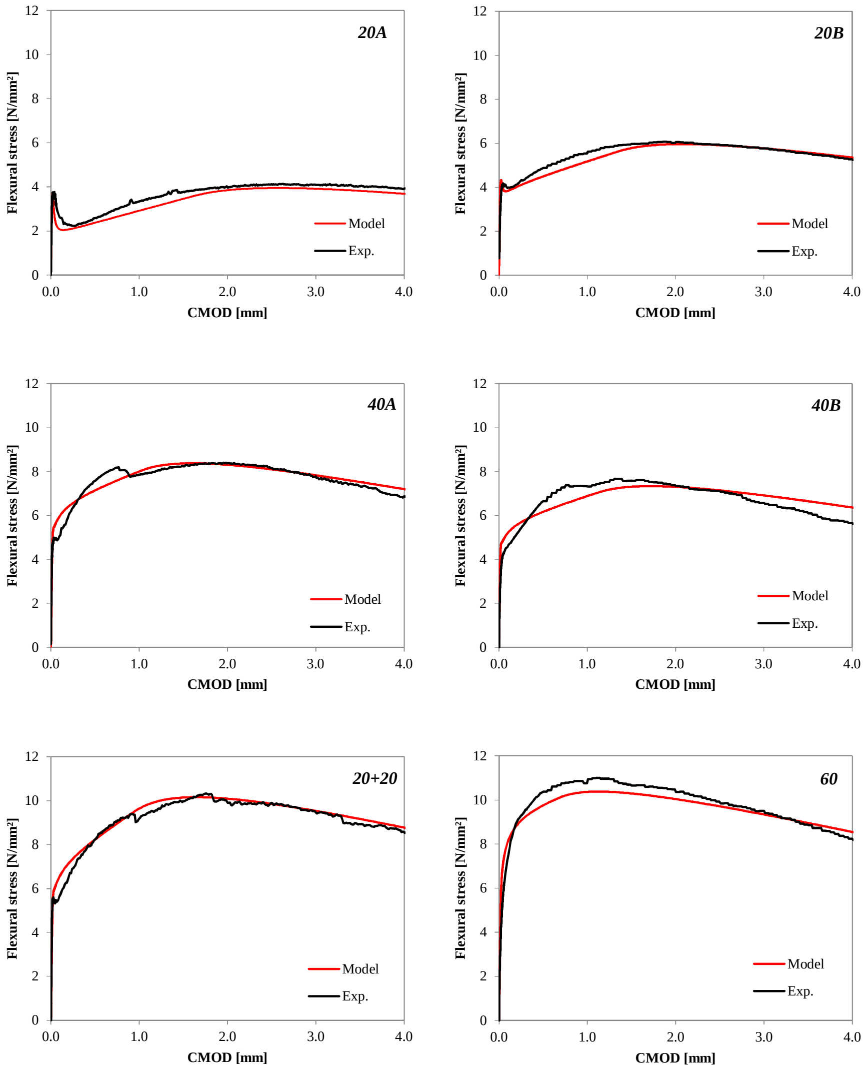

Fig. 6.3 – Comparison between modelled and experimental average three-point bending test results

As can be seen from Fig. 6.3, the proposed tri-linear model can be successfully used to model both the pseudo-hardening and pure hardening post-cracking behaviour of SFRC subjected to a standard three-point bending test. Further evaluation of the accuracy has been done by considering the error between the average experimental curve and the modelled flexural behaviour. In Fig. 6.4, this relative error is plotted as a function of CMOD.

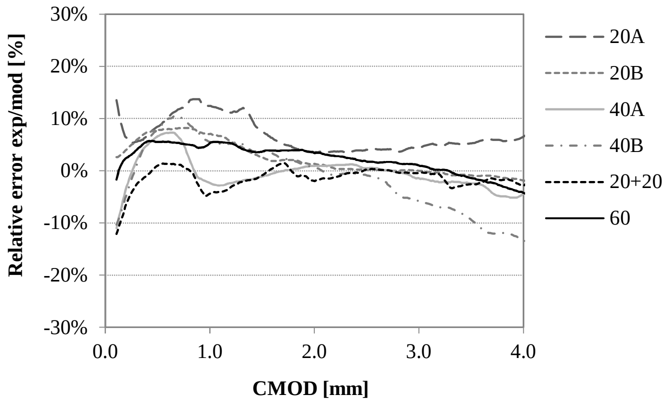

Fig. 6.4 – Relative error between model and experimental result as a function of CMOD

In general, the relative error (Fig. 6.4) is lower than +/-10% for all of the considered SFRC mixes. For a CMOD value lower than 2 mm, the use of the proposed tri-linear model tends to yield mostly an underestimation of residual flexural strength between 0 and 10 %, while for CMOD-values higher than 2 mm, a better prediction is made, except for the SFRC mix 40B. This can be attributed to the mixture of both short and long fibres, for which the adopted model is not calibrated. For mix 20A, this general trend is not observed and the model error has been found to be more constant for about 5-10 %.

For the post-cracking tensile stress-strain response of girders without SFRC and with tradional stirrups, a tensions stiffening law is adopted according to Eq. 6.4 (see also Chapter 2).

$$f_{1,res}\left(\varepsilon_1\right) = \left(\frac{C_1}{1+\sqrt{C_2\varepsilon_1}}\right)\sqrt{f_{cm}} \qquad \text{Eq. 6.4}$$

In which C_1 is taken equal to 0.375, and C_2 is taken equal to 1500 in case of the presence of a web reinforcement. For the combination of stirrups and steel fibres, the proposed model can not be used and further research is needed to derive empirical values for C_2.

For all of the plain concrete girders [REF] and [REF/TR]-Phase 1, the adopted post-cracking softening law is assumed to be bi-linear as described in Section 4.2.4, Fig. 4.12 and the tension stiffening effect is not considered.

6.2.2.2 SFRC in compression

For the case of compression of the concrete, the constitutive law as described in fib bulletin 42 “constitutive modelling of high strength / high performance concrete” [3] is considered. This constitutive relationship is a function of the principal compressive strain (Fig. 6.5).

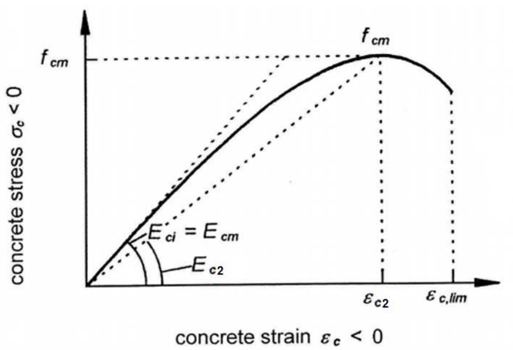

Fig. 6.5-Schematic representation of the uni-axial stress-strain compressive curve for concrete (adapted from fib bulletin 42 [3])

By assuming this compressive law, the effect of fibres on the post-peak toughness in compression is neglected. However, it is assumed to be less important with respect to the evaluation of the shear behaviour, since no compressive shear failure has been observed. The secant modulus, E_{c1} is defined as the slope between the points zero stress and maximum stress f_{cm}.

The compressive stress strain curve shown in Fig. 6.5 is mathematically described by means of the following relationship:

$$\sigma_{c2} = -f_{cm}\left(\frac{k\eta - \eta^2}{1+(k-2)\eta}\right) \quad \text{for} \quad |\varepsilon_c| < |\varepsilon_{c,lim}| \qquad \text{Eq. 6.5}$$

with

$$k = \frac{E_{cm}}{E_{c2}} \qquad \text{Eq. 6.6}$$

$$\eta = \frac{\varepsilon_c}{\varepsilon_{c2}} \qquad \text{Eq. 6.7}$$

In which E_{cm} and E_{c2} are the tangential and secant modulus of elasticity, ε_{c2} is the compressive strain at maximum compressive stress (f_{cm}) and $\varepsilon_{c,lim}$ is the ultimate compressive strain.

By fitting the compressive stress strain curves derived from compression tests on cylinders at the age of 28 days (all individual test result can be found in Appendix B), the values of k and ε_{c2} have been determined for the concrete in this test programme (see Chapter 5, Section 5.2.3). An overview of all values obtained from this curve fitting analysis is given in Table 6.2.

Table 6.2 – Compressive stress-strain curve shape parameters

Girder	f_{cm} [N/mm²]	E_{cm} [N/mm²]	k	ε_{c2} [-10^{-3}]
20A	41.0	31900	1.65	-2.10
20B	64.8	36750	1.50	-2.75
40A	70.4	40150	1.50	-2.60
40B	58.8	35350	1.60	-2.65
20+20	56.2	34950	1.55	-2.65
60	66.5	37700	1.40	-2.60
REF	68.5	37600	1.45	-2.65
REF/TR	57.8	36450	1.50	-2.45
TR	73.2	39850	1.50	-2.80

6.2.2.3 Reinforcement

The mechanical properties of the mild reinforcement steel used for the stirrups, are determined by means of an axial tensile tests on two different bars extracted from the girder [TR]. The stress-strain response of both reinforcement bars is shown in Fig. 6.6 (left). After reaching the maximum tensile stress at a strain of 0.045, a descending branch has been adopted in order to provide numerical stability for large strain deformations (up to 0.15 mm/mm). In order to model the stress-strain relationship of the prestressing strands, a multi-linear stress strain relationship is assumed as shown in Fig. 6.6 (right).

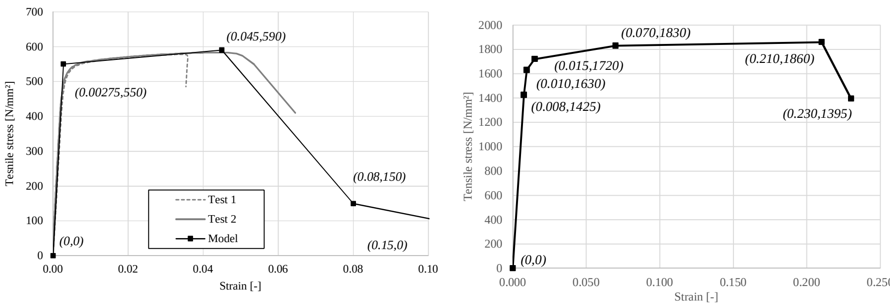

Fig. 6.6 – Adopted stress-strain curve for reinforcement steel (left) and prestressing strands (right)

6.2.3 Layer equilibrium

For every layer, the equilibrium and compatibility conditions according to the Modified Compression Field Theory has to be fulfilled. For each 'sectional' iteration in between incremental shear deformation steps, the longitudinal, vertical and shear strains are known for every layer. The calculation procedure initiates with the calculation of principal tensile strain (ε_1), compressive strain (ε_2) and the inherent inclination of the compression struts (θ). The convention of signs is according to Fig. 6.7:

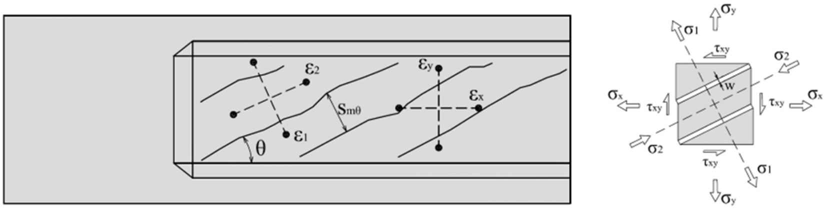

Fig. 6.7 – Definition and conventions of signs for local and principal strains and stresses.

In Fig. 6.7 (right), a cracked element subjected to the in-plane shear and normal stresses is shown. The element contains two cracks width equal crack widths (w), dependent on the principal tensile strain (ε_1) and average crack distance ($s_{m\theta}$).

For plain stress analysis, the strain compatibility equations as derived by Mohr's circle can be obtained [1, 2, 4, 5].

$$\varepsilon_1 = \frac{\varepsilon_x + \varepsilon_y}{2} + \frac{\sqrt{\left(\varepsilon_y - \varepsilon_x\right)^2 + \gamma_{xy}^2}}{2} \qquad \text{Eq. 6.8}$$

$$\varepsilon_2 = \frac{\varepsilon_x + \varepsilon_y}{2} - \frac{\sqrt{\left(\varepsilon_y - \varepsilon_x\right)^2 + \gamma_{xy}^2}}{2} \qquad \text{Eq. 6.9}$$

In which ε_x is the longitudinal strain, ε_y is the transverse strain and γ_{xy} is the shear strain.

To avoid further rotating of the principals stresses after crack formation, the calculation of the inclination angle will only be performed before cracking occurs [6, 7]. Hence, the inclination of the compressive struts is calculated by:

$$\theta = \arctan\left[2\frac{\left(\varepsilon_x - \varepsilon_2\right)}{\gamma_{xy}}\right] \qquad \varepsilon_1 \leq \varepsilon_{cr}$$

Eq. 6.10

$$\theta = \theta_{cr} \qquad \varepsilon_{cr} < \varepsilon_1$$

In which the cracking strain is given by:

$$\varepsilon_{cr} = \frac{f_{ct}}{E_{cm}} \qquad \text{Eq. 6.11}$$

After reaching the tensile strength of concrete, the post-cracking residual tensile strength of SFRC is evaluated as a function of the crack width w. This crack width is calculated as the product of the principal tensile strain ε_1 and the average shear crack spacing $s_{m\theta}$ (see Eq. 6.12 and Eq. 6.13).

$$w = s_{m\theta}\varepsilon_1 \qquad \text{Eq. 6.12}$$

$$s_{m\theta} = \frac{1}{\dfrac{\sin\theta}{s_x} + \dfrac{\cos\theta}{s_y}} \qquad \text{Eq. 6.13}$$

With s_x the distance between horizontally aligned longitudinal reinforcement and s_y the distance between stirrups. In case of absence of stirrups, s_y can be taken equal to the specimen dimensions. For the conducted analysis of the tested girders, the crack spacing values for s_x and s_y are taken equal to the internal lever arm of the cross-section (i.e. 836 mm) and the height of the thin web (i.e. 615 mm) respectively.

When the principal tensile (σ_1) and compressive stresses (σ_2) are known, the local stresses in the layers can be obtained. Therefore, the principal secant stiffness matrix is assembled and then converted to a local secant stiffness matrix. The principal stiffness matrix D_c is given as:

$$[D_c] = \begin{bmatrix} E_{c2} & 0 & 0 \\ 0 & E_{c1} & 0 \\ 0 & 0 & \dfrac{E_{c1}E_{c2}}{E_{c1}+E_{c2}} \end{bmatrix} \qquad \text{Eq. 6.14}$$

The values of E_{c2} and E_{c1} in the stiffness matrix D_c are the secant moduli in compression and tension respectively, given by:

$$E_{c2} = \frac{\sigma_2}{\varepsilon_2} \qquad \text{Eq. 6.15}$$

$$E_{c1} = \frac{\sigma_1}{\varepsilon_1} \qquad \text{Eq. 6.16}$$

In which σ_1 is obtained by means of the tri-linear stress-crack opening law defined in Section 6.2.2.1(Fig. 6.2 and Table 6.1) and σ_2 is obtained by means of the constitutive law defined in Section 6.2.2.2.

Then, the stiffness matrix in the principal axis coordinate system is converted to the local coordinate system using the transformation matrix T:

$$\left[D_{c,loc}\right] = [T]^T [D_c][T] \qquad \text{Eq. 6.17}$$

In which T is given by

$$T = \begin{bmatrix} \cos^2\theta & \sin^2\theta & -\cos\theta\sin\theta \\ \sin^2\theta & \cos^2\theta & \cos\theta\sin\theta \\ 2\cos\theta\sin\theta & -2\cos\theta\sin\theta & \cos^2\theta-\sin^2\theta \end{bmatrix} \qquad \text{Eq. 6.18}$$

With the angle θ, the inclination of the compressive strut according to Eq. 6.10.

For each layer containing either longitudinal or transverse reinforcement, the local stiffness matrix is updated as follows

$$[D_{tot}] = \left[D_{c,loc}\right] + \begin{bmatrix} \rho_l E_s & 0 & 0 \\ 0 & \rho_t E_s & 0 \\ 0 & 0 & 0 \end{bmatrix} \qquad \text{Eq. 6.19}$$

For each layer, the stresses in the local coordinate system can be derived by

$$\begin{bmatrix} \sigma_x \\ \sigma_y \\ \tau_{xy} \end{bmatrix} = \left[D_{tot}\right] \begin{bmatrix} \varepsilon_x \\ \varepsilon_y \\ \gamma_{xy} \end{bmatrix} \qquad \text{Eq. 6.20}$$

The local stresses in both the reinforcement (longitudinal and vertical) and the (fibre reinforced) concrete are obtained by

$$\sigma_{sx} = \varepsilon_x E_s \qquad \text{Eq. 6.21}$$

$$\sigma_{sy} = \varepsilon_y E_s \qquad \text{Eq. 6.22}$$

$$\sigma_{cx} = \sigma_x - \rho_s \sigma_{sx} \qquad \text{Eq. 6.23}$$

One of the assumptions of the sectional analysis implies that no vertical concrete stresses act in the cross section. In order to obtain a stress state in each layer for which the vertical stress component is equal to zero, each time before performing the next iteration step, the vertical strains are updated as follows:

$$\varepsilon_{y,i+1} = \varepsilon_{y,i} - \frac{\sigma_{y,i}}{\left[D_{tot,i}\right]_{22}} \qquad \text{Eq. 6.24}$$

With $[D_{tot,i}]_{22}$ the element of the total local stiffness matrix located at the second row and second column.

6.2.4 Section equilibrium

At the beginning of each incremental deformation step, the deformation of the cross section is defined in terms of average longitudinal strain $\overline{\varepsilon}$, curvature χ and average shear strain $\overline{\gamma}$ (see Eq. 6.25).

$$[U]=\begin{bmatrix}\bar{\varepsilon}\\ \chi\\ \bar{\gamma}\end{bmatrix} \qquad \text{Eq. 6.25}$$

The value of average strain and curvature of the cross-section defines the strain at each layer by

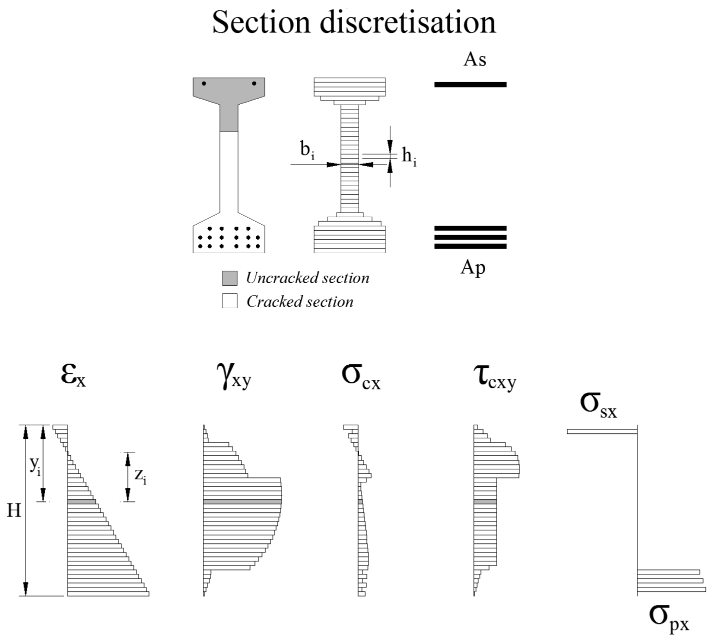

Fig. 6.8 – Schematic of the layer discretisation of the cross-section and inherent strain and stress profiles.

$$\varepsilon_{x,i}=\bar{\varepsilon}-\chi\left[\frac{H}{2}-y_i\right] \qquad \text{Eq. 6.26}$$

The stresses in the section are obtained per layer element as explained in Section 6.2.3. By summing the stress resultant for every layer of the cross-section, the normal force is obtained as follows:

$$N=\sum_{i=1}^{n}\sigma_{cx,i}h_i b_i + A_s\sigma_{sx} + A_p\sigma_{px} \qquad \text{Eq. 6.27}$$

In which tensile and compressive stresses are taken positive and negative respectively. The internal bending moment and shear load are given by Eq. 6.28 and Eq. 6.29 respectively.

$$M = \sum_{i=1}^{n} z_i \sigma_{cx,i} h_i b_i + z_i A_s \sigma_{sx} + z_i A_p \sigma_{px} \qquad \text{Eq. 6.28}$$

$$V = \sum_{i=1}^{n} \tau_{cxy,i} h_i b_i \qquad \text{Eq. 6.29}$$

Equilibrium is obtained when the internal forces resultants N, M and V in the cross-section equals the external forces. Hence, for a prestressed cross-section subjected to both a shear and bending load, N equals zero (tensile stresses in the prestress strands are in equilibrium with the compressive stresses in the concrete) and M has to be equal to the external moment taken as the shear load V multiplied with the distance from the analysed cross-section to the nearest support. According to Bentz [8], the cross-section that has to be taken into consideration to evaluate the shear strength is situated at a distance d from the loading point (see Fig. 6.9).

In order to reach equilibrium of sectional forces, the assumed longitudinal strain distribution ($\bar{\varepsilon},\chi$; Eq. 6.27) has to be updated in the iterative process. This is done by means of the linear elastic axial and bending stiffness of the cross-section as follows:

$$\bar{\varepsilon}_{i+1} = \bar{\varepsilon}_i + \frac{N_{ext} - N_{int}}{A_c E_c} \qquad \text{Eq. 6.30}$$

$$\chi_{i+1} = \chi_i + \frac{Va - M_{int}}{E_c I_c} \qquad \text{Eq. 6.31}$$

For the update of the shear strain distribution over the cross-section depth, the method as described by Vecchio [2] is adopted. Basically, the rate of change of longitudinal stresses between two sections defines the shear stress acting on the considered layer (see Fig. 6.9).

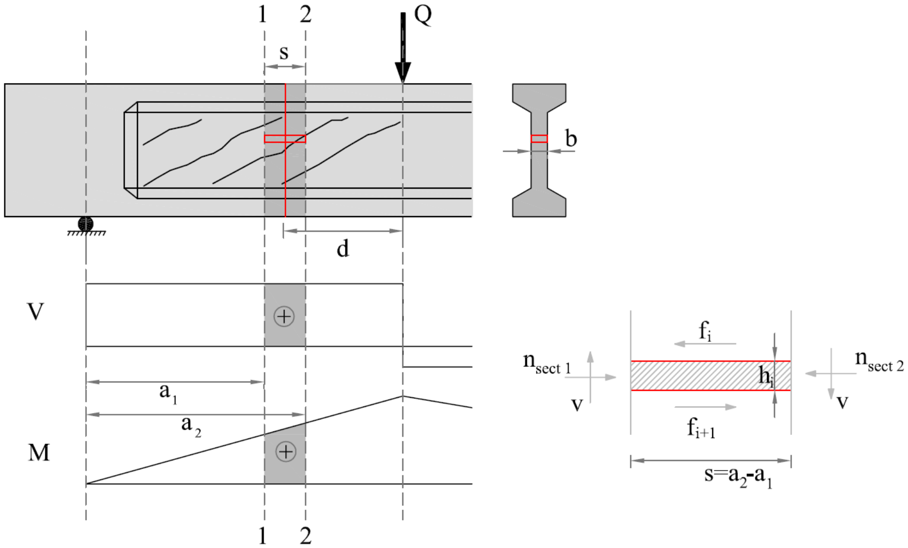

Fig. 6.9 – Shear and moment at the analysed section (left) and the free body diagram (right) for the dual section analysis.

Considering two sections, located on a fixed distance s from each other, the normal force Eq. 6.32 acting on a layer at the left section and the right section are in equilibrium when a given horizontal shear component f_i is acting in between the layers (Eq. 6.33).

$$n = \sigma_{cx,i} h_i b_i + A_s \sigma_s + A_p \sigma_{sp} \qquad \text{Eq. 6.32}$$

$$f_{i+1} = f_i + n_{sect2} - n_{sect1} \qquad \text{Eq. 6.33}$$

Based on the reciprocity principal of shear stresses, rotational equilibrium of the free body diagram (Fig. 6.9, right) yields the expression to calculate the shear force v_i.

$$v_i s = \frac{f_i + f_{i+1}}{2} h_i \qquad \text{Eq. 6.34}$$

From which the updated shear stresses can be computed as

$$\tau_{cxy,i} = \frac{v_i}{b_i h_i} \qquad \text{Eq. 6.35}$$

The derived updated shear stress profile is then compared with the initially assumed profile and when the error is too large, the derived updated shear stress profile is then assumed for the next iteration step.

For each load step, the calculation converges when the iteratively updated strain profile (ε_x) and shear strain profile (γ_{xy}) result in (1) internal forces (Eq. 6.27 till Eq. 6.29) which match those corresponding with the acting loads, and (2) the shear stress profile as derived by Eq. 6.20 which matches the shear stress profile as derived by Eq. 6.35.

6.3 Model validation

6.3.1 General description of the model output

Fig. 6.10, shows a typical shear force-strain behaviour obtained by the model. In general, five key points can be defined which characterise the entire analytically obtained shear behaviour of the prestressed SFRC girders. By monotonically increasing the shear strain, the first phase consist of a linear elastic increase (A) of the shear load until first cracking occurs (B). At this point, a first layer of the thin web will be cracked and the sectional stiffness reduces further upon more layers reaching a principal tensile stress in excess of the tensile strength of concrete (taking into account the biaxial stress state). The softening phase of the girder section is maintained until cracks have been formed over the entire height of the web (C).

After the formation of cracks for all of the web layers the shear load increases further thanks to the fibres acting. Hereby, the post-cracking tensile stress reaches a peak for a crack width value about equal to w_2 in the tri-linear constitutive law (see Table 6.1). At this point (D), the post-cracking shear curve tends to flatten because the secant stiffness E_{c1} for each layer will decrease as a function of increasing shear strain (and inherent principal tensile strain). Finally, the ultimate shear strength is reached (E) for a given deformation state of the analysed section. After point (E), the increase of shear deformation will cause an average decrease of shear stresses in the considered section and a residual branch is observed. The calculation procedure is then stopped to avoid excessive deformations.

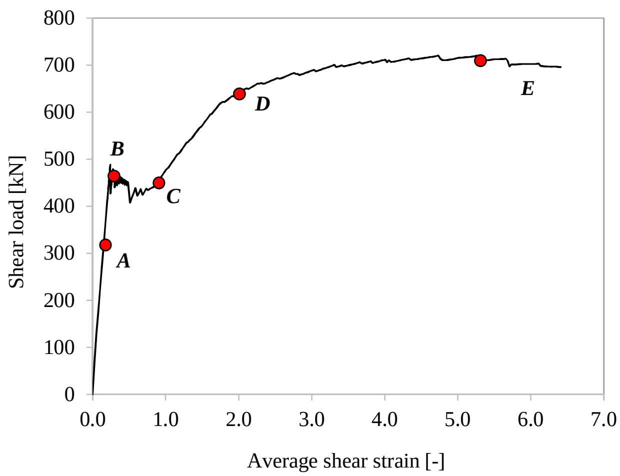

Fig. 6.10 – General output of the sectional model with indication of key points A-E

In order to get more insight into the complete shear behaviour of a given section of a SFRC girder, subjected to the combined effects of prestress, curvature and shear deformation, reference is made to Fig. 6.11 till Fig. 6.13 (this calculation corresponds with a prestressed girder with geometrical properties similar to the girders studied in Chapter 5 and with arbitrarily chosen material parameters). These figures show the evolution of shear strains and stresses, crack width, orientation angle, and principal compressive and tensile stresses; and are shown with respect to the 5 key points as defined in Fig. 6.10.

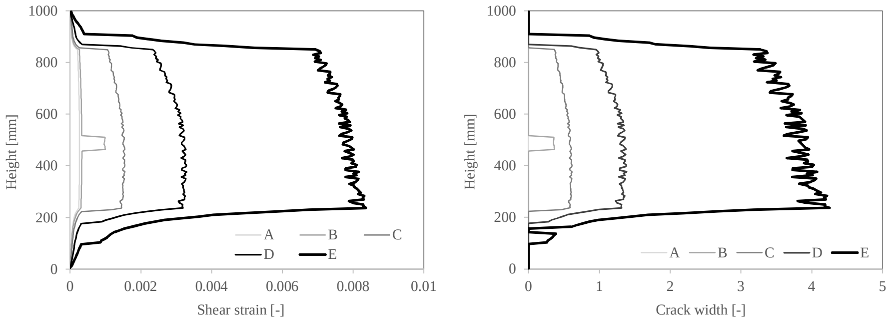

Fig. 6.11 – Evolution of shear strain (left) and crack width (right).

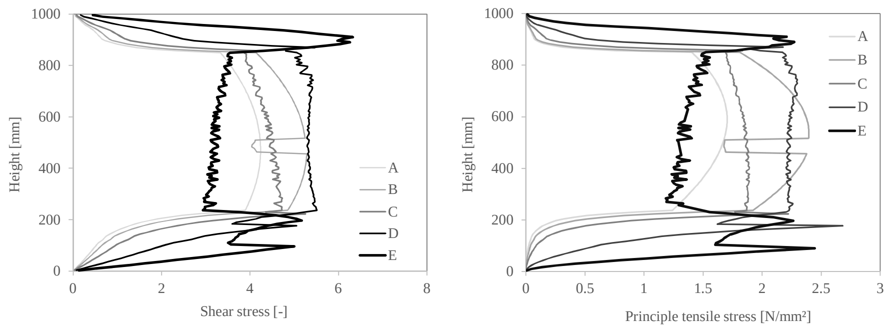

Fig. 6.12 – Evolution of shear stresses (left) and principal tensile stresses (right).

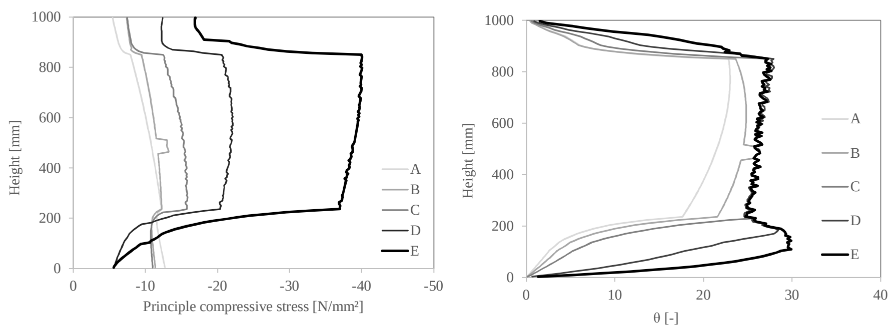

Fig. 6.13 – Evolution of principal compressive (left) and orientation angle of principal stresses (right).

In general, the evolution of the shear strain profile is very similar to the evolution of the crack width. Hence, the crack width is a multiple of the principal tensile strain which is directly influenced by the acting shear strain. As a consequence, for I-shaped girders, the sectional analysis tool can be used to understand how the section fails and how cracks propagate for increasing shear deformation. By means of the model, both the crack opening as well as the crack orientation can be modelled.

In Fig. 6.12 (right), it can be seen that the principal tensile stresses increase between points B and D, and that for higher crack openings, the post-cracking tensile strength is decreasing. When the stiffness of the web is reduced significantly at higher crack widths, the shear stresses developed in the thin web are decreasing and the shear stresses in the upper and lower flanges are further increasing. At the top and bottom flanges, the same is observed in terms of the principal tensile stresses, yet these remain relatively low in contrast with the principal compressive stresses. Due to the presence of the wider flanges with relatively high shear and compression stresses, the cross-section can build up residual shear capacity after excessive cracking of the web until ultimate failure is reached.

As a concluding remark, it has to be emphasised that the cross-sectional analysis method is most suitable to analyse a beam-type shear failure rather than an arch-type shear failure. Therefore, it can be expected that the shear strength of girders will be underestimated for lower values of shear span to depth ratio and more accurate predictions will be obtained for higher values of a/d.

6.3.2 Influence of crack spacing

The link between the principal tensile strains and the corresponding crack opening is the crack spacing. Hence, an incorrect implementation of the crack spacing can lead to a different post-cracking shear behaviour of the cross-section. This can be considered as the main drawback in the use of the MCFT cross-sectional model.

In order to verify the influence of the crack spacing $s_{m\theta}$ (s_x, s_y, θ) on the shear behaviour, four different combinations of the distances s_x and s_y (Eq. 6.13) have been chosen arbitrarily to run different analyses. The following combinations are being investigated (compared to the original analysis, with distances s_x = 836 mm and s_y = 615 mm):

- 200 mm by 200 mm
- 200 mm by 2000 mm
- 2000 mm by 200 mm
- 2000 mm by 2000 mm

A comparison between all obtained shear responses is shown in Fig. 6.14 (this calculation corresponds with girder 40A).

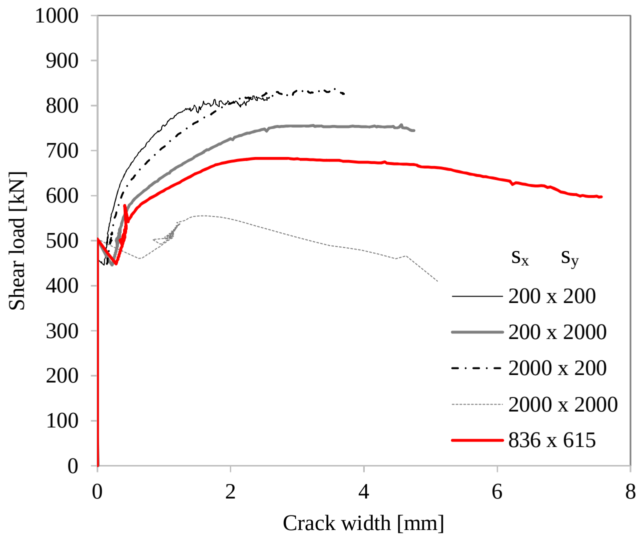

Fig. 6.14 – Influence of crack spacing (s_x and s_y) on the modelled post cracking shear behaviour of prestressed SFRC girder 40A (test 2.5-2).

The stiffest response is obtained for an assumed crack spacing of 200 mm by 200 mm (more yet finer cracks). A large reduction of residual shear strength is observed for a crack spacing equal to 2000 mm by 2000 mm (larger cracks). From Fig. 6.14, it can be further observed that the shear response is most influenced when both distances s_x and s_y are increased simultaneously. When only one of both is increased while the other is maintained constant, only a limited reduction in the post-cracking capacity is observed. On overall, the sensitivity of the model with respect to the predicted crack spacing remains acceptable. The assumed approach to estimate the crack spacing gives more or less accurate predictions of the crack width, as illustrated in the next section.

6.3.3 Crack opening behaviour

For the conducted shear tests, the crack opening behaviour has been measured by means of either the DIC technique (see Chapter 4) or by means of the grid of extensometers (see Appendix C). Since the sectional shear behaviour model can be used to calculate the relationship between applied shear load and corresponding average crack width (see Fig. 6.15 till Fig. 6.22), the experimentally observed shear behaviour is compared with respect to the modelled post-cracking shear behaviour. The experimental curves in Fig. 6.15 till Fig. 6.22 are taken as follows: for the shear crack opening curves obtained by the DIC-technique the black-grey lines represent the individual crack propagation behaviour of the critical shear cracks, denoted in the legend by crack 1, crack 2, etc. In case of tests on girders for which the crack propagation is evaluated by means of a grid of extensometers, the applied shear load is plotted against the extensometer elongation (in the legend of the figure, the extensometer number is given). When multiple cracks pass through the measurement range of the extensometer, the represented crack openings are cumulated and hence, these curves are less accurate than those obtained by means of the DIC-technique.

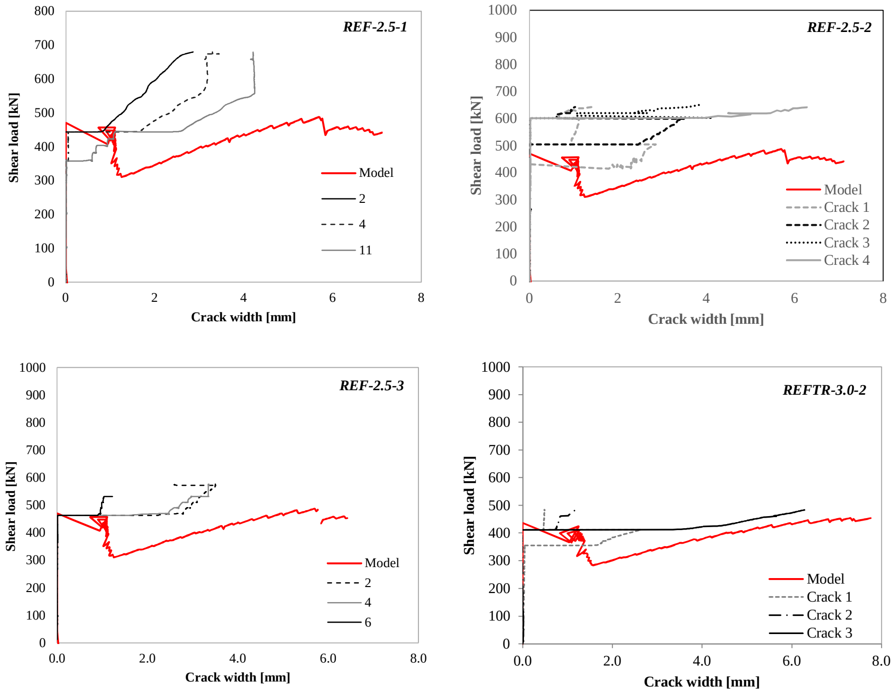

Fig. 6.15 – Comparison between experimentally obtained and modelled shear load –crack opening behaviour for the girders without shear reinforcement.

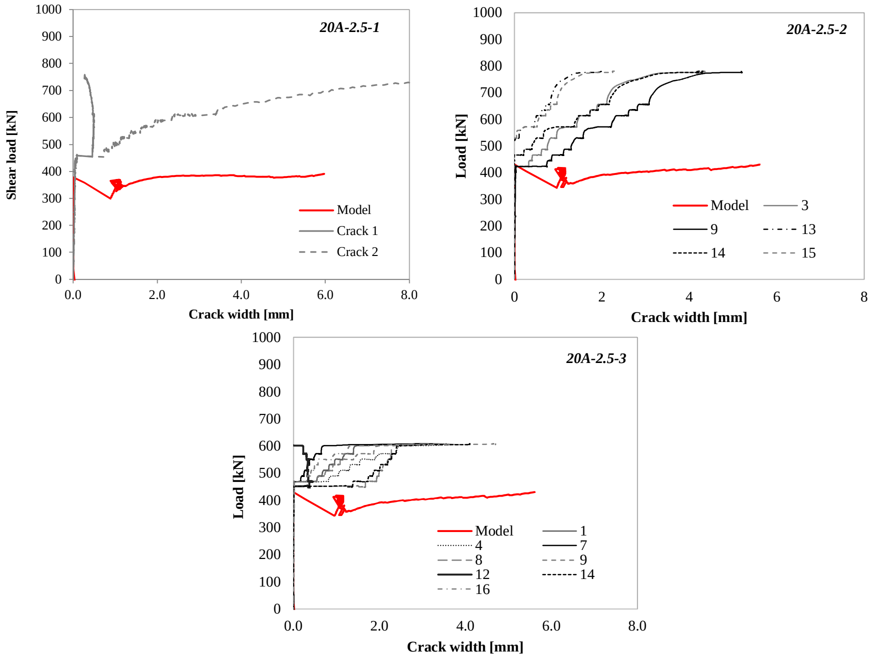

Fig. 6.16 – Comparison between experimentally obtained and modelled shear load –crack opening behaviour for the girder [20A]

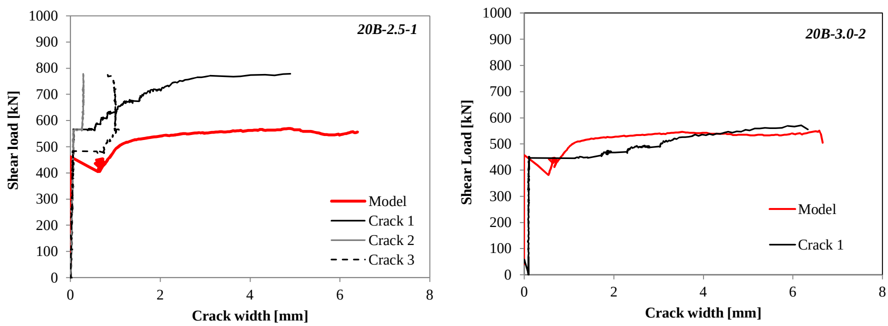

Fig. 6.17 – Comparison between experimentally obtained and modelled shear load –crack opening behaviour for the girder [20B]

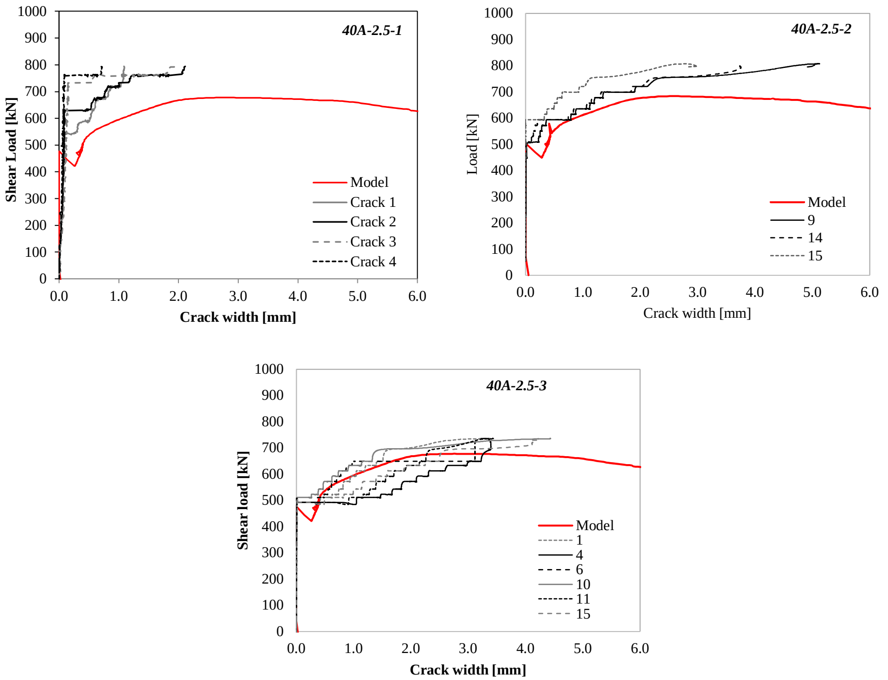

Fig. 6.18 – Comparison between experimentally obtained and modelled shear load –crack opening behaviour for the girder [40A]

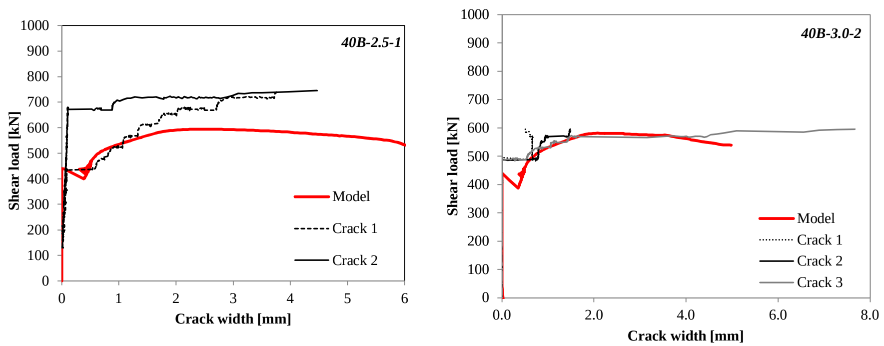

Fig. 6.19 – Comparison between experimentally obtained and modelled shear load –crack opening behaviour for the girder [40B]

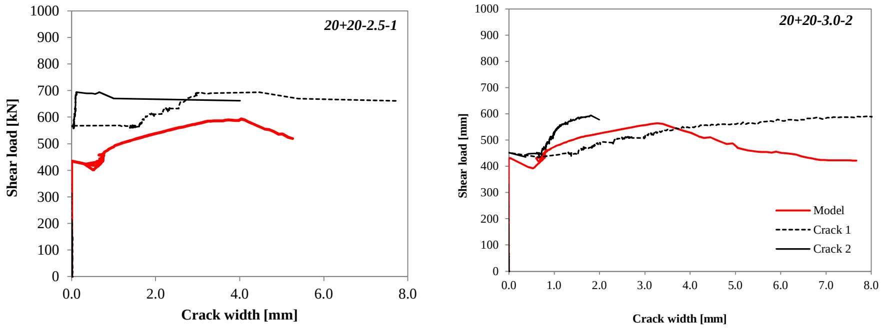

Fig. 6.20 – Comparison between experimentally obtained and modelled shear load –crack opening behaviour for the girder [20+20]

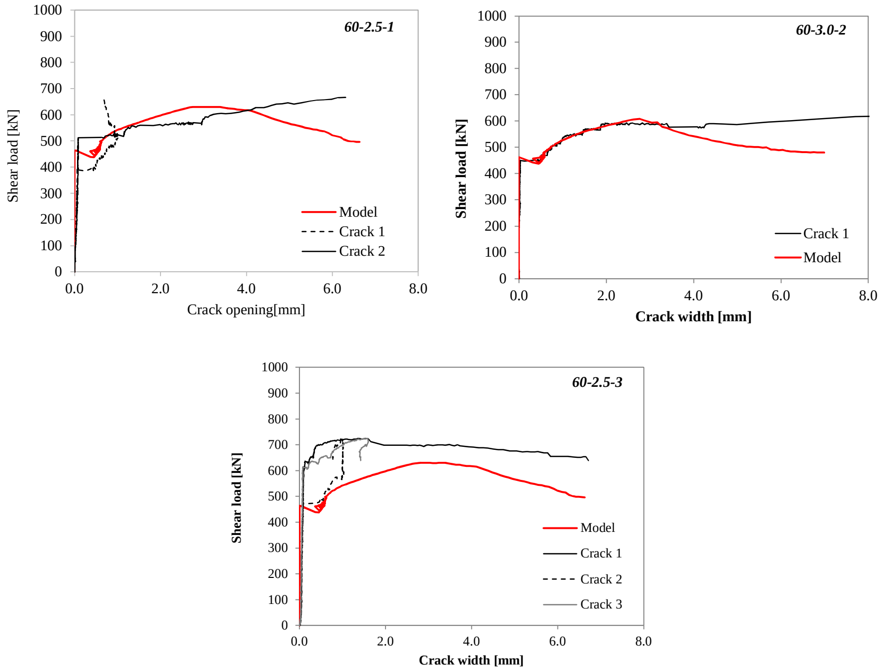

Fig. 6.21 – Comparison between experimentally obtained and modelled shear load –crack opening behaviour for the girder [60]

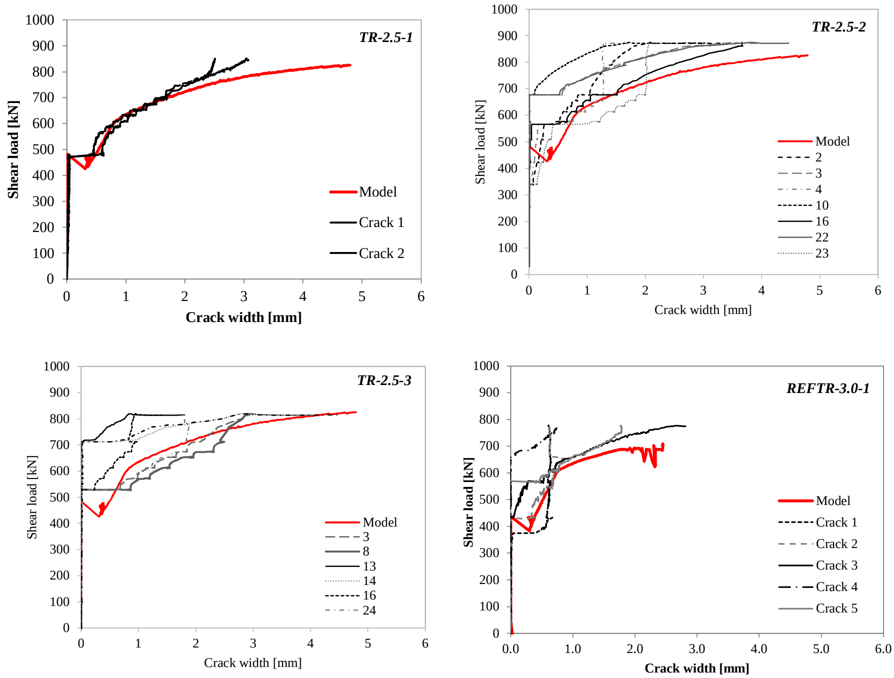

Fig. 6.22 – Comparison between experimentally obtained and modelled shear load –crack opening behaviour for the girders with traditional stirrups

As can be seen from the comparison between modelled and experimentally observed shear crack opening behaviour, the developed model is underestimating the shear strength shear strength for the girders tested with an a/d ratio equal to 2.5. For the tests conducted with an a/d ratio equal to 3.0, the sectional analysis tool provides better predictions. This observation can be explained by the increase of the shear strength due to arch action, which will have more influence on the observed shear capacities at a/d = 2.5 compared to a/d = 3.0 (see Section 6.1).

6.3.4 Shear strength prediction

Fig. 6.23, shows the parity between the experimentally obtained and calculated shear strength. In addition to the comparison between the maximum shear loads, another comparison is made for the shear strengths obtained at a critical shear crack opening equal to 2.5 mm.

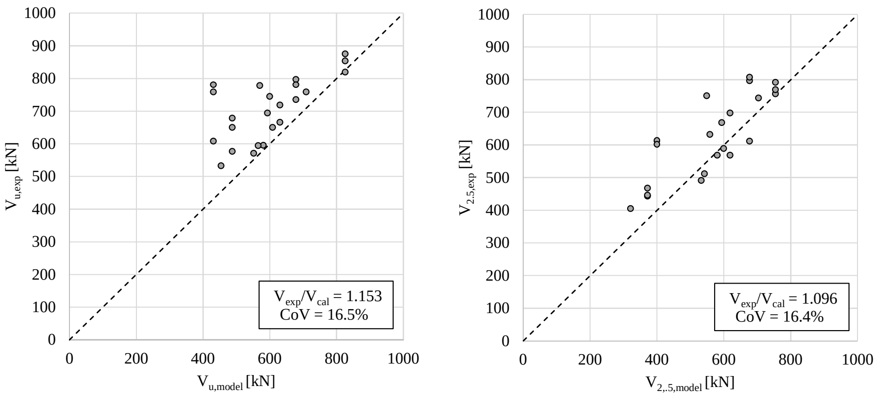

Fig. 6.23 – Parity diagram for experimental and modelled ultimate shear load (left) and shear load at a crack opening equal to 2.5 mm (right).

As can be seen from Fig. 6.23, the sectional model is yielding a conservative prediction of the maximum shear strength. When considering the shear capacity at a crack opening of 2.5 mm, the model is more accurate and less conservative. This reveals again that the model is unable to reflect the experimentally observed additional capacity due to a degree of direct load transfer.

The influence of residual stress f_{R3} on the shear capacity at 2.5 mm crack opening is shown in Fig. 6.24. It can be observed that for the girders with traditional shear reinforcement, a good prediction has been made with the sectional model and for girders made of SFRC with f_{Ftu}-values higher than 2 N/mm². For girders with relatively low values of f_{Ftu} (i.e. lower than 2 N/mm² and plain concrete), the shear capacity has been systematically underestimated.

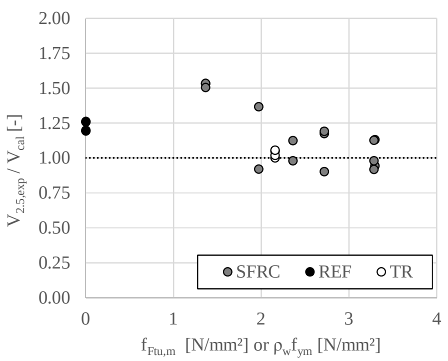

Fig. 6.24 –$V_{2.5,exp}/V_{cal}$ as a function of f_{Ftum} (SFRC and REF) or $\rho_w f_{ym}$ (TR).

6.4 Conclusions

Based on the equilibrium and compatibility equations from the modified compression field theory, a sectional model to analyse the shear response of a prestressed fibre reinforced concrete cross-section has been developed. Thereby, existing sectional modelling tools are taken as the basis for further development by including the post-cracking tensile strength of SFRC through a tri-linear constitutive law as proposed in Chapter 4.

In order to understand possible modelling errors because of the assumption of a simplified tri-linear constitutive relationship for SFRC, the modelled stress-CMOD curves have been verified with respect to the average experimentally obtained three-point bending test results (SFRC quality control tests on standard prisms). In general, it can be concluded that the adopted tri-linear post-cracking tensile law for SFRC is yielding a modelling error of less than 10 % over the CMOD range up to 4 mm. The modelling error due to the adopted compressive stress-strain law implemented is kept minimal by curve fitting the experimental cylinder compressive test results.

This analysis tool is used to obtain the relationship between general deformations in terms of shear strain, curvature and crack width propagation with respect to the applied shear load. The model output is compared with the experimental results in terms of both shear crack opening behaviour and shear capacity. An accurate yet somewhat underestimating prediction of the maximum shear capacity is obtained, with an average ratio between V_{exp} and V_{cal} of 1.153 and a CoV equal to 16.5%. Looking to the shear strength at a critical shear crack opening equal to 2.5mm ($V_{2.5,exp}$), the model strength prediction is slightly more accurate with an average ratio of $V_{2.5,exp}/V_{cal}$ equal to 1.096 and a CoV of 16.4%.

It is emphasised that the modelling of the shear behaviour of SFRC elements is sensitive to the assumed average crack spacing. The assumption of to low crack spacing will lead to an overestimation of the shear capacity, while for very high crack spacing, the crack widths are higher for comparable levels of strain. Consequently, the stiffness reduction will be much higher and the obtained shear capacity will be lower. Further research evidence is needed in order to predict the correct crack spacing. To avoid unsafe shear strength prediction however, the adoption of maximum crack spacing as a function of member size yields satisfactory shear strength predictions.

6.5 References

[1] Vecchio, F. J., Collins, M. P. (1986). "The Modified Compression-Field Theory for Reinforced Concrete Elements Subjected to Shear". *ACI Journal*, Vol. 83(22), pp. 219-231.

[2] Vecchio, F. J., Collins, M. P. (1988). "Predicting the Response of Reinforced Concrete Beams Subjected to Shear Using Modified Compression Field Theory". *ACI Structural Journal*, Vol. 85(3), pp. 258-268.

[3] fib. (2008). "Bulletin No. 42: Constitutive modelling of high strength / high performance concrete (HSC/HPC)". Lausanne, Switzerland.

[4] Bentz, E. C., Vecchio, F. J., Collins, M. P. (2006). "Simplified Modified Compression Field Theory for Calculating Shear Strength of Reinforced Concrete Elements". *ACI Structural Journal*, Vol. 103(4), pp. 614-624.

[5] Minelli, F., Vecchio, D. J. (2006). "Compression Field Modeling of Fiber-Reinforced Concrete Members Under Shear Loading". *ACI Structural Journal*, Vol. 103(2), pp. 244-252.

[6] Vecchio, F. J. (2001). "Disturbed Stress Field Moel for Reinforced Concrete: Implementation". *Journal of Structural Engineering (ASCE)*, Vol. 127(1), pp. 12-20.

[7] Vecchio, F. J. (2000). "Disturbed Stress Field Model for Reinforced Concrete: Formulation". *Journal of Structural Engineering (ASCE)*, Vol. 126(9), pp. 1070-1077.

[8] Bentz, E. C. (2000). "*Sectional Analysis of Reinforced Concrete Members*" (PhD-thesis), University of Toronto, Department of Civil Engineering.

7 SHEAR STRENGTH DESIGN MODELS

7.1 Introduction

Recent developments and ongoing research in the field of fibre reinforced concrete (FRC) have led to the implementation of FRC into national and international design codes and guidelines [1-3], as discussed in Chapter 3. Since fibres are promising as an alternative for (minimum) shear reinforcement [4-9], special attention is given towards new shear design provisions for FRC elements. Although these design models are available and validated with respect to research results, the application of fibres as shear reinforcement for both reinforced (RC) and prestressed concrete (PC) beams is rather limited in daily practice. This may be due to a lack of:

- Experience in the engineering community with respect to these design guidelines, also given the fact that they have been verified based on specific experimental data sets which are not always representative for real scale elements.

- Knowledge on the model uncertainty, making these design guidelines less well defined in terms of proper safety factors.

Based on a thorough literature survey (Chapter 4), the most important shear design models available for SFRC elements are evaluated in this chapter, with respect to the obtained test results from the full scale shear tests (Chapter 5) and test results reported in literature. The considered shear design equations [1, 2, 6] are selected in such way that they can deal with the presence of a prestressing force and that the effect of fibres can be taken into account by means of strength parameters obtained from standardised tests on the FRC composite.

In addition to the existing shear strength equations, an alternative shear strength equation for prestressed SFRC elements is proposed. This new engineering model is a derivation of the developed detailed analytical procedure given in Chapter 6, and takes into account the effect of broadly accepted shear influencing parameters such as size effect, reinforcement ratio, prestress, shear-span-to-depth ratio, concrete strength and effect of fibres. The proposed engineering model is formulated in a way that it is feasible to implement into daily practice of design engineers.

The considered shear design equations are presented in the following and their theoretical or empirical background is shortly discussed. Furthermore, the accuracy of the models is verified against a shear test database containing test results of 99 FRC elements (69 RC and 30 PC). The shear test database is assembled taking into account specific selection criteria and relevance towards the intended assessment of the design models (i.e. detailed information should be available of the post-cracking strength of the FRC). To allow the comparison with shear test data, the design equations are converted into shear strength equations by taking all partial safety factors equal to unity, and by considering mean values of the material properties

Based on the obtained insights on the accuracy of the shear resistance models, model safety factors are evaluated by means of a Monte Carlo method [10] taking into account the scatter of concrete compressive strength and post-cracking capacity of FRC. In order to evaluate the predictive capacity of the models and inherent safety levels, a distinction is made between reinforced and prestressed members. Based on the obtained model uncertainties and scatter of base variables the existing safety margins as currently provided in design codes and guidelines are discussed.

7.2 Shear strength models

The shear strength models that are evaluated in this chapter must satisfy the following requirements:

- The influence of fibre reinforcement has to be taken into account based on the residual flexural parameters $f_{R,i}$ (Chapter 2, Eq. 2.8), determined by means of a standardized test method [11]. Shear strength models based on a fibre volume fraction and a fibre effectiveness are only considered to be valid in specific cases and hence, not widely applicable for design purposes.
- The beneficial effect of a prestress force should be consistently taken into account.

In this study, four existing shear strength models are withhold: (1) the RILEM TC 162 model, (2) the fib MC2010 adapted shear model for reinforced concrete without stirrups, (3) the fib MC2010 iterative model based on the MCFT, and (4) the iterative model based on plasticity theory. These formulations are briefly discussed in the following sections, in terms of resistance models (all partial safety factors are set equal to unity and average values are used instead of characteristic ones) In addition, a new engineering resistance model is proposed.

7.2.1 RILEM TC 162-TDF

The RILEM model considers a separate term for the shear capacity of the fibres (see Chapter 3, Section 3.2.3.2), in addition to the contribution of plain concrete and prestressing. A further extension of the design model was done, based on available information in literature [12, 13], in order to be able to deal with a variation of shear span to depth ratio. The shear strength model V_{RILEM} is given as follows:

$$V_{RILEM} = \left[0.18\sqrt[3]{3\frac{d}{a}}k\left[\left(100\rho_l f_{cm}\right)^{1/3}\right] + 0.15\sigma_{cp} + 0.5\frac{d}{a}k_f k f_{Rm,4}\right]b_w d \qquad \text{Eq. 7.1}$$

with definition of symbols as provided in Section 3.2.3, and with the SFRC being characterized by the post-cracking tensile strength $f_{Rm,4}$ at a CMOD of 3.5 mm.

7.2.2 Model Code 2010 - A

More recently, Model Code 2010 [1] proposed two fundamentally different design approaches. The first model (denoted as MC2010-A) is mainly an adaptation of the shear design equation for plain concrete. It is assumed [5, 14] that fibres enhance the aggregate interlock mechanism and hence, the beneficial effects of fibres is taken into account by increasing the longitudinal reinforcement ratio with a factor that includes the post-cracking tensile strength of fibre reinforced concrete.

$$V_{MC2010,A} = \left(0.18\cdot\sqrt[3]{3\frac{d}{a}}\cdot k\cdot\left[100\cdot\rho_l\left(1+7.5\cdot\frac{f_{Ftum}}{f_{ctm}}\right)\cdot f_{cm}\right]^{1/3} + 0.15\cdot\sigma_{cp}\right)\cdot b_w\cdot d \qquad \text{Eq. 7.2}$$

with definition of symbols as provided in Section 3.1.5, and with the SFRC being characterized by the post-cracking tensile strength $f_{R,3m}$ at a CMOD of 2.5 mm (whereby $f_{Ftum} = f_{R,3m}/3$).

7.2.3 Model Code 2010 - B

The second design approach is presented in the MC2010 commentary section. The model is based on shear design provisions for concrete members considering the calculation procedure for a Level III of Approximation (LoAIII) [1]. This procedure, based on the formulations of the Modified Compression Field Theory (MCFT) [1, 15, 16] is discussed in more detail in Chapter 2.

The shear strength is calculated as follows:

$$V_{MC2010-B} = \left(k_v \sqrt{f_{cm}} + f_{Ftum} \cot\theta\right) b_w z \qquad \text{Eq. 7.3}$$

The first term between the brackets is counting for the concrete contribution as a result of aggregate interlocking in which the strain effect factor k_v [16] is given by:

$$k_v = \frac{0.4}{1+1500\varepsilon_x} \frac{1300}{1000+s_{xe}} \qquad \text{Eq. 7.4}$$

with

$$s_{xe} = \frac{35 s_x}{a_g + 16} \qquad \text{Eq. 7.5}$$

As suggested in [16], s_x is taken equal to the distance between horizontally aligned reinforcement. As the assembled shear database does not contain beams with horizontal reinforcement at mid-depth, Eq. 7.5 can be rewritten as

$$s_{xe} = 0.9d\left(\frac{35}{a_g + 16}\right) \qquad \text{Eq. 7.6}$$

In Eq. 7.6, the aggregate size a_g is representative for the roughness of cracks and their capacity to transmit shear stresses. However, when the concrete compressive strength class is higher than C50/60, cracks will rather go through the aggregates than around them [17]. Therefore, the value of a_g is taken equal to 0 when f_{cm} is higher than 58 N/mm².

The inclination of the compression strut is calculated by means of Eq. 7.7.

$$\theta = \left(29^\circ + 7000\varepsilon_x\right)\left(0.88 + \frac{s_{xe}}{2500}\right) \qquad \text{Eq. 7.7}$$

Both Eq. 7.6 and Eq. 7.7 require the strain at the cross-section mid-depth ε_x to be known. This strain can be estimated by taking half of the strain at the cross-section bottom [1, 18].

$$\varepsilon_x = \frac{\frac{M}{z} + 0.5\cot\theta \cdot V_{MC2010-B} - \eta\left(A_{p,bot} + A_{p,top}\right) f_{p0}}{2\left(E_s A_s + E_p\left(A_{p,bot} + A_{p,top}\right)\right)} \quad \text{Eq. 7.8}$$

with M the flexural moment in the middle of the shear span, a the length of the shear span, η the ratio of prestress losses, f_{p0} the initial prestress in the prestress strands, A_{bot} the section of the lower reinforcement and A_{top} the upper reinforcement, E the modulus of elasticity, whereby the indices s, p and c stand for steel, prestress strand and concrete, respectively. Since the value of ε_x depends on the maximum shear force $V_{MC2010\text{-}B}$, the set of equations Eq. 7.5 to Eq. 7.8 is solved iteratively.

If a compressive force is acting on the fibre at mid-depth of the section (when $\varepsilon_x < 0$), the additional stiffness of the uncracked concrete section A_{ct} will be taken into account. The strain ε_x is then calculated as follows:

$$\varepsilon_x = \frac{\frac{M}{d} + 0.5\cot\theta \cdot V_{MC2010-B} - \eta\left(A_{p,inf} + A_{p,sup}\right) f_{p0}}{2\left(E_s A_s + E_p\left(A_{p,inf} + A_{p,sup}\right) + E_c A_{ct}\right)} \quad \text{Eq. 7.9}$$

With A_{ct} the area of uncracked concrete, which can be taken as $A_c/2$.

7.2.4 Plasticity model

The plasticity model is typically an upper bound estimation of the resistance, considering large deformations in a critical shear crack. The approach is discussed in Section 3.2.3.1. Based on [19, 20], V_{PLM} is given as follows:

$$V_{PLM} = \frac{1}{2} f_t^* b \frac{h^2 + x^2}{a} + \frac{\sum \eta P_0 d}{a} = \frac{1}{2} f_c^* bh \left(\sqrt{1 + \left(\frac{x}{h}\right)^2} - \frac{x}{h}\right) \quad \text{Eq. 7.10}$$

with definition of symbols as provided in Section 3.2.3.1, and with the SFRC being characterized by the post-cracking tensile strength $f_{Rm,3}$ at a CMOD of 2.5 mm (whereby $f_{Ftum} = f_{Rm,3}/3$).

7.2.5 Proposed shear strength model

Although the strength models based on the MCFT (Section 7.2.3) or the plasticity theory (Section 7.2.4) provide a more rational approach to the problem of shear, these models are considered to be more difficult to be implemented in the daily practice of design engineers. In order to overcome the iterative solution procedure, an easy to use alternative model has been developed which provide a more simplified yet safe shear design of FRC elements. By means of a thorough literature investigation, a detailed analysis of existing design models, and the analytical approach described in Chapter 6, the most important shear influencing parameters are used to propose a new shear capacity model which can deal with both reinforced and prestressed concrete elements.

The formulation of the new shear strength model will be based on both physical approaches and empirically evidenced assumptions. In its general form the proposed engineering model can be written as:

$$V_{PROPOSED} = \left(A\sqrt{f_{cm}} + Bf_{Ftum}\right)b_w z \qquad \text{Eq. 7.11}$$

In which the first term will be the concrete contribution and the second term is representing the contribution of fibre reinforcement. As a consequence, Eq. 7.11is basically similar to the model as proposed by MC2010 based on the MCFT. The function A will be dependent on parameters deterministic for the concrete contribution: the effective depth of the beam d, the longitudinal reinforcement ratio ρ_l (cf. dowel action), the shear-span-to-depth ratio a/d, the compressive stress σ_{cp} due to prestressing and an overall correlation factor C. The function B is representative for the fibre contribution and is taken in relation to the inclination of the compressive strut θ and a fibre effectiveness factor α_{red}.

$$A = C \cdot f\left(a, d, \rho_l, \sigma_{cp}\right) \qquad \text{Eq. 7.12}$$

$$B = f\left(\theta, \alpha_{red}\right) \qquad \text{Eq. 7.13}$$

Hereby the above mentioned parameters to determine A and B, are considered as follows.

- Shear span to depth ratio

To take into account the increase of shear strength for lower values of a/d due to the arch effect [21], the following factor will be taken into account:

$$f\left(\frac{a}{d}\right) = \left(3\frac{d}{a}\right)^{\frac{1}{3}} \qquad \text{Eq. 7.14}$$

- Size effect

A size effect factor will be taken into account by means of the empirical factor as included in the current Eurocode 2:

$$f\left(d\right) = 1 + \sqrt{\frac{200}{d}} \qquad \text{Eq. 7.15}$$

- Dowel action

The contribution of dowel action is directly related to the longitudinal reinforcement ratio. Based on earlier research by Zsutty [22] and Kordina [23], the shear strength of beams without web reinforcement is correlated to the longitudinal reinforcement ratio with a factor given by Eq. 7.16:

$$f\left(\rho_l\right)=\left(\rho_l\right)^{\frac{1}{3}} \qquad \text{Eq. 7.16}$$

- Prestress

Prestressing results in increased shear capacity due to increased shear cracking load and longer horizontal projection length of the critical shear crack. To avoid excessive conservatism when determining the shear strength of prestressed elements, these beneficial effects of the prestressing should be dually considered. Considering a Mohr's circle [24], the influence of the prestressing on the cracking shear strength is taken into account by Eq. 7.17.

$$f\left(\sigma_{cp}\right)=\sqrt{1+\left(\frac{\sigma_{cp}}{f_{ctk}}\right)} \qquad \text{Eq. 7.17}$$

Secondly, the inclination of the shear crack is calculated by:

$$\cot\theta=1+4\left(\frac{\sigma_{cp}}{f_{ck}}\right) \qquad \text{Eq. 7.18}$$

Given the above parameters (Eq. 7.14 till Eq. 7.18), the functions A (concrete contribution) en B (fibre contribution) can be obtained as follows.

The concrete contribution to the shear capacity, basically given by aggregate interlocking, can be related to a strain effect factor k_v (Eq. 6.5). This factor k_v as determined by the iterative MCFT based procedure described in Section 7.2.3, appears to correlate in a linear way with the product of the above mentioned parameters:

$$f\left(a,d,\rho_l,\sigma_{cp}\right)=\left(1+\sqrt{\frac{200}{d}}\right)\left(3\frac{d}{a}\rho_l\right)^{\frac{1}{3}}\sqrt{1+\left(\frac{\sigma_{cp}}{f_{ctk}}\right)} \qquad \text{Eq. 7.19}$$

The obtained correlation between k_v and f(a, d, ρ_l, σ_{cp}) is plotted in Fig. 7.1. By means of a linear regression analysis the correlation factor (C) between these two parameters is found to be 0.388. Hence, instead of using the more complex iterative procedure, the factor k_v expressing the concrete contribution to the shear capacity can be more simply estimated as A = 0.388 f(a, d, ρ_l, σ_{cp}).

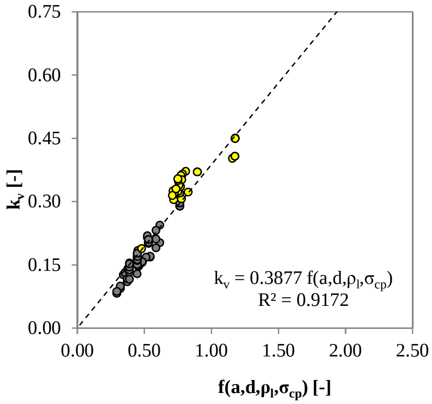

Fig. 7.1 – Relationship between factor k_v (Eq. 7.4) and f(a, d, ρ_l, σ_{cp}) (Eq. 7.19).

The fibre contribution can be expressed as cot(θ) times f_{Ftum}. Hence, the factor B is equal to cot(θ) given by Eq. 7.18. Furthermore, it should be understood that the value of f_{Ftum} should be limited, given the limitation of stresses that can be transmitted across the shear crack (see Section 6.2.2.1).Indeed, given the biaxial stress state, the strength f_{Ftum} might not be fully developed (especially for high forces acting in the compression strut) and hence, the value of f_{Ftum} shall be limited to:

$$f_{Ftu*} = \min \begin{cases} f_{Ftum} \\ f_{ctm}\left(1 - \dfrac{2\sigma_{cp}}{f_{cm}}\right) \end{cases} \qquad \text{Eq. 7.20}$$

Based on the above assumptions, the proposed shear strength equation can be written in its complete form as:

$$V_{proposed} = \left[0.388\sqrt{1+\frac{\sigma_{cp}}{f_{ctk}}}\left(1+\sqrt{\frac{200}{d}}\right)\left(3\frac{d}{a}\rho\right)^{\frac{1}{3}}\sqrt{f_{cm}} + f^{*}_{Ftu}\left(1+4\frac{\sigma_{cp}}{f_{ck}}\right)\right]b_w z \qquad \text{Eq. 7.21}$$

As can be noted from the above derivation procedure the proposed engineering model can be regarded as a closed form version of the MC2010 MCFT approach (model MC2010-B).

7.3 Analysis of shear test database

7.3.1 Selection of test results

Despite the large number of conducted shear tests and corresponding results reported in the past, few research reports are available in which the residual flexural strength parameters of the adopted SFRC-mix is obtained by means of the standard three point bending test [11]. In some cases, these material parameters are simply not reported. The lack of sufficient information can be attributed to the historical use of the concept of the fibre effectiveness factor [25, 26] which cannot represent the real composite post-cracking behaviour for a wide range of combinations of fibre type, dosage and concrete strength. As a consequence, the most important selection criterion for the implementation of shear test results into the database is the availability of measured residual tensile stresses ($f_{R,i}$). Furthermore, the following conditions were considered in order to add test results to the database: the failure aspect of the FRC element is characterized by a shear failure, and only complete replacement of stirrups by fibres is included in this study. Because the evaluated resistance models include the plasticity model, which cannot be solved when there is no prestress force and no fibre reinforcement at the same time, the combination reinforced concrete without stirrups was also excluded from the database.

Based on these criteria, a total of 99 fibre reinforced beams (30 prestressed and 69 reinforced) are withheld in order to evaluate the considered models (see Appendix A):

- Brite Euram project 97-4163: "Test and Design Methods for Steel Fibre Reinforced Concrete", as reported in [13] and [27]
- Parmentier [28]
- Minelli [14]
- Cuenca [29]
- Soetens [30]
- Conforti [31]

A summary of the most important material properties, beam geometries and test results can be found in Appendix A. The range of values of all parameters influencing the shear strength are summarized in Table 7.1.

Table 7.1 – Minimum, maximum and average (avg.) of test parameters for the considered database.

Parameter	Min.	Max.	Avg.
h [mm]	300	1000	584
f_{cm} [N/mm²]	19.6	78.9	46.1
f_{R3} [N/mm²] [(1)]	1.14	9.88	4.54
a/d [-]	0.5	4.04	2.64
σ_{cp} [N/mm²]	0	15.54	3.23
b_w [mm]	80	890	178
ρ_l [%]	0.99	5.61	1.89

[(1)] for the beams tested by Minelli [14] the residual flexural parameters are derived by means of the Italian standard test method. The equivalent tensile strengths $f_{eq,0.6\text{-}3}$, is taken equal to f_{R3}.

7.3.2 Database analysis

The database of shear test results is used to evaluate the shear strength models given in Section 7.2. The experimentally obtained shear strength (V_{exp}) is compared with respect to the corresponding modelled shear strength (V_{cal}) by means of parity diagrams (Fig. 7.2) These diagrams give a representation of the predictive capacity of the resistance models in terms of overall correctness (global bias with respect to the parity line) and magnitude of variability in the predictions (magnitude of bias of the individual data points).

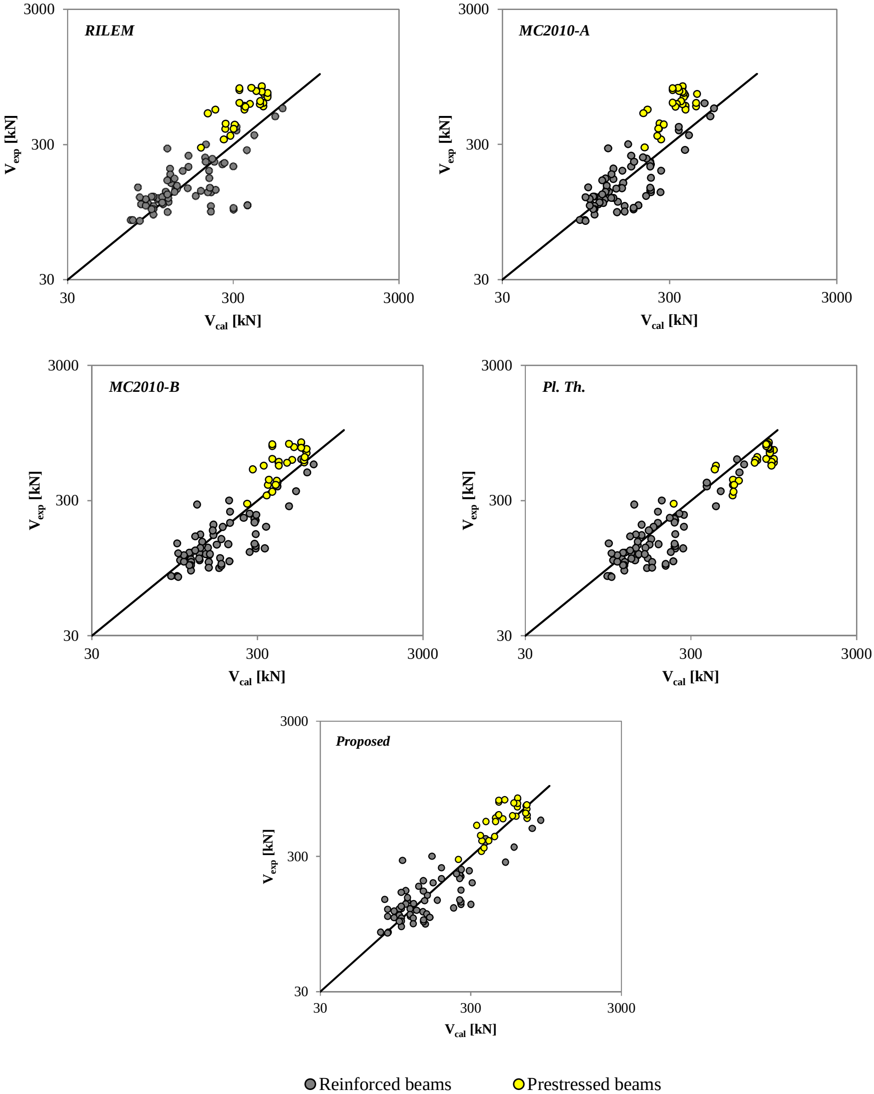

Fig. 7.2 – Comparison between experimentally obtained (V_{exp}) and calculated shear capacity (V_{cal}) of FRC beams

If the resistance model is exact, all of the points ($V_{exp,i}$, $V_{cal,i}$) would lie on the parity line. However, since the values of V_{exp}/V_{cal} are not perfectly collinear, a model uncertainty has to be dealt with and hence, the shear strength can be expressed in terms of a correction factor (b) and a model error term (δ) as follows (Eurocode 0 procedure for statistical determination of resistance models [32]):

$$V_{exp} = b\delta V_{cal} \qquad \text{Eq. 7.22}$$

In which b is derived by applying the "least square" best-fit to the slopes of Fig. 7.2, so that the model correction factor b can be calculated as:

$$b = \frac{\sum V_{exp,i} V_{cal,i}}{\sum V_{cal,i}^{\ 2}} \qquad \text{Eq. 7.23}$$

The error term δ_i for each points ($V_{exp,i}$, $V_{cal,i}$) is given as:

$$\delta_i = V_{exp,i} /(bV_{cal,i}) \qquad \text{Eq. 7.24}$$

It should be noted that the error term δ is lognormal distributed. The coefficient of variation of δ (CoV_δ) is given by:

$$CoV_\delta = \sqrt{e^{\sigma^2_{LN\delta}} - 1} \qquad \text{Eq. 7.25}$$

with $\sigma^2_{LN\delta}$ the variance of the term δ.

For all of the considered shear strength models, the values of b and CoV_δ are calculated for the complete database and the subsets of reinforced and prestressed concrete elements, respectively. All values are given in Table 7.2.

Table 7.2 – Average relative error b and coefficient of variation of δ (between parentheses) with respect to the considered database subset

Subset	N° of tests	RILEM	MC2010-A	MC2010-B	Plasticity theory	Proposed
All	99	1.213 (0.448)	1.234 (0.406)	1.002 (0.372)	0.864 (0.284)	1.079 (0.333)
RC beams	69	1.027 (0.424)	0.984 (0.313)	0.864 (0.330)	0.891 (0.312)	1.023 (0.359)
PC beams	30	1.639 (0.198)	1.810 (0.213)	1.320 (0.223)	0.803 (0.202)	1.207 (0.200)

Based on the parity diagrams shown in Fig. 7.2 and the values reported in Table 7.2, it can be concluded that the empirically based equations (RILEM and MC2010-A) yield more conservative predictions than the more rational approaches based on the MCFT (MC2010-B) and the plasticity theory in case of prestressed elements. Hereby, it should also be noted that the empirical equations (RILEM and MC2010-A) are developed based on test results with flexural shear failure mechanism. Hence, these models are not generally applicable, which is considered as a main drawback by the author. On the contrary, the more rational approaches deal consistently with the presence of a prestress force and, as a result, are less conservative in case of prestress.

The relative frequency distribution of the ratio V_{exp}/V_{cal} is compared (Fig. 7.3) with the theoretical lognormal distribution function based on the values b and CoV_{δ} given in Table 7.2.

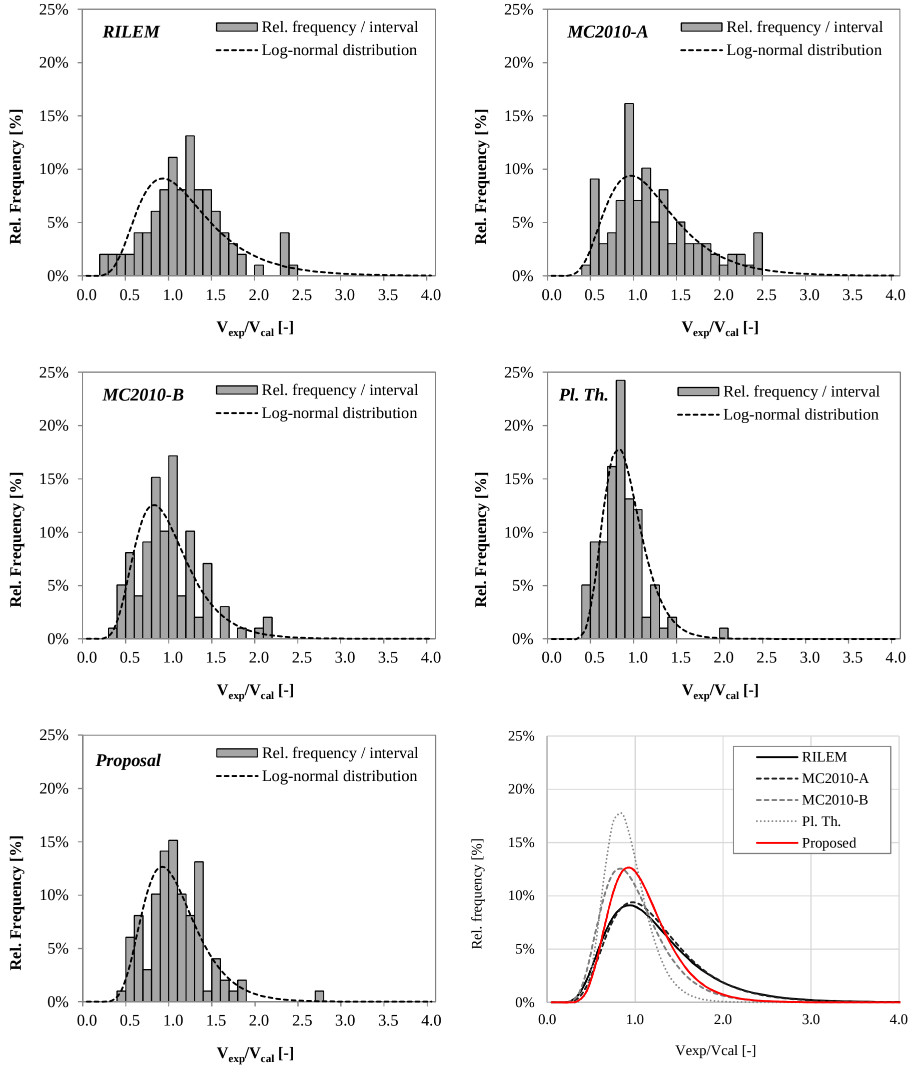

Fig. 7.3 – Relative frequencies for the shear capacity models with corresponding lognormal distribution function

Considering the correction factor b in Table 7.2 and the complete set of test data, the empirical based models RILEM and MC2010-A provide in general conservative predictions by underestimating the shear strength for about 21% and 23%, respectively. For the model based on the plasticity theory, the shear capacity is overestimated for about 14%. The MC2010-B model and the newly proposed engineering model give accurate predictions (correction factor b ≈ 1). Regarding the values of coefficient of variation CoV_{δ} in Table 7.2, for the empirical equations, a higher model uncertainty (CoV around 40-45%) is observed than for the rational approaches (28-38 %). Nevertheless, the obtained values of the coefficient of variation are not lower than 28%, as is common observation for the problem of shear [33]. For the proposed engineering model the CoV equals 33%, which is amongst the lowest of all the considered models. Given the larger scatter for the prediction of the shear strength of both models RILEM and MC2010-A and its tendency to underestimate the shear capacity, it is clear that using these models as design equations will lead to (very) conservative designs. Therefore, it should be encouraged to use more rational approaches based on the Modified Compression Field Theory (MC2010-B and newly proposed engineering model) or the Plasticity Theory.

Also looking into the subsets of reinforced or prestressed concrete members, the proposed engineering model gives the best performance in terms of having a correction factor b close to unity and a relatively low CoV (see Table 7.2).

When a distinction is made between reinforced and prestressed concrete beams (Fig. 7.4), a remarkable difference between the considered models has been found. Evaluation of the models for the 69 RC beams (Fig. 7.4 and Table 7.2), in a similar way, all the models yield fairly good predictions of the ultimate shear strength, with average V_{exp}/V_{cal} values towards unity. The CoV for the RILEM model is higher (42%) than for the other models which have a value of CoV around 30-35%.

In case of prestressed beams (30 test results), Table 7.2 shows that the plasticity theory yields unsafe shear strength predictions while for most of the other models an excessive conservatism has been observed with average V_{exp}/V_{cal} values up to 1.8 for the MC2010-A model. The RILEM and MC2010-B model have an average V_{exp}/V_{cal} ratio of about 1.6 and 1.3, respectively.

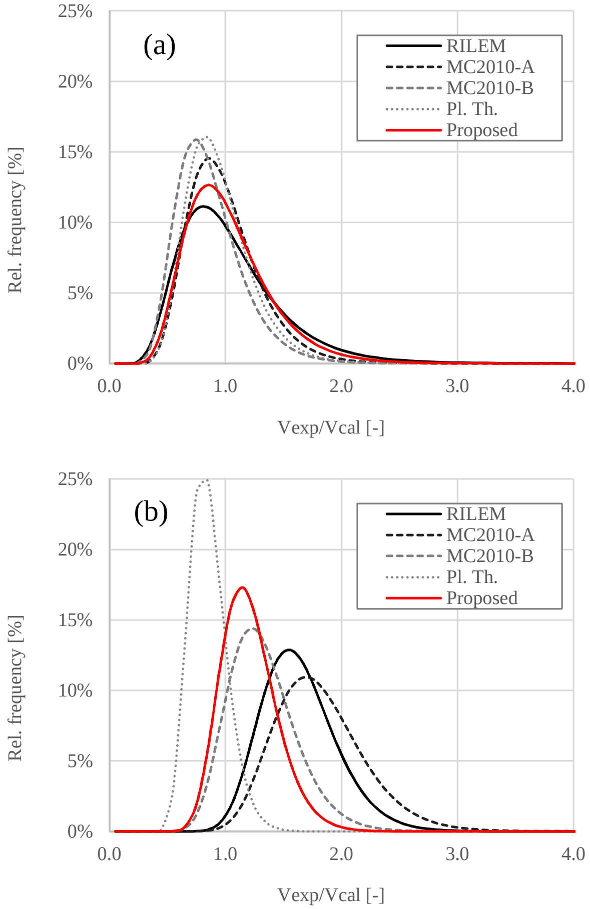

Fig. 7.4 – Distribution function of V_{exp}/V_{cal} for the subset of reinforced beams (a) and prestressed beams (b)

7.4 Influence of main parameters

The observed scatter of shear test results and inherent model uncertainties can be attributed to:

- The complex mechanisms involved in the shear failure of reinforced and prestressed concrete beams, as also reflected by the model error term δ.
- The scatter of the main material parameters itself. Hereby, the most important parameters are the concrete compressive strength and the post-cracking tensile strength of FRC. This is further discussed in the following sections.

In the following, the influence of the material parameters residual flexural stress f_{R3} and the concrete compressive strength on the model uncertainty has been discussed in more detail. For the influence of the main geometrical parameters, reference is made to Appendix D.

7.4.1 Influence of f_{R3}

In case of traditionally reinforced elements, it is often observed that the uncertainty of shear strength models decreases as a function of transverse reinforcement ratio [33]. The ratio of V_{exp}/V_{cal} as a function of residual flexural stress of the FRC is shown in Fig. 7.5. Hereby the CoV of the error term δ can be calculated for the RC and PC subsets (Section 7.3.2) for a predefined interval of the residual flexural stress $f_{Rm,3}$ at CMOD 2.5 mm, or the related post-cracking stress $f_{Ftum} = f_{Rm,3}/3$. This allows to compare the CoV_{δ} for lower versus higher values of f_{Ftum}. The chosen f_{Ftum} interval levels and corresponding coefficient of variation are summarized in Table 7.3 and visualised in Fig. 7.6.

Table 7.3 – Influence of post-cracking stress f_{Ftu} on the values of CoV_{δ} for each model.

Subset	# tests	$f_{Ftu, min}$ [N/mm²]	$f_{Ftu,max}$ [N/mm²]	f_{Ftum} [N/mm²]	RILEM	MC2010-A	MC2010-B	Pl. Th.	Proposed
RC	28	0.38	0.97	0.75	0.470	0.341	0.317	0.358	0.340
	41	1.00	2.00	1.54	0.384	0.313	0.324	0.296	0.332
PC	15	1.00	1.99	1.48	0.219	0.222	0.263	0.234	0.222
	15	2.08	3.29	2.80	0.150	0.183	0.160	0.172	0.155

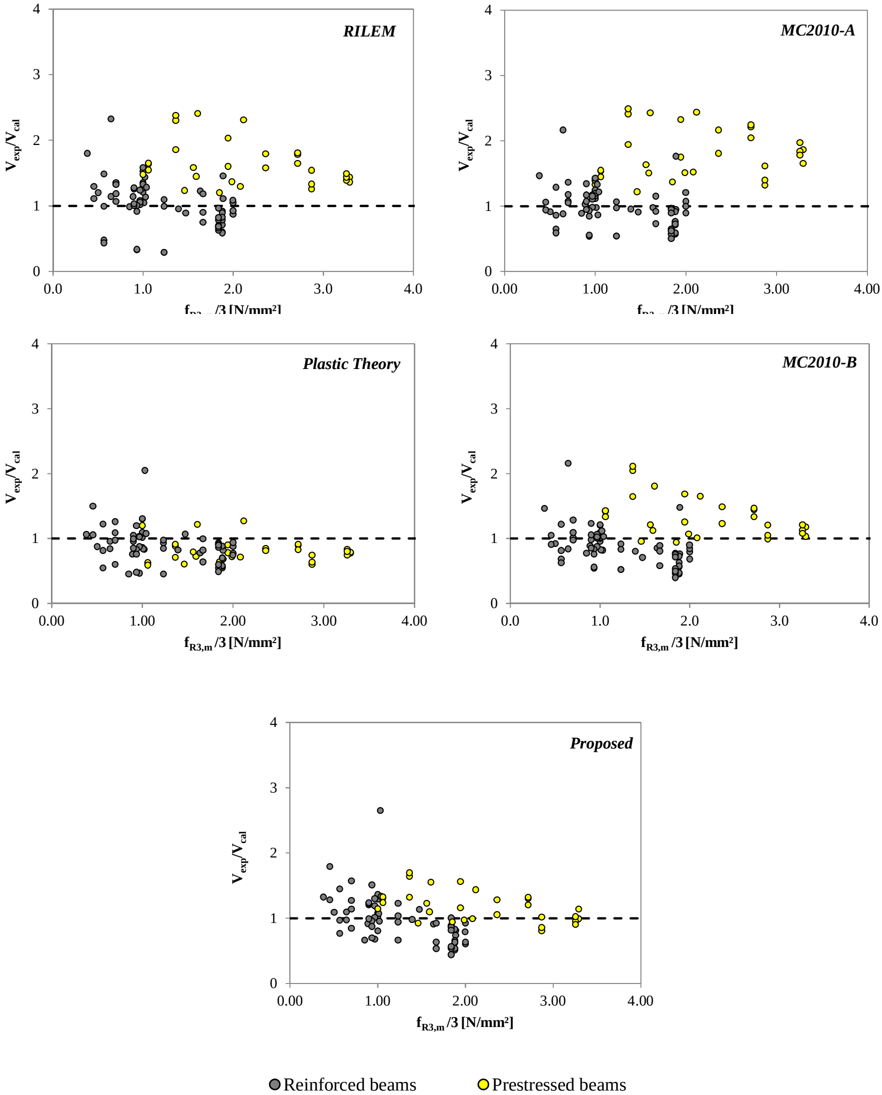

Fig. 7.5 – Ratio of V_{exp}/V_{cal} as a function of average residual stress for all of the considered models

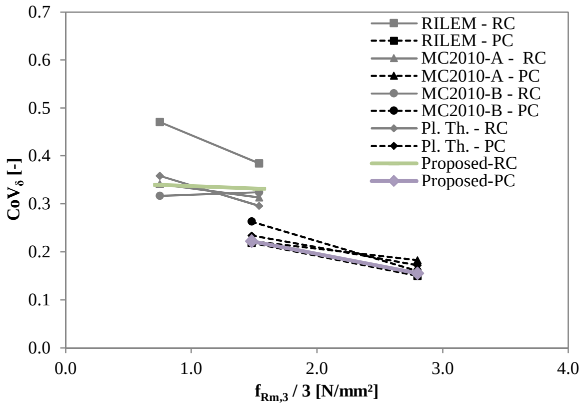

Fig. 7.6 – CoV_δ as a function of average residual stress for RC and PC beams

From Fig. 7.6, it can be observed that for higher values of residual stress f_{R3m}, all the models yield more accurate shear strength predictions. For RC beams, the proposed engineering model has one of the lowest CoV (about 30%), while the RILEM model has CoV values between 40-50%. For the subset of PC beams, all the considered models reveal a clear decrease of CoV ranging from 25% to 15%.

7.4.2 Influence of compressive strength

In a similar way as discussed in Section 7.4.1, the influence of the concrete compressive strength on the prediction accuracy of the models is analysed. The individual data points are shown in Fig. 7.7. The calculation of the CoV_δ for predefined concrete compressive strength intervals is reported in Table 7.4 and Fig. 7.8. Hereby, for the PC subset, typically higher concrete compressive strengths are applicable than for the RC subset.

Table 7.4 – Influence of concrete compressive stress on the values of CoV_δ for each model.

Subset	# tests	f_{cm} [N/mm²]	$f_{c,min}$ [N/mm²]	$f_{c,max}$ [N/mm²]	RILEM	MC2010-A	MC2010-B	Pl. Th.	Proposed
RC	40	35.1	19.6	39.9	0.334	0.294	0.324	0.284	0.349
	29	42.5	40.1	48.3	0.528	0.328	0.283	0.345	0.310
PC	11	49.4	34.3	59.5	0.237	0.216	0.253	0.216	0.223
	19	67.9	62.0	78.9	0.132	0.213	0.163	0.128	0.178

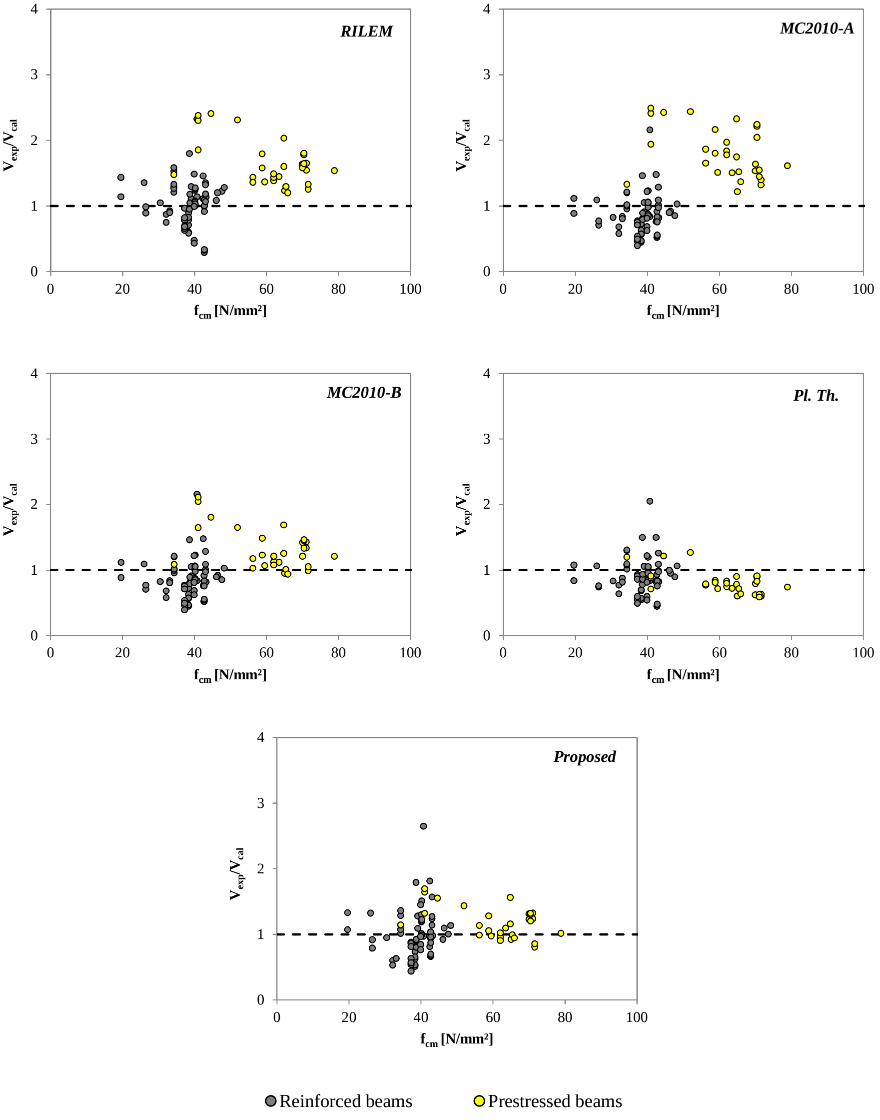

Fig. 7.7 – Ratio of V_{exp}/V_{cal} as a function of average concrete compressive strength

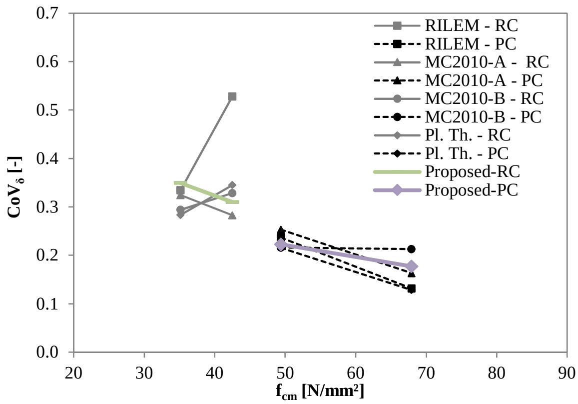

Fig. 7.8 – CoV_δ as a function of concrete compressive strength for RC and PC beams

From Fig. 7.8 and Table 7.4, it can be observed that the accuracy of shear strength prediction increases for higher concrete compressive strength (though not always consistently observed for the RC subset). This observed trend is similar to the observed effect of values of $f_{Rm,3}$.

7.5 Safety levels for design

Given the obtained values for the model uncertainties of the evaluated shear strength models, it is of great importance to use an appropriate safety factor for design. Based on the obtained values of b and CoV_δ, design values can be obtained for all of the considered shear resistance model. For the models RILEM, MC2010-A and the proposed engineering model, which are all available in a closed form solution, the procedure given in Eurocode 0 (EC0) for design by testing can be used in a straight forward way. However, for the iterative models based on the MCFT and the plasticity theory, the method described in EC0 cannot be implemented directly. To deal with this aspect, and to implement variation of material parameters more easily, evaluation of the safety levels of the considered models will be done by means of the EC0 procedure (see further) in combination with Monte Carlo sampling [10].

By means of a shear resistance model, the shear strength of FRC beams can be predicted. However, due to the observed model uncertainties and additional scatter of material parameters, a proper margin of safety has to be taken into account in order to sufficiently reduce the risk of failure. Hence, a target reliability index β as defined in Eurocode 0 can be guaranteed.

Given that R is the resistance and E is the effect of load actions, a performance function g = R-E can be considered. Hereby, the failure boundary for design can be taken as g = 0. Following the approach for calibration of design values given in Eurocode 0, starting from a known resistance model (R) and a pre-defined target reliability index β, the design value of the resistance R_d can be defined such that the probability of having a more unfavourable value $P[R \leq R_d]$ is limited as follows (whereas for the specific case of the shear resistance models, R can be replaced by V_R and R_d by V_{Rd}):

$$P\left[V_R \leq V_{Rd}\right] \leq \Phi\left(-\alpha_R \beta\right) \qquad \text{Eq. 7.26}$$

In which Φ is the cumulative distribution function of the standardised normal distribution, β is the target reliability index and α_R is a FORM (first order reliability method) sensitivity factor for resistance according to EC0. For a design life span of 50 years and reliability class RC2, a value of 3.8 is adopted for β. Due to the relatively high scatter of the observed model uncertainty, the sensitivity factor for resistance α_R is considered to be a dominant variable and the value of α_R is taken equal to 0.8 as specified in EC0. Taking this into account, the failure probability has to be lower than 0.118%.

A schematic representation of the above procedure of assessing the safety factor is given in Fig. 7.9. By means of the procedure a safety factor γ_M is evaluated which combines uncertainty in material properties (safety factor γ_M) and model uncertainty in structural resistance (safety factor γ_{Rd}).

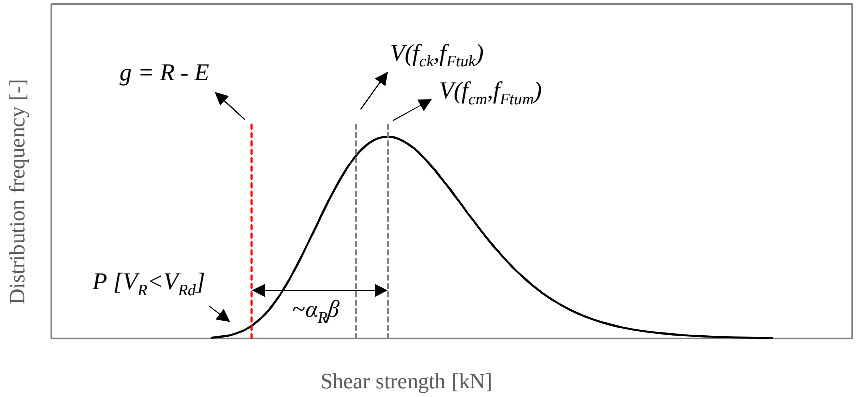

Fig. 7.9 – Shear strength distribution obtained from Monte Carlo sampling

V_R is evaluated by taking into account the scatter of both model uncertainty and the mean shear strength influencing parameters (i.e. concrete compressive strength and post-cracking tensile stress of SFRC), as given in Eq. Eq. 7.22.

$$V_R = b\delta V_{cal}(f_c, f_{Ftu}) \qquad \text{Eq. 7.27}$$

The design value of the shear resistance V_d can be expressed as follows:

$$V_{Rd} = \frac{1}{\gamma_M} V_{cal}(f_{ck}, f_{Ftuk}) \qquad \text{Eq. 7.28}$$

In which f_{ck} and f_{Ftuk} are the characteristic values of concrete compressive strength and post-cracking tensile strength of FRC respectively. The variables f_c, and f_{Ftu} are lognormal distributed. γ_M is the safety factor, which is then obtained by dividing $V_{cal}(f_{ck}, f_{Ftuk})$ by V_{Rd}. Under the assumption that the model uncertainty is the only parameter involved in obtaining a sufficient safety margin, Eurocode 0 defines that V_{Rd} can be derived on the basis of Eq. 7.27 as follows:

$$V_{Rd} = b\left[\exp\left(-\alpha_R \beta \sigma_{LN(V_R)} - 0.5\left(\sigma_{LN(V_R)}\right)^2\right)\right] V_{cal}(f_{cm}, f_{Ftum}) \qquad \text{Eq. 7.29}$$

Since two of the considered resistance models involve an iterative calculation procedure and to allow for the treatment of f_{cm} and f_{Ftum} as stochastic parameters, the evaluation of the safety factors has been systematically done by performing Monte Carlo sampling [10]. Hereby, the following aspects are considered:

- A distinction is made between a reinforced concrete and a prestressed concrete beam. The cross-sectional dimensions and material characteristics are summarised in Table 7.5.
- The safety factor γ_M is evaluated per resistance model, for different values of f_{Ftum}, given the differences of the CoV_δ of the resistance models for the f_{Ftum} intervals assumed in Section 7.4.1 (Fig. 7.6).
- The evaluation is done for a chosen RC and PC beam, with predefined geometrical dimensions (Table 7.5). It is hence assumed (due to limited available data this assumption could not be thoroughly verified) that the geometrical dimensions have no significant influence on the CoV_δ of the resistance models. It is further assumed that the geometrical dimensions should not be treated as stochastic parameters. Indeed, to limit the Monte Carlo sampling space it is assumed that the concrete strength properties are the main governing stochastic parameters in the resistance models.
- The concretes strength properties f_{cm} and f_{Ftum} are treated as stochastic parameters, with a coefficient of variation on the concrete compressive strength and on the residual flexural strength equal to 15% and 30%, respectively. These coefficients of variation are typical values reported in literature (e.g. [34] for residual stress and for concrete compressive strength [35]).
- The evaluation is done for a preset value f_{cm} of 30 N/mm², to be representative for the RC beam, and 60 N/mm² for the PC beam. Hereby, it is assumed that the CoV_δ of the resistance models is more or less constant for the RC and PC subset (see Section 7.4.2 and Fig. 7.8).

Table 7.5 – Stochastic variables and according safety factors relative to the average shear strength V_{cal} (f_{cm}, f_{Ftum})

Property	Reinforced [cf. Minelli]	Prestressed [cf. this study]
h [mm]	500	1000
d [mm]	435	886
b_w [mm]	200	100
b_f [mm]	200	400
h_f [mm]	0	130
ρ_l [%]	1.04	1.78
σ_{cp} [N/mm²]	0	9.24
a/d [-]	2.51	3
f_{cm}	30	60
f_{R3m}	2.25-4.62	4.44-8.40

By using the Monte Carlo tool, 500000 different beam configurations are calculated for each considered shear resistance model. By means of the Monte Carlo method, the log-normal distribution function of the calculated shear strength V_R (Eq. 7.27) is obtained (see Fig. 7.9). As a result, the standard deviation $\sigma_{LN\delta}$ is known, and the safety factor can be determined by means of Eq. 7.28 and Eq. 7.29.

The calculation of design shear strength V_{Rd} and inherent safety margin γ_M is mainly affected by the adopted values for b and CoV_δ as obtained from the accuracy analysis of the resistance models versus a collected database of test results (Section 7.3). As this accuracy analysis has been performed on the complete database (Table 7.2) as well as the RC and PC subsets (Table 7.3), the same approach can be done for the evaluation of the safety margin. In Fig. 7.10 till Fig. 7.13, all the obtained values of V_{Rd} (denoted in these figures as V_d) and corresponding safety factors with respect to the shear strength $V(f_{ck},f_{Ftuk})$, are given.

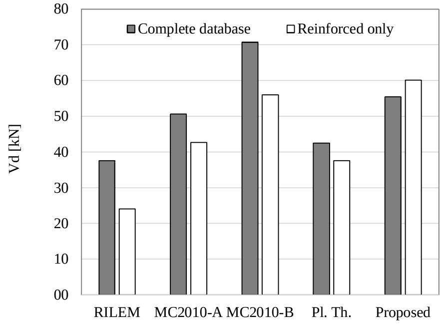

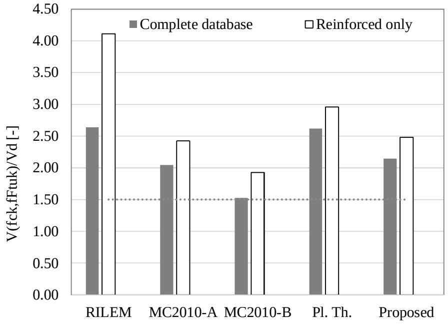

Fig. 7.10 – Design shear strength (left) and corresponding safety margins (right) for the reinforced concrete beam case with $f_{Rm,3}$ = 2.25 N/mm²

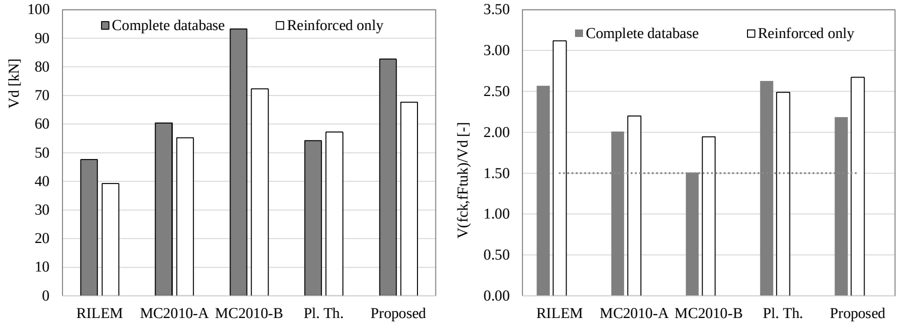

Fig. 7.11 – Design shear strength (left) and corresponding safety margins (right) for the reinforced concrete beam case with $f_{Rm,3}$ = 4.62 N/mm²

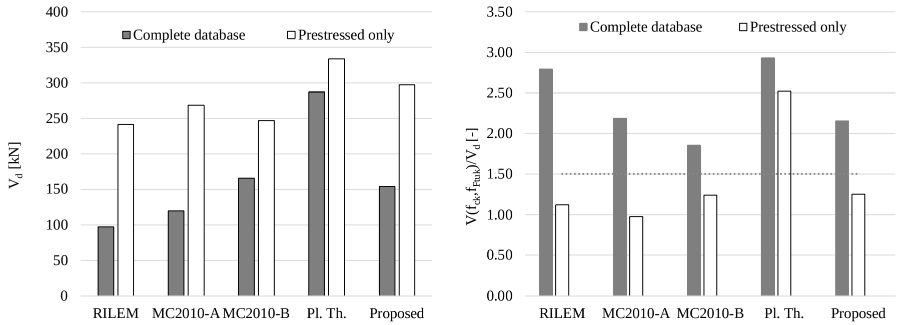

Fig. 7.12 – Design shear strength (left) and corresponding safety margins (right) for the prestressed concrete beam case with $f_{Rm,3}$ = 4.44 N/mm²

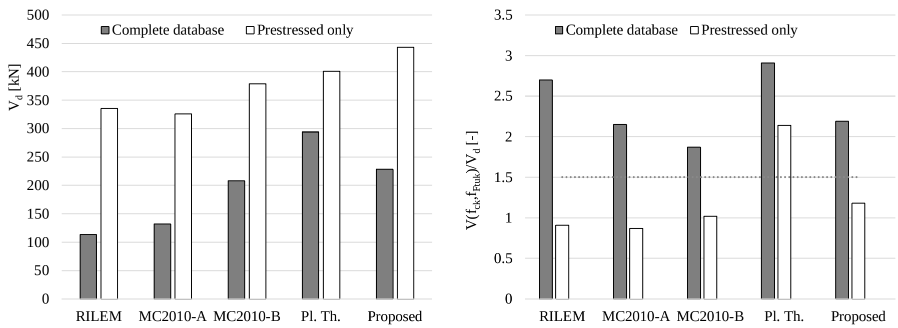

Fig. 7.13 – Design shear strength (left) and corresponding safety margins (right) for the prestressed concrete beam case with $f_{Rm,3}$ = 8.40 N/mm²

For the case of the reinforced concrete beam, the design capacity considering the uncertainty parameters (b, CoV_δ) of the complete database is slightly higher than when the subset of RC beams is considered. However, this difference is relatively low (20%). Given their higher accuracy and lower coefficient of variation, the shear strength models

MC2010-B and the proposed engineering model provide the highest design shear capacity for both cases of $f_{R3,m}$ equal to 2.25 N/mm² and 4.62 N/mm² while for the RILEM and MC2010-A, the lowest shear design strengths are obtained. Given that the calculated safety factors in Fig. 7.11 and Fig. 7.12 are in the order of magnitude of 2 to 3, the safety factors as currently adopted in design codes (i.e. 1.5) is insufficient to obtain safe design.

For the case of prestressed concrete beams, different conclusions can be drawn. When considering the model uncertainty obtained from the complete database, the design shear strengths are in general much lower than in case of considering the subset of PC beams only. For the models RILEM and MC2010-A, this difference is higher than a factor 2. This difference is lower for the proposed engineering model and MC2010-B, as they take the effect of prestressing more thoroughly into account. Given the calculated safety factors in Fig. 7.12 and Fig. 7.13, it can be concluded that adopting a value of 1.5 for the case of prestressed elements will lead to over conservative designs.

The overall prediction consistency of the proposed engineering model and MC2010-B model is in general better than for the other models considered in this study. The safety factor estimated for these two resistance models, to fulfil a target reliability index $\beta = 3.8$, is given in Table 7.6.

Table 7.6 – Safety factor γ_M to be applied for a target reliability $\beta = 3.8$

V_{Rd} of SFRC for	MC2010-B iterative model	Proposed engineering model
RC	1.94	2.58
PC	1.13	1.22

7.6 Conclusions

Based on the analysis of a shear test database containing 99 shear test results from prestressed (30) and reinforced (69) concrete beams, it can be concluded that the empirical based formulations (RILEM, MC2010-A) have a higher model uncertainty than the more rational models (MC2010-B and plasticity theory) when the complete database is considered. However, when analyzing the subsets of reinforced and prestressed concrete beams only, all models yield similar predictions for the case of reinforced beams. The RILEM and MC2010-A are derived for the particular case of shear flexural failure mechanisms of reinforced beams. This is reflected by the high conservatism of these models with respect to the more rational approaches in case of prestressing.

A new engineering model is proposed in order to obtain more accurate shear strength predictions and without increasing the level of calculation effort (e.g. no iterations). Thereby, attention is paid towards physical phenomena influencing the shear strength such as dowel action, shear span to depth ratio, size effect, and level of prestress. In fact, the model is a derivation of the more complex MCFT iterative procedure described in the Model Code 2010 (MC2010-B model). By comparing the experimental with the predicted shear test results, the proposed engineering model has been found to be feasible for both prestressed and reinforced concrete cases. Together with the model MC2010-B, it gives the most consistent and accurate predictive capacity for the complete range of variables.

Further to the evaluation of the resistance models, their representation as design models aiming for a target reliability index $\beta = 3.8$ has been evaluated as well. It has been found that for the RILEM, MC2010-A and plasticity theory models, the currently specified safety factor equal to 1.5 is insufficient to provide a safe design. This value should be between 2 and 3, depending on the considered model. For the MC2010-B model and the proposed engineering model, the model safety factor is in the range of 1.50-2.25 (when considering the complete database).

7.7 References

[1] fib. (2010). "Model Code for Concrete Structures 2010". Lausanne, Switzerland, fédération internationale du béton.

[2] RILEM. (2003). "Final Recommendation of RILEM TC 162-TDF: Test and design methods for steel fibre reinforced concrete sigma-epsilon-design method". *Materials and Structures,* Vol. 36(262), pp. 560-567.

[3] CNR. (2006). "CNR DT 204/2006 - Guidelines for the design, construction and production control of fiber reinforced concrete structures".

[4] Gustafsson, J., Noghabai, K. (1999). "Steel fibers as shear reinforcement in high strength cocnrete beams". *Bi annual report - Nordic Concrete Research (NCR)*, Vol. 1, pp. 1-18.

[5] Minelli, F., Plizzari, G. (2013). "On the Effectiveness of Steel Fibres as Shear Reinforcement". *ACI Structural Journal*, Vol. 110(3), pp. 379-389.

[6] Voo, Y. L., Foster, S. J. (2008). "Shear strength of steel fiber reinforced ultra-high performance concrete beams without stirrups". *5th international Specialty Conference on Fibre Reinforced Materials,* pp. 177-184.

[7] Cucchiara, C., La Mendola, L., Papia, M. (2004). "Effectiveness of stirrups and steel fibres as shear reinforcement". *Cement and Concrete Composites,* Vol. 26(7), pp. 777-786.

[8] Swamy, R. N., Bahia, H. M. (1985). "The effectiveness of steel fibers as shear reinforcement". *Concrete International*, Vol. March, pp. 35-40.

[9] Brandt, A. M. (2008). "Fibre reinforced cement-based (FRC) composites after over 40 years of development in building and civil engineering". *Composite Structures*, Vol. 86(1-3), pp. 3-9.

[10] Liu, J. S. (2008) "*Monte Carlo Strategies in Scientific Computing*". USA: Springer.

[11] CEN. (2005). "EN 14651 - Test method for metallic fibered concrete - measuring the flexural tensile strength". Brussels, Belgium, CEN.

[12] CEB-FIP. (1990). "Model Code 1990: Design code". Lausanne, Switzerland.

[13] Dupont, D., Vandewalle, L. (2002). "Dwarskrachtcapaciteit van staalvezel-betonbalken". *Cement*, Vol. 8.

[14] Minelli, F. (2005). "*Plain and Fibre Reinforced Concrete Beams under Shear Loading: Structural Behaviour and Design Aspects*" (PhD-thesis). Brescia, University of Brescia.

[15] Vecchio, F. J., Collins, M. P. (1986). "The Modified Compression-Field Theory for Reinforced Concrete Elements Subjected to Shear". *ACI Journal*, Vol. 83(22), pp. 219-231.

[16] Bentz, E. C., Vecchio, F. J., Collins, M. P. (2006). "Simplified Modified Compression Field Theory for Calculating Shear Strength of Reinforced Concrete Elements". *ACI Structural Journal*, Vol. 103(4), pp. 614-624.

[17] Sagaseta, J. (2008). "*The influence of aggregate fracture on the shear strength of reinforced concrete beams*". London, Imperial College London.

[18] Collins, M. P., Mitchell, D. (1991) "*Prestressed Concrete Structures*". Englewood Cliffs, New Jersey: Prentice-Hall, p. 766.

[19] Spinella, N., Colajanni, P., Recupero, A. (2010). "Simple plastic model for shear critical SFRC beams". *Journal of Structural Engineering*, Vol. April, pp. 390-400.

[20] Voo, Y. L., Foster, S. J., Gilbert, R. I. (2006). "Shear Strength of Fiber Reinforced Reactive powder Concrete Prestressed Girders without Stirrups". *Journal of Advanced Concrete Technology*, Vol. 4(1), pp. 123-132.

[21] Kani, G. N. J. (1964). "The Riddle of Shear Failure and Its Solution ". *Journal of the American Concrete Institute*, Vol. 61(4), pp. 441-468.

[22] Zsutty, T. (1971). "Shear Strength Prediction for Separate Catagories of Simple Beam Tests". *ACI Journal*, Vol. 68(2), pp. 138-143.

[23] Kordina, K., Blume, F. (1985). "Empirische Zusammenhänge zur Ermittlung der Schubtragfähigkeit stabförmiger Stahlbetonelemente". Berlin, Sohn Eu.

[24] Ramirez, J. A., Breen, J. E. (1991). "Evaluation of a Modified Truss-Model Approach for Beams in Shear". *ACI Structural Journal*, Vol. 88(5), pp. 562-571.

[25] Narayanan, R., Kareen-Palanjian, A. S. (1986). "Factors Influencing the Strength of Steel Fibre Reinforced Concrete". *Third International Rilem Symposium*.

[26] Aoude, H., Mehdi, B., Cook, W. D., Mitchell, D. (2012). "Response of Steel Fiber-Reinforced Concrete Beams with and without Stirrups". *ACI Structural Journal*, Vol. 109(3), pp. 359-367.

[27] Rosenbusch, J., Teutsch, M. (2003). "Shear Design with σ-ε Method". *RILEM TC 162-TDF Workshop, Bochum, Germany*.

[28] Parmentier, B., Cauberg, N., Vandewalle, L. (2012). "Shear resistance of macro-synthetic and steel fibre reinforced concrete beams without stirrups". *BEFIB 2012, Guimaraes*.

[29] Cuenca, E., Serna, P. (2013). "Shear behavior of prestressed precast beams made of self-compacting fiber reinforced concrete". *Construction and Building Materials*, Vol. 45(August 2013), pp. 145–156.

[30] Soetens, T., Matthys, S. (2014). "Shear design of full-scale prestressed SFRC girders". *FRC 2014 Joint ACI-fib International Workshop - Fibre Reinforced Concrete: from Design to Structural Applications, Montréal, Canada*, pp. 123-133.

[31] Conforti, A., Tinini, A., Minelli, F., Plizzari, G., Moro, S. (2014). "Structural applicability of polypropylene fibres: deep and wide-shallow beams subjected to shear". *FRC 2014 Joint ACI-fib International Workshop - Fibre Reinforced Concrete: from Design to Structural Applications, Montréal, Canada*, pp. 341-355.

[32] CEN. (2002). "EN 1990 - Eurocode 0: Basis of structural design". Brussels, Belgium, CEN.

[33] Schlune, H., Plos, M., Gylltoft, K. (2011). "Safety formats for nonlinear analysis tested on concrete beams subjected to shear forces and bending moments". *Engineering Structures,* Vol. 33(8), pp. 2350-2356.

[34] Parmentier, B., Vandewalle, L., Van Rickstal, F. (2008). "Evaluation of the scatter of the postpeak behaviour of fibre reinforced concrete in bending: a step towards reliability". *7th international RILEM symposium on Fibre Reinforced Concrete, Chennai, India*, pp. 133-143.

[35] Holický, M., Sýkora, M. (2010). "Stochastic Models in Analysis of Structural Reliability". *The International Symposium on Stochastic Models in Reliability Engineering, Life Sciences and Operations Management, Beër Sjeva, Israël*.

8 DESIGN OF SFRC ROOF GIRDERS

8.1 Introduction

The applicability for steel fibres as shear reinforcement will be of most economical for slender beams subjected to a high bending moment and relatively low shear load. Hence, two prestressed roof girders with a span of 20m and 23m, and taking into account realistic design loads, were selected for a design case. The roof girders, also designated as IV-girders, have a variable height (roof-shaped). In Chapter 7, existing design models and a newly proposed design engineering model have been evaluated by means of a shear test database and conclusions have been drawn with respect to the overall applicability in terms of accuracy and inherent safety levels. Applying the developed design procedure of Chapter 7, the roof girders have been dimensioned. As a result of the design process, a target value of the post-cracking strength $f_{Rk,3}$ is specified, which needs to be converted to a SFRC mix and corresponding fibre dosage. This has been done on the bases of the SFRC material characterisation given in Chapter 5. Following, the girders have been manufactured and tested in shear at both sides and the obtained shear test results are compared with the calculated design value of the shear capacity.

8.2 Design calculation

8.2.1 Strength of materials

For the roof girders, the concrete strength class is C50/60, the mild steel reinforcement is grade BE500-S and the characteristic yield stress of the prestressing strands is equal to 1860 N/mm². The concrete mix composition is equal to the one used for the girders tested in Chapter 5 (see Table 5.2), and for which the constitutive material behaviour is reported in Section 6.2.2.

8.2.2 Element geometry & design loads

All geometrical properties of both roof girders 1 and 2 are summarized in Table 8.1. The critical cross-section for the shear design is found at the location where the I-shaped cross-section is the nearest to the end-blocks. At this point, the shear design loads are the highest and the resistance to shear will be the lowest (given the lower height of the roof-shaped girder near its ends). The considered acting loads for the girders 1 and 2 are summarized in Table 8.1, in terms of characteristic values of the self-weight (g_k), additional dead load (p_k) and a life load (q_k). Taking into account the self-weight of the girders and the uniformly distributed loads, the design shear load and bending moment for both girders 1 and 2 is given in Table 8.1.

Table 8.1 – Distributed loads and corresponding design values for bending and shear.

Property	Girder 1	Girder 2
p_k [kN/m]	2.20	4.28
q_k [kN/m]	3.69	3.75
g_k [kN/m]	4.32	5.90
Span length [m]	20.7	22.5
Max. height [mm]	1000	1100
$M_{Sd,mid}$ [kNm]	771	1227
$V_{Sd,crit}$ [kN]	120	203

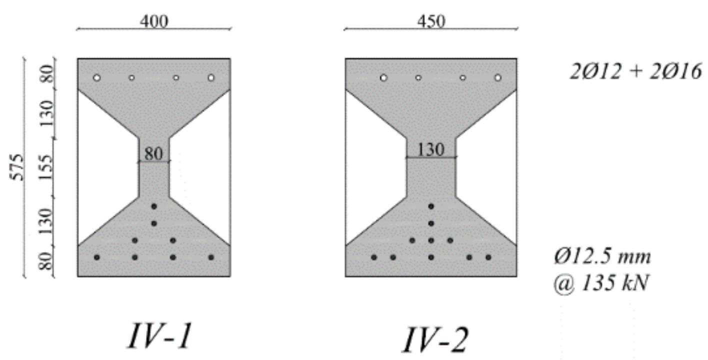

Fig. 8.1 – Cross-section of girders IV-1 and IV-2

The amount of longitudinal reinforcement and inherent configuration of the prestressing strands is calculated by taking into account the value of M_{Sd} at midspan. The adopted prestressing strand configuration is shown in Fig. 8.1 for the considered shear critical cross-section. All of the geometrical properties are summarized in Table 8.2.

Table 8.2 – Geometrical properties of both girders 1 and 2

Girder	Girder 1	Girder 2
$\#N_p$	8	10
Prestress strand configuration	4 – 2 – 1 – 1	5 – 3 – 1 – 1
Web width [mm]	80	130
Flange width [mm]	400	450
Length of I-section [m]	17.0	21.0
h_{crit} [mm]	575	575
h - d [mm]	89	86
A_c [mm²]	145100	174400

8.2.3 Dimensioning of the girders in terms of required post-cracking strength

Based on the above mentioned geometrical and material properties and applying the different design models of Chapter 7, the design value V_{Rd} of the roof girders has been calculated as a function of the post-cracking strength $f_{Rk,3}$. The results are given in Fig. 8.2 for girder IV-1 and in Fig. 8.5 for girder IV-2, for a design safety factor as defined in Section 7.5 for the case of model uncertainty corresponding with prestressed girders only (PC subset in Chapter 7).

8.2.4 Determination of nominal fibre content

Since the increase of shear strength of prestressed girders due to the addition of fibres is taken into account by means of the characteristic value of the residual flexural strength ($f_{Rk,3}$) at CMOD equal to 2.5 mm, it is necessary to define the nominal fibre content as a function of $f_{Rk,3}$. Hence, for a specific SFRC mix with a nominal fibre content and as validated by standard bending tests according to EN 14651, a corresponding value of $f_{Rk,3}$ can be specified.

8.2.4.1 Girder IV-1

In Fig. 8.2, the relationship between the characteristic value of residual strength $f_{Rk,3}$ and the design shear strength for all of the considered models is shown and compared with the design value of the shear force acting on the shear critical section of the beam. The intersection between the design shear strength and the horizontal line representing V_{Sd} yields the required value of $f_{Rk,3}$ to obtain a safe design.

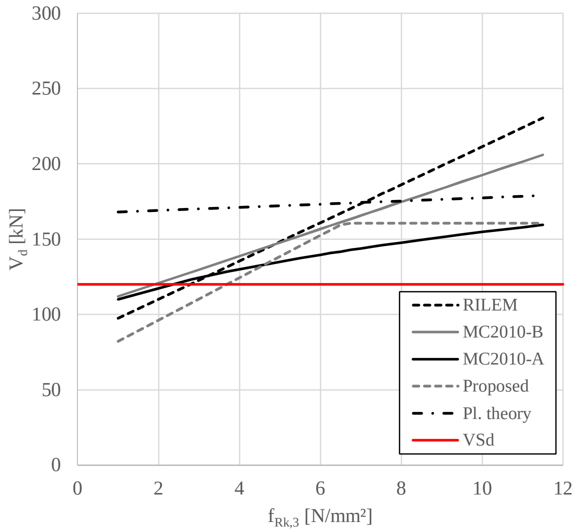

Fig. 8.2 – Comparison between V_{Sd} and V_{Rd} as a function of $f_{Rk,3}$ for the design of girder IV-1

In order to obtain a practical value for the fibre dosage, the three-point bending test result database available from the testing of 7 different SFRC-mixes as discussed in Chapter 5 are used to determine the amount of fibres needed to obtain a characteristic value of $f_{R,3}$. The relationship between the values of $f_{R,3}$ and the nominal fibre dosage is shown in Fig. 8.3. The characteristic line is shown as a red dotted line.

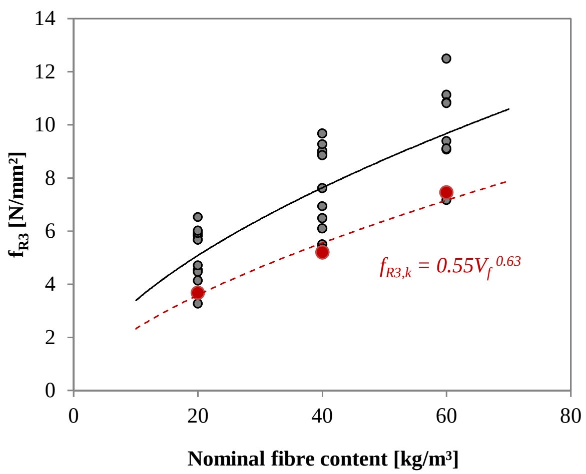

Fig. 8.3 – Relationship between $f_{Rk,3}$ and nominal fibre dosage based on Chapter 5

Given the correlation between $f_{Rk,3}$ and V_f shown in Fig. 8.3, the practical fibre dosage is obtained by the following relationship:

$$f_{Rk,3} = 0.55V_f^{0.63} \quad \text{Eq. 8.1}$$

From which the fibre dosage can be obtained as

$$V_f = \left(\frac{f_{Rk,3}}{0.55}\right)^{1.59} \quad \text{Eq. 8.2}$$

Finally, the calculated value of V_f is then rounded to the nearest upper multiple of 5 kg/m³. For the considered shear design models, the required nominal fibre dosages are summarized in Table 8.3.

Table 8.3 – Required characteristic value of $f_{R3,k}$ and corresponding nominal fibre content V_f

Model	$f_{R3,k}$ [N/mm²]	$V_{f,req}$ [kg/m³]
RILEM	2.8	14
MC2010-A	2.3	10
MC2010-B	1.9	8
Proposed	3.7	21
Pl. Theory.	0	0

From both Fig. 8.3 and Table 8.3, it is clear that the use of the plasticity model yields a safe design for a concrete girder without fibres. This should however be disregarded, as for a plain concrete girder without prestress the derived plasticity model is not valid. For the other models, the required nominal fibre content ranges between 8 and 21 kg/m³. From a practical point of view it is decided to use an SFRC mix containing 20 kg/m³ of fibres for girder IV-1.

As a remark, it should be noted that Eq. 8.1 can only be used for the considered type of fibre and concrete. When girders are made with a different concrete mix composition or fibre type, a shear design can only be done when a new relationship between V_f and $f_{Rk,3}$ is established. Therefore it is recommended to perform a sufficient number of standard bending tests which characterize the SFRC mix quality for daily practice. In this way, the scatter inherent to both the mix procedure and material performance of the SFRC is taken into account. Per SFRC mix, a database of quality control tests according to EN 14651 can be used to update the relationship between V_f and $f_{Rk,3}$. This will eventually lead to a stable and reliable relationship between V_f and $f_{R3,k}$. From this point of view, the design of girder IV-2 shall be done by taking also into account the quality control bending test results obtained from the SFRC batch of girder IV-1. The obtained post-cracking bending tensile stress curves for SFRC mix IV-1 are shown in Fig. 8.4. The black solid line is the average post-cracking response and the dotted red line is the characteristic line of residual flexural stresses. In Table 8.4, the corresponding residual tensile stresses are summarized.

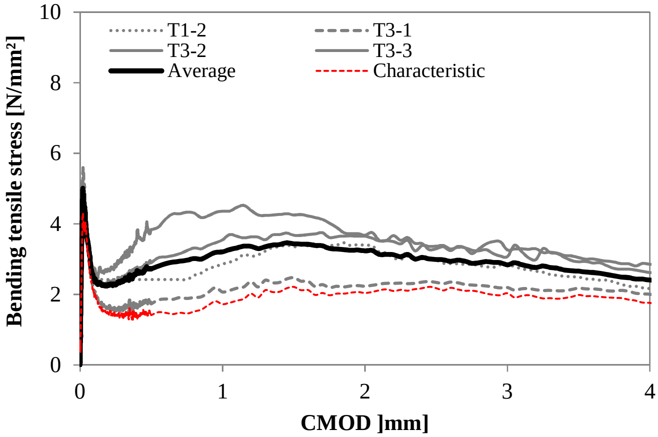

Fig. 8.4 – Stress-CMOD curves for SFRC mix IV-1

Table 8.4 - SFRC properties

Girder	Test	f_L [N/mm²]	$f_{R,1}$ [N/mm²]	$f_{R,2}$ [N/mm²]	$f_{R,3}$ [N/mm²]	$f_{R,4}$ [N/mm²]
IV-1	1	-	-	-	-	-
	2	5.18	2.42	3.34	2.97	2.49
	3	-	-	-	-	-
	4	5.60	1.73	2.47	2.34	2.18
	5	4.65	2.90	3.68	3.37	2.93
	6	5.29	3.84	4.25	3.29	3.05
	Average	5.18	2.72	3.44	2.99	2.66
	Char. value	4.45	1.10	2.06	2.13	1.92

8.2.4.2 Girder IV-2

Similar to the determination of the required $f_{Rk,3}$ of girder IV-1, the intersection between the shear design load V_{Sd} and shear design capacity V_{Rd} is used to obtain the required value of $f_{Rk,3}$ (see Fig. 8.5). The value of $f_{Rk,3}$ is further translated to a practical fibre dosage V_f, making use of the quality control tests database of Chapter 5, this time including the obtained results of SFRC mix IV-1. Hereby, it is observed that the obtained values of $f_{Rk,3}$ for SFRC mix IV-1 are lower than expected, compared to the results obtained in Chapter 5. Taking into account the values of $f_{Rk,3}$ for mix IV-1 the database is updated and an updated correlation between $f_{Rk,3}$ and V_f is obtained (see Fig. 8.6).

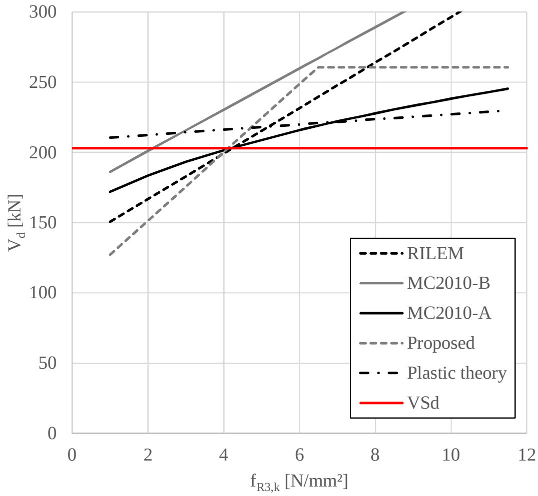

Fig. 8.5 – Design shear strength as a function of f_{R3k}

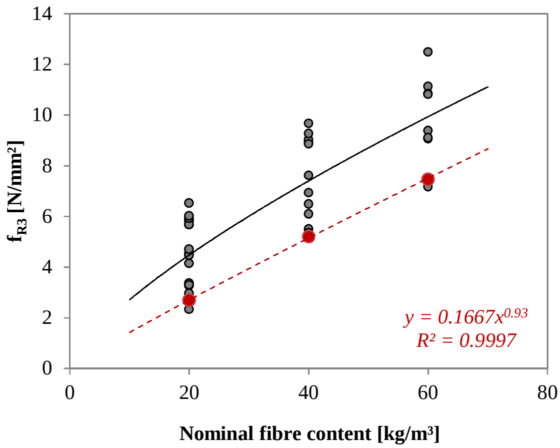

Fig. 8.6 – Relationship between $f_{Rk,3}$ and nominal fibre dosage based on Chapter 5 and mix IV-1

Given the correlation between $f_{Rk,3}$ and V_f shown in Fig. 8.3, the practical fibre dosage is obtained by the following relationship:

$$f_{Rk,3} = 0.167 V_f^{\,0.93} \qquad \text{Eq. 8.3}$$

From which the fibre content can be obtained as

$$V_f = \left(\frac{f_{Rk,3}}{0.167}\right)^{1.075} \qquad \text{Eq. 8.4}$$

For the design of girder IV-2, the required nominal fibre dosages are summarized in Table 8.5. Based on these values, it is decided to use a fibre dosage equal to 35 kg/m³.

Table 8.5 – Required characteristic value of $f_{R3,k}$ and corresponding nominal fibre content V_f

Model	$f_{Rk,3}$ [N/mm²]	$V_{f,req}$ [kg/m³]
RILEM	4.25	33
MC2010-A	4.2	33
MC2010-B	2.15	16
Proposed	4.11	32
Pl. Theory	0	0

Again, the post-cracking bending stress CMOD response is evaluated by means of standard three-point bending quality control tests. Fig. 8.7 shows the individual results as well as the average and characteristic line. In contrast to the SFRC mix IV-1 containing 20 kg/m³ of fibres, this SFRC mix shows a quasi pure-hardening behaviour and the performance of the SFRC is better than expected. Table 8.6 gives an overview of all obtained values of f_L and $f_{R,i}$.

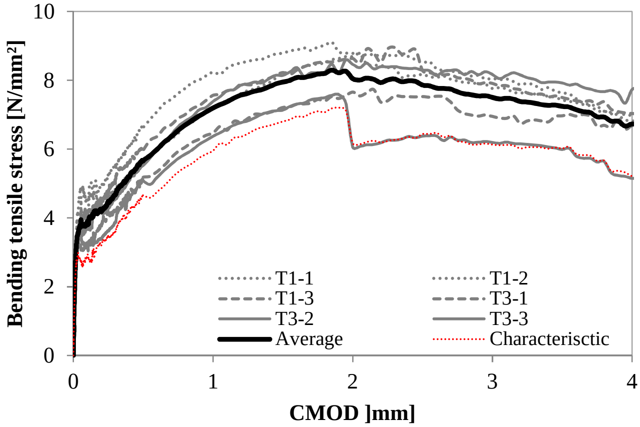

Fig. 8.7 – Stress-CMOD curves for SFRC mix IV-2

Table 8.6 - SFRC properties

Girder	Test	f_L [N/mm²]	$f_{R,1}$ [N/mm²]	$f_{R,2}$ [N/mm²]	$f_{R,3}$ [N/mm²]	$f_{R,4}$ [N/mm²]
IV-35	1	4.87	6.63	8.79	8.51	7.63
	2	3.97	5.64	8.19	8.17	7.42
	3	3.34	5.18	7.21	7.53	6.97
	4	3.79	5.98	8.23	8.29	7.50
	5	3.70	5.53	8.14	8.29	7.92
	6	3.50	5.07	7.13	6.38	5.99
	Average	3.81	5.67	7.95	7.86	7.24
	Char. Value	2.99	4.66	6.80	6.44	6.02

The difference between the post-cracking performance of both mixes IV-1 and IV-2 is relatively large. Fig. 8.8 shows the CoV over the entire range of CMOD.

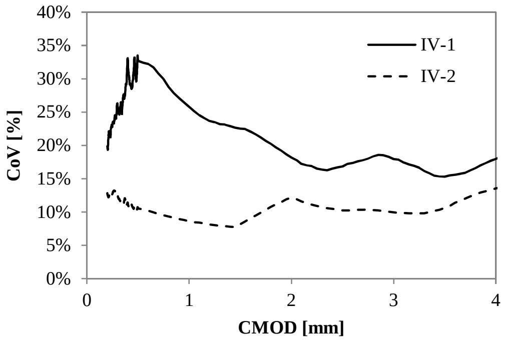

Fig. 8.8 – Variation of the scatter of residual stress as a function of CMOD for SFRC mix IV-1 and IV-2

From Fig. 8.8, it can be concluded that the overall quality performance of SFRC mix IV-1 is lower than expected and the CoV is higher than 15 %. In contrast, the CoV for SFRC mix IV-2 is about 10% only. This indicates a relatively better mix quality.

To exclude the possibility that this difference is due to an erroneous fibre content, the fibre content is verified both in the fresh and hardened state of the SFRC. The adopted methods to derive these contents are described in Chapter 5. The obtained measurement results are given in Table 8.7 and Table 8.8, indicating no significant anomalies in the fibre content (except for IV-2 (phase 2) for which somewhat lower fibre content has been measured).

Table 8.7 – Fibre content in the fresh state

Girder	T1 [kg/m³]	T2 [kg/m³]	T3 [kg/m³]	Average$V_{f,exp}$ [kg/m³]	St. Dev. [kg/m³]	COV
IV-1	23.6	-	19.6	21.6	2.8	13 %
IV-2	39.0	-	33.0	36.1	4.6	12 %

Table 8.8 – Fibre content in the hardened state

Girder	C1	C2	C3	C4	C5	Min. [kg/m³]	Max. [kg/m³]	Avg. [kg/m³]	CoV [-]
IV-1 (Phase 1)	22	-	21	20	-	20	22	21	5%
IV-1 (Phase 2)	15	23	19	24	17	15	24	20	20%
IV-2 (Phase 1)	39	27	39	39	-	27	39	36	17%
IV-2 (Phase 2)	29	31	26	31	-	26	31	29	8%

Finally, the bending quality control test database is further updated by implementing the three-point bending test results obtained for SFRC mix IV-2. Since, the performance of this mix is relatively better than all of the previously tested mixes, a beneficial effect on the correlation between $f_{Rk,3}$ and V_f is obtained. The newly updated relationship is shown in Fig. 8.9.

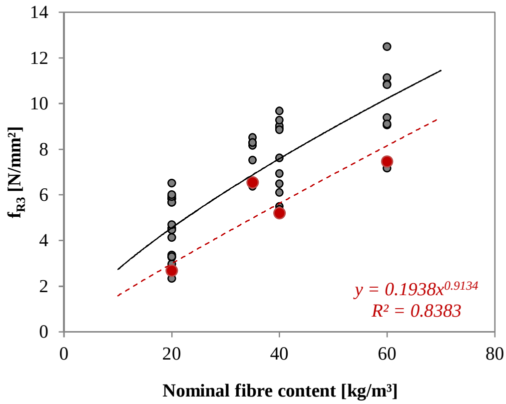

Fig. 8.9 – Correlation between $f_{Rk,3}$ and V_f taking into account bending test results of Chapter 5 and both girders IV-1 and 2.

8.3 Shear tests on the roof girders

8.3.1 Concrete strength properties

In the framework of full scale testing of the roof girders, additional quality control testing has been performed to determine the concrete strength properties of the SFRC in terms of concrete compression strength and post-cracking tensile strength. For the latter, 3-point bending tests have been performed according to EN 14651 [1]. The obtained results have been discussed in Section 8.2.4.

Compression tests have been performed to obtain the compressive cube strength at 2, 7, 14 and 28 days, as well as the cylinder strength at 7 and 28 days. The strength evolution of girders IV-1 and IV-2 is shown in Fig. 8.10. The measured strength values are given in Table 8.9 and Table 8.10.

Table 8.9 – Concrete cube strength at different ages

Girder	Age [days]	$f_{c,cub,1}$ [N/mm²]	$f_{c,cub,1}$ [N/mm²]	$f_{c,cub,1}$ [N/mm²]	$f_{c,cub,m}$ [N/mm²]	CoV
IV-1	3	52.1	56.0	57.5	55.2	5.1%
	7	66.4	58.6	52.9	59.3	11.4%
	14	73.0	70.8	70.8	71.5	1.8%
	28	65.0	81.1	79.4	75.2	11.8%
IV-2	2	49.5	48.7	47.9	48.7	1.6%
	7	63.4	63.4	59.0	61.9	4.1%
	14	58.9	68.4	64.6	64.0	7.5%
	28	74.7	71.3	76.9	74.3	3.8%

Table 8.10 – Concrete cylinder strength and modulus of elasticity at 7 and 28 days

Girder	Age [days]	$f_{c,cyl,1}$ [N/mm²]	$f_{c,cyl,2}$ [N/mm²]	$f_{c,cyl,3}$ [N/mm²]	$E_{c,cyl1}$ [N/mm²]	$E_{c,cyl1}$ [N/mm²]	E_{cm} [N/mm²]
IV-1	7	59.4	60.5	60.0	38250	35750	36100
	28	75.2	73.1	74.2	36450	37800	38000
IV-2	8	56.9	56.9	56.9	32550	32300	32400
	42	70.5	71.8	71.1	37900	35600	36750

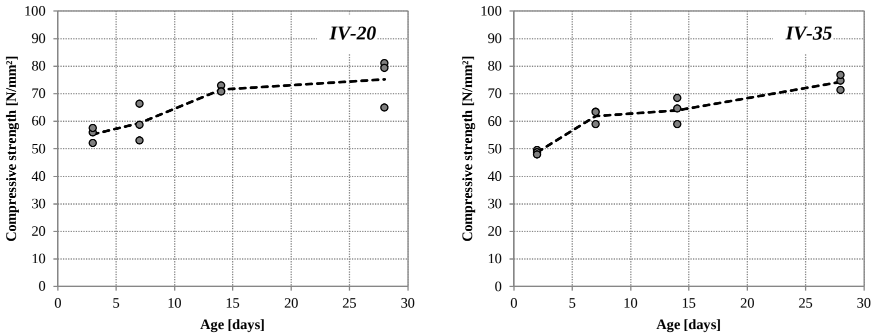

Fig. 8.10 – Cube compression strength development for girders IV-1 and IV-2

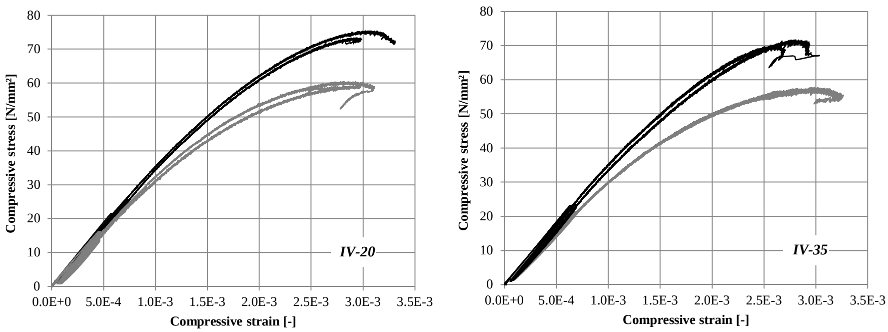

Fig. 8.11 – Compressive stress strain curves for girders IV-1 and IV-2.

As can be seen from Fig. 8.10 and Fig. 8.11, the required values of both cylinder and cube compressive strength for this concrete type C50/60 is obtained for both girders IV-1 and IV-2.

8.3.2 Shear test setup and measurement equipment

The maximum shear strength capacity of the girders IV-1 and IV-2 has been determined in laboratory conditions. For each girder, the shear strength is tested at both girder ends. In a first phase, the complete girder span is used and the shear span to depth ratio is taken equal to 2.5. In a second phase, the a/d-ratio is increased to 3.0 and the supports are moved in order to avoid influence of the first shear test (see Fig. 8.12).

The testing approach is quite similar as for the test series described in Chapter 5. The deflections under the load, at midspan and an extra third point are recorded. The load is applied deformation controlled with a hydraulic jack with a capacity of 1000 kN. For both the right and left supports, the girders can move freely in the longitudinal directions and the point at which the load is applied is assumed to be fixed.

The crack displacement behaviour is measured by means of horizontally and inclined (45°) extensometers with a base length of 200 mm and a maximum crack width measurement range of about 3-4 mm. The positioning of the extensometers is shown in Appendix F.

Further, the strain deformation is measured along the height at the section where the point load is applied. The strain deformation is both measured manually (top, bottom and centre) and digitally (only top and bottom). In this way the load-curvature of the beam can be obtained.

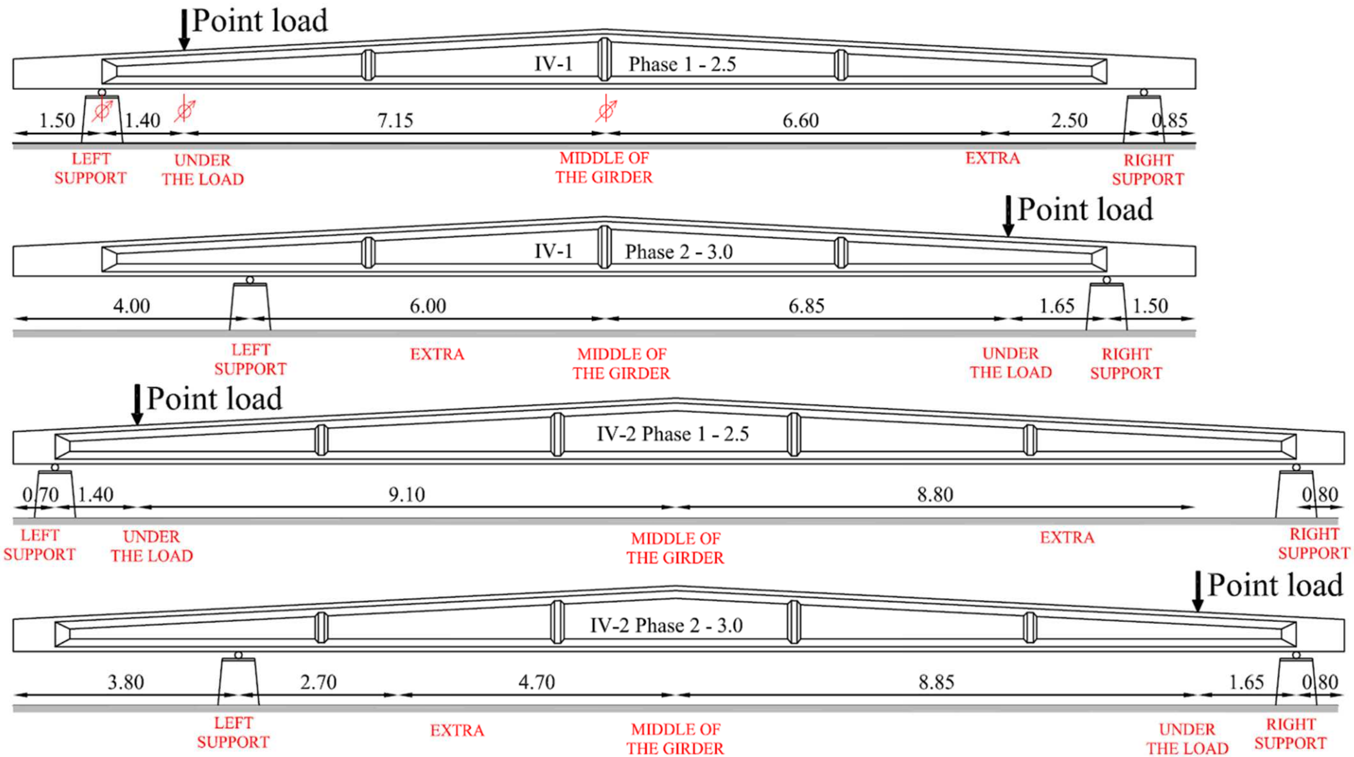

Fig. 8.12 – Schematic of the test setups adopted to determine the shear strength of girders IV-1 and IV-2

8.4 Test results & discussion

Both of the girders IV-1 and IV-2 have been tested with a shear span-to depth ratio respectively equal to 2.5 in phase 1 and 3.0 in phase 2. The obtained load-deflection curves for the conducted shear tests in both phase 1 and 2 are shown in Fig. 8.13 till Fig. 8.16.The black solid line is the load-deflection curve measured under to point-load and the solid grey line is the one measured under the midspan.

For shear test IV-2-2.5 (girder IV-2 tested in phase 1), it is remarked that prior to the application of a deflection-controlled loading, the girder has been accidentally subjected to a pre-loading equal to 400 kN, with the occurrence of shear cracks. However, the girder clearly did not fail during this accidental pre-loading and it was decided to restart the test under controlled conditions. Hence, the first branch of both the load deflection response and the shear crack propagation behaviour for the shear test IV-2-2.5 differ with the curves obtained for the other tests and the value at which first shear cracking occurs (V_{cr}) cannot be reported. Nevertheless, the shear test results are withhold for further investigation.

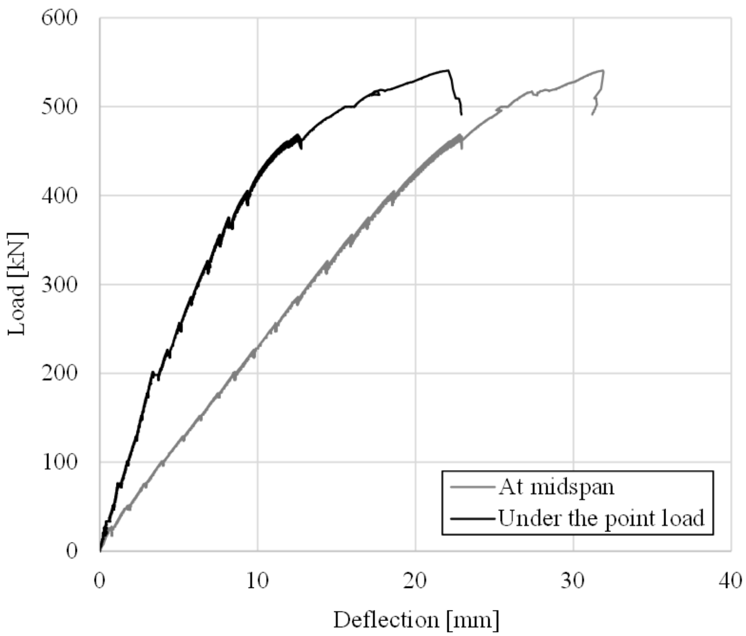

Fig. 8.13 – Load deflection response of girder IV-1 a/d=2.5

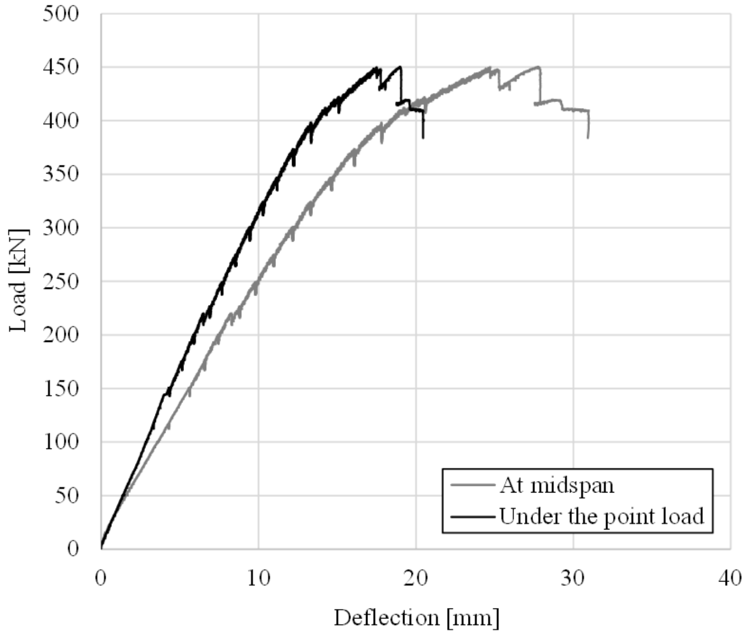

Fig. 8.14 – Load deflection response of girder IV-1 a/d=3.0

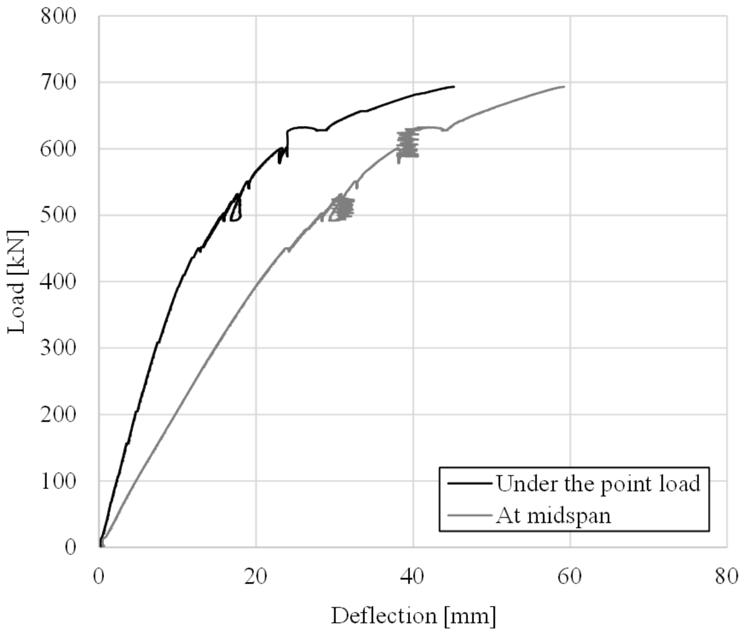

Fig. 8.15 – Load deflection response of girder IV-2 a/d=2.5

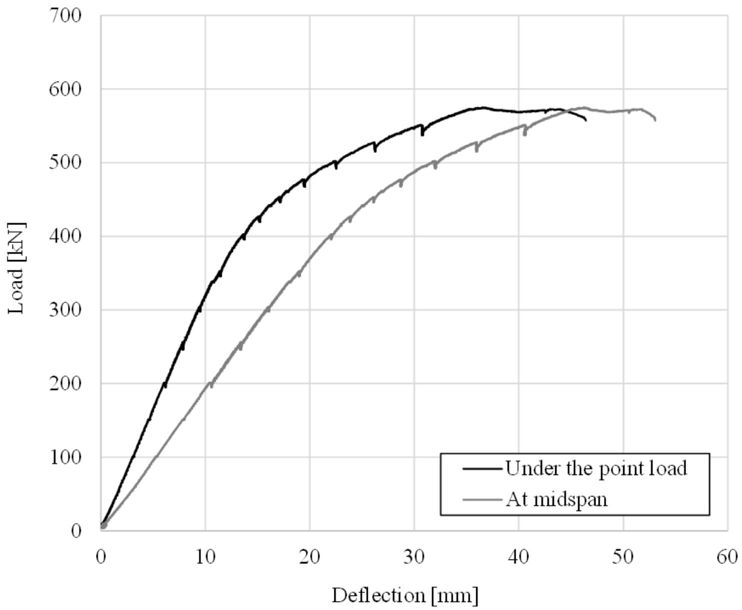

Fig. 8.16 – Load deflection response of girder IV-2 a/d=3.0

For girder IV-1, the first shear cracking load for both phase 1 and 2 is reached at a point-load for about 200 kN. Around a load of 350 to 400 kN, the first flexural cracks start to develop and the deflection tends to increase more rapidly for increasing shear loads. Finally, a shear failure has been observed for both phases. For the girder IV-2 tested in phase 2, the first shear cracks developed around 350 kN. At this load, the first flexural cracks also started to propagate.

The complete load-crack opening behaviour for the shear tests on the IV-girders is given in Appendix E.

In Table 8.11, the design shear strength V_{Rd} is compared with the cracking shear strength V_{cr}, the shear strength $V_{2.5}$ at a crack opening of 2.5 mm and the maximum obtained shear strength V_{max}.

Table 8.11 – Summary of design shear strength V_{Rd}, versus main shear load test results (V_{cr}, $V_{2.5}$, V_{max})

Girder test	V_{Rd} [kN]	V_{cr} [kN]	$V_{2.5}$ [kN]	V_{max} [kN]	V_{max}/V_{Rd}
IV-1-2.5	120	180	410	492	4.10
IV-1-3.0	120	189	344	398	3.31
IV-2-2.5	203	N/A	595	648	3.19
IV-2-3.0	203	320	512	523	2.58

A large safety factor between the design resistance V_{Rd} and shear load test results (V_{cr}, $V_{2.5}$, V_{max}) is observed. This means that at the load level V_{Rd} the girders are still uncracked.

Furthermore, a ratio V_{max}/V_{Rd} of 2.5 or more is obtained. With respect to the observed model uncertainty in Section 7.4, the obtained ratio's between V_{max} and V_{Rd} yield a target reliability index higher than β=3.8 (cf. Eq. 7.29).

8.5 Conclusions

The feasibility of the considered design models, among which the proposed engineering model, for the design calculation of prestressed precast girders has been demonstrated for the specific case of IV-shaped roof girders. After being designed, the two considered roof girders were produced and tested, demonstrating the applicability of SFRC for the shear strength of prestressed precast girders, both in terms of design and resulting safe resistance performance.

As the design models allow the dimensioning of the girders in terms of the characteristic post-cracking tensile strength ($f_{Rk,3}$) to be achieved by the SFRC, a SFRC mix design is needed to guarantee the required post-crakcing tensile strength. The SFRC mix design correlates the post-cracking tensile strength with a practical fibre dosage (V_f). On the other hand, frequent testing of the flexural response of SFRC mixes has to be done in order to evaluate the evolution of SFRC mix quality and to obtain proper correlations between $f_{R3,k}$ and V_f. It is clear that for economical applications of steel fibres as shear reinforcement, high quality SFRC mixes should be executed in the production environment so that scatter on the post-cracking tensile response of the SFRC is kept within boundaries and hence more beneficial values of $f_{R3,k}$ are obtained for a given concrete type, fibre type and fibre dosage. In the framework of the SFRC mix of the two tested girders IV-1 and IV-2, it was observed that the SFRC post-cracking tensile response of IV-1 was somewhat lower than expected, while the opposite was obtained for IV-2.Only when the increase of $f_{Rk,3}$ values (increased quality of the SFRC mix in production environment) can be guaranteed for a sufficiently long manufacturing period, the relationhsip between V_f and $f_{Rk,3}$ can be optimized. From the moment quality control tests yield lower values, immediate remediation actions may be needed in order to safely garantee a $f_{Rk,3}$ value as a function of fibre dosage. Mix quality can be increased by increasing the volume of SFRC being cast in one batch, by adding fibres automatically, improve concrete mix proportions as a function of fibre type and dosage, etc.

For the tested roof girders a large safety margin (factor 2.58 and higher) was confirmed between the design value of the shear resistance (V_{Rd}) and the experimentally obtained shear capacity (V_{max}). This corresponds with the intended design approach, and so to fulfil the required target reliability index β = 3.8.

8.6 References

[1] CEN. (2005). "EN 14651 - Test method for metallic fibered concrete - measuring the flexural tensile strength". Brussels, Belgium, CEN.

9 CONCLUSIONS AND FUTURE PERSPECTIVES

9.1 General

In the framework of this doctoral study, analytical, numerical and experimental work has been conducted in order to investigate the mechanics of SFRC on both the micro, meso- and macroscale level, in relation to the shear behaviour of SFRC and in view of using SFRC to replace traditional stirrups in prestressed precast girders.

On the micro-scale level, existing models describing the pull-out behaviour of hooked-end fibres are evaluated and a new method to implement the single fibre pull-out behaviour into a finite element model has been proposed. This finite element model gives a good exposure on the 3D numerical prediction of SFRC quality control tests in 3 or 4-point bending. The model includes the use of stochastic sampling of the fibre distribution in the concrete matrix. This allows to numerically estimate the scatter which can be obtained on the post-cracking tensile behaviour of SFRC. The model proved also to be feasible for the prediction of bending behaviour involving multiple cracking.

On the meso-scale level, both the post-cracking behaviour of SFRC subjected to Mode I and a mixed mode crack opening behaviour has been studied. Based on the bending tests conducted on notched prisms and inherent inverse analysis, a simplified yet accurate tri-linear Mode I constitutive law for SFRC has been proposed. Further, the physical meaning of the post-cracking resistance under Mode I have been confirmed by comparing the trilinear curve with respect to an analytical procedure which calculates the Mode I constitutive behaviour, starting from the single fibre pull-out behaviour. For the latter, a revised model as developed as part of the micro-scale level study is applied.

The mixed mode or shear friction behaviour of SFRC has been studied by means of direct shear push-through tests. It was found that the obtained shear stress capacity of cracked SFRC linearly increases with fibre dosage and concrete compressive strength. The observed crack dilatation is not affected by fibre dosage nor concrete strength and hence being significantly dependent on the adopted test setup.

Similar to the model developed to obtain a mode I constitutive law, a direct shear behaviour model has been developed based on the experimental observation, taking into account aggregate interlock, crack dilatation and the transverse pull-out of fibres. However, in order to verify the more general applicability of the developed model for the shear friction capacity of SFRC, further testing is needed by the international research community. This testing should involve test methods with accurate measurement of both crack opening and dilatation. Indeed, this level of detail in testing of the direct shear behaviour was not found to be reported in most literature accessible to the author, yet is a basic requirement to use literature data for evaluation of the proposed model.

On the macro-scale level, extensive experimental work has been conducted on full scale prestressed precast girders. This testing involved 23 tests on 9 I-shaped girders and 4 tests on 2 IV-shaped roof girders. This experimental work has been further extended in the analytical prediction of shear resistance models as well as shear design models, compliant with a target reliability index.

In the framework of the analytical study of the full scale girders, a shear behaviour model has been developed. This model is conceived as a sectional analysis tool based on the Modified Compression Field Theory (MCFT), which is modified in order to deal with the constitutive laws for SFRC. The model gives a thorough implementation of physical behaviour aspects related to the shear mechanism and allows detailed and fairly accurate prediction of the shear behaviour, e.g. in terms of shear capacity and shear load-crack width propagation. Based on the comparison between modelled and experimental curves, and performing a sensitivity analysis, it is found that the average crack distance is one of the major parameters involved to accurately estimate the shear strength of SFRC by means of the sectional model.

Whereas the developed MCFT sectional analysis tool predicts the complete shear response, the MCFT approach can also be used to evaluate only the ultimate shear strength.

This makes the MCFT model less complex, yet it remains an iterative calculation procedure. Such a MCFT approach for shear strength evaluation of SFRC member has been introduced relatively recently in the Model Code 2010 (mentioned in the commentary sections, and designated in this work as MC2010-B model).

Given that the iterative calculation procedure of the MCFT approach is less desirable for straightforward design calculations in engineering practice, a new resistance model is proposed in this work. This proposed engineering model is based on the iterative MCFT model, yet converting it in a closed-form solution through observed correlations with physical phenomena influencing the shear strength such as dowel action, shear span to depth ratio, size effect and level of prestress.

Finally, a shear test database has been assembled comprising 99 test results on reinforced and prestressed concrete members. The assembled database only contains shear test data with sufficient level of detail in the characterisation of the post-cracking behaviour of the related SFRC mix. Based on this database, the accuracy has been evaluated of different resistance models provided in design guidelines, as well as for the newly proposed engineering model. It can be concluded that the empirical based formulations (RILEM, MC2010-A) have a higher model uncertainty than the more rational models (MC2010-B, proposed engineering model and plastic theory), especially for the case of prestressed concrete members. The proposed engineering model has been found to be feasible for both prestressed and reinforced concrete cases. Together with the MC2010-B model, it gives the most consistent and accurate predictive capacity for the complete range of variables.

9.2 Recommendations for design

Further to the evaluation of the resistance models, their use as design models aiming for a target reliability index $\beta = 3.8$ has been evaluated, given the observed accuracy of the resistance models with respect to the database of test results. It has been found that for the RILEM, MC2010-A and plasticity theory models, the currently specified safety factor equal to 1.5 is insufficient to provide a safe design. This value should be between 2 and 3, depending on the considered model. For the MC2010-B model and the proposed engineering model, the model safety factor is in the range of 1.5-2.25.

The feasibility of the considered design models, among which the proposed engineering model, for the design calculation of the shear capacity when replacing stirrups by SFRC has been demonstrated in this work. This includes the proposal of adapted safety factors to fulfill the required target reliability index and focussing on the design of prestressed precast girders.

As the design models deal with the dimensioning of the girders in terms of the characteristic post-cracking tensile strength ($f_{Rk,3}$) to be achieved by the SFRC, a SFRC mix design is needed to guarantee the required post-cracking tensile strength. The SFRC mix design correlates the post-cracking tensile strength with a practical fibre dosage (V_f). For an economical application of steel fibres as shear reinforcement, high quality SFRC mixes should be executed in the precast production environment so that scatter on the post-cracking tensile response of the SFRC is kept within boundaries and hence more beneficial values of $f_{R3,k}$ are obtained for a given concrete type, fibre type and fibre dosage.

Resulting from this doctoral study the following design engineering model is proposed:

$$V_{Rd,proposed} = \frac{1}{\gamma_M}\left[0.388\sqrt{1+\frac{\sigma_{cp}}{f_{ctk}}}\left(1+\sqrt{\frac{200}{d}}\right)\left(3\frac{d}{a}\rho_l\right)^{\frac{1}{3}}\sqrt{f_{ck}}+f^*_{Ftu}\left(1+4\frac{\sigma_{cp}}{f_{ck}}\right)\right]b_w z$$

In which γ_M is the model safety factor for design, σ_{cp} is the compressive stress at neutral axis; f_{ctk} is the characteristic tensile strength of the concrete, d is the effective depth, a is the shear span, ρ_l is the longitudinal reinforcement ratio, f_{ck} is the characteristic concrete cylinder strength, f_{cm} is the average concrete cylinder strength, b_w is the web width, z is the internal lever arm and f^*_{Ftu} is the post-cracking tensile capacity of SFRC given by

$$f^*_{Ftu} = \min\begin{cases} f_{Ftuk} \\ f_{ctk}\left(1-\frac{2\sigma_{cp}}{f_{cm}}\right)\end{cases}$$

9.3 Recommendations for future research

The research work performed in this doctoral study has contributed to obtain a better understanding of the shear behaviour of SFRC, as well as the predictive modelling of this behaviour, especially towards the replacement of traditional stirrups by SFRC for prestressed precast concrete girders. In line with the obtained results in this work, further research topics in this field can be suggested as follows.

For higher fibre dosages, mutual interaction of fibres has been observed to become more important. This means that local damage of the concrete at the fibre exit point with respect to single fibre pull-out during crack bridging, may influence the fibre anchorage capacity of nearby fibres as well. The proposed models in this work describing the post-cracking material behaviour in tension or direct shear are not taking this phenomenon of mutual fibre interaction into account in a systematic way, and gives room for further improvement of the developed analytical models.

In modelling the SFRC constitutive behaviour in bending, a finite element model has been proposed. This non-linear two-phase model (concrete and single fibres) makes use of specific fibre elements, whereby the fibres are modelled as cable elements with fixed ends and whereby an equivalent stress-strain constitutive law has been developed to match the behaviour of the cable elements with the pull-out behaviour of single fibres. This approach allows to avoid the introduction of more complex interface elements between concrete and fibres. This FEM approach allows to predict the multi-cracking behaviour of SFRC in bending, as well as the stochastic treatment of fibres distribution and orientation in a SFRC volume. The latter aspect can be used to estimate numerically the scatter of the post-cracking tensile behaviour of SFRC. The feasibility to apply the FEM approach for more large scale members subjected to bending has however not yet been verified. Also, to extend the finite element approach into shear behaviour, a new crack model should be developed by taking into account the crack opening behaviour for different combinations of crack opening and slip. As a result, a constitutive law for SFRC has to be determined in a three dimensional space.

Reviewing the available literature on direct shear tests on SFRC, it was observed that mostly only the ultimate shear strength is reported and detailed information on the shear crack propagation behaviour in direct shear is missing. This shear crack propagation behaviour was however found to be quite different depending on the applied direct shear test method, making comparison of reported data on direct shear strength difficult. Further research work in this direction is needed to increase the understanding of the direct shear behaviour of SFRC and its correlation (or lack thereof) with the mode I material characterization more standardly performed on SFRC mixes.

Increasing the shear capacity of concrete members by SFRC also means that higher forces will act in the compression struts in between the shear cracks. As a result, in the fibre anchorage zone of the concrete adjacent to the shear crack, a biaxial stress state is acting which becomes more important for increasing stress levels (for increasing fibre dosage and related shear capacity). In this doctoral study, this phenomenon has been observed and taken into consideration by means of reduction factor on the post-cracking tensile capacity of the SFRC. Further research is however needed for a more proper coverage of the biaxial stress state, and to derive improved proposals for the aforementioned reduction factor for design.

As outcomes of this study a detailed analytical MCFT model has been derived, as well as an engineering model for design purpose, in predicting the shear behaviour and capacity of SFRC members. These models are based on physical parameters and behavioural aspects, opposite to more empirical based models which are only applicable for specific SFRC mixes. This ability of the proposed models to be more generic applicable, needs however to be verified further by the international research community. Hence, additional testing of girders should be performed for varying parameters such as a/d-ratio, concrete compressive strength, amount of prestressing, etc.

Looking into design models, it is important that model safety factors are calibrated in a proper way, to guarantee the target reliability index specified in Eurocode 0. In current design provisions the safety factors for SFRC shear design are often taken nominally equal to those usually applied in concrete calculations (i.e. 1.5), because of lack of information to establish the safety factor. In this study, a thorough study has been made to calculate the required design safety factors, making use of assumptions and established accuracy of models with respect to a database of test results. Upon coming more information available and further improving on the methodology and assumptions applied in this work to calculate the safety factors, this work can be further extended in the future, so to establish proper safety factors and to avoid over-conservative designs.

APPENDIX A SHEAR TEST DATABASE

A.1 BRITE EURAM [1] - 2002

d [mm]	A_c [mm²]	ρ_l [%]	σ_{cp} [Mpa]	h_f [mm]	b_f [mm]	b_w [mm]	a/d	f_{cm} [Mpa]	Fibre Type	$f_{R3,m}$ [Mpa]	V_{test} [kN]
260	60000	1.81	0.00	0	200	200	1.54	42.4	RC 65-60 BN	4.87	300
260	60000	1.81	0.00	0	200	200	4.04	42.4	RC 65-60 BN	4.87	117
260	60000	2.83	0.00	0	200	200	3.50	38.3	RC 65-60 BN	4.85	113
460	100000	2.73	0.00	0	200	200	3.37	38.3	RC 65-60 BN	4.85	136
560	120000	2.73	0.00	0	200	200	3.48	38.3	RC 65-60 BN	4.85	192
460	124000	2.80	0.00	80	500	200	3.37	38.3	RC 65-60 BN	4.85	169
460	130000	2.80	0.00	100	500	200	3.37	38.3	RC 65-60 BN	4.85	133
460	145000	2.80	0.00	150	500	200	3.37	38.3	RC 65-60 BN	4.85	138
460	169000	2.80	0.00	230	500	200	3.37	38.3	RC 65-60 BN	4.85	214
260	60000	2.83	0.00	0	200	200	3.50	37.2	RC 65-60 BN	4.74	95
410	90000	3.09	0.00	0	200	200	3.34	37.2	RC 65-60 BN	4.74	125
560	120000	2.73	0.00	0	200	200	3.48	37.2	RC 65-60 BN	4.74	133
460	130000	2.80	0.00	100	500	200	3.37	37.2	RC 65-60 BN	4.74	143
460	145000	2.80	0.00	150	500	200	3.37	37.2	RC 65-60 BN	4.74	223
460	182500	2.80	0.00	150	750	200	3.37	37.2	RC 65-60 BN	4.74	219
460	220000	2.80	0.00	150	1000	200	3.37	37.2	RC 65-60 BN	4.74	206
260	60000	3.55	0.00	0	200	200	3.46	47.6	RC 65-60 BN	4.22	155
260	60000	1.16	0.00	0	200	200	2.50	38.6	RC 65-60 BN	3.59	108
260	60000	3.55	0.00	0	200	200	3.46	43.2	RC 65-60 BN	2.65	120
260	60000	1.81	0.00	0	200	200	1.54	40.7	RC 65-60 BN	1.66	280
260	60000	1.81	0.00	0	200	200	4.04	40.7	RC 65-60 BN	1.66	83
260	60000	3.55	0.00	0	200	200	3.46	46.4	RC 65-60 BN	1.30	110

d [mm]	A_c [mm²]	ρ_l [%]	σ_{cp} [Mpa]	h_f [mm]	b_f [mm]	b_w [mm]	a/d	f_{cm} [Mpa]	Fibre Type	$f_{R3,m}$ [Mpa]	V_{test} [kN]
260	60000	1.16	0.00	0	200	200	2.50	39.1	RC 65-60 BN	1.17	83
260	60000	1.81	0.00	0	200	200	2.50	39.1	RC 65-60 BN	1.17	108
260	60000	1.81	0.00	0	200	200	2.50	38.6	RC 65-60 BN	0.98	144

A.2 Conforti [2] - 2014

d [mm]	A_c [mm²]	ρ_l [%]	σ_{cp} [Mpa]	h_f [mm]	b_f [mm]	b_w [mm]	a/d	f_{cm} [Mpa]	Fibre Type	$f_{R3,m}$ [Mpa]	V_{test} [kN]
763	170000	1.32	1.30	0	150	150	2.49	34.3	PP	3.00	284
295	195700	1.22	0.00	0	890	890	2.50	26.0	PP	3.00	605
761	260000	0.99	0.00	0	300	300	2.50	34.3	PP	3.00	381
761	260000	0.99	0.00	0	300	300	2.50	34.3	PP	3.00	405
763	170000	1.10	0.00	0	150	150	2.49	34.3	PP	3.00	205
763	170000	1.10	0.00	0	150	150	2.49	34.3	PP	3.00	247
563	140000	1.12	0.00	0	150	150	2.50	34.3	PP	3.00	166
563	140000	1.12	0.00	0	150	150	2.50	34.3	PP	3.00	198

A.3 Cuenca [3]- 2013

d [mm]	A_c [mm²]	ρ_l [%]	σ_{cp} [Mpa]	h_f [mm]	b_f [mm]	b_w [mm]	a/d	f_{cm} [Mpa]	Fibre Type	$f_{R3,m}$ [Mpa]	V_{test} [kN]
675	151000	1.87	11.05	100	260	100	3.00	65.0	65/40BN	4.38	326
675	165000	1.87	10.11	100	400	100	3.00	63.5	65/40BN	4.77	390
675	165000	1.87	10.11	100	400	100	3.00	70.0	65/40BN	4.68	428
720	170000	1.75	9.81	100	400	100	2.80	59.5	65/40BN	5.96	420
675	185000	1.87	9.02	100	600	100	3.00	65.4	65/40BN	6.24	392
675	185000	1.87	9.02	100	600	100	3.00	65.9	65/40BN	5.55	347
440	125000	1.12	0.00	0	250	250	3.00	38.7	Hooked 50/.80	6.00	235
940	250000	1.07	0.00	0	250	250	3.00	32.1	Hooked 50/.80	6.00	351

d [mm]	A_c [mm²]	ρ_l [%]	σ_{cp} [Mpa]	h_f [mm]	b_f [mm]	b_w [mm]	a/d	f_{cm} [Mpa]	Fibre Type	$f_{R3,m}$ [Mpa]	V_{test} [kN]
1440	375000	1.01	0.00	0	250	250	3.00	33.1	Hooked 50/.80	6.00	554
440	125000	1.12	0.00	0	250	250	3.00	38.7	Hooked 50/.80	5.00	240
940	250000	1.07	0.00	0	250	250	3.00	32.1	Hooked 50/.80	5.00	272
1440	375000	1.01	0.00	0	250	250	3.00	33.1	Hooked 50/.80	5.00	484

A.4 Minelli [4]- 2005

d [mm]	A_c [mm²]	ρ_l [%]	σ_{cp} [Mpa]	h_f [mm]	b_f [mm]	b_w [mm]	a/d	f_{cm} [Mpa]	Fibre Type	$f_{R3,m}$ [Mpa]	V_{test} [kN]
630	200000	5.61	15.54	125	600	120	3.49	78.9		8.61	709
630	200000	5.61	15.54	125	600	120	3.49	71.6		8.61	573
630	200000	5.61	15.54	125	600	120	3.49	71.6		8.61	607
630	200000	5.61	15.54	125	600	120	3.49	70.0		3.18	574
630	200000	5.61	15.54	125	600	120	3.49	71.1		3.18	579
630	200000	5.61	15.54	125	600	120	3.49	71.1		3.18	542
435	96000	1.04	0.00	0	200	200	2.51	46.1	-	5.99	223
435	96000	1.04	0.00	0	200	200	2.51	26.5	-	4.42	142
435	96000	1.04	0.00	0	200	200	2.51	48.3	-	3.12	191
435	96000	1.04	0.00	0	200	200	2.51	19.6		3.06	180
435	96000	1.04	0.00	0	200	200	2.51	30.5	-	3.03	141
435	96000	1.04	0.00	0	200	200	2.51	19.6	-	2.67	134
435	96000	1.04	0.00	0	200	200	2.51	26.5	-	2.55	120

A.5 Parmentier [5] - 2012

d [mm]	A_c [mm²]	ρ_l [%]	σ_{cp} [Mpa]	h_f [mm]	b_f [mm]	b_w [mm]	a/d	f_{cm} [Mpa]	Fibre Type	$f_{R3,m}$ [Mpa]	V_{test} [kN]
270	60000	1.16	0.00	0	200	200	0.5	42.7	UN	3.7	106.1
270	60000	1.16	0.00	0	200	200	0.5	42.7	UN	3.7	106.1

d [mm]	A_c [mm²]	ρ_l [%]	σ_{cp} [Mpa]	h_f [mm]	b_f [mm]	b_w [mm]	a/d	f_{cm} [Mpa]	Fibre Type	$f_{R3,m}$ [Mpa]	V_{test} [kN]
270	60000	1.16	0.00	0	200	200	2.5	42.7	UN	3.7	122.4
270	60000	1.16	0.00	0	200	200	2.5	42.7	UN	3.7	111.3
270	60000	1.16	0.00	0	200	200	1.5	40.1	CF	2.9	140.1
270	60000	1.16	0.00	0	200	200	1.5	40.1	CF	2.9	148.4
270	60000	1.16	0.00	0	200	200	2.5	40.1	CF	2.9	104.9
270	60000	1.16	0.00	0	200	200	2.5	40.1	CF	2.9	123
270	60000	1.16	0.00	0	200	200	0.5	42.7	CF	2.8	98.7
270	60000	1.16	0.00	0	200	200	0.5	42.7	CF	2.8	101.5
270	60000	1.16	0.00	0	200	200	2.5	42.7	CF	2.8	99.5
270	60000	1.16	0.00	0	200	200	2.5	42.7	CF	2.8	90.6
270	60000	1.16	0.00	0	200	200	1.5	40.2	UNCF	2.7	167.4
270	60000	1.16	0.00	0	200	200	1.5	40.2	UNCF	2.7	133.4
270	60000	1.16	0.00	0	200	200	2.5	40.2	UNCF	2.7	123
270	60000	1.16	0.00	0	200	200	2.5	40.2	UNCF	2.7	99.4
270	60000	1.16	0.00	0	200	200	1.5	43.1	Sy	2.1	128.1
270	60000	1.16	0.00	0	200	200	1.5	43.1	Sy	2.1	162.6
270	60000	1.16	0.00	0	200	200	2.5	43.1	Sy	2.1	105.5
270	60000	1.16	0.00	0	200	200	2.5	43.1	Sy	2.1	118
270	60000	1.16	0.00	0	200	200	0.5	39.9	UN	1.7	104.8
270	60000	1.16	0.00	0	200	200	0.5	39.9	UN	1.7	95.2
270	60000	1.16	0.00	0	200	200	2.5	39.9	UN	1.7	81.3
270	60000	1.16	0.00	0	200	200	2.5	39.9	UN	1.7	121.9

A.6 De Pauw [6] - 2008

d [mm]	A_c [mm²]	ρ_l [%]	σ_{cp} [Mpa]	h_f [mm]	b_f [mm]	b_w [mm]	a/d	f_{cm} [Mpa]	Fibre Type	$f_{R3,m}$ [Mpa]	V_{test} [kN]
813	144878	1.57	8.19	110	300	80	2.75	52.0	RC 80 60 BP	6.35	542
813	144878	1.57	8.19	110	300	80	2.75	44.6	RC 80 60 BP	4.82	509

A.7 Current study

d [mm]	A_c [mm²]	ρ_l [%]	σ_{cp} [Mpa]	h_f [mm]	b_f [mm]	b_w [mm]	a/d	f_{cm} [Mpa]	Fibre Type	$f_{R3,m}$ [Mpa]	V_{test} [kN]
886	198600	1.78	9.23	125	400	100	2.5	56.2	RC 80 30 CP + RC 80 60 BP	9.88	696
886	198600	1.78	9.23	125	400	100	3	56.2	RC 80 30 CP + RC 80 60 BP	9.88	594
886	198600	1.78	9.23	125	400	100	2.5	62.0	RC 80 30 CP	9.77	672
886	198600	1.78	9.23	125	400	100	3	62.0	RC 80 30 CP	9.77	627
886	198600	1.78	9.23	125	400	100	2.5	62.0	RC 80 30 CP	9.77	721
886	198600	1.78	9.23	125	400	100	2.5	70.4	RC 80 30 CP	8.15	798
886	198600	1.78	9.23	125	400	100	2.5	70.4	RC 80 30 CP	8.15	809
886	198600	1.78	9.23	125	400	100	2.5	70.4	RC 80 30 CP	8.15	737
886	198600	1.78	9.23	125	400	100	2.5	58.8	RC 80 30 CP	7.08	744
886	198600	1.78	9.23	125	400	100	3	58.8	RC 80 30 CP	7.08	599
886	198600	1.78	9.23	125	400	100	2.5	64.8	RC 80 30 CP	5.83	786
886	198600	1.78	9.23	125	400	100	3	64.8	RC 80 30 CP	5.83	570
886	198600	1.78	9.23	125	400	100	2.5	41.0	RC 80 30 CP	4.09	756
886	198600	1.78	9.23	125	400	100	2.5	41.0	RC 80 30 CP	4.09	781
886	198600	1.78	9.23	125	400	100	2.5	41.0	RC 80 30 CP	4.09	609

A.8 References

[1] Rosenbusch, J., Teutsch, M. (2003). "Shear Design with σ-ε Method". *RILEM TC 162-TDF Workshop, Bochum, Germany*.

[2] Conforti, A., Tinini, A., Minelli, F., Plizzari, G., Moro, S. (2014). "Structural applicability of polypropylene fibres: deep and wide-shallow beams subjected to shear". *FRC 2014 Joint ACI-fib International Workshop - Fibre Reinforced Concrete: from Design to Structural Applications, Montréal, Canada*, pp. 341-355.

[3] Cuenca, E., Serna, P. (2013). "Shear behavior of prestressed precast beams made of self-compacting fiber reinforced concrete". *Construction and Building Materials*, Vol. 45(August 2013), pp. 145–156.

[4] Minelli, F. (2005). "*Plain and Fibre Reinforced Concrete Beams under Shear Loading: Structural Behaviour and Design Aspects*" (PhD-thesis). Brescia, University of Brescia.

[5] Parmentier, B., Cauberg, N., Vandewalle, L. (2012). "Shear resistance of macro-synthetic and steel fibre reinforced concrete beams without stirrups". *BEFIB 2012, Guimaraes*.

[6] De Pauw, P., Taerwe, L., Van den Buverie, N., Moerman, W. (2008). "Steel fibre concrete as an alternative for traditional shear reinforcement in pretensioned concrete beams". *7th international RILEM symposium on fibre reinforced concrete: design and applications (BEFIB 2008)*, pp. 887-898.

APPENDIX B SFRC PROPERTIES OF GIRDERS

B.1 BENDING TENSILE STRENGTH

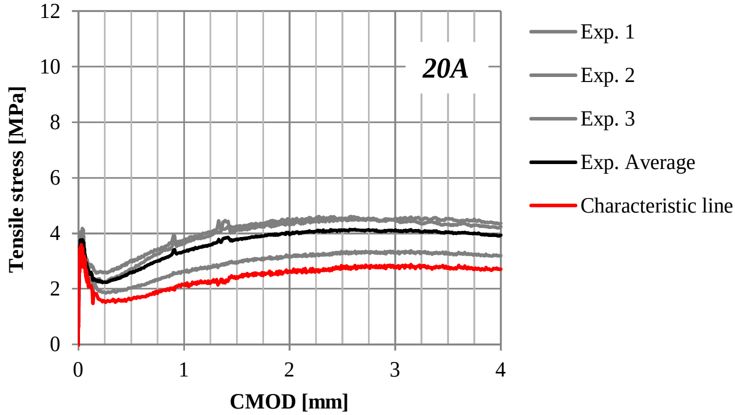

Fig. B1 – Bending tensile stress – CMOD curves for girder 20A

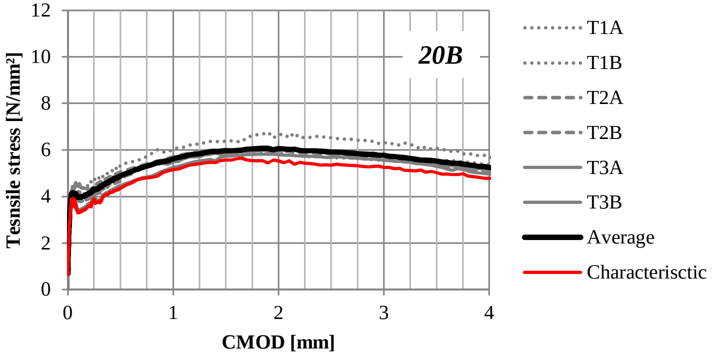

Fig. B2 – Bending tensile stress – CMOD curves for girder 20B

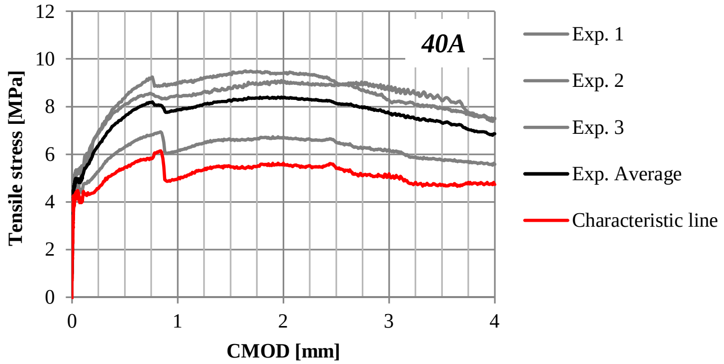

Fig. B3 – Bending tensile stress – CMOD curves for girder 40A

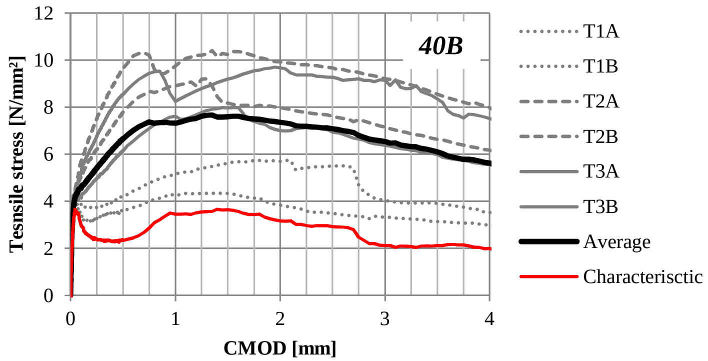

Fig. B4 – Bending tensile stress – CMOD curves for girder 40A

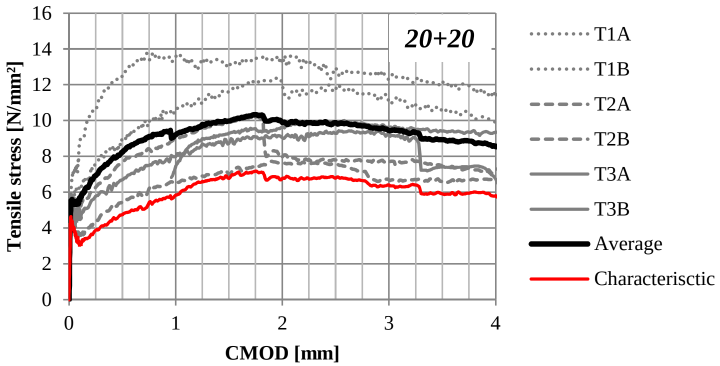

Fig. B5 – Bending tensile stress – CMOD curves for girder 40A

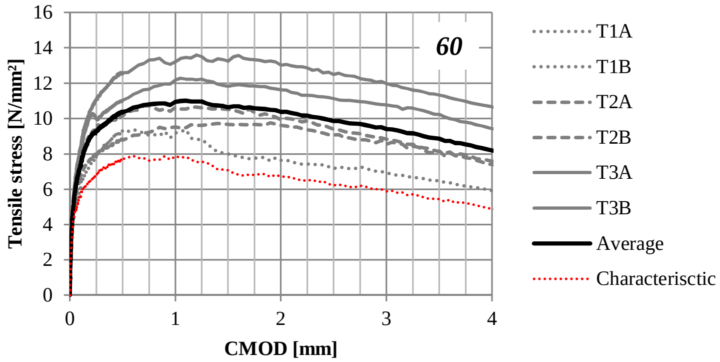

Fig. B6 – Bending tensile stress – CMOD curves for girder 40A

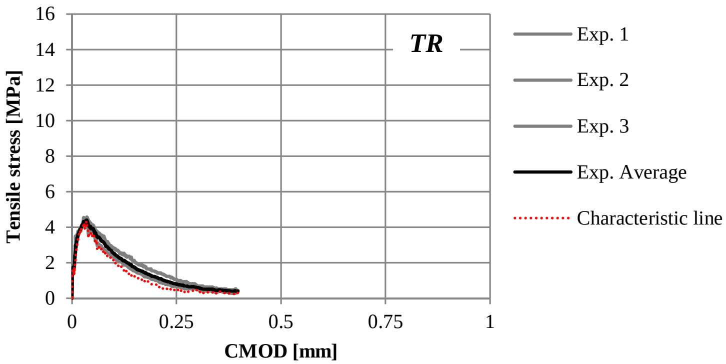

Fig. B7 – Bending tensile stress – CMOD curves for girder 40A

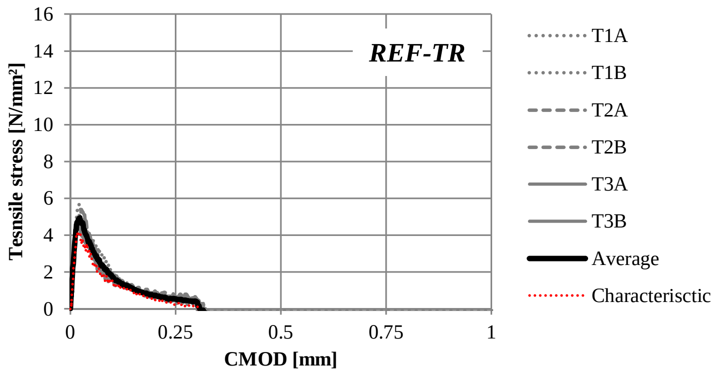

Fig. B8 – Bending tensile stress – CMOD curves for girder 40A

Table B1 - f_{Ri} values for all tested girders

Girder	Test	f_L [N/mm²]	f_{R1} [N/mm²]	f_{R2} [N/mm²]	f_{R3} [N/mm²]	f_{R4} [N/mm²]
20A	1	3.76	3.03	4.26	4.55	4.31
	2	3.55	2.71	4.11	4.46	4.53
	3	3.49	2.04	2.98	3.27	3.26
40A	1	4.77	8.09	8.76	8.93	8.25
	2	4.77	6.31	6.60	6.49	5.76
	3	5.29	8.37	9.37	9.02	7.96
20B	1	4.16	4.88	5.92	5.67	5.56
	2	4.14	5.29	4.67	4.81	4.86
	3	3.88	4.43	4.74	4.69	4.67
	4	4.03	4.88	4.67	4.70	4.70
	5	3.82	4.47	4.57	4.55	4.55
	6	4.31	4.94	4.88	4.91	4.91
40B	1	3.89	4.21	5.62	5.50	3.91
	2	3.80	3.59	4.34	3.49	3.14
	3	4.72	7.79	8.17	7.62	6.63
	4	4.93	9.66	10.24	9.67	8.55
	5	4.62	8.55	9.19	9.27	8.35
	6	4.13	6.16	7.96	6.94	5.99
20+20	1	6.00	11.67	12.37	11.80	11.14
	2	6.07	8.88	11.67	11.85	10.68
	3	5.28	7.66	9.92	7.79	7.44
	4	4.74	5.46	6.99	7.56	6.58
	5	-	-	9.31	9.84	9.41
	6	5.86	6.68	8.72	9.29	7.41
60	1	-	-	-	-	-
	2	3.97	9.32	8.00	7.17	6.44
	3	4.80	8.78	9.67	9.06	8.17
	4	5.01	10.16	10.51	9.39	8.12
	5	4.98	12.57	13.24	12.49	11.33
	6	4.91	11.04	11.82	11.13	10.23

B.2 CYLINDER COMPRESSIVE STRENGTH AND MODULUS OF ELASTICITY

Table B2 - $f_{c,cyl}$ and Modulus of elasticity test result for all griders

Girder	Age	Cyl 1	Cyl 2	Average	$E_{c,cyl1}$	$E_{c,cyl2}$	Average
20A	7	32.9	32.8	32.8	32000	31000	31500
	30	40.0	41.9	41.0	31900	31900	31900
20B	6	45.7	56.5	51.1	32400	32900	32650
	27	64.8	64.8	64.8	36750	36700	36750
40A	7	58.2	59.6	58.9	39700	36800	38250
	26	70.2	70.5	70.4	40800	39500	40150
40B	7	52.4	52.8	52.6	32350	30400	31350
	28	60.4	57.3	58.8	35200	35500	35350
20+20	7	52.5	50.9	51.7	31500	31550	31500
	28	52.3	60.0	56.2	34450	35500	34950
60	15	58.0	59.9	58.9	37800	34550	36150
	47	65.1	67.9	66.5	36350	39050	37700
REF	7	60.0	59.0	59.5	35750	36000	35900
	28	69.1	67.8	68.5	37600	37550	37600
REF/TR	6	46.2	44.8	45.5	32100	32700	32400
	28	61.0	54.5	57.8	37700	35250	36450
TR	7	59.1	55.1	57.1	38900	36950	37900
	28	70.6	75.8	73.2	40600	39150	39850

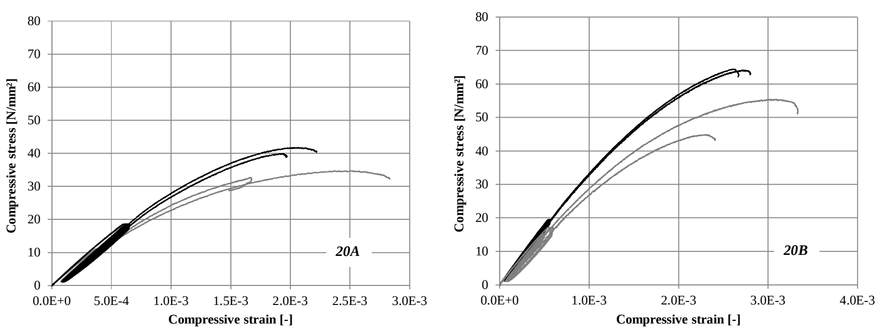

Fig. B9 – Compressive stress strain curve at 7 and 28 days for girders 20A and 20B

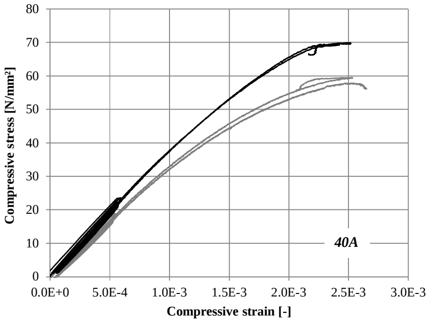

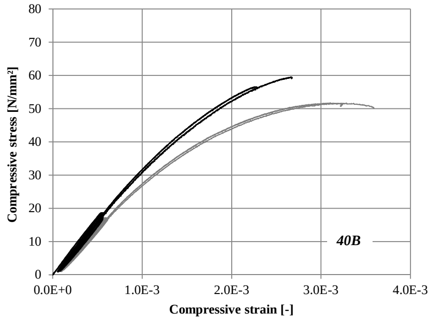

Fig. B10 - Compressive stress strain curve at 7 and 28 days for girders 40A and 40B

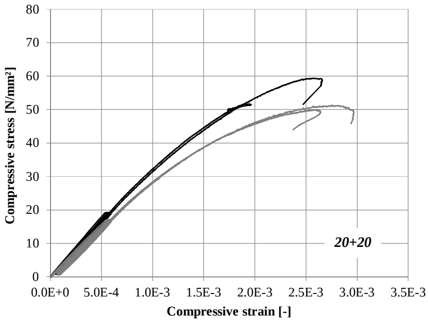

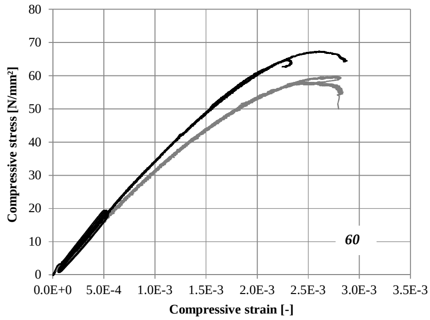

Fig. B11 - Compressive stress strain curve at 7 and 28 days for girders 20+20 and 60

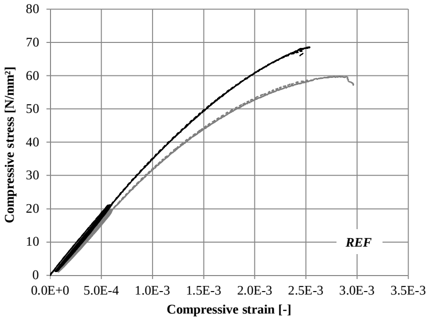

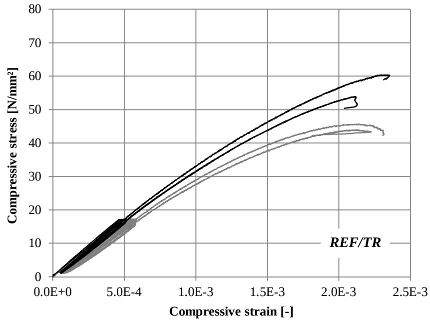

Fig. B12- Compressive stress strain curve at 7 and 28 days for girders REF and REF/TR

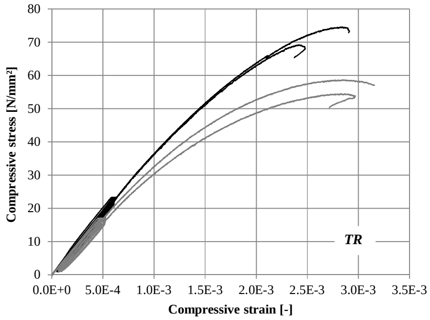

Fig. B13 - Compressive stress strain curve at 7 and 28 days for girder TR

B.3 Cube compression strength

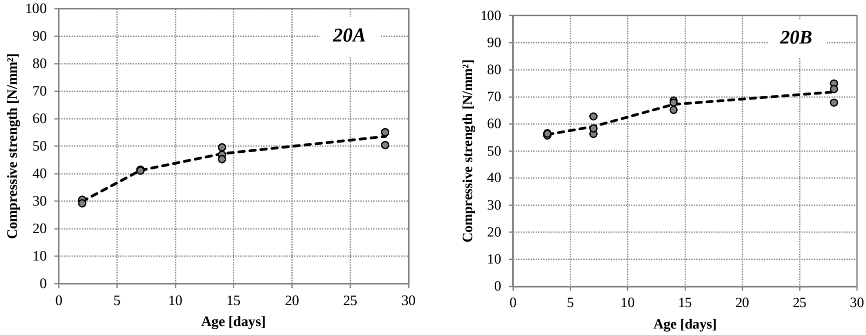

Fig. B14 - Cube compressive strength evolution for girders 20A and 20B

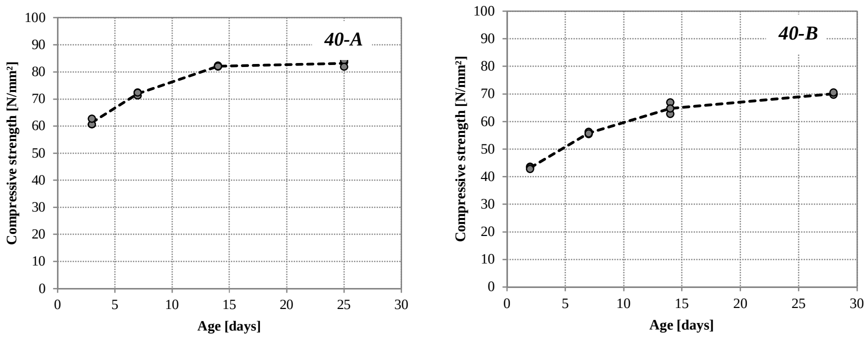

Fig. B15 - Cube compressive strength evolution for girders 40A and 40B

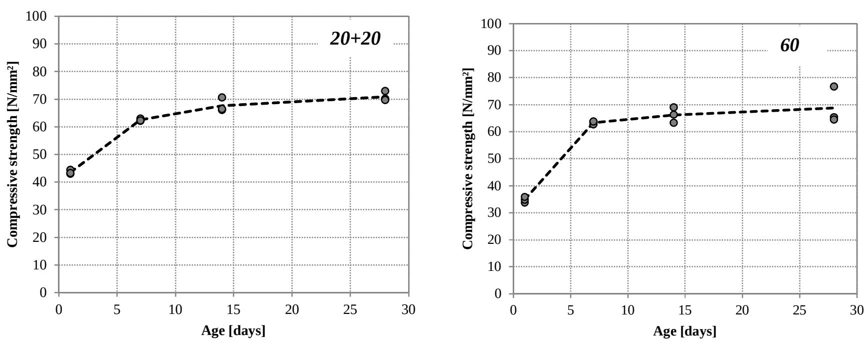

Fig. B16 - Cube compressive strength evolution for girders 20+20 and 60

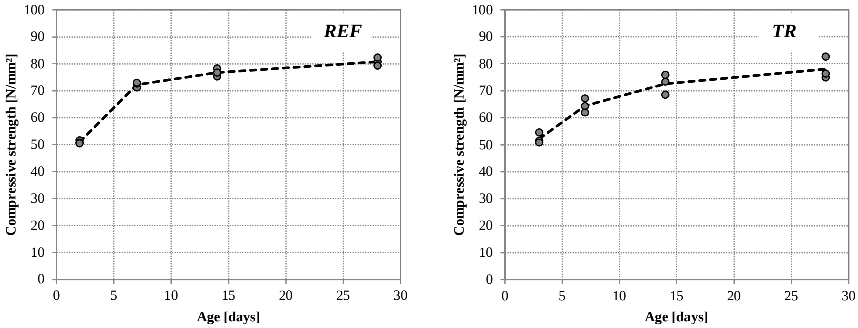

Fig. B17 - Cube compressive strength evolution for girders REF & REF/TR

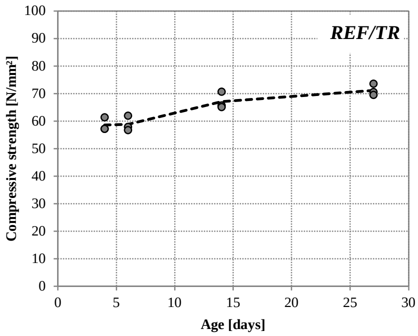

Fig. B18 - Cube compressive strength evolution for girder TR

Table B3 - Cube compressive strength as a function of the age

Girder	Age [days]	Cube 1	Cube 2	Cube 3	Average	CoV [%]
REF	2	51.7	50.7	50.5	51.0	1.2%
	7	71.2	72.7	73.0	72.3	1.3%
	14	75.3	78.3	76.7	76.8	1.9%
	28	80.8	79.3	82.3	80.8	1.8%
20A	2	30.2	30.5	29.3	30.0	2.2%
	7	41.2	41.6	41.1	41.3	0.6%
	14	46.9	49.6	45.3	47.3	4.5%
	28	55.1	50.4	55.1	53.6	5.1%
20B	3	55.7	56.5	56.3	56.2	0.7%
	7	56.2	62.7	58.3	59.1	5.6%
	14	68.6	65.1	67.8	67.2	2.7%
	28	74.9	72.8	67.8	71.8	5.0%
40A	3	60.6	60.6	62.6	61.3	1.9%
	7	72.4	71.2	72.3	72.0	0.9%
	14	81.9	82.3	82.0	82.0	0.2%
	25	83.5	84.2	81.8	83.2	1.5%
40B	2	43.6	43.3	42.7	43.2	1.0%
	7	56.2	55.4	55.6	55.7	0.7%
	14	66.8	62.6	64.7	64.7	3.2%
	28	70.0	69.6	70.5	70.0	0.7%
20+20	1	43.0	44.3	43.2	43.5	1.6%
	7	63.0	62.1	62.3	62.5	0.7%
	14	66.0	66.4	70.5	67.6	3.7%
	28	72.9	70.0	69.7	70.9	2.5%
60	1	33.8	34.8	35.9	34.8	3.0%
	7	63.7	62.6	63.8	63.4	1.0%
	14	66.3	63.3	69.0	66.2	4.3%
	28	65.3	76.7	64.4	68.8	9.9%
REF/TR	4	61.4	57.2	57.2	58.6	4.1%
	6	57.8	61.9	56.7	58.8	4.7%
	14	65.7	70.6	65.1	67.1	4.5%
	27	73.6	70.6	69.5	71.2	2.9%
TR	3	54.5	51.5	50.8	52.3	3.8%
	7	64.3	67.2	61.9	64.4	4.1%
	14	68.5	73.4	75.9	72.6	5.1%
	28	74.9	76.3	82.6	78.0	5.3%

B.4 Creep and Shrinkage

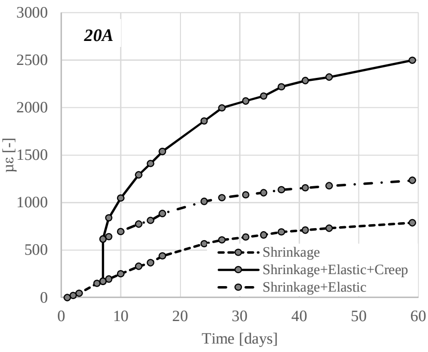

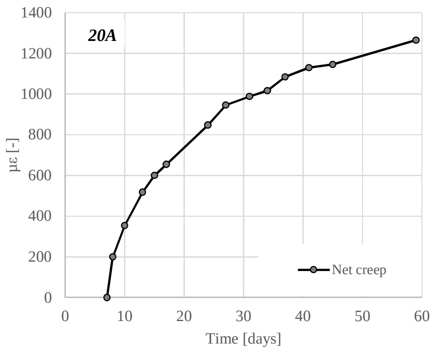

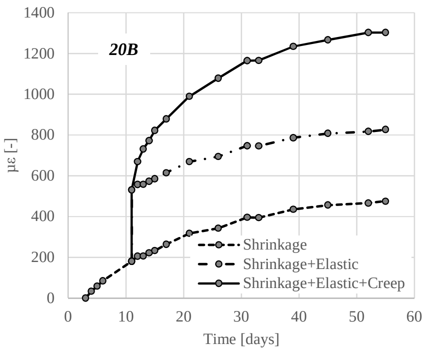

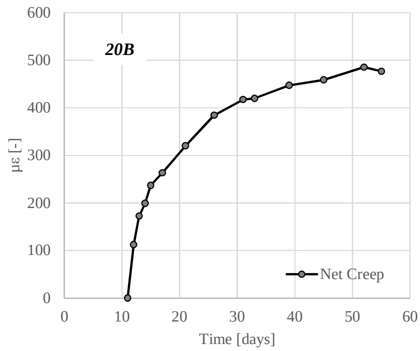

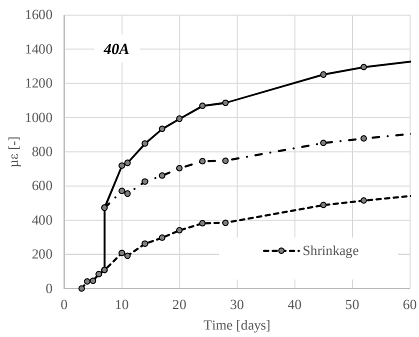

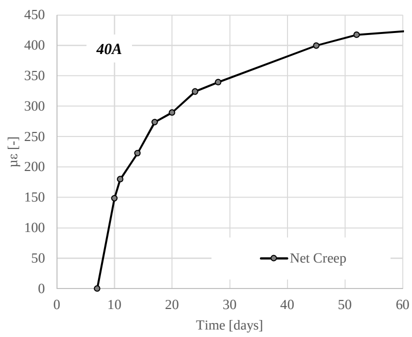

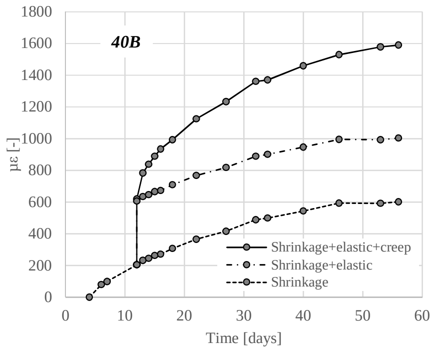
40B
με [-]
Time [days]
Shrinkage+elastic+creep
Shrinkage+elastic
Shrinkage

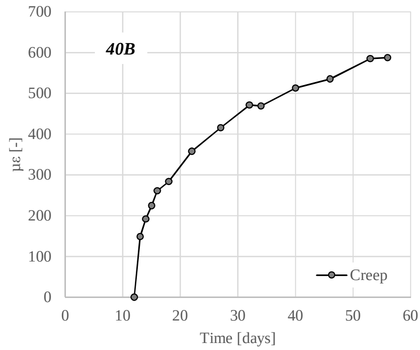
40B
με [-]
Time [days]
Creep

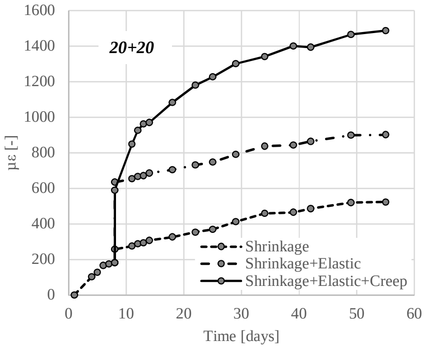
20+20
με [-]
Time [days]
Shrinkage
Shrinkage+Elastic
Shrinkage+Elastic+Creep

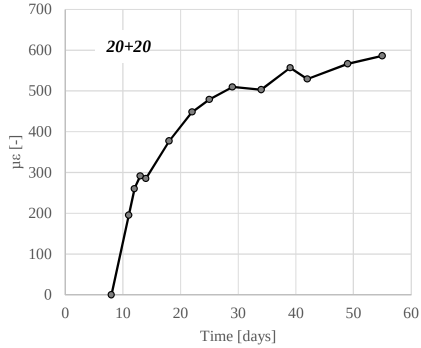
20+20
με [-]
Time [days]

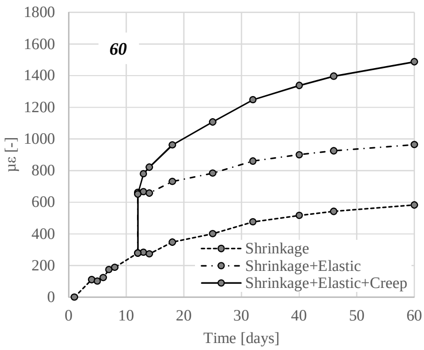
60
με [-]
Time [days]
Shrinkage
Shrinkage+Elastic
Shrinkage+Elastic+Creep

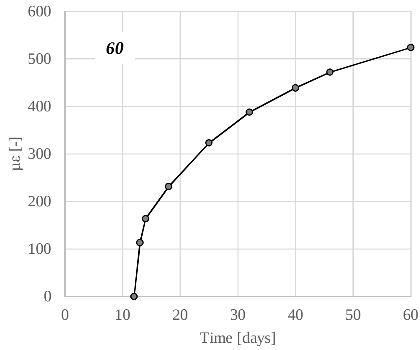
60
με [-]
Time [days]

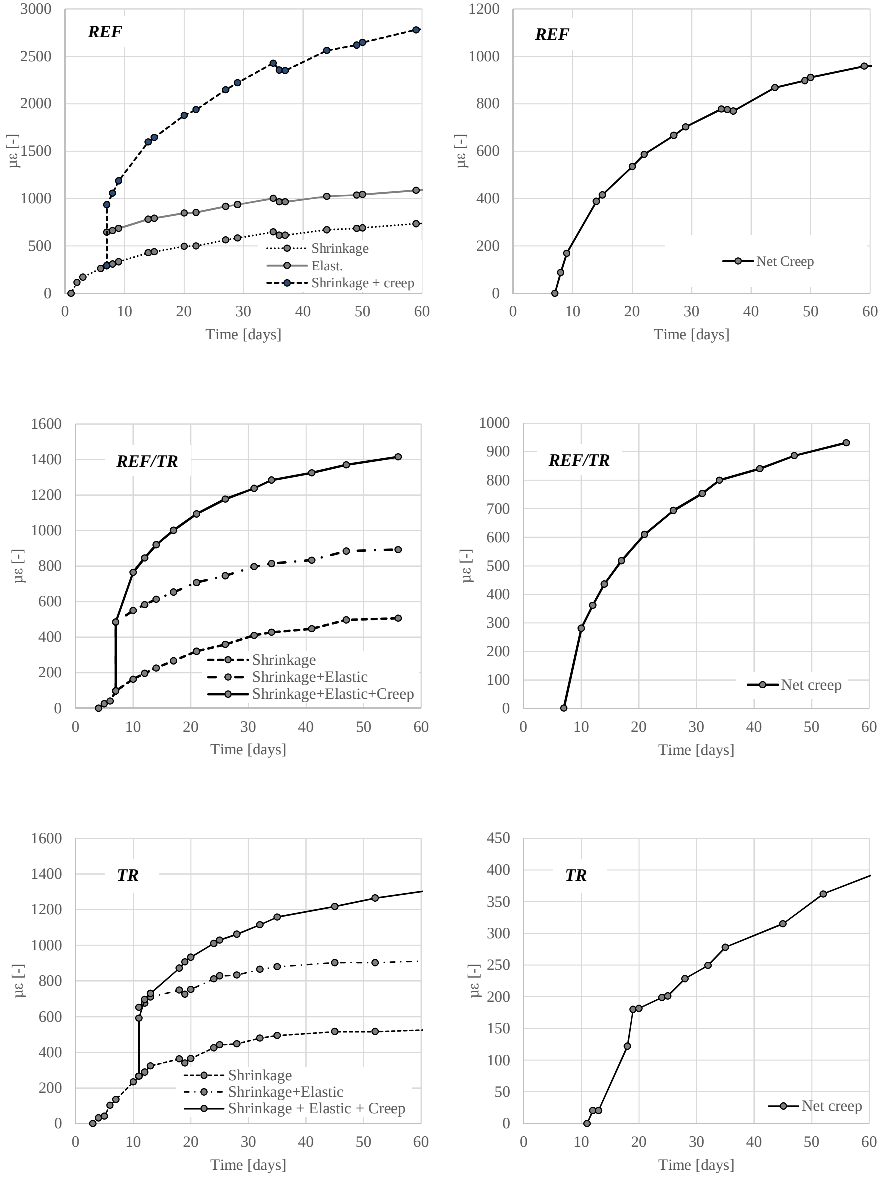
REF
με [-]
Time [days]
Shrinkage
Elast.
Shrinkage + creep
REF
Net Creep
REF/TR
Shrinkage
Shrinkage+Elastic
Shrinkage+Elastic+Creep
REF/TR
Net creep
TR
Shrinkage
Shrinkage+Elastic
Shrinkage + Elastic + Creep
TR
Net creep

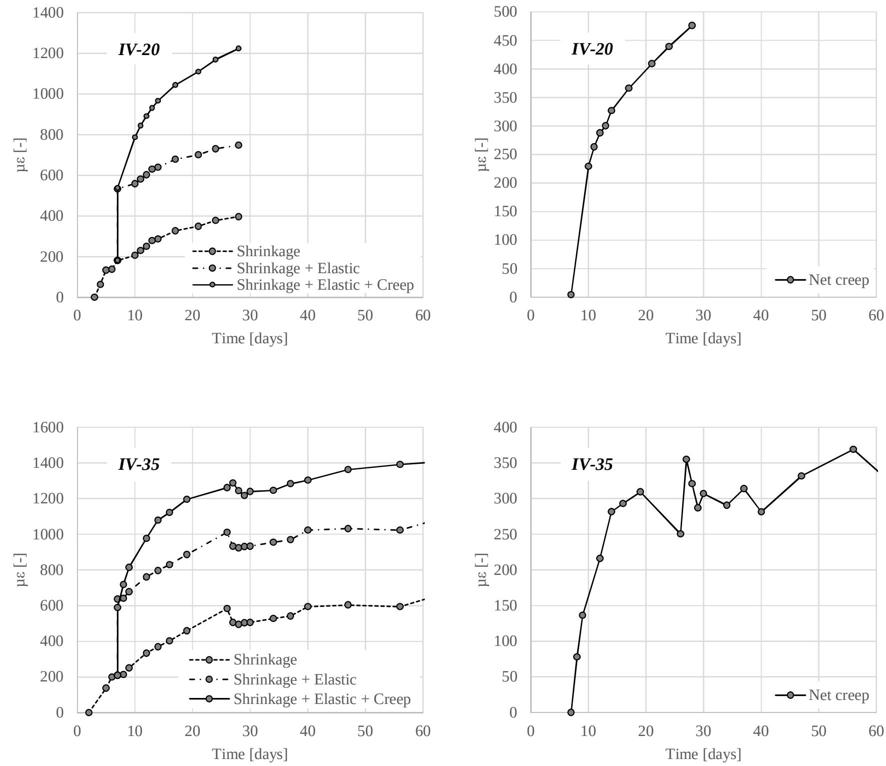

Fig. 9.1 – Shrinkage and creep strain evolution between 0-60 days

APPENDIX C FULL SCALE SHEAR TEST RESULTS

C.1 CRACK PROPAGATION BEHAVIOUR

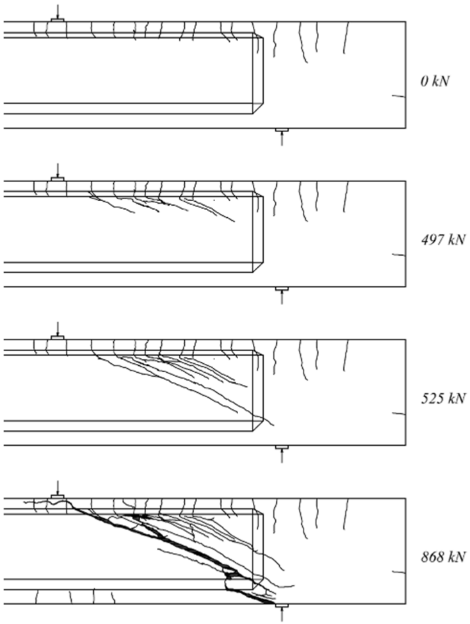

Fig. C1 - Crack development [20A – 2.5 – 1]

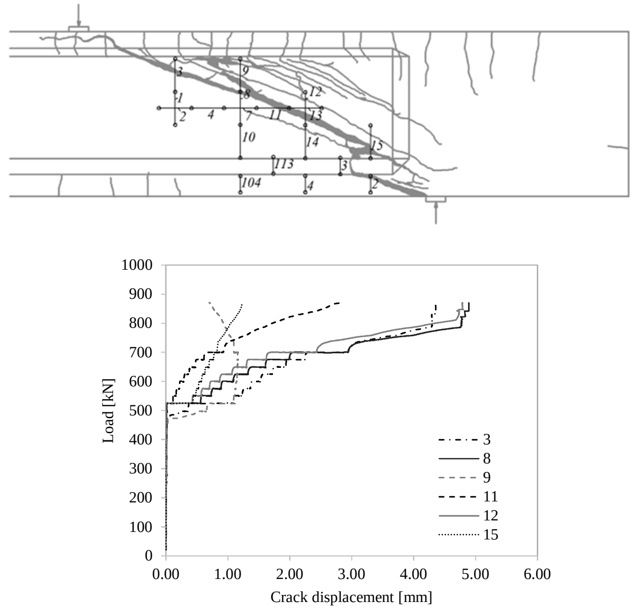

Fig. C2 – Load vs. shear crack displacement [20A – 2.5 – 1]

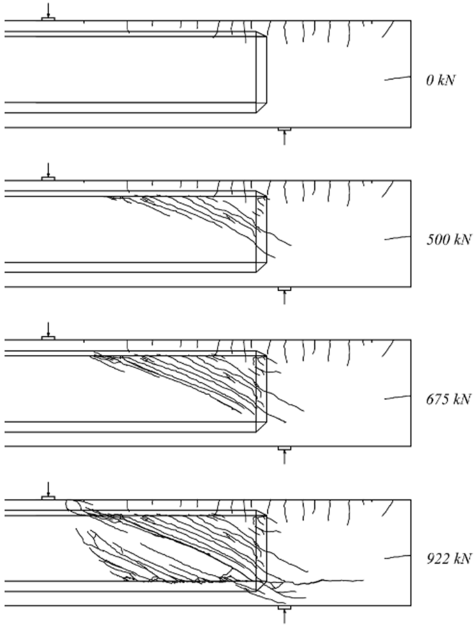

Fig. C3 - Crack development for girder [20A – 2.5 – 2]

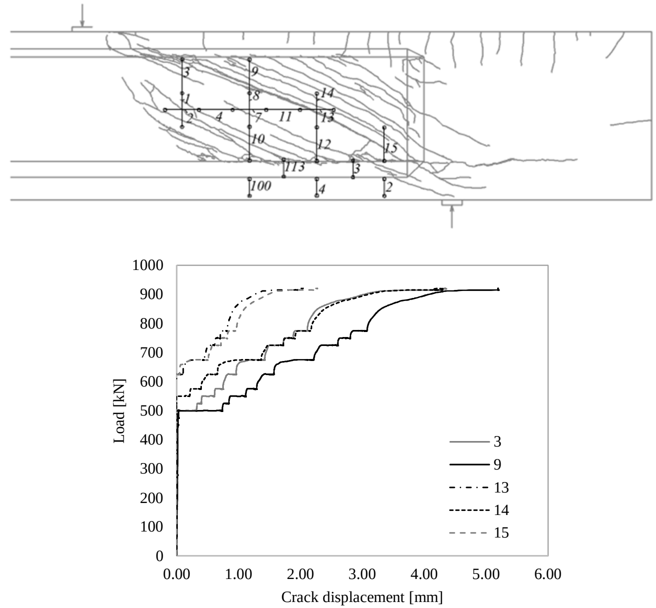

Fig. C4 - Load vs. shear crack displacement [20A – 2.5 – 2]

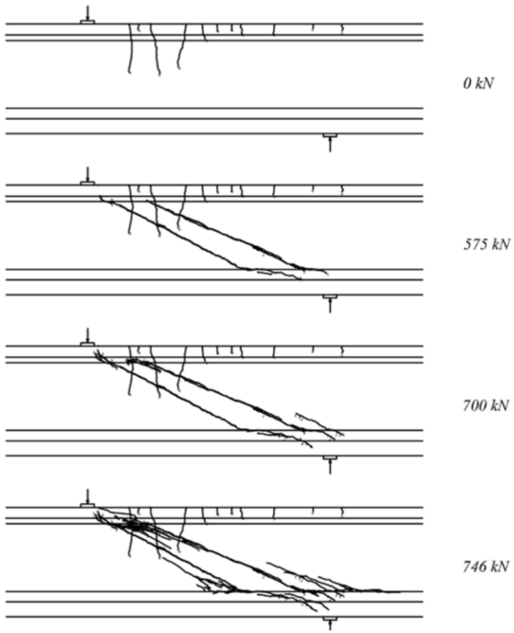

Fig. C5 - Crack development [20A – 2.5 – 3]

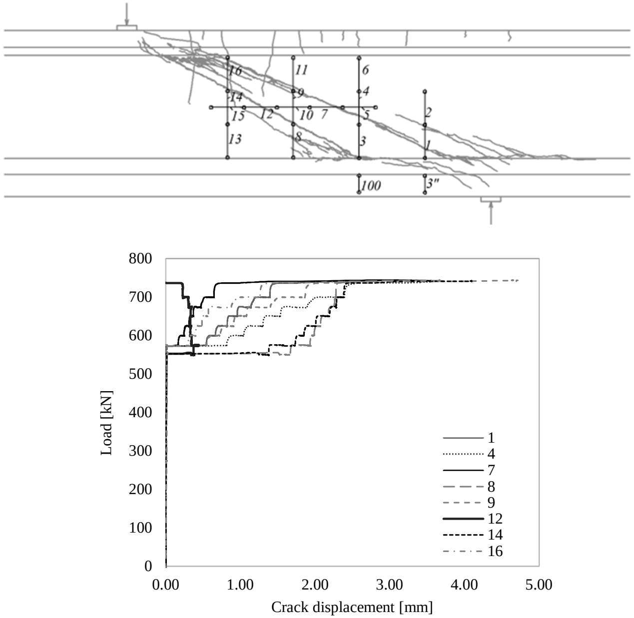

Fig. C6 - Load vs. shear crack displacement [20A – 2.5 – 3]

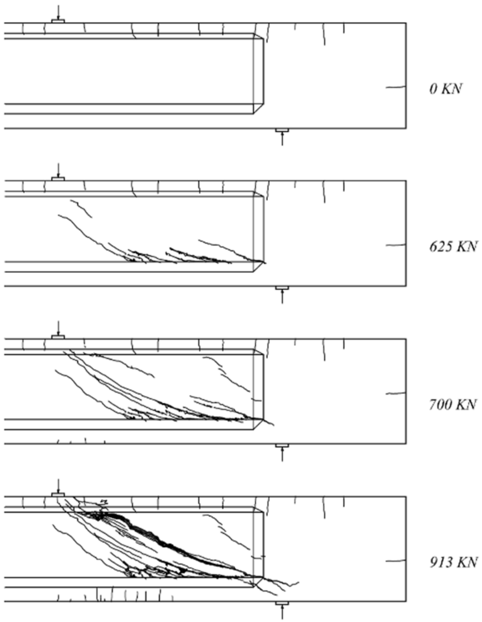

Fig. C7 - Crack development [40A – 2.5 – 1]

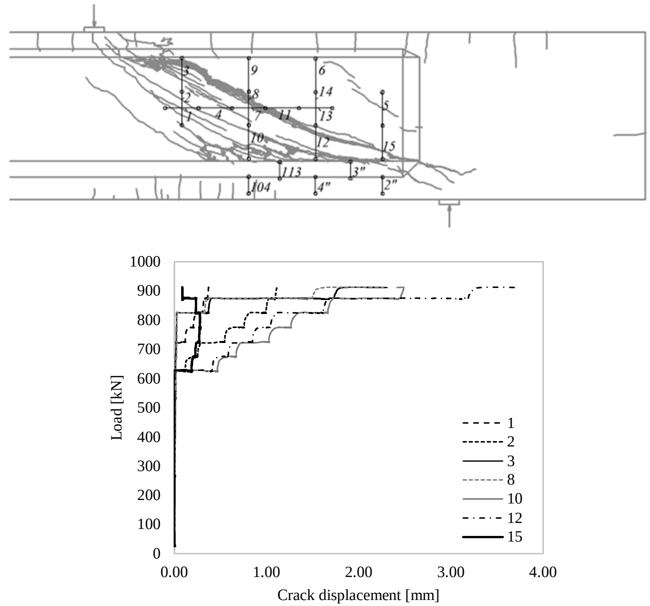

Fig. C8 - Load vs. shear crack displacement [40A – 2.5 – 1]

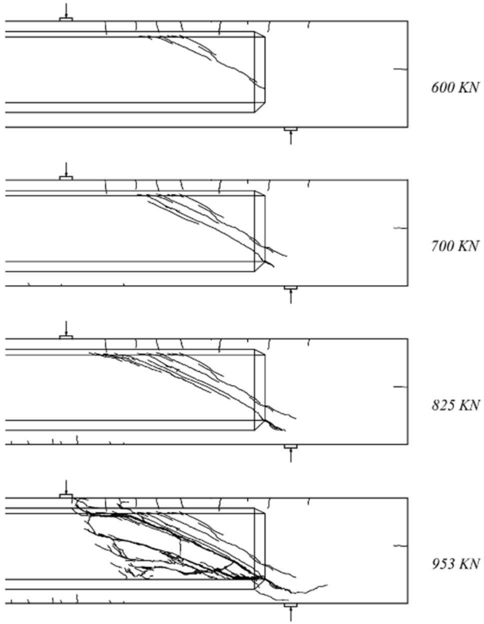

Fig. C9 - Crack development [40A – 2.5 – 2]

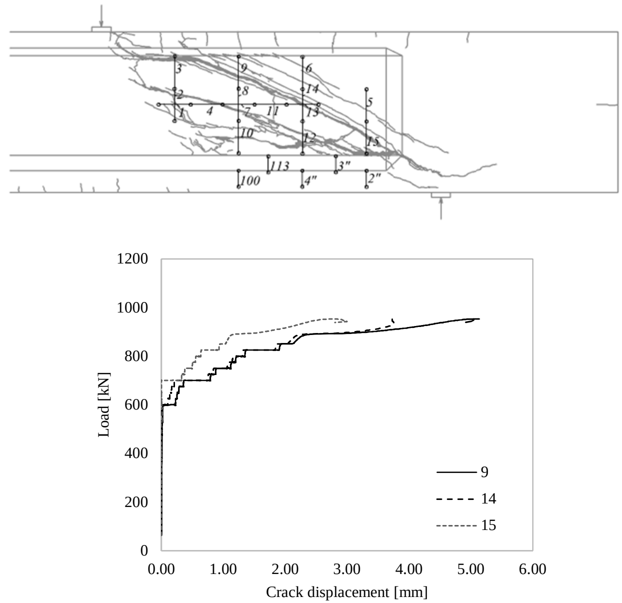

Fig. C10 - Load vs. shear crack displacement [40A – 2.5 – 2]

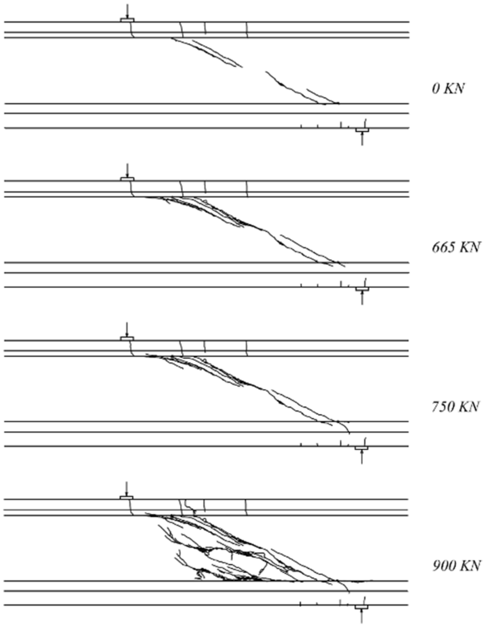

Fig. C11 - Crack development [40A – 2.5 – 3]

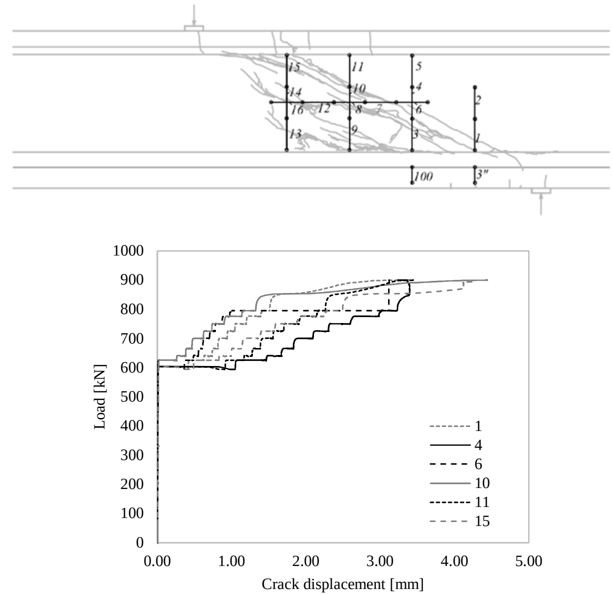

Fig. C12 - Load vs. shear crack displacement [40A – 2.5 – 3]

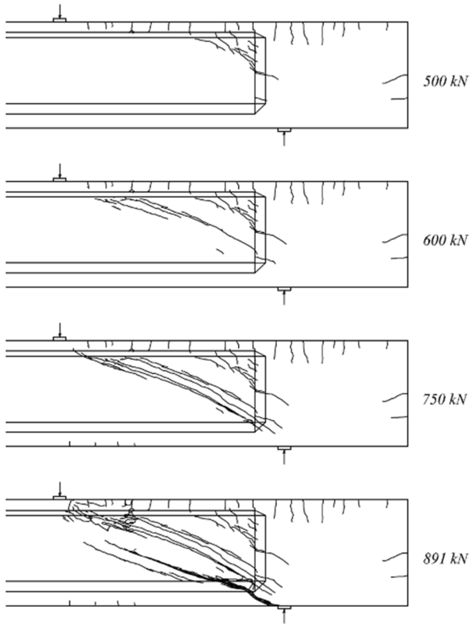

Fig. C13 - Crack development [20B – 2.5 – 1]

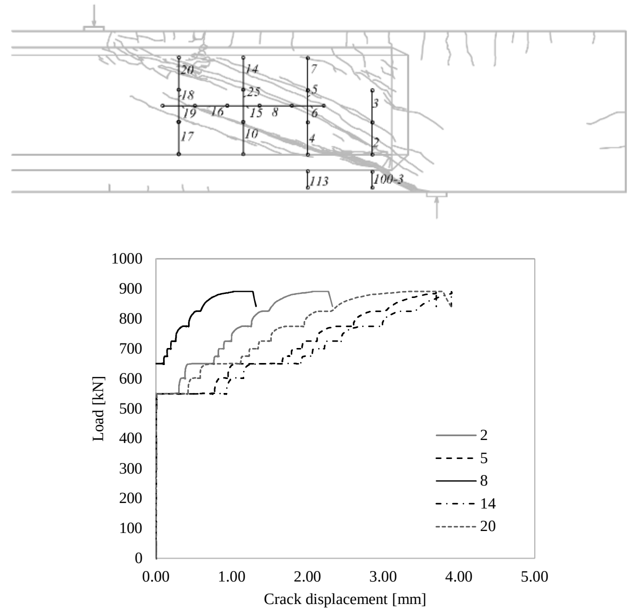

Fig. C14 - Load vs. shear crack displacement [20B – 2.5 – 1]

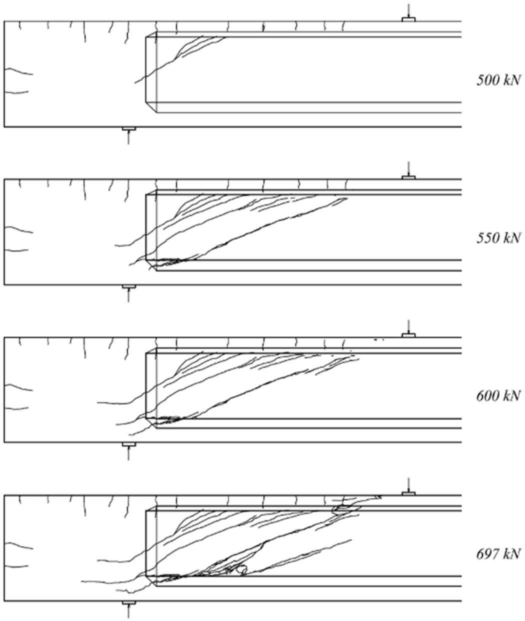

Fig. C15 - Crack development [20B – 3.0 – 2]

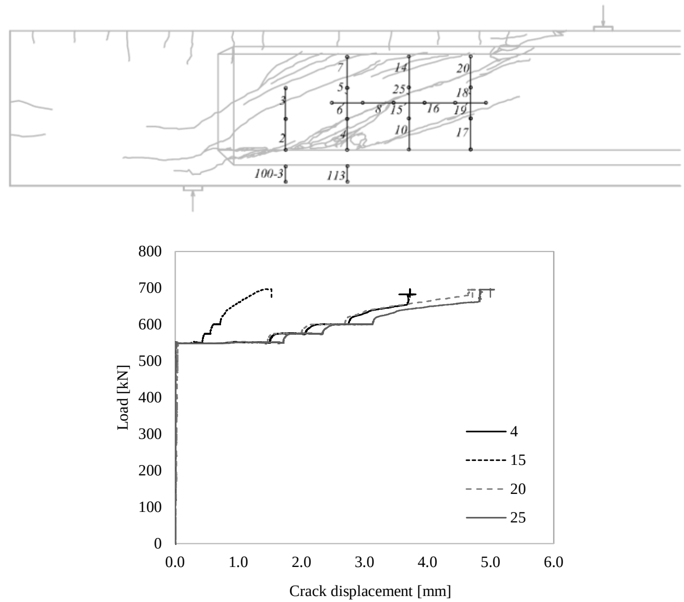

Fig. C16 - Load vs. shear crack displacement [20B – 3.0 – 2]

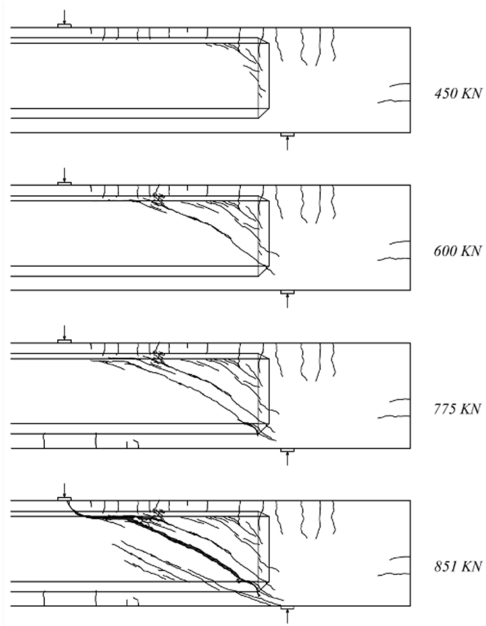

Fig. C17 - Crack development [40B –2.5 – 1]

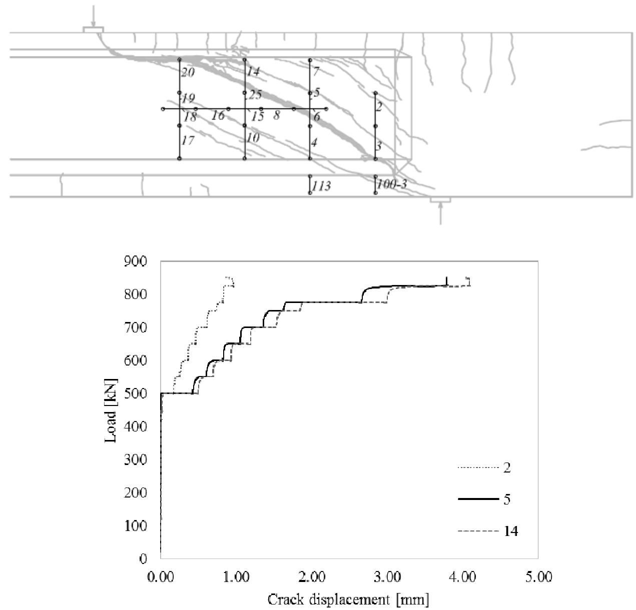

Fig. C18 - Load vs. shear crack displacement [40B – 2.5 – 1]

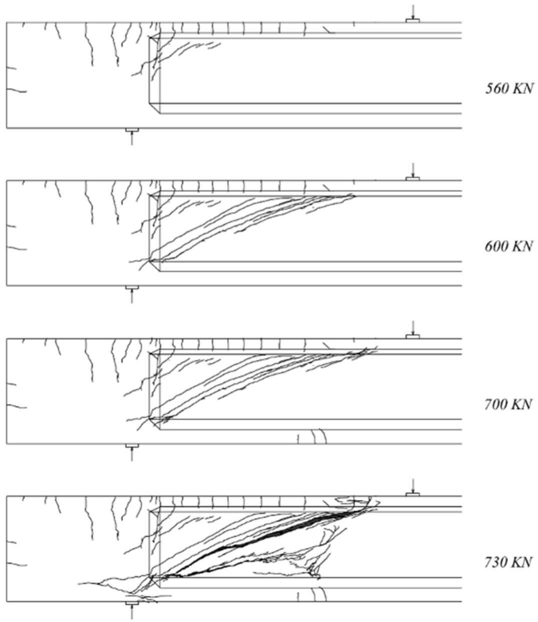

Fig. C19 - Crack development [40B –3.0 – 2]

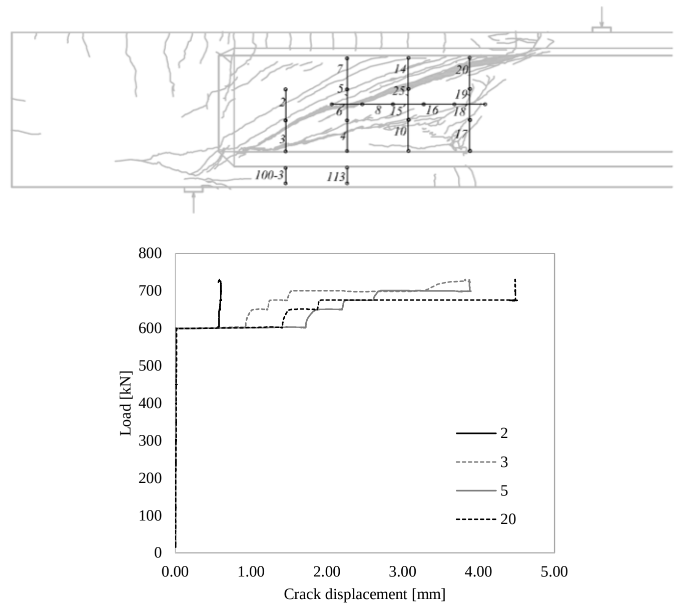

Fig. C20 - Load vs. shear crack displacement [40B –3.0 – 2]

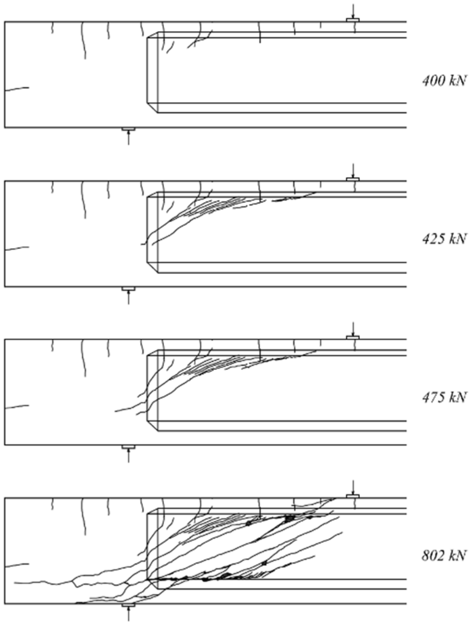

Fig. C21 - Crack development [REF –2.5 – 1]

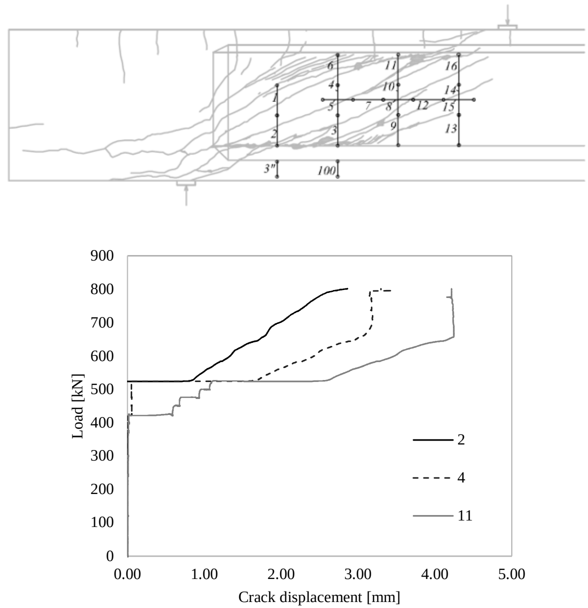

Fig. C22 - Load vs. shear crack displacement [REF –2.5 – 1]

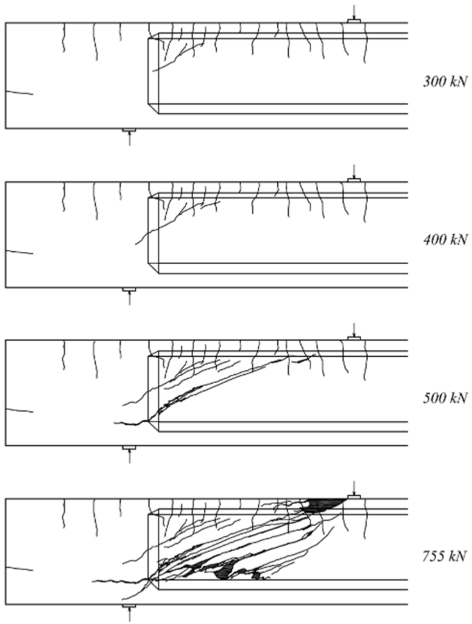

Fig. C23 - Crack development [REF –2.5 – 2]

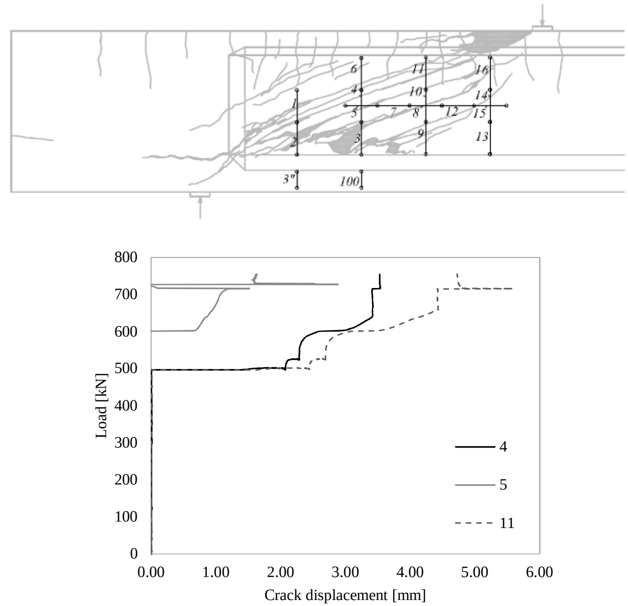

Fig. C24 - Load vs. shear crack displacement [REF –2.5 – 2]

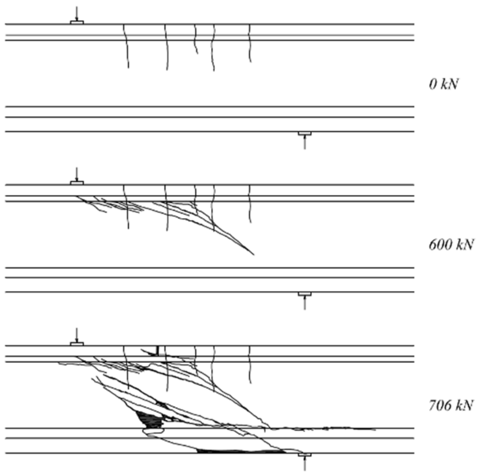

Fig. C25 - Crack development [REF –2.5 – 3]

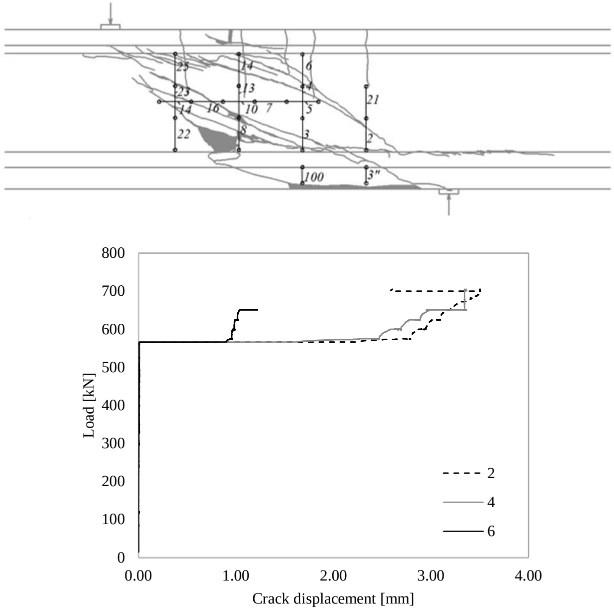

Fig. C26 - Load vs. shear crack displacement [REF –2.5 – 3]

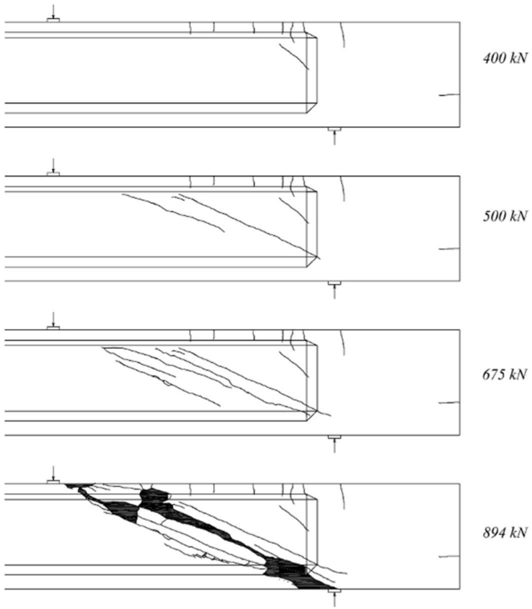

Fig. C27 - Crack development [REFTR – 3.0 – 1]

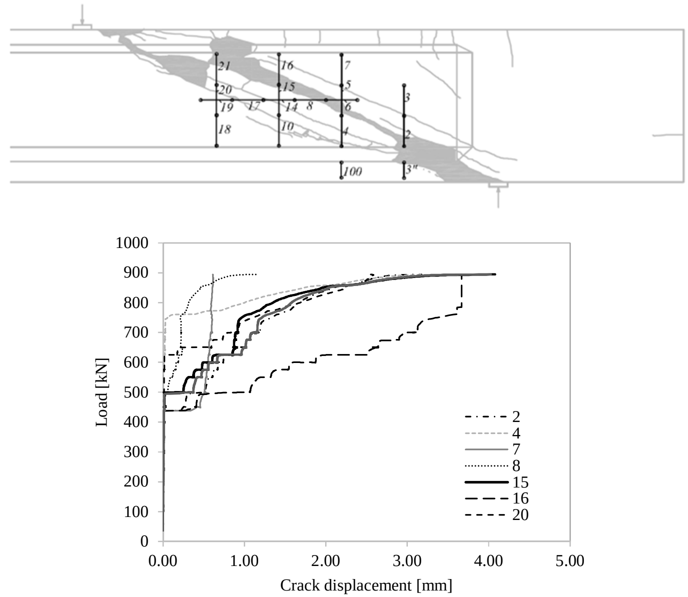

Fig. C28 - Load vs. shear crack displacement [REFTR – 3.0 – 1]

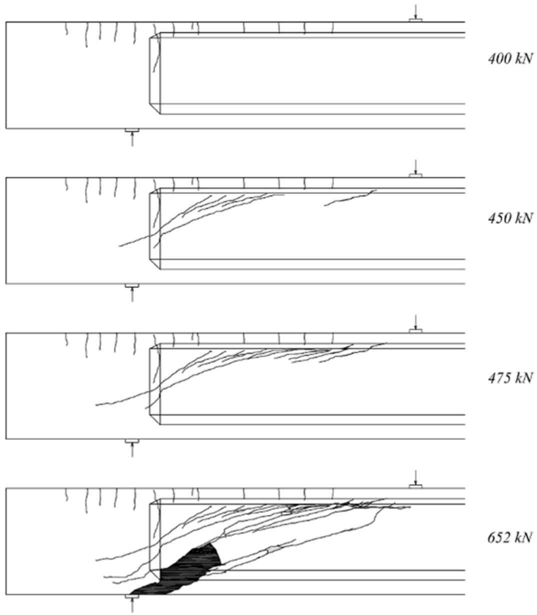

Fig. C29 - Crack development [REFTR – 3.0 – 2]

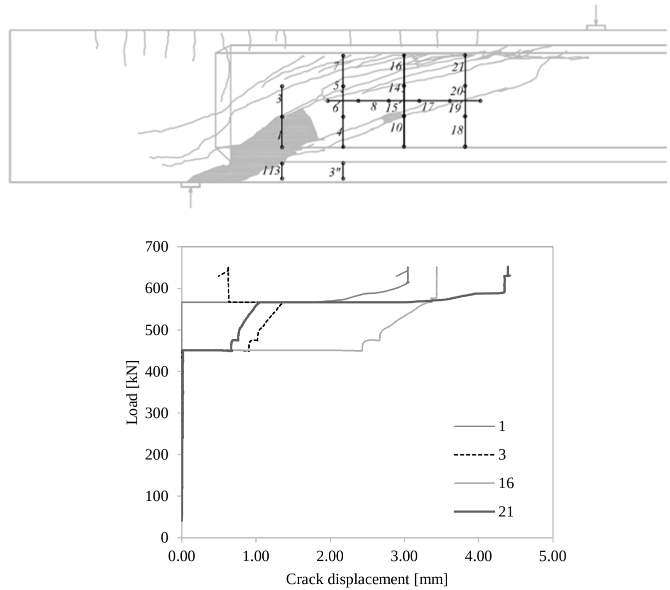

Fig. C30 - Load vs. shear crack displacement [REFTR – 3.0 – 2]

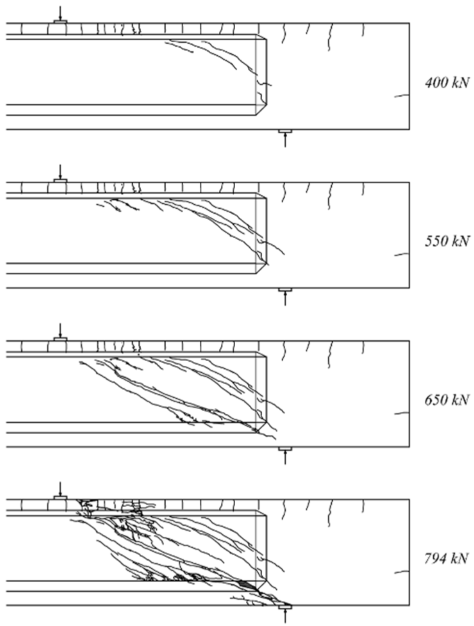

Fig. C31 - Crack development [2020 – 2.5 – 1]

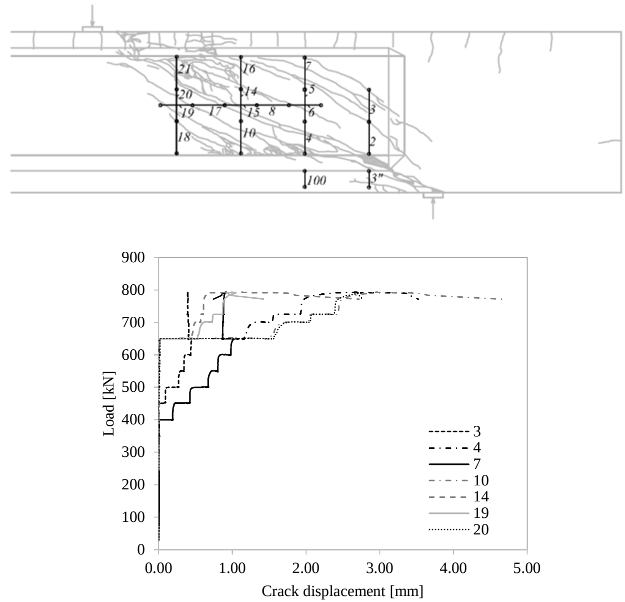

Fig. C32 - Load vs. shear crack displacement [2020 – 2.5 - 1]

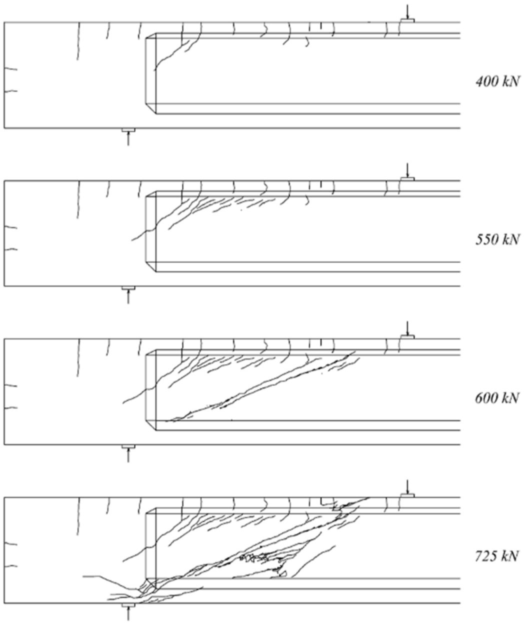

Fig. C33 - Crack development [2020 – 3.0 – 2]

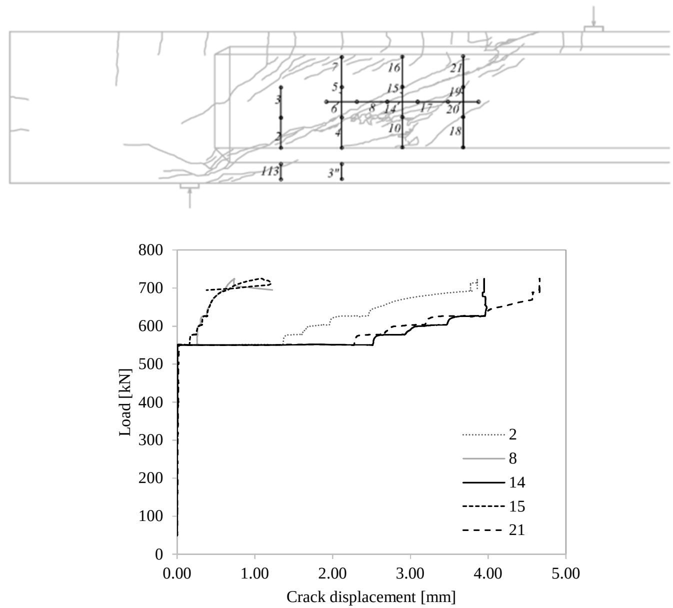

Fig. C34 - Load vs. shear crack displacement [2020 – 3.0 – 2]

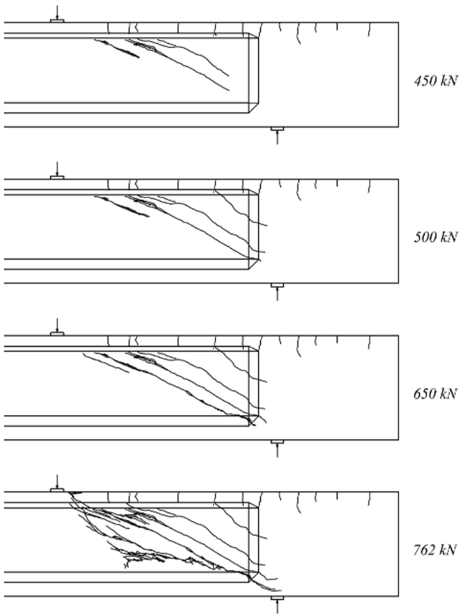

Fig. C35 - Crack development [60 – 2.5 – 1]

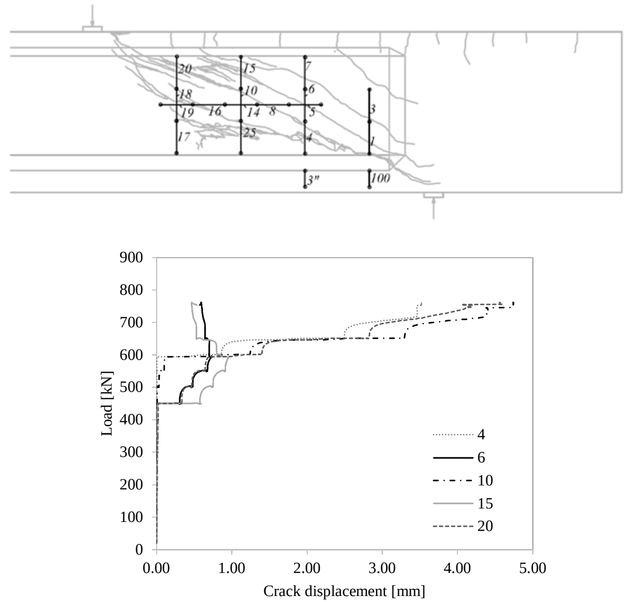

Fig. C36 - Load vs. shear crack displacement [60 – 2.5 – 1]

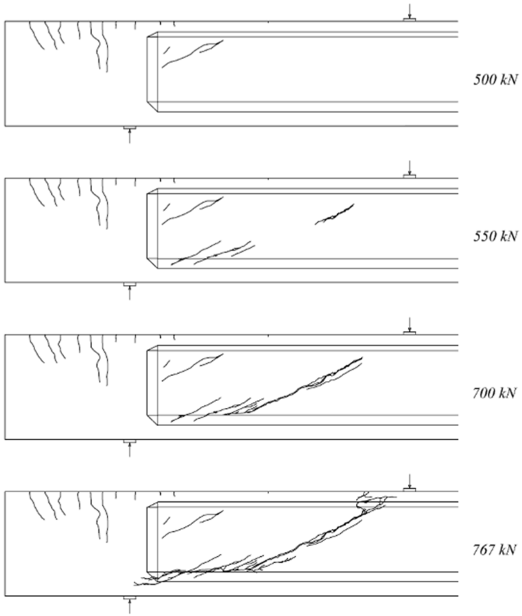

Fig. C37 - Crack development [60 – 3.0 – 2]

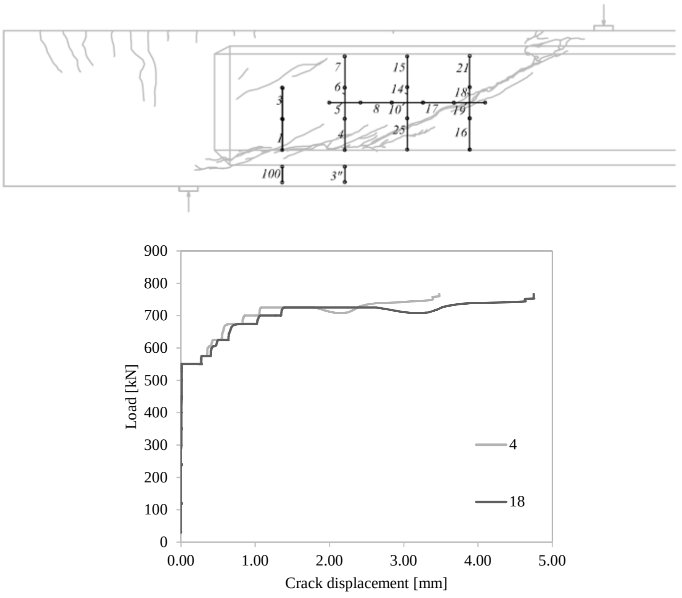

Fig. C38 - Load vs. shear crack displacement [60 – 3.0 – 2]

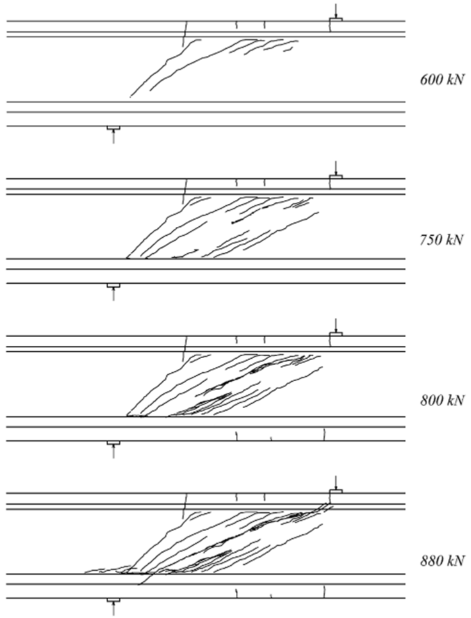

Fig. C39 - Crack development [60 – 2.5 – 3]

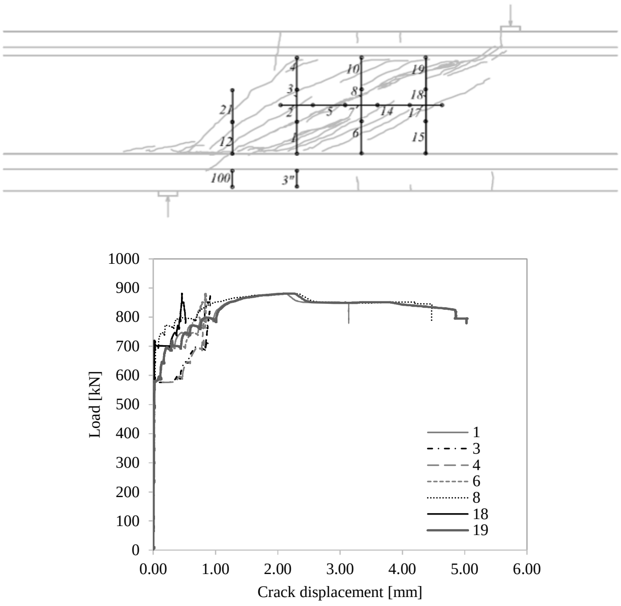

Fig. C40 - Load vs. shear crack displacement [60 – 2.5 – 3]

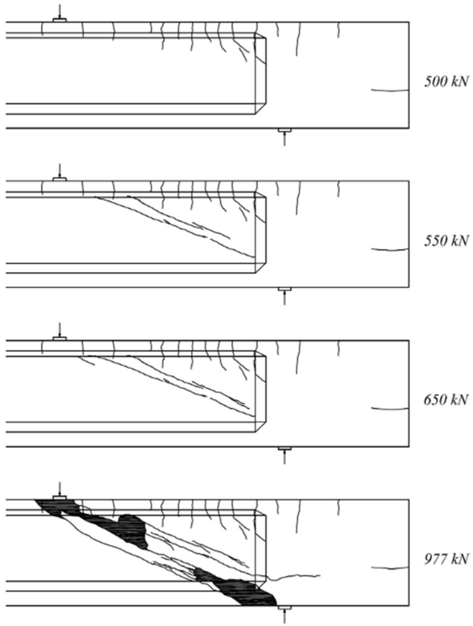

Fig. C41 - Crack development [TR – 2.5 – 1]

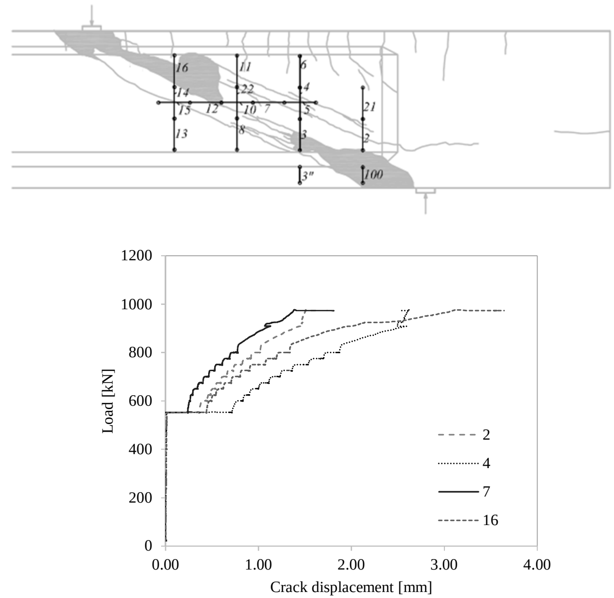

Fig. C42 - Load vs. shear crack displacement [TR – 2.5 – 1]

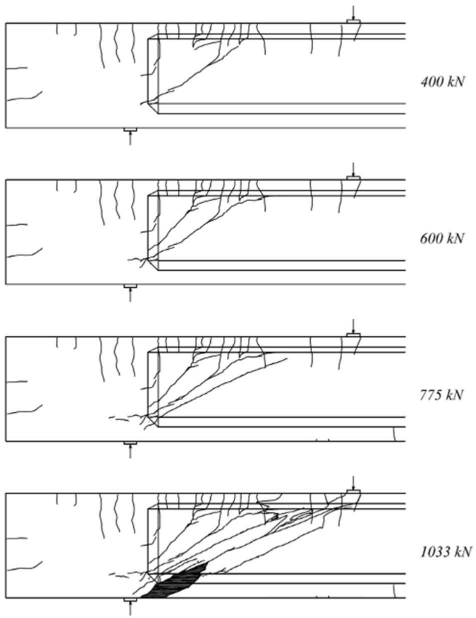

Fig. C43 - Crack development [TR – 2.5 – 2]

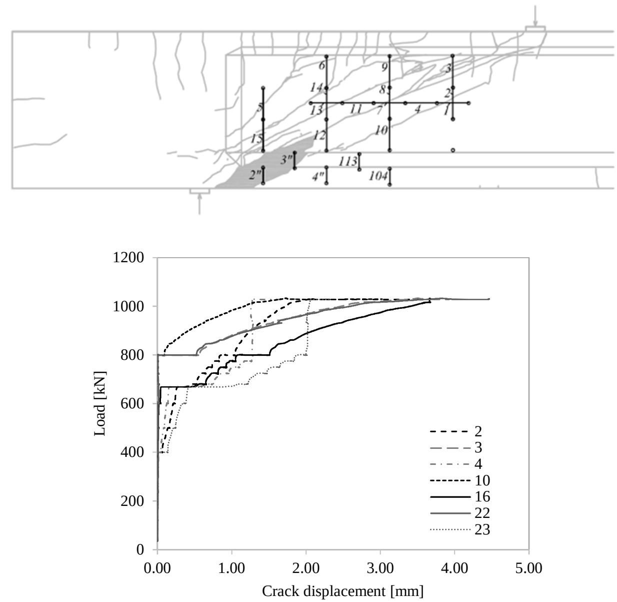

Fig. C44 - Load vs. shear crack displacement [TR – 2.5 – 2]

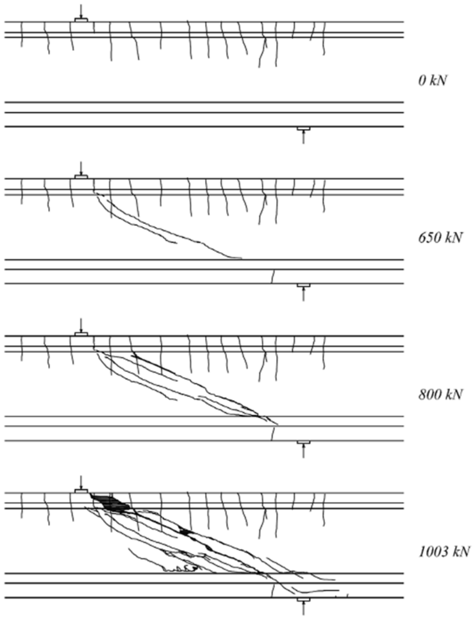

Fig. C45 - Crack development [TR – 2.5 – 3]

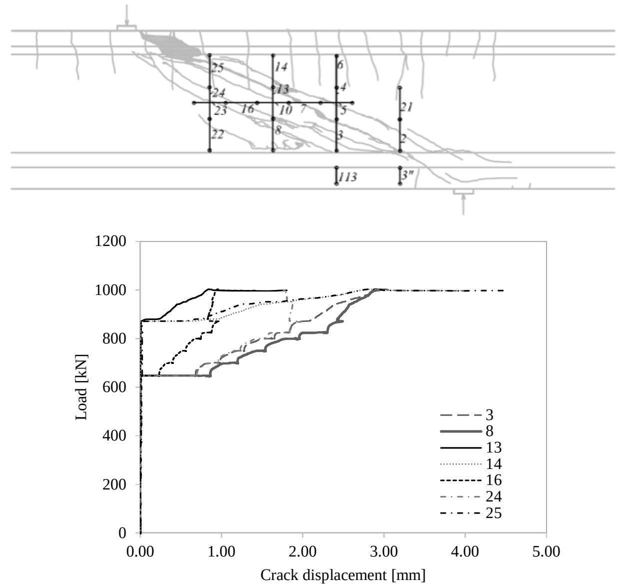

Fig. C46 - Load vs. shear crack displacement [TR – 2.5 – 3]

C.2 FIBRE DOSAGE IN THE HARDENED STATE

Table C1 – Fibre content measured in the hardened state

Girder test	Core nr.						$V_{f,min}$ [kg/m³]	$V_{f,max}$ [kg/m³]	$V_{f,avg}$ [kg/m³]	CoV [-]
	1	2	3	4	5	6				
20A-2.5-1	23.7	15.8	17.6	15.4	16.3	16.7	15.4	23.7	17.6	17%
20A-2.5-2	22.8	18.3	17.0	16.6	18.8	18.1	16.6	22.8	18.6	12%
20A-2.5-3	18.8	18.5	16.3	18.5	16.3	18.5	16.3	18.8	17.8	7%
20B-2.5-1	20.7	20.2	18.1	19.6	18.0	18.4	18.0	20.7	19.2	6%
20B-3.0-2	16.4	19.4	17.7	23.0	22.5	19.9	16.4	23.0	19.8	13%
40A-2.5-1	42.5	44.4	43.2	48.3	41.9	40.3	40.3	48.3	43.4	6%
40A-2.5-2	38.1	41.4	51.2	48.1	50.4	42.0	38.1	51.2	45.2	12%
40A-2.5-3	46.2	39.3	40.5	38.6	42.1	43.7	38.6	46.2	41.7	7%
40B-2.5-1	39.0	41.7	35.7	37.7	50.0	45.2	35.7	50.0	41.5	13%
40B-3.0-2	43.8	38.5	37.1	49.6	40.0	37.1	37.1	49.6	41.0	12%
2020-2.5-1	34.4	-	39.2	45.6	-	37.3	34.4	45.6	39.1	12%
2020-3.0-2	37.0	41.7	43.5	45.6	39.4	43.3	37.0	45.6	41.8	7%
60-2.5-1	68.2	64.3	61.8	60.5	60.5	67.8	60.5	68.2	63.8	5%
60-3.0-2	63.7	60.8	60.6	61.6	58.4	67.0	58.4	67.0	62.0	5%
60-2.5-3	63.6	60.9	70.8	61.1	60.8	59.5	59.5	70.8	62.8	7%

APPENDIX D EVALUATION OF SHEAR STRENGTH MODELS

D.1 INFLUENCE OF EFFECTIVE DEPTH

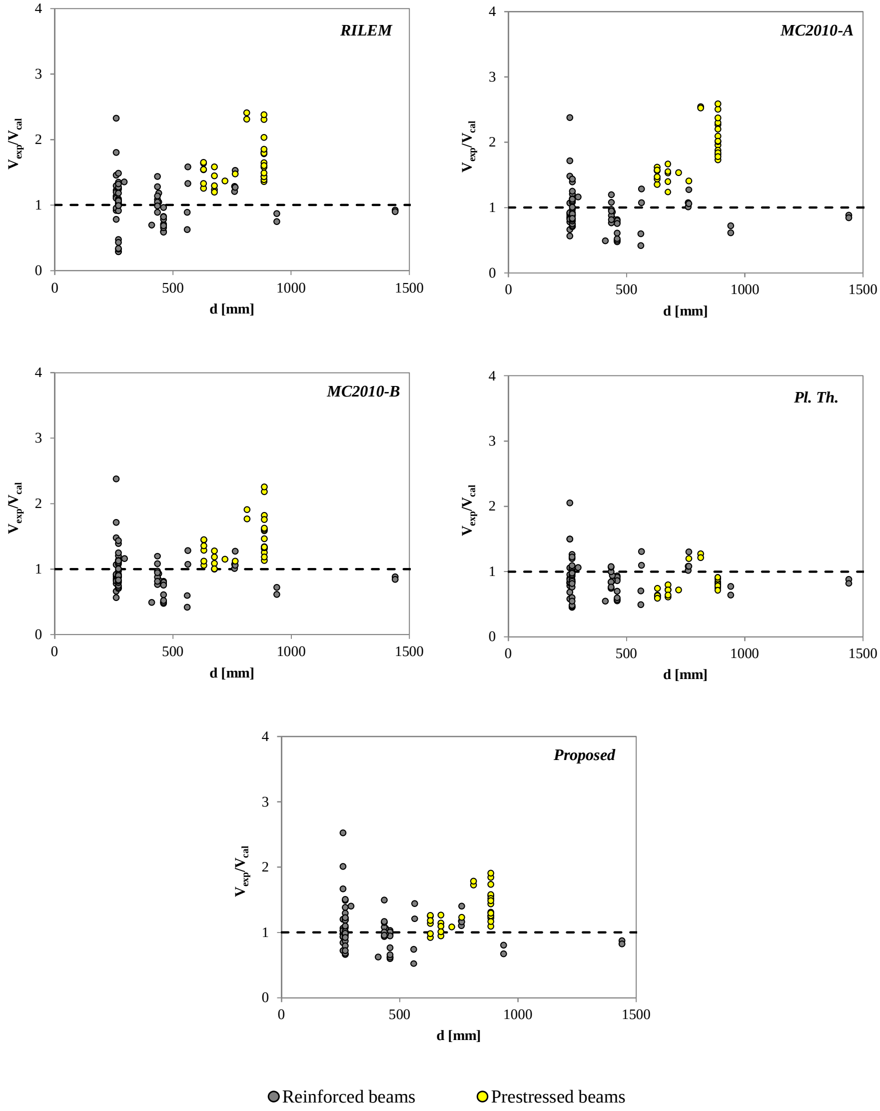

Fig. D1 – Influence of effective depth to the shear strength model error

D.2 INFLUENCE OF LONGITUDINAL REINFORCEMENT RATIO

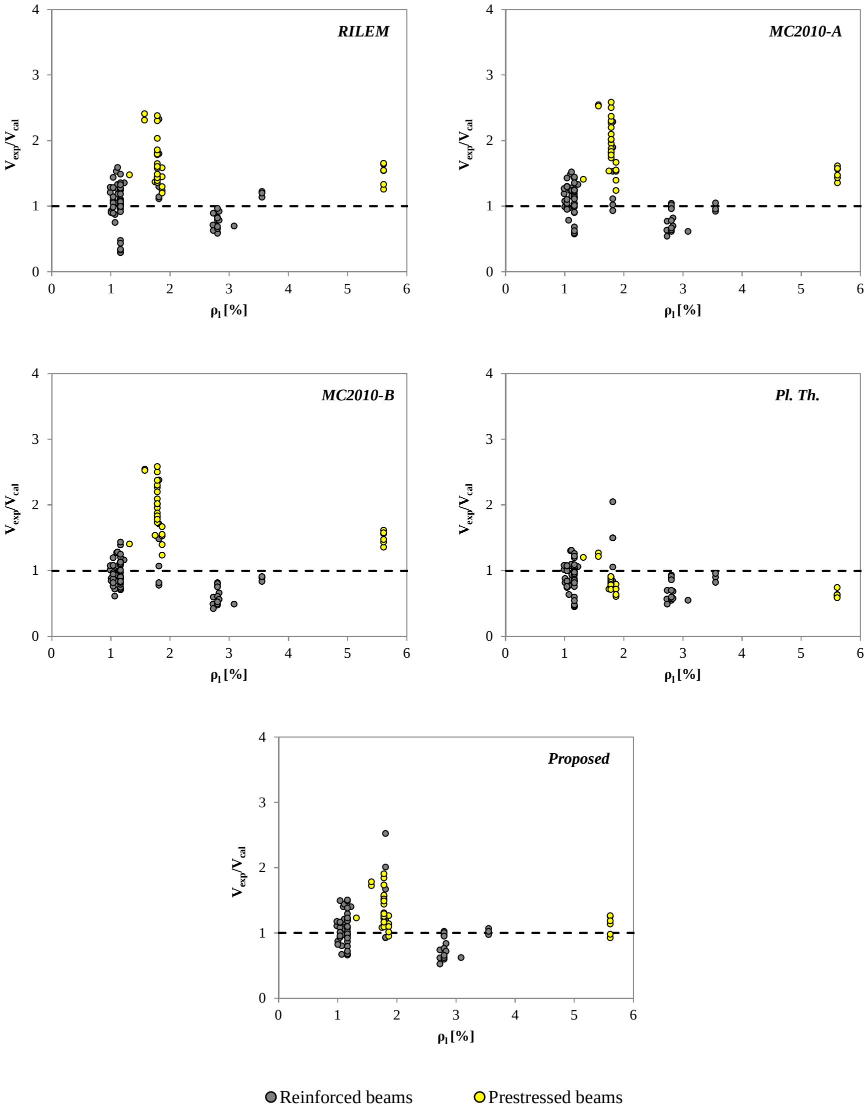

Fig. D2 – Influence of longitudinal reinforcement ratio to the shear strength model error

D.3 INFLUENCE OF SHEAR SPAN TO DEPTH RATIO

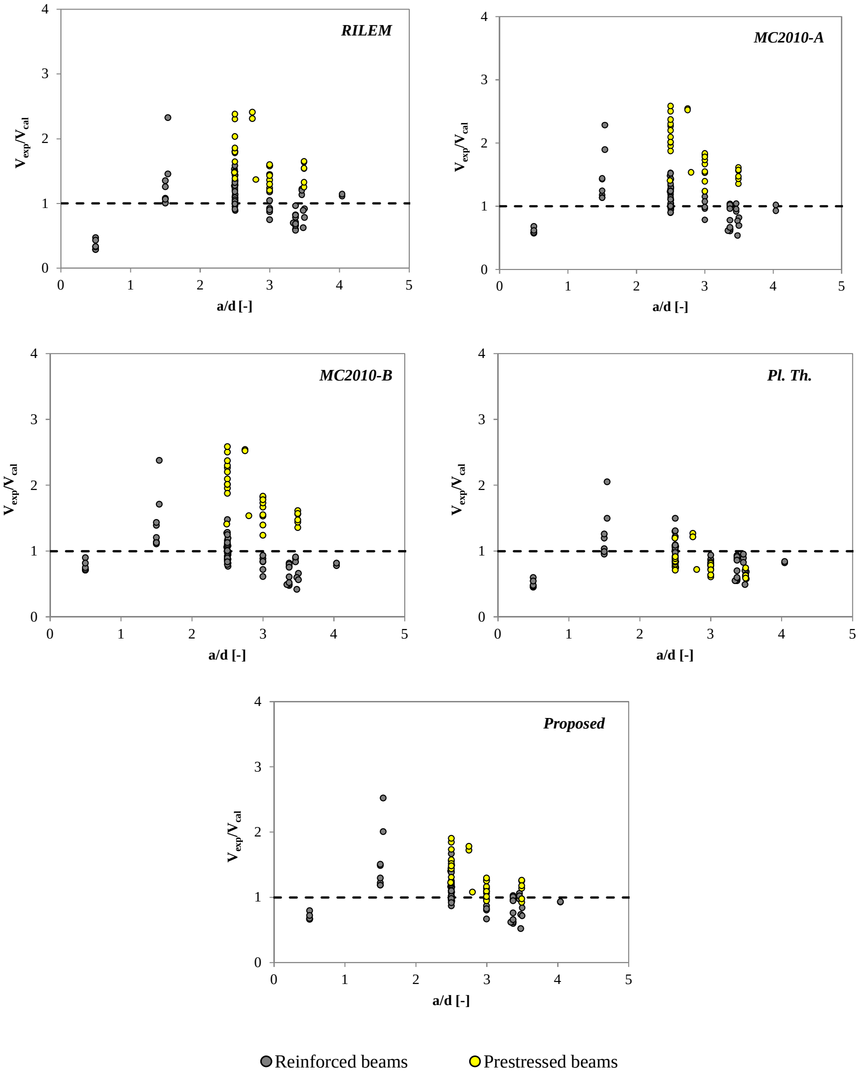

Fig. D3 – Influence of a/d to the shear strength model error

APPENDIX E CRACK PROPAGATION OF IV-GIRDERS

E.1 GIRDER IV-1

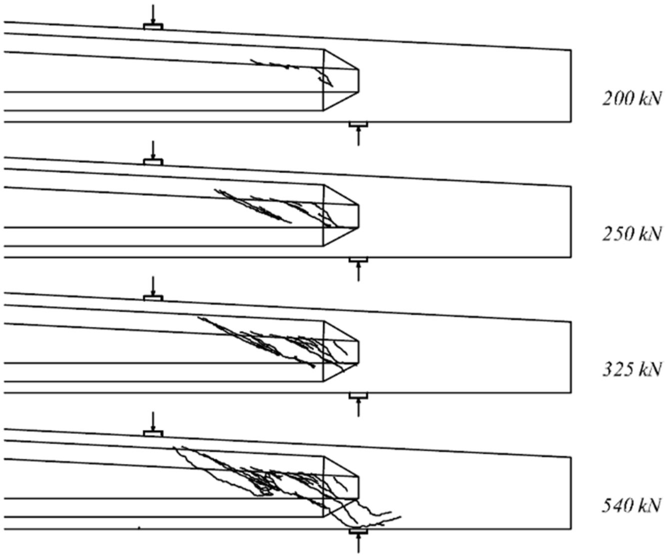

Fig. E1 - Crack development for griderd IV-20 – 2.5 – 1

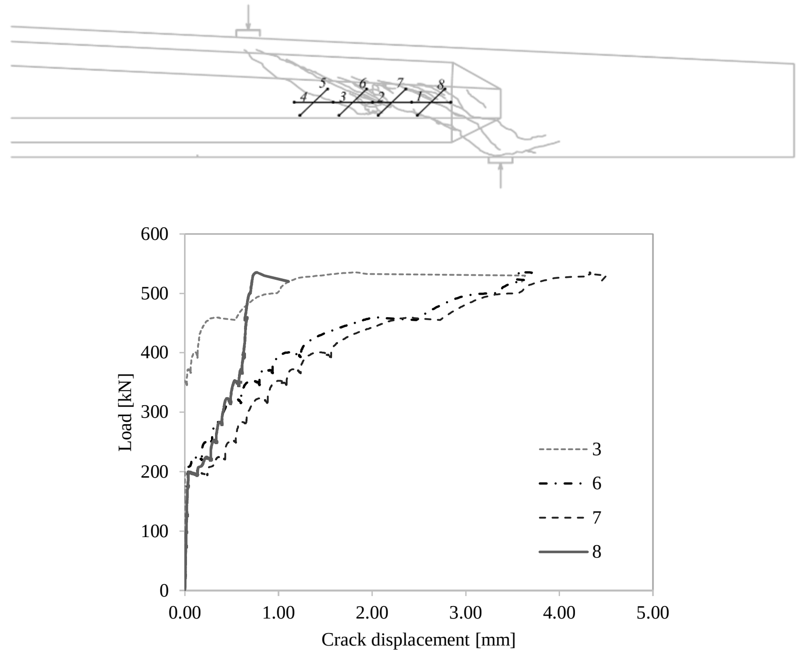

Fig. E2 - Load vs. shear crack displacement [IV-20 – 2.5 -1]

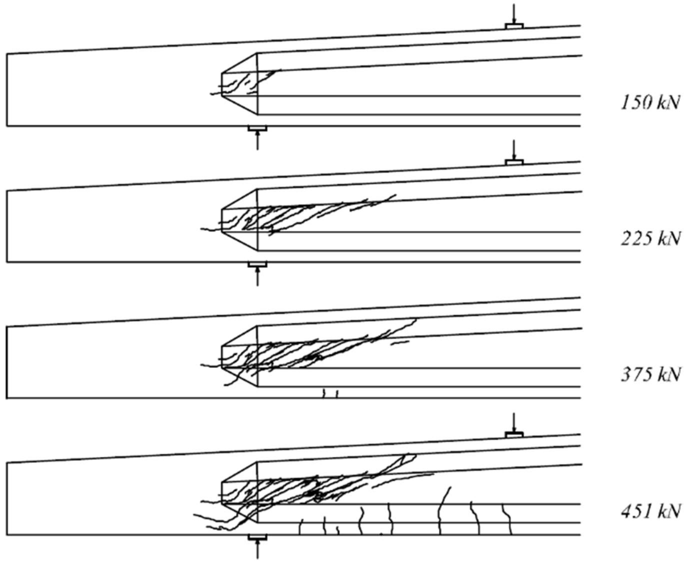

Fig. E3 - Crack development for griderd IV-20 – 3.0 – 2

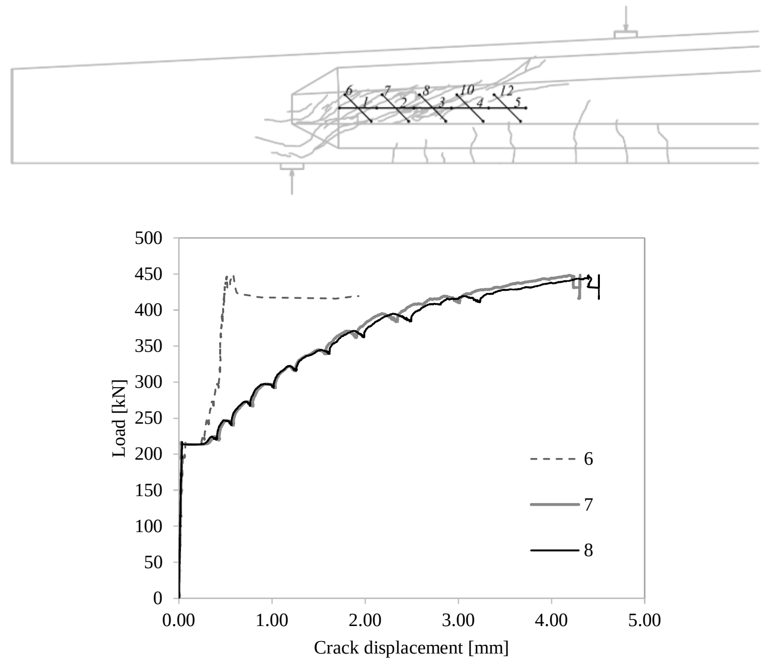

Fig. E4 - Load vs. shear crack displacement [IV-20 – 3.0 - 2]

E.2 GIRDER IV-2

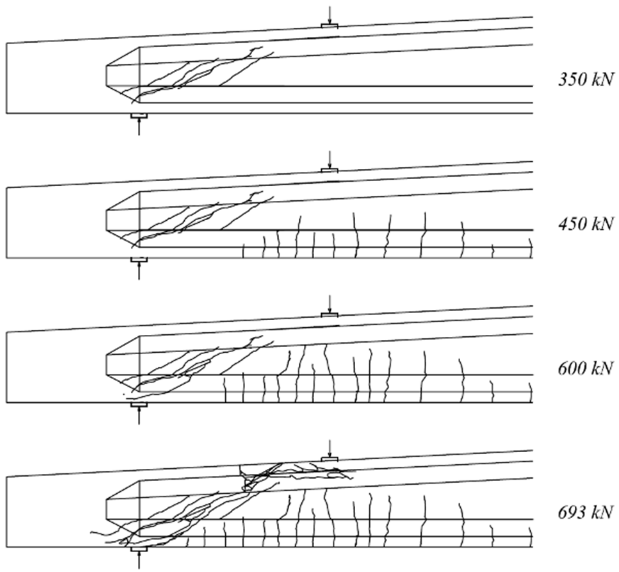

Fig. E5 - Crack development for griderd IV-35 – 2.5 – 1

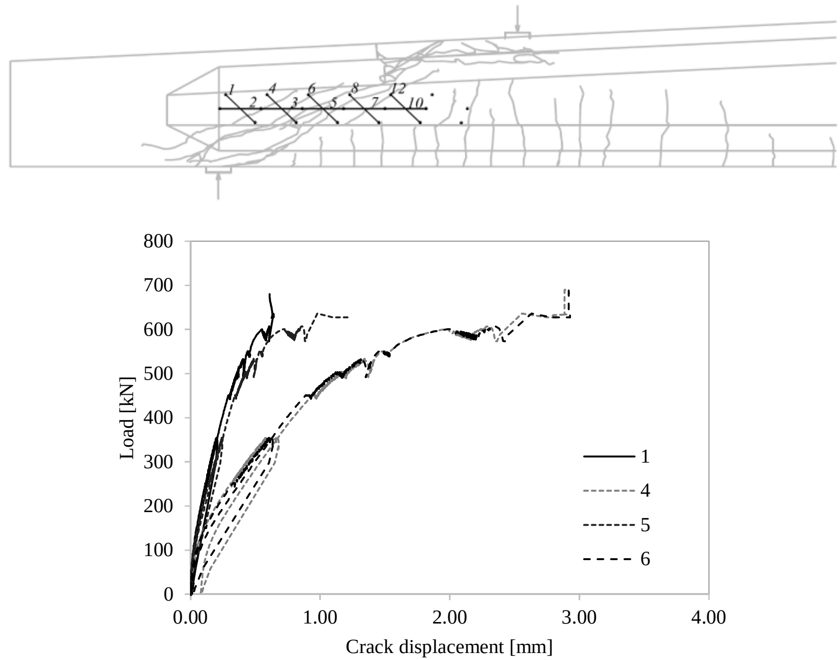

Fig. E6 - Load vs. shear crack displacement [IV-35 – 2.5 - 1]

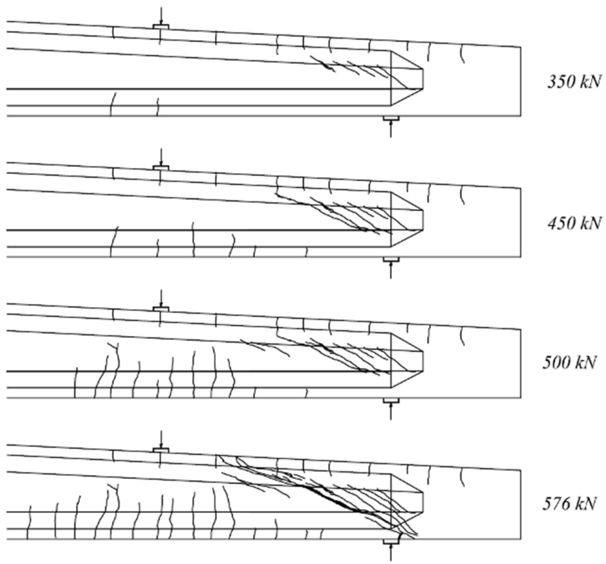

Fig. E7 - Crack development for griderd IV-35 – 3.0 – 2

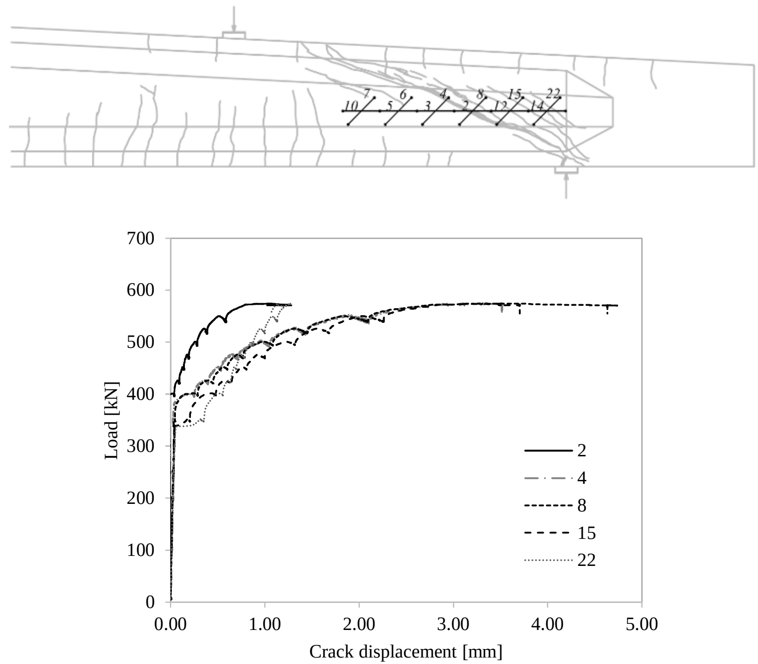

Fig. E8 - Load vs. shear crack displacement [IV-35 – 3.0 - 2]

Curriculum vitae

Personalia

Name	Tim Soetens
Date of birth	05/08/1987
Place of birth	Sint-Niklaas, Belgium
Address	Elzenstraat 38, 9112 Sinaai
Phone	+32 (0) 494 62 39 72
E-mail	tim.soetens@sanacon.be tim.soetens@ugent.be

Education

1998-2004	General Secondary Education: Science-Mathematics Broederschool, Sint-Niklaas
2004-2008	Master of Science in Industrial Engineering: Construction Graduated magna cum laude Master thesis: Non-traditional reinforcement of concrete members to resist stress tensile stress under flexural load
2008-2010	Master of Science in Civil Engineering: Construction design Graduated magna cum laude Master thesis: Design and verification of concrete hypar shell roofs

Employment

January 2015 – …

Owner of SANACON bvba - UGent spin-off

- Concrete consultancy – damage diagnostics and repair of concrete structures

August 2010 – April 2015

Researcher at the Magnel Laboratory for Concrete research, Ghent University.

- PhD research: Design models for the shear strength of prestressed precast SFRC girders.
- Teaching: Prestressed and Reinforced Concrete
- Services: Damage diagnostics and repair of concrete structures.

Scientific Publications

A1- Journal Papers

Soetens T, Matthys S. "Different Methods to Model the Post-cracking Behaviour of Hookend-end Steel Fibre Reinforced Concrete." *CONSTRUCTION AND BUILDING MATERIALS* 73 (2014): 458–471.

Soetens T, Van Gysel A, Matthys S, Taerwe L. "A Semi-analytical Model to Predict the Pull-out Behaviour of Inclined Hooked-end Steel Fibres." *CONSTRUCTION AND BUILDING MATERIALS* 43 (2013): 253–265.

Soetens T, Matthys S. "Shear Stress Transfer across a Crack in Steel Fibre Reinforced Concrete." Submitted to CEMENT AND CONCRETE COMPOSITES (Currently under review).

P1 - International Conference Proceedings

Soetens T, Matthys S, Taerwe L, Van Gysel A. "Basis of a Finite-element Simulation Tool to Predict the Flexural Behavior of SFRC Prisms."HPFRCC 6. *RILEM Bookseries, Vol. 2*. Ed. Gustavo J Parra-Montesinos, Hans W Reinhardt, & Antoine E Naaman. Berlin, Germany: Springer, 2011. 91–98.

C1 - International Conference Proceedings

Soetens T, Matthys S. "Shear Design of Full-scale Prestressed SFRC Girders." 2nd FRC International Workshop (1st ACI–fib Joint Workshop) on Fibre Reinforced Concrete: from Design to Structural Applications, Proceedings. Eds. Bruno Massicotte, Giovanni Plizzari, Barzin Mobasher, Jean-Philippe Charron, 24-25 July 2014, Montreal (Quebec) Canada.

Soetens T, Matthys S. "A Simple Model to Estimate Shear Stress Transfer in Cracked SFRC." *10th Fib International PhD Symposium in Civil Engineering, Proceedings*. Ed. Josée Bastien et al. 2014. 461–466.

Soetens T, Matthys S. "Evaluation of MC2010 Models for Prestressed SFRC Beams Subjected to Shear." *7th International Conference "Fibre Concrete 2013 : Technology, Design, Application", Proceedings*. Ed. Alena Kohoutkova. 2013. 1–10.

Soetens T, Matthys S. "A Semi-analytical Model to Simulate the Direct Shear Pull-out Behaviour of Hooked-end Steel Fibres." *8th Rilem International Symposium on Fibre Reinforced Concrete : Challenges and Opportunities (BEFIB 2012), Proceedings*. Ed. Joaquim Barros et al. Bagneux, France: RILEM Publications, 2012. 1–12.

Soetens T, Matthys S. "Implementation of Fibre Pull-out Behaviour in a Finite Element Model for SFRC." *Bond in Concrete 2012 : Bond, Anchorage, Detailing : Detailing 4th International Symposium, Proceedings*. Ed. John W Cairns, Giovanni Metelli, & Giovanni A Plizzari. Vol. 2. Brescia, Italy: Publisher Creatings, 2012. 941–945.

Soetens T, Matthys S. "A Formula to Predict the Maximum Direct Shear Load of SFRC." *CCC2011: Innovative Materials and Technologies for Concrete Structures : Proceedings of the Fib Congress*. Ed. György L Balazs & Eva Lubloy. Balatonfüred, Hungary: Budapest University of Technology and Economics, 2011. 99–102.